Synthesis of Graphene Oxide from Different Precursors and its Fiber-Reinforced Nanocomposites

Thesis submitted for the award of degree of

Doctor of Philosophy

Submitted by

Anushka Garg

(Regn. No. 901909025)

Under the guidance of

Dr. Rajeev Mehta

Professor- Department of Chemical Engineering

Coordinator- Center of Excellence in Emerging Materials (TIET-VT, CEEMS)

TIET, Patiala-147004

Dr. Soumen Basu

Professor- Department of Chemistry & Biochemistry

Affiliate Faculty- Center of Excellence in Emerging Materials (TIET-VT, CEEMS)

TIET, Patiala-147004

Dr. Roop L. Mahajan

L.E. Hester Chair Professor

Department of Mechanical Engineering, Virginia Tech, USA

Chair Professor, (TIET-VT, CEEMS)

Department of Chemistry & Biochemistry

Thapar Institute of Engineering & Technology, Patiala-147004

Certificate

This is to certify that the thesis entitled, "**Synthesis of Graphene Oxide from Different Precursors and its Fiber-Reinforced Nanocomposites**" being submitted by Ms. Anushka Garg in fulfilment of the requirement for the award of Degree of Doctor of Philosophy in the Department of Chemistry and Biochemistry, Thapar Institute of Engineering and Technology, Patiala, is a record of the candidate's own work carried out by her from December 2019 to February 2024 in this institute under our supervision. The matter presented in this thesis has not been submitted in part or full for the award of any degree in any other University or Institute.

(Supervisor)

Dr. Rajeev Mehta

Professor- Department of Chemical Engineering

Coordinator- Center of Excellence in Emerging Materials (TIET-VT, CEEMS)

TIET, Patiala-147004

(Supervisor)

Dr. Soumen Basu

Professor- Department of Chemistry & Biochemistry

Affiliate Faculty- Center of Excellence in Emerging Materials (TIET-VT, CEEMS)

TIET, Patiala-147004

(Supervisor)

Dr. Roop L. Mahajan

L.E. Hester Chair Professor

Department of Mechanical Engineering, Virginia Tech, USA

Chair Professor, (TIET-VT, CEEMS)

(Head)

Dr. Manmohan Chhibber

Professor & Head

Department of Chemistry & Biochemistry

Thapar Institute of Engineering & Technology, Patiala-147004

Candidate's Declaration

I, hereby declare that the work presented in the thesis entitled **"Synthesis of Graphene Oxide from Different Precursors and its Fiber-Reinforced Nanocomposites", in fulfilment of the requirement for the award** of the Degree of Doctor of Philosophy in the Department of Chemistry and Biochemistry, Thapar Institute of Engineering and Technology, Patiala, is an authentic record of my own work carried out under the supervision of Dr. Rajeev Mehta (Professor & Head, Department of Chemical Engineering, TIET), Dr. Soumen Basu (Professor, Department of Chemistry and Biochemistry, TIET) and Dr. Roop L. Mahajan (Chair Professor, TIET-VT, CEEMS). The matter presented in this thesis has not been submitted in part or full for the award of any degree in India or Abroad.

Anushka Garg

Acknowledgments

"सर्व शक्तिमते परमात्मने, श्री रामाय नमः"

First and foremost, I sincerely express my gratitude to the divine power for granting me the fortitude, patience, endurance, and determination to complete this work.

I am deeply thankful to my academic supervisors, **Dr. Rajeev Mehta** (Professor, CHED), **Dr. Soumen Basu** (Professor, DCBC), and **Dr. Roop L. Mahajan** (Chair Professor, TIET-VT, CEEMS) for their unwavering guidance, invaluable insights, and continuous support throughout this research endeavor. Their mentorship has been instrumental in shaping the direction of my work and fostering my academic growth. They have consistently been accessible whenever needed, even during the odd hours of their jobs.

I owe sincere gratitude to **Dr. Manmohan Chhibber**, Professor and Head, DCBC, TIET, Patiala. I extend my heartfelt thanks to the members of my doctoral committee, **Dr. Kulvir Singh** (Professor & Head, Department of Physics and Materials Science), **Dr. Bonamali Pal** (Professor, DCBC), and **Dr. Banibrata Maity** (Assistant Professor, DCBC), for their constructive feedback during half-yearly progress reports and dedication to ensuring the rigor and quality of my research. My sincere thanks also goes to **Mr. Mayank Sharma** (DCBC) and **Mrs. Mrinmoyee Kanjilal Chakroborty** (TIET-VT, CEEMS) for all the support in documentation work. A special thanks to **Mr. Munish, Mr. Daljit, Mr. Bharat, Mr. Chander Thakur, Mr. Hemant Sharma, Mr. Vishwanath, and Mr. Shekhar** for their help as per the need.

I am grateful to **Dr. Padmakumar Nair**, Director, TIET, and **Dr. N. Tejo Prakash**, Dean of Research and Development Cell (DoRDC), TIET for providing a conducive research environment and access to resources essential for the successful execution of my project. The help from different laboratories like SAI labs, DPMS Instrumental Facilities, SAIF Labs, PU, IIT-Mumbai Sprint Testing Solutions, and CIPET, Amritsar is highly acknowledged. I also want to acknowledge all the faculty members in the Department of Chemistry and Biochemistry for their cooperation and support. I am also thankful to **Dr. Kamaldeep Paul,** Deputy Coordinator, TIET-VT, CEEMS for his valuable suggestions during seminars. I am thankful to **Dr. Gautam Setia**, Assistant Professor, MED, **Dr. Neetu Singh**, Associate Professor, CHED for the occasional support and suggestions, **Dr. Haripada Bhunia**, Professor, CHED, for providing me with the UTM facility, and **Mr. Varinder**, for helping me in the testing of my samples. I am also thankful

to **Mr. Manpreet Singh** (Account Section) for his cooperation. The academic and administrative staff have been instrumental in creating a supportive atmosphere for intellectual exploration.

My appreciation extends to my seniors and lab mates, **Dr. Aashna Nagar, Dr. Zaid B. Siddique, Dr. Daksh Shelly, Dr. Shelly Singla, Dr. Surbhi Sharma, Dr. Neeraj Sohal, Dr. Aanchal Rathi, Dr. Shagun Kainth, Mr. Nikhil Sharma, Ms. Simran, Mrs. Ravinder Kaur, Mr. Shubham Bansal, Mr. Pritam Hait, Mr. Ranjeet, Ms. Palkaran, Ms. Manpreet, Mr. Padam,** and **Ms. Bhavika** who have shared their knowledge, insights, and camaraderie throughout this academic journey. I am especially thankful to **Dr. Divya Monga** who cared for me and motivated me in every aspect. The collaborative spirit within the academic community has enriched my experience and broadened my perspective.

My friends, **Mr. Sachin Jaidka, Mr. Vikash Ranjan, Ms. Akanksha Ranade, Ms. Mandeep, Dr. Aayushi, Mr. Ayush, Ms. Anjali, Ms. Harmeet, Ms. Komal, Mrs. Neha, Mrs. Sonali, Ms. Disha, Mr. Shiv,** and **Mr. Sourabh** for their emotional support and their presence in any way it could have been which has been a constant source of strength.

I owe a debt of gratitude to my family, my father, **Mr. Sanjay Garg**, my mother, **Mrs. Anuradha Garg**, and my grandfather, **Mr. Barkha Nath Garg**, for their unwavering encouragement, understanding, sacrifices, and patience during the challenging phases of my doctoral studies. To my support system from childhood, **Mr. Akshit, Mr. Ankush, Mr. Advitya, Ms. Akanksha, Ms. Akshita, Mr. Arpit, Ms. Shivika,** and **Mrs. Pooja,** your love and affection has been my anchor, and I am grateful for the joy and laughter you guys bring into my life. I extend my gratitude to my uncles, **Mr. Sanjeev Garg** and **Mr. Rajeev Garg,** and my aunts, **Mrs. Rajni Garg** and **Mrs. Mamta Garg** who have always looked after me no matter where I have been. I am truly thankful for their belief in my abilities. This thesis is as much a reflection of their support as it is of my academic endeavors. A special thanks to **Mr. Akshat Mittal** for all the phenomenal care and support during the ending phase of this work.

Last but not least, I want to express my deepest gratitude to **TIET-VT, Center of Excellence in Emerging Materials (CEEMS)**, whose financial support made this research possible.

This journey has been both challenging and rewarding, and I am fortunate to have had the support and encouragement of so many wonderful individuals. Thank you all for being an integral part of my academic and personal growth.

This thesis is dedicated to my "Father"- *The one who believed in Me.!*

Table of Contents

CHAPTER- 1

Introduction and Literature Review

CHAPTER- 2

One-Pot Synthesis of Graphene Oxide from Different Coals and its Application in Enhancing the Mechanical Performance of GFRP Nanocomposites

CHAPTER- 3

Enhancing the Mechanical Performance of E-Glass Fiber Epoxy Composites using Coal-Derived Graphene Oxide

CHAPTER- 4

Enhancement in Mechanical Properties of GFRP-Coal-derived Graphene Oxide Composites by Addition of Multiwalled Carbon Nanotubes and Halloysite Nanotubes: A Comparative Study

List of Figures

CHAPTER- 1

CHAPTER- 2

CHAPTER- 3

CHAPTER- 4

List of Tables

CHAPTER- 1

CHAPTER- 2

List of Symbols

Symbol	
W/mK	Watts per meter-Kelvin
Ω	Ohm
cm	Centimetre
GPa	Gigapascal
π	Pie
TPa	Terapascal
Å	Angstrom
cm^{-1}	Unit for wavenumber
°	Degree
nm	Nanometre
θ	Theta
°C	Degree centigrade
M	Molar
λ	Lambda
eV	Electron volt
phr	Parts per hundred resin
rpm	Rotations per minute
µm	Micrometer

List of Abbreviations

Abbreviation	
2D	Two-dimensional
GO	Graphene oxide
rGO	Reduced Graphene oxide
MLG	Multilayer Graphene
MWCNT	Multi-walled Carbon Nanotube
HNT	Halloysite Nanotube
PAC	Purified Semianthracite Coal
PBC	Purified Bituminous Coal
NPAC	Non-purified Semianthracite Coal
NPBC	Non-purified Bituminous Coal
AC-GO	Semianthracite Coal derived Graphene oxide
BC-GO	Bituminous Coal derived Graphene oxide
MHM	Modified Hummers'method
Gr-GO	Graphite derived Graphene oxide
AC-GO (MHM)	Semianthracite Coal derived Graphene oxide synthesized through Modified Hummers'method
MHM-GO	Graphite derived Graphene oxide synthesized through Modified Hummers'method
GIC	Graphite Intercalation Compound
PGO	Pristine Graphene oxide
FLG	Few Layer Graphene
SWCNT	Single-walled Carbon Nanotube
LDH	Layered double hydroxide
$NaNO_3$	Sodium nitrate
$KMnO_4$	Potassium permanganate
$KClO_3$	Potassium chlorate
ClO_2	Chlorine dioxide

OH	Hydroxyl
H_2O_2	Hydrogen peroxide
Cu	Copper
Al	Aluminium
HCl	Hydrochloric acid
AA	Ascorbic acid
CAGR	Compound Annual Growth Rate
XRD	X-ray Diffraction
FTIR	Fourier Transform Infrared Spectroscopy
SEM	Scanning Electron Microscopy
EDX	Energy Dispersive X-ray
AFM	Atomic Force Microscopy
TEM	Transmission Electron Microscopy
DLS	Dynamic Light Scattering
BET-BJH	Brunauer-Emmett-Teller - Barrett-Joyner-Halenda
XPS	X ray Photoelectron Spectroscopy
LRS	Laser Raman Spectroscopy
SAED	Selected Area (Electron) Diffraction
CVD	Chemical Vapor Deposition
vol.%	Volume percentage
wt.%	Weight percentage
Nc	No. of graphene stacked layers
Lc	Crystallite height
La	Crystallite size
h	Hour
min.	Minutes
ASTM	American Society for Testing and Materials
Tg	Glass Transition Temperature
PVP	Polyvinylpyrrolidone
PVC	Polyvinyl chloride

HDPE	High-density polyethylene
PAMAM	Poly (amidoamine)
PES	Polyethersulfone
EGFPs/GFRP	E-glass fiber-reinforced polymer composites
CFRP	Carbon Fiber reinforced polymer composites
VARIM	Vacuum Assisted Resin Infusion Molding
$GFRP_0$	E-Glass fiber reinforced with epoxy without any nanofiller
$A\text{-}EGF_{0.0625}$	0.0625 phr AC-GO reinforced E-Glass Fiber Epoxy Composite
$A\text{-}EGF_{0.125}$	0.125 phr AC-GO reinforced E-Glass Fiber Epoxy Composite
$A\text{-}EGF_{0.25}$	0.25 phr AC-GO reinforced E-Glass Fiber Epoxy Composite
$A\text{-}EGF_{0.50}$	0.50 phr AC-GO reinforced E-Glass Fiber Epoxy Composite
$A\text{-}EGF_{0.75}$	0.75 phr AC-GO reinforced E-Glass Fiber Epoxy Composite
$B\text{-}EGF_{0.125}$	0.125 phr BC-GO reinforced E-Glass Fiber Epoxy Composite
$B\text{-}EGF_{0.25}$	0.25 phr BC-GO reinforced E-Glass Fiber Epoxy Composite
$B\text{-}EGF_{0.50}$	0.50 phr BC-GO reinforced E-Glass Fiber Epoxy Composite
$B\text{-}EGF_{0.75}$	0.75 phr BC-GO reinforced E-Glass Fiber Epoxy Composite
$Gr\text{-}EGF_{0.125}$	0.125 phr Gr-GO reinforced E-Glass Fiber Epoxy Composite
$Gr\text{-}EGF_{0.25}$	0.25 phr Gr-GO reinforced E-Glass Fiber Epoxy Composite
$Gr\text{-}EGF_{0.50}$	0.50 phr Gr-GO reinforced E-Glass Fiber Epoxy Composite
$Gr\text{-}EGF_{0.75}$	0.75 phr Gr-GO reinforced E-Glass Fiber Epoxy Composite
0.125 HAGRP	(0.125 phr AC-GO + 0.125 phr HNT) reinforced E-Glass Fiber Epoxy Composite
0.25 HAGRP	(0.125 phr AC-GO + 0.25 phr HNT) reinforced E-Glass Fiber Epoxy Composite
0.50 HAGRP	(0.125 phr AC-GO + 0.50 phr HNT) reinforced E-Glass Fiber Epoxy Composite
0.75 HAGRP	(0.125 phr AC-GO + 0.75 phr HNT) reinforced E-Glass Fiber Epoxy Composite
0.125 CAGRP	(0.125 phr AC-GO + 0.125 phr MWCNT) reinforced E-

	Glass Fiber Epoxy Composite
0.25 CAGRP	(0.125 phr AC-GO + 0.25 phr MWCNT) reinforced E-Glass Fiber Epoxy Composite
0.50 CAGRP	(0.125 phr AC-GO + 0.50 phr MWCNT) reinforced E-Glass Fiber Epoxy Composite
0.75 CAGRP	(0.125 phr AC-GO + 0.75 phr MWCNT) reinforced E-Glass Fiber Epoxy Composite
1 CAGRP	(0.125 phr AC-GO + 1 phr MWCNT) reinforced E-Glass Fiber Epoxy Composite

List of Publications

A. Related to PhD Work

- **Garg, A.**, Basu, S., Lee, S. Y., Mahajan, R. L., & Mehta, R. (2023). Simplified One-Pot Synthesis of Graphene Oxide from Different Coals and its Potential Application in Enhancing the Mechanical Performance of GFRP Nanocomposites. *ACS Applied Nano Materials, 6(15),* 14594-14608. **(I.F.- 5.9)**

- **Garg, A.**, Basu, S., Mehta, R., & Mahajan, R. L. (2023). Enhancing the mechanical performance of E-glass fiber epoxy composites using coal-derived graphene oxide. *Polymer Composites, 45(3),* 2444-2461. **(I.F.- 5.2)**

Indian Patent (Status: Filed)

Garg, A., Basu, S., Mahajan, R. L., & Mehta, R. (2023). AN E-GLASS FIBER REINFORCED EPOXY NANOCOMPOSITES & PROCESS THEREFORE. **(Docket No.- 21653)**

B. Other Publications

- **Garg, A.,** Basu, S., Shetti, N. P., & Reddy, K. R. (2021). 2D materials and its heterostructured photocatalysts: Synthesis, properties, functionalization and applications in environmental remediation. *Journal of Environmental Chemical Engineering*, *9*(6), 106408.

- **Garg, A.,** Shetti, N. P., Basu, S., Nadagouda, M. N., & Aminabhavi, T. M. (2023). Treatment technologies for removal of per-and polyfluoroalkyl substances (PFAS) in biosolids. *Chemical Engineering Journal*, *453*, 139964.

- **Garg, A.,** Chauhan, A., Agnihotri, C., Singh, B. P., Mondem, V., Basu, S., & Agnihotri, S. (2023). Sunlight active cellulose/g-C_3N_4/TiO_2 nano-photocatalyst for simultaneous degradation of methylene blue dye and atenolol drug in real wastewater. *Nanotechnology, 34(50),* 505705.

- **Garg, A.,** Basu, S., Shetti, N. P., Bhattu, M., Alodhayb, A., & Pandiaraj, S. (2024). Biowaste to bioenergy nexus: Fostering sustainability and circular economy. *Environmental Research, 250,* 118503.

C. Book Chapters

- **Anushka Garg,** Aayushi Kundu, Soumen Basu, Rajeev Mehta, "GRAPHENE, THE NEXT GENERATION NANOCARBON: SYNTHESIS, PROPERTIES AND ITS APPLICATIONS", Futuristic Trends in Chemical, Material Sciences & Nano Technology, Volume 2, Book 13, Part 1, Chapter 2, November, 2022, 11-19, 978-93-95632-67-6, https://www.rsquarel.org/assets/docupload/rsl2023CA75D9CAC1CE41A.pdf

- Aayushi Kundu, **Anushka Garg,** Banibrata Maity, Soumen Basu, "FLUORESCENT CARBON QUANTUM DOTS FOR METAL ION SENSING", Futuristic Trends in Chemical, Material Sciences & Nano Technology, Volume 2, Book 13, Part 1, Chapter 1, November, 2022, 1-10, 978-93-95632-67-6, https://www.rsquarel.org/assets/docupload/rsl20232F0DFB9056E979E.pdf

Abstract

Graphene oxide stands out as a promising candidate for numerous potential applications owing to its superior characteristics. Graphene oxide is primarily synthesized using Hummers' method or its modified version, involving a reaction with oxidizing agents like potassium permanganate ($KMnO_4$), potassium chlorate ($KClO_3$), or sodium nitrate ($NaNO_3$) in corrosive oxidizing acid mixtures (H_2SO_4, H_3PO_4, HNO_3). These multi-step methods generate hazardous gases (NO_x, SO_x) and carcinogens. The process also produces significant wastewater with residual acids and heavy metals, posing challenges in chemical waste disposal. Moreover, the rising cost of graphite makes the procedure unsuitable for large-scale production.

In the light of above addressed issues, there has been very few reports published working on development of a facile and efficient method utilizing cost-effective precursors. Amongst the available methods for synthesis, the one-pot method has recently gained attention utilizing HNO_3 as a single oxidant and Coal as the precursor. The present work has aimed to explore this one-pot process for its applicability to Indian coals and conversion to Graphene oxide. Then the potential of this coal-derived GO has been studied for its use as a nanofiller in enhancing the mechanical properties of E-Glass fiber-based epoxy composites.

This thesis entitled "**Synthesis of Graphene Oxide from Different Precursors and its Fiber-Reinforced Nanocomposites**" embodies the subject matter resulting out of this study and is divided into four Chapters.

Chapter 1:

It describes the background of nanomaterials, carbon-based nanomaterials including graphene and its derivatives along with literature survey and scope of the work. This Chapter discusses the detailed information about different synthesis methods for graphene from different precursors, i.e., coal and graphite and related advancements along with the limitations, utilization of these

types of nanofiller in polymer composites for improved mechanical performance. A thorough literature survey has been done to understand the reinforcement of different nanofillers in the E-Glass based epoxy composites.

Chapter 2:

This chapter presents new data on the feasibility of using a facile one-pot process with HNO_3 to synthesize graphene oxide (GO) from bituminous coal (BC) as well as anthracite coal procured from coalfields in India. The experiments demonstrate that a reduced concentration of 5M HNO_3 and a shorter oxidation time period of 5 hours are sufficient for bituminous coal, whereas semi-anthracite coal (AC) requires 16M HNO_3 and 72 hours of oxidation time. The synthesized graphene oxide from bituminous coal (BC-GO) and semi-anthracite coal (AC-GO) was characterized using various techniques including SEM-EDX, FTIR, XRD, XPS, BET-BJH, LRS, TEM, SAED, AFM, and DLS. These results were then compared with those for GO derived from graphite and purified AC using modified Hummers' method. The characterization data revealed both similarities and significant differences in the properties of these materials. While TEM analysis revealed similar sheet-like morphology for both coal-derived and graphite-derived GO, XPS and FTIR data indicated the presence of graphitic compositions with observable peaks for C=C and C=O, as well as abundant functional groups containing oxygen and nitrogen. Surface and structure properties differed between coal-derived and graphite-derived GOs. Raman spectra of BC-GO showed a lower I_D indicating fewer defects and preserved graphitic domains due to the use of less concentrated HNO_3. Furthermore, the study explores the potential application of coal-derived GO by studying the mechanical properties of glass fiber-reinforced polymer nanocomposites with AC-GO as a nanofiller. The results demonstrate that coal-derived GO effectively enhances the mechanical properties of the nanocomposites.

Chapter 3:

In this chapter, we have compared the effect of various precursor-based graphene oxide (GO) nanofillers on enhancing the mechanical performance of E-glass fiber reinforced epoxy resin composites (EGFPs). GO derived from bituminous coal (BC-GO) and graphite (Gr-GO) were dispersed into epoxy resin matrix. The resulting mixture was combined with E-glass fiber mats using vacuum-assisted resin infusion molding. Notable improvements (38.9 % in flexural strength, 22.9 % in tensile strength, and 21.6 % in impact strength) were observed in BC-GO reinforced EGFPs at 0.25 phr loading of BC-GO. The improvements for Gr-GO reinforced EGFPs were 28 %, 9.3 %, and 6.8 %, respectively. XRD analysis of BC-GO showed a diffraction peak at $2\theta = 20.9°$. Except for this peak, no other crystalline peaks were observed when BC-GO was incorporated into EGFPs. FTIR spectra of both composite samples, with or without the nanofiller, were similar due to the spectral peaks overlap. TEM demonstrated exfoliated morphology of BC-GO in EGFPs. These findings underscore the potential of BC-GO as a cost-effective reinforcement for polymer nanocomposites across various industrial applications, including the development of lightweight and strong materials for aerospace and automotive industries, protective coatings, petroleum, and aerospace production systems.

Chapter 4:

In this chapter, a comparative study depicting the synergistic performance of two different nanofillers, namely halloysite nanotubes (HNT) clay and multiwalled carbon nanotubes (MWCNT), in conjunction with a fixed concentration (0.125 phr) of semi-anthracite coal-derived graphene oxide (AC-GO) on enhancing the mechanical properties of E-glass fiber reinforced epoxy resin composites (EGFPs) is shown. The dispersion of AC-GO with HNT clay (GO-H) and AC-GO with MWCNT (GO-C) within the epoxy resin matrix was achieved using sonication and homogenization techniques. The resulting mixture was incorporated into E-glass fiber mats employing the “vacuum-

assisted resin infusion molding" (VARIM) technique. Notable improvements (18.3% in flexural strength, 14.6% in tensile strength, and a slight increase in impact strength (1.8%)) were observed in EGFPs reinforced with GO-H at a 0.50 phr loading of HNT, with an AC-GO concentration maintained at 0.125 phr. Correspondingly, optimal values for GO-C reinforced EGFPs at 0.25 phr were 40.3%, 18.7%, and a 10.5% decrease in impact strength, respectively. Analytical techniques such as XRD, FESEM, EDX mapping, and FTIR revealed the presence of relatively abundant functional groups and strong interfacial adhesion between AC-GO and HNT, as well as AC-GO and MWCNT, contributing to enhanced mechanical properties through a synergistic combination of reinforcement, filler-matrix interaction, and particle packing density. Importantly, considering that the cost of HNT clay is approximately 15 times cheaper than industrial-grade MWCNTs, these findings underscore the potential of GO-H as a very cost-effective reinforcement alternative to GO-C for polymer nanocomposites for various industrial applications.

Chapter 1. *Introduction and Literature Review*

1.1. Graphene oxide

The graphene unveiling in 2004 by Andre Geim and Konstantin Novoselov has spurred widespread exploration within the science community to uncover myriad potential utilizations of this material [1]. Graphene is frequently described as a 2D (two-dimensional) layer, comprising carbon atoms with sp^2 hybridization arranged in a honeycomb-like or hexagonal structure [2]. Its thickness equals the diameter of an individual atom. Moreover, graphene is composed of pure carbon, where each carbon atom forms covalent bonds in same plane arrangement, and monolayer of graphene are interconnected through van der Waals forces [3]. To grasp the essence of graphene, one can view it as a smaller component of graphite with only a few layers. From this perspective, the concept of graphene and its characteristics is not a recent revelation, and its history extends back approximately 500 years [4]. Even during the middle ages, graphite was utilized to craft pencils for writing [5]. The remarkable properties of graphite, encompassing high thermal conductivity (around 3000 W/mK), in-plane electrical conductivity (approximately 104 $\Omega^{-1}cm^{-1}$), and the mechanical stiffness of its hexagonal network (1060 GPa), have rendered graphite indispensable across various industries and applications [6]. The global annual demand for graphite has soared to one million tons [7]. Extensively explored in various fields, graphene materials, and their derivatives, like GO (graphene oxide), and rGO (reduced graphene oxide) have garnered consideration [8]. This interest is driven by the existence of aromatic rings, reactive functionalities, and free π-π electrons in these materials [9]. Graphene derivatives share closely related 2D structures, yet subtle distinctions between them give rise to divergent physico-chemical properties. Numerous comprehensive reviews have chronicled the outstanding performance exhibited by graphene materials [10][11][12][13].

In graphene, the in-plane bond arises from sp^2 hybridized orbitals, comprising s, p_x, and p_y orbitals, with the p_z orbital being unbound and perpendicular to the plane. This configuration

results in a 2D plane with sigma bonds featuring very short interatomic lengths (~1.42 Å), imparting greater strength compared to the sp^3 hybridized orbital in diamond. This robust C-C-C in-plane bond underlies the remarkable mechanical resistance of a graphene monolayer, evident in intrinsic tensile strength (130.5 GPa) and Young's modulus (1 TPa), respectively [14]. Furthermore, the half-filled π band contributes to a zero-band gap between valence and conductive bands, allowing for free-moving electrons within the graphene monolayer. The weak π bonds also result in a feeble Van der Waals interaction between monolayers, facilitating movement upon each other under very weak shear stress [15]. The primary objective of graphene derivatization is to customize its physical characteristics, including electronic structure, resistivity, surface energy, optical transmittance, luminescence, and mechanical behavior. GO serves as a representative instance of graphene modified through the incorporation of oxygen functionalities. A notable distinction lies in the ability to attach various types of functionalities to the graphene framework. Achieving the introduction of a single type of oxygen functionality onto graphene in a singular step is generally challenging. However, the oxidation of graphite-to-graphite oxide, followed by exfoliation to produce GO, tends to introduce different functionalities in varying proportions based on the conditions. Significantly, GO finds extensive use as an initial material for synthesizing other graphene derivatives and reduced graphene. Chemical, photochemical, thermal, microwave, and solvothermal methods stand out as the most commonly employed approaches for reducing GO [16]. Evidently, the potential applications of graphene derivatives are expanding at a rapid pace, keeping pace with the evolution of this material family.

1.2. Synthesis approaches for GO

Efficient and cost-effective synthesis of graphene continues to pose a challenge. Well before the recent surge in interest in graphene-based composites, significant progress had been made in the synthesis of GO. GO was first synthesized by Benjamin Brodie in 1859, predating the formal discovery of graphene. Brodie devised a method for producing graphite oxide, involving the

oxidation and exfoliation of natural crystalline graphite, which undoubtedly yielded a noticeable amount of single-layer GO [17]. Unfortunately, during that era, the significance of graphene was not yet known. It was only more than a century and a half later, following "The Rise of Graphene [18]," that Brodie's old invention was revisited as an efficient and economical means of producing this novel and promising material. Current approaches for producing GO leverage the notable intercalation capability of layered graphite. This involves allowing atoms of active metals and certain oxidation agents to permeate the spaces between the flat carbon layers of crystalline graphite. This process increases the interlayer distance and modifies the layer surfaces through the formation of chemically bonded functional groups. The synthesis method significantly impacts the structure of graphene products, often introducing defects, but not all defects necessarily degrade graphene properties; some can be beneficial [19]. Controlled defects may find applications in specific contexts. Various researchers have studied defects in graphene structures, categorizing them into two types: point defects and one-dimensional line defects. Liu et al. [20] delved into the specifics of graphene defects, citing examples like Stone-Wales dislocations, single vacancies, and clustered vacancies as point defects. Additionally, defects can occur at the graphene edges, resulting from local variations in reconstruction type or continuous removal of carbon atoms from the backbone [21].

Ultimately, the application of suitable oxidation agents induces the complete disassembly of the graphitic crystal into individual carbon monolayers with chemically modified surfaces [22]. Established techniques for producing graphene oxide (such as those by Brodie [23], Staudenmaier, and Hoffman [24]) involve the use of potent acids (nitric acid (HNO_3) and/or sulphuric acid (H_2SO_4)) along with potassium chlorate ($KClO_3$) as shown in figure 1.1. The widely adopted Hummers'-Offeman method utilizes a combination of concentrated H_2SO_4, $NaNO_3$, and $KMnO_4$. This method yields well and is more time-efficient compared to earlier approaches [25]. Hummers' method offers several benefits over conventional methods like the $KMnO_4$ usage as an

oxidizing agent (instead of $KClO_3$, that evolves toxic gaseous ClO_2) and the addition of $NaNO_3$ (resulting in in situ formation of HNO_3 instead of utilizing HNO_3 as solvent) [26]. Still, disadvantages of using it cannot be underestimated which include intensive oxidation and mechanical exfoliation to form GO [27]. The graphene production can be categorized by distinguish methods: Top-down method (mechanical and chemical exfoliation, chemical fabrication) and Bottom-up approach (pyrolysis, epitaxial growth, plasma synthesis, and chemical vapor deposition). Any approach which enhances the synthesis route as well as the final product proposed by Hummers' is referred to as "modified Hummers' method". Figure 1.1 represents a brief history synthesis of graphene.

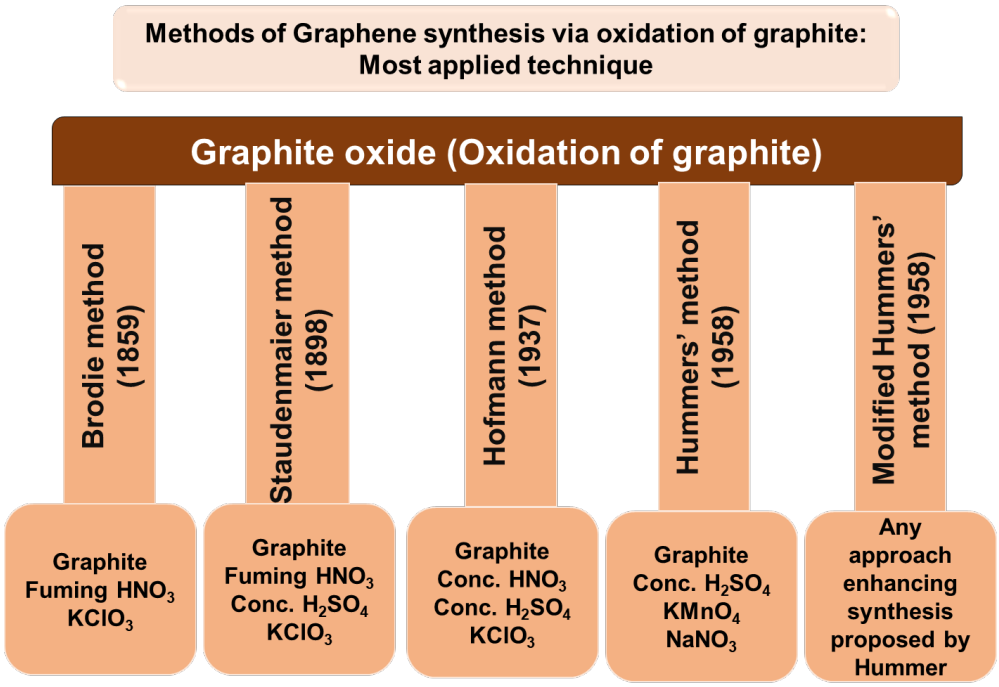

Figure 1.1. A summarized history of events in the evolution of graphene derivatives

In recent years, Tour et al. [28] showed the improved synthesis of GO via natural graphite flake (precursor). However, graphite flakes used are ultra-purified using harsh acid washing and then are used for GO synthesis. They used $KMnO_4$, oxidant and H_3PO_4/H_2SO_4 in ratio 1:9 eliminating the use of $NaNO_3$. Their improved phenomena provided a larger quantity of hydrophilic oxidized

material in comparison with other conventional methods. GO exhibits distorted sp^2 bonding, and restoration of its honeycomb lattice, reduction approaches are frequently employed [29]. The reduction method often leads to elimination of most oxygen-based functionalities, like hydroxyl, carbonyl, and carboxylic in GO. However, achieving reduction of GO completely to yield pure graphene remains challenging. The resulting rGO typically exhibits a strong similarity to pristine graphene but with a dimensional variances and few defects [30]. The rGO quality is influenced through factors like the kind of reductant and process optimizations, including pressure, reduction time, temperature, and voltage [31]. Additionally, the C/O ratio indicates the effectiveness of reducing agent. A higher C/O ratio proposes a more extensive de-oxygenation, leading to rGO of higher quality [32]. Thermal, chemical, and electrochemical reduction methods are majorly used methods. Table 1.1 shows the recent literature on GO synthesis using graphite as the precursor.

Table 1.1. Literature review on synthesis of graphene oxide from graphite

S.No.	Materials used	Technique	Key results	References
1.	Precursor: Natural graphite	Three variations of Hummers' method utilizing three distinct acid blends	Explored safe and facile approaches for synthesizing rGO and GO of high-quality, avoiding the generation of toxic gases and keeping production temperatures low. The structural examinations indicated the existence of a crystalline phase of GO and established the GO reduction to rGO following 1h exposure to ultrasound. XPS and EDS analyses affirmed a notable rise in atomic concentration of oxygen-containing functional groups, in both GO-I and GO-II. FTIR findings validated the higher concentration of oxygen-based groups in GO-1 comparative to the other prepared GO samples.	[33]
2.	Precursor: Graphite	Tour method	Synthesized GO using the Tour method and reduced GO using	[34]

	powder		different parameters. Various factors considered included reaction duration, temperature, and concentration levels to examine the extent of graphite oxidation to graphene oxide. Findings indicated that subjecting graphite powder to a combination of $KMnO_4$ (1:9) and concentrated H_2SO_4/H_3PO_4 acids at 50°C for 12 h yielded a superior degree of oxidation.	
3.	Precursor: Natural graphite flake	Modified Hummers' method	Several necessary processing materials were evaluated explicitly concerning the size distribution of GO sheets produced based on each set of these parameters. The use of larger graphite flakes did not produce large GO sheets. Increasing the degree of oxidation beyond that required for exfoliation resulted in small-sized GO sheets. Thermal expansion was found to be better than the exfoliation step.	[35]
4.	Precursor: Natural graphite powder	Modified Hummers' method	Proposed an enhanced approach to the Hummers' method for synthesizing GO, denoted as GO1 without $NaNO_3$ or as GO2 with $NaNO_3$, and purified through dialysis and centrifugation. Improved synthesis method resulted in a maintained product yield and emergence of toxic gaseous N_2O_4/NO_2. The yields of GO1 and GO2, expressed as the ratio of the weight of GO to the weight of graphite powder, were determined to be 92% ± 3% and 96% ± 2%, respectively. XPS results confirmed, GO1 and GO2 have comparable oxidization degrees. Zeta potentials of GO1 and GO2 suspensions came out to be 43.8 ± 1.3 and 45.6 ± 0.6 mV because of the presence of carboxyl groups providing a negative charge. Additional findings reveal that GO produced by both the refined and	[36]

			traditional Hummers' techniques exhibit nearly identical dispersibility, chemical structures, thicknesses, and lateral dimensions.	
5.	Precursor: Multiwalled-carbon nanotubes	Longitudinal unzipping of MWCNTs	Different reaction conditions were investigated to assess the importance of each variable in the synthesis of GO nanoribbons. Discovered that adequate H_2SO_4 (90 vol%) was vital for the complete formation and exfoliation of the nanoribbons, while raising the reaction temperature to 60°C was essential. Moreover, introducing 10 vol% of a secondary acid such as TFA or H_3PO_4 significantly improved the quality of the resulting nanoribbons. GO nanoribbons were produced with fewer defects, maintained < 100 nm wide, and maximized greater aspect ratio.	[37]
6.	Precursor: Purified natural graphite	Hummers' method	Investigated production of graphene-based nanosheets through the chemical reduction of exfoliated graphite oxide. Reduction of exfoliated GO sheets in water with hydrazine results in a material with graphitic characteristics comparable to pristine graphite. Various characterization techniques of the reduced GO indicate that the hydrazine treatment results in unsaturated and conjugated carbon atoms, which in turn imparts electrical conductivity.	[38]
7.	Precursor: Natural graphite powder	Improved Tour method followed by reduction using ascorbic acid (AA)	In GO FTIR spectra, peak at 1066 cm^{-1} corresponds to C-O stretch, while the peak at 1288 cm^{-1} is identified as C-O-C bending. Additionally, C-OH bending is observed at 1587 cm^{-1}. Carbonyl groups are evident at 1724 cm^{-1}, indicating C=O stretching. A prominent peak observed at 3448 cm^{-1} is assigned to the O-H stretching vibration of C-OH groups and the moisture content within the material. Conversely, in rGO, the peaks at	[39]

			1066, 1288, 1724, and 3448 cm^{-1} disappear or notably diminish.	
8.	Precursor: Natural graphite	Modified Hummers' approach following reduction using Fe powder	Microscopic images reveal that the rGO material consists of thin, crumpled sheets that are randomly aggregated and closely interwoven with each other. XRD spectra show the peak at 10.3°, originally present in GO, got eliminated, while a broad peak at 24.3° emerges. This shift signifies the extensive reduction of GO and the exfoliation of layered graphene nanosheets.	[40]
9.	Precursor: Natural graphite powder	Vacuum-assisted thermal exfoliation and in situ reduction of graphite oxide	The resulting graphene sheets, averaging 0.9 nm in thickness and possessing a specific surface area of 758 m^2g^{-1}, match the characteristics of conventional graphene produced at 1050°C under atmospheric pressure (700 m^2g^{-1}).	[41]
10.	Precursor: Graphite powder	Chemical cleavage followed by reduction process and through liquid-phase exfoliation methods	GO synthesized by modified Hummers' method had carboxylic acid, hydroxyl, and ether groups confirming that graphite was successfully oxidized. Consisted of 12 layers and the layer distance was in the range of 0.67–0.72 nm. Inter-layer spacing of graphite was expanded from 0.3356 to 0.3364 nm in the case of the liquid exfoliation process.	[42]
11.	Precursor: Graphite powder	Modified Hummers' method, followed by reduction with N_2H_4	XRD findings suggest the disappearance of the 2θ at 26.4° peak, associated with d (002) of 0.335 nm in graphite powder, indicates its transformation. A significant peak at 2θ=11.95°, conforming to a d-spacing of 0.754 nm, suggests successful graphite oxidation and GO formation. Subsequently, a distinct diffraction peak at 2θ=22.5° signifies the formation of rGO flakes through	[43]

			hydrothermal reduction.	
12.	Precursor: Natural graphite	Modified Hummers' method without using $NaNO_3$ (Drying temperatures, 60 °C and 90 °C used)	FTIR analysis reveals the existence of various functionalities, hydroxyl, carboxyl, and carbonyl. XRD results indicate a slightly larger interlayer spacing in GO60 (dried at 60 °C) compared to GO90 (dried at 90 °C). SEM images depict a uniform network of GO layers ranging from approximately 6 to 9 nm.	[44]
13.	Precursor: Graphite flakes	Modified Hummers' method	Decrease in the interlayer spacing for rGO (0.36 nm) when compared to GO (0.98 nm) confirmed the recovery of sp^2 carbon atoms and the reduction of functionalities in GO. Higher C/O atomic ratio for rGO (4.44) than GO (1.59) obtained from the XPS data showed that reducing the graphite oxide with N_2H_4 reduced the oxygen-based functionalities. Confirmation of presence of GO and rGO were evident by the absorption peaks observed at 235 nm and 277 nm.	[45]
14.	Precursor: Graphite powder	Modified Hummers' method	FTIR spectra indicated the existence of oxygen-containing functional groups, ensuring the thorough exfoliation of graphite into GO. XRD of the product showed the diffraction peak at ($2\theta = 26.7°$) with d-spacing of 0.334 nm.	[46]
15.	Precursor: Pure graphite powder	Modified Hummers' method	SEM results indicate the acquisition of GO in several square microns. GO FTIR spectra reveal the existence of various functionalities in both samples, including hydroxyl, epoxy, carboxyl, and carbonyl.	[47]

The majority of the literature, as documented in Table 1.1, outlines the synthesis of GO through approaches like the Hummers' method, its modified form, and the Tour method, followed by reduction methods to produce rGO.

Higginbotham et al. [48] utilized multiwalled CNTs and produced GO nanoribbons via their longitudinal zipping. This approach generates GO nanoribbons with reduced holes or defects on basal plane, preserves narrow ribbons measuring less than 100 nm in width, and increases high aspect ratio.

Other than that, most of the conventional methods widely utilize graphite as the precursor for obtaining GO. Hummers' method offers several benefits over conventional methods like the use of $KMnO_4$ as an oxidizer and the addition of $NaNO_3$. Still, disadvantages of using the advanced Hummers' method cannot be underestimated since it includes intensive oxidation and mechanical exfoliation to form GO. The utilization of multiple oxidants at multiple steps makes the process tedious and presents health hazards. All these limitations associated with different approaches make the investigations till now inappropriate for inexpensive potential mass scalability. Therefore, it calls for a relatively inexpensive method, which is environmentally more benign and can be customized to different sources of precursors such as coal, plastics, biomass, etc.

1.3. Different precursors for GO synthesis: Coal vs Graphite

Over the past decade, significant advancements have been made in the commercially feasible, large-scale graphene production, an advanced carbon nanomaterial with diverse applications in composites, energy storage, sensors, and membranes owing to its excellent properties (figure 1.2). The growing demand has driven numerous global research initiatives, resulting in significant breakthroughs in both fundamental science and state-of-the-art utilizations. Previous literature on graphene highlighted a common challenge: increased production yield often accompanied substandard graphene quality, limiting commercial viability. However, recent studies in graphene synthesis reveal an emerging trend—utilizing naturally available carbonaceous sources to produce low-cost graphene derivatives [49]. Till date, graphite stands as primary precursor for GO synthesis. Graphitic materials fall into two primary categories based on the arrangement of their

graphene layers. The first category features a hexagonal lattice of carbons, commonly known as graphite. This structure is characterized by a thermodynamically stable, regularly packed layered arrangement denoted as … ABAB …, bonded together by van der Waals forces. The second category is turbostratic carbon, where graphene layers are organized in a disordered fashion, exhibiting tilts, bends, random orientations, translations with each other, and rotations concerning the normal of the graphene layers. Through series of chemical processes, typically involving strong acids and oxidizing agents, graphite undergoes oxidation and exfoliation, transforming into graphene oxide [50]. The initial layered structure of graphite is disrupted, introducing oxygen-based functionalities such as carbonyl, hydroxyl, and carboxyl, onto the layers of graphene. This modification imparts hydrophilicity and enhanced reactivity to the resulting GO [51]. The versatility of graphite as a precursor underscores its significance in the production of GO, a material valued for its wide-ranging applications in various fields, including composites, sensors, and energy storage devices [52].

Being an exemplar of Bernal (or AB)-stacked graphitic material, both natural and synthetic graphite present their own set of challenges. The cost of the precursor material, graphite, has experienced a consistent upward trend in recent years. This rise is attributed to the escalating demand driven by the expanding electric car battery markets and lithium-ion battery manufacturers [53][54]. As per the Canaccord Genuity report in 2017, the overall demand for graphite from lithium-ion batteries is projected to surge from 150 kilotons in 2015 to over 1 million tons in 2025, indicating a compound annual growth rate (CAGR) of 23% [55]. Also, natural graphite is constrained by geographical limitations and is typically localized establishing a dependency on imports for the production of these materials. Furthermore, the synthesis of graphite involves substantial costs, primarily stemming from the use of petroleum byproducts as precursors and the exceptionally high temperatures required, which can reach up to 3000°C [56].

Unlocking the complete potential of graphene as a revolutionary material (remarkable properties shown in figure 1.2) with diverse applications impacting various facets of our daily lives requires the exploration of alternative precursor materials and environmentally friendly processes for cost-effective mass production. Unsurprisingly, this constitutes a vibrant and ongoing research focus in both academic and industrial spheres [57].

Coal, a naturally abundant fossil fuel, serves as a rich source of carbon globally [58]. Through the bio-geochemical process of coalification, involving high heat and pressure acting on plant materials, the organic species (C, H, S, O, and N) undergo metamorphic transformation. This process destroys organic molecules while preserving carbon. The content of carbon varies based on the coalification level, resulting in a range from low to high grade [59]. Coal is typically divided into lignite (70 wt%), bituminous (75–85 wt%), and anthracite (95 wt%). These coal types can be converted to graphitic structures through shear stress, elevated temperature, and pressure [60][61]. Coal is a heterogeneous nanostructure formed by the arrangement of aromatic units, characterized by a three-dimensional crosslinked interconnected network arising from short aliphatic and ether bonds [62]. Also, coal consists of crystalline carbon with Å or nm-scaled graphitic domains featuring short-range graphite-like order and a few layers. This structure is commonly referred to as turbostratic graphitic structure (figure 1.2). Additionally, coal contains completely amorphous carbon, lacking a crystalline structure, alongside polymerized aromatic hydrocarbon units and defects interconnected by cross-links, with variable amounts of other elements [63]. The term turbostratic carbon denotes a lower stacking order between adjacent graphene layers and a larger interlayer spacing (>0.342 nm), in contrast to the crystalline graphite's interlayer spacing, which is generally 0.335 nm [64]. According to findings in [65], the structural model of pyrolyzed carbon suggests a composition of perfect, planar graphite-like layers alongside a highly disordered form, lacking mutual orientations. As discussed earlier, the physico-chemical properties of coal vary based on its location and grade, but they consistently exhibit

numerous poly-aromatic structures akin to the sp^2 bonding character of graphene. Consequently, coal emerges as a promising precursor for carbonaceous nanomaterials, including graphene [66].

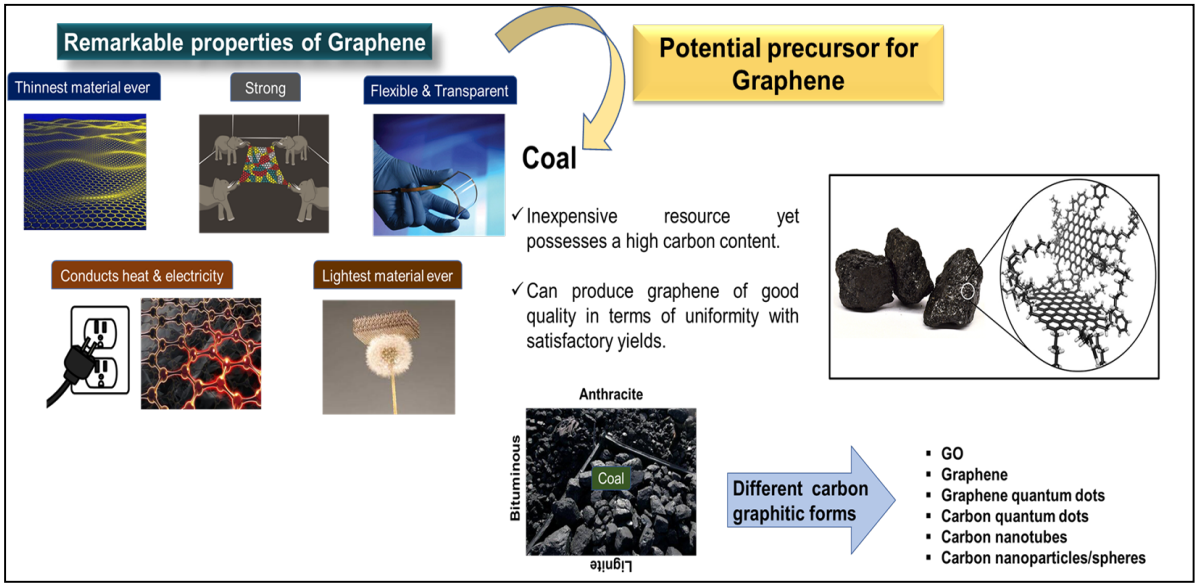

Figure 1.2. Properties of graphene oxide and its potential precursor for synthesis

The primary focus of academic researchers has been on transforming coal into highly ordered graphitic carbon, subsequently employing a chemical-intensive oxidation process. Pakhira et al. [67] documented their research on GO synthesis by leaching low-grade coal with HNO_3. Following the thermal removal of excess acid, they generated large GO sheets. Nevertheless, these sheets demonstrated instability in an acidic environment and adopted a spherical morphology, exhibiting both closed and open characteristics. Yan et al. [68] outline a convenient method for directly converting anthracite into multilayer graphene sheets in the presence of molten iron. By adjusting the ratio of iron to anthracite in the initial reactant, they can control the morphology and layer number of the resulting multilayer graphene sheets. Their findings indicate that when the iron to anthracite ratio is approximately 10:1, multilayer graphene sheets with around 2–4 layers can be obtained. Purwandari et al. [69] utilized bituminous coal and employed a combination of exfoliation and Hummers' method to isolate graphite. They observed a higher d-spacing in GO compared to coal-graphite, along with the presence of various functional groups. In a similar

approach, Savitskii et al. [70] explored the chemical oxidation of different coal types, including brown coal, anthracite, low-volatile bituminous, and bituminous coal. Their findings indicated anthracite coal as an effective precursor for the colloidal dispersion of GO, with a size distribution in the range of 122−190 nm. Additionally, the existence of oxygen functionalities at 3420 cm^{-1} (OH), 1053 and 1226 cm^{-1} (C−O), and 1293 and 1720 cm^{-1} (C=O) was reported. Table 1.2 shows the literature on the synthesis of graphene derivatives from coal using different approaches.

Table 1.2. Literature review on synthesis of GO from coal

S.No.	Material used	Technique	Key results	References
1.	Bituminous coal (coal mine in Sawahlunto-Sinjunjung, West Sumatra, Indonesia)	Exfoliation with modified Hummers' method	XRD diffraction peak at 2Θ= 11.08°, derived from inter-GO diffraction from bituminous coal with 0.72nm interlayer distance resulting from oxidation of coal; used the coal without any pre-treatment. SEM revealed a smooth and crimped surface of GO.	[69]
2.	Semi-bituminous coal (eastern Indian region)	Treatment of the demineralized coal in concentrated H_2SO_4 followed by modified Hummers' method (involving ultra-sonication)	XRD diffraction peak at 2θ = 12.5° corresponds to the (001) plane, with a d-spacing of ~0.789 nm, thereby confirming the formation of GO; synthesized GO has a d-spacing larger than the commercially available graphite (0.343 nm). Raman spectra of GO reveal two peaks at 1350 cm^{-1} (D-band) and 1590 cm^{-1} (G-band), with an I_D/I_G value of approximately 1.04.	[71]
3.	Coal (China)	Solution phase technique	Results revealed the small and monolayer GO sheet. XRD diffraction peak at 2Θ= 21.5°, which came from the inter-GO diffraction, shows a d-spacing of 0.41 nm; d-spacing is a little larger than that of the normal graphite for the present of functional groups but smaller than that of GO from	[72]

			graphite.	
4.	Bituminous coal	Improved modified Hummers' method	XRD peak of GO appeared at a value of 2θ = 11.3°, with a d spacing corresponding to 0.8 nm, revealing the laminar structure with increased d-spacing in GO. Additionally, the peak at 2θ = 25.01° indicates that the distance between graphite layers has been significantly increased during the thermal treatment.	[73]
5.	Sub-bituminous coal (Pakistan)	Hummers' method followed by reduction through N_2H_4	A broad shoulder was observed in GO analysis from 15º to 22º, indicating that the graphene oxide produced is amorphous. This shoulder after reduction shifted towards a higher degree, confirming that the material has exfoliated after reduction, and the rGO produced has smaller interplanar spacing than GO.	[74]
6.	Lignite (Puhe Coal Mine, Shenbei Mining Area, Liaoning Province, China)	Conventional Hummers' method	Computed interlayer spacing derived from the (002) peak of GO is 8.27 Å (2θ = 10.7º), surpassing the value for synthetic graphite (3.38 Å), while raw coal typically exhibits a 2θ around 24º.	[75]
7.	Coal (Dera Underground Mines, Talcher, Angul, Odisha, India)	Modified Hummers' method	Mineralized coal showcases a diffraction peak at roughly 2θ of 26.05°, corresponding to an interlayer spacing (d) of 3.423 Å with Miller indices (002), validating the presence of graphitic layers within the coal. Furthermore, the coal powder manifests two peaks at 41.51° and 55.97° attributed to the (101) and (004) diffraction planes of its graphitic layers. In contrast, GO exhibits a notable diffraction peak at approximately 2θ of 14.26° with an interplanar spacing of 6.2 Å assigned to the (001) diffraction plane. Moreover, a broad peak at about 42.25°, corresponding to the (100) plane, signifies the short-range order in the graphene nanolayers, confirming the successful GO	[76]

			synthesis from coal.	
8.	Low-quality subbituminous coals (Changki colliery, CC), Nagaland and Jadi colliery (Garo Hills, Meghalaya) located in the NER of India	Ultrasonic-assisted production of activated carbons	The XRD peak of raw coal CC and oxidized coal CC at 2θ = 26º can be interpreted with reference to the small-dimension crystallites which are perpendicular to aromatic layers whereas in case of other coal the oxidation results in peak shift to 2θ = 24.01º.	[77]
9.	Sub-bituminous coal (Indonesia)	Pyrolysis of coal followed by hydrothermal process and exfoliation	Coal XRD displays a peak at 21.40° indicating carbonyl groups (d = 7.336 Å) and peaks at 24.86° and 43.96° confirm graphene nanosheets (d = 2.583 Å) (right shift indicating reduction).	[78]
10.	Sub-bituminous coal (Uluiwoi, Kolaka Timur, South East Sulawesi, Indonesia)	Modified Hummers' method	XRD pattern of coal shows an amorphous pattern with a wide peak at 2θ position of 15 – 20°; after the coal was processed into GO, the XRD spectrum was changed with the emergence of new peaks at 2θ position of 12.2°.	[79]
11.	Sub-bituminous powder river basin coal from Wyoming	Multistep coal fractionation followed by Chemical Vapor Deposition (CVD)	11-layered defect-free graphene on Ni and graphite with high defects on Cu was obtained.	[80]
12.	Australian bituminous coal	Catalytic process (Fe) under microwave heat treatment	In Raman mapping, the sample loaded with the catalyst exhibited a uniform distribution, indicating the presence of a few-layer graphene (FLG). AFM measured the FLG thickness around 4.5 nm	[81]
13.	Sub-bituminous coal	CVD on copper (Cu) substrates	Raman spectra of graphene films reveal the 1350 cm^{-1} (D band), at 1575 cm^{-1} (G band), and at 2700 cm^{-1} (2D band). TEM shows the edge of the	[82]

			graphene film revealing the bi-layers of the coal-derived graphene films.	
14.	Coal	Modified Hummers' method	Presence of edge oxygen functionalities in coal-derived graphene sheets induces fluorescent properties. XRD, FESEM, and HRTEM findings suggest the creation of micro-sized 2D sheets comprising a few layers of sp^2-bonded carbons.	[83]
15.	Sub-bituminous Wyodak coal	CVD on Cu substrates	The graphene films over a large area displayed uniformity and continuity, as evident from the AFM and TEM images.	[84]
16.	Powder River Basin coal	HNO_3 method along with disparities of Hummers' method	In graphene nanomaterials derived from coal, an additional Raman feature, D″, associated with the amorphous phase is identified. Annealing (1000°C) significantly diminishes the oxygen in graphene oxide derivative from coal, with the restoration of the graphitic d-spacing occurring at 1500 °C.	[85]
17.	Dried electrolyzed coal char	CVD	Raman spectrum of the synthesized films shows the 2D band feature of graphene. TEM images and SAED pattern show morphology and typical hexagonal crystalline structure of graphene films.	[86]
18.	Sub-bituminous coal	Oxidation of coal with mineral acid	Within the coal structure, the crystalline carbon is more readily displaced by mineral acid oxidation, leading to the formation of nm-sized graphitic sheets. Raman analysis indicates the formation of finite-sized, less defective, few-layer graphene through the chemical leaching of coal.	[87]
19.	Coal marcels	Improved Hummers' method followed by	XRD data demonstrates that at high-temperature graphitization, the layer spacing d002 for each sample is reduced to less than 0.3400 nm.	[88]

		chemical reduction through $N_2H_4.H_2O$	Additionally, the lamellar crystallite sizes L_a and L_c range from 7.70 to 21.09 nm and 11.53 to 16.94 nm, respectively, in coal-based graphene. SEM and TEM data indicate that inertinite tends to adopt a flat graphene structure with four to six layers, displaying favorable light transmission properties.	
20.	Sub-bituminous coal, Shaanxi Province (China)	High temperature graphitization followed by modified Hummers' method	Prepared a composite of GO and rGO with TiO_2, therefore, weak characteristic peaks of the functional groups related to GO and rGO were observed due to low graphene content. Furthermore, in XRD, the diffraction peaks of isolated GO or rGO were not observed, likely attributed to the limited quantity of GO or rGO in the composites.	[89]
21.	Semi-anthracite coal region in Northeast Pennsylvania, USA	Facile one-pot method using a single oxidant, HNO_3 followed by thermal reduction	The surface features of Coal-GO reveal presence of nitrogen, both originating from the raw coal and introduced during the process. Coal-rGO featured multilayer graphene nanosheets with lateral sizes ranging from 300 to 700 nm (TEM and AFM). In Coal-GO, the predominant evolution of carboxylic groups occurs at edges of the graphene.	[90][91]

From table 1.2, it can be inferred that references, [69], [71], [73], [74], [75], [76], [79], [83], [85], [88], [89] follows the conventional approach, i.e., Hummers' method, modified Hummers' method, improved Hummers' method. Das et al. [71] employed demineralization using H_2SO_4 (concentrated) in the $NaNO_2$ presence followed by HNO_3 addition in an ultrasonication system at 80 °C to obtain GO. Kumar et al. [73] used an improved modified Hummers' method with few modifications in which bituminous coal powder was combined with $NaNO_3$ and H_2SO_4 and stirred

at 80°C for 24 hrs. Further cooling to room temperature, solution was diluted with 1M HNO_3, leading to the precipitation of GO at 7200 rpm centrifugation for 10 min. Resulting powder was washed and this solution was applied to quartz surfaces using piranha, followed by thermal treatment under argon flow at 900 °C for 5 hours to produce graphene. These procedures involve many steps and generate harmful NO_x (nitrogen oxides), SO_x (sulfur oxides), as well as some carcinogens, during the oxidation process. Moreover, substantial amounts of untreated water constituting heavy metals and residual acids metals pose challenges for chemical waste discarding [92]. Also, the bottom-up approaches like CVD are highly expensive and unsuitable for large-scale production [93]. Leandro et al. [85] used the HNO_3 method with few changes to Hummers' approach. In their method, coal powder sample was combined with 70% concentrated HNO_3 as an oxidizing agent (replaced with harsh oxidants) which was diluted using distilled water (3:1 volume ratio). At 70 °C, after an ultrasonic bath, sample was further diluted with water to 1:10 ratio. The solution underwent filtration till the achievement of pH level of about 6.5, followed by freeze-drying to obtain GO. Moreover, to showcase the utility of HNO_3-derived GO, GO was subjected to high-temperature thermal reduction. Annealing at 1000 °C significantly decreases the content of oxygen in GO obtained from coal, leading to the restoration of graphitic interlayer spacing at 1500 °C. Further annealing at temperatures till 2500 °C transforms the morphology from large aggregates to micron-sized layered structures. Also, HNO_3 reduced GO showed the substantial number of defects.

Several researchers have documented the extraction and separation of carbon nanomaterials, such as graphene oxide, carbon dots, few-layered graphene, etc., from coal possessing crystalline domains. This process involves severe oxidation-exfoliation method employing a mixture of concentrated acids and oxidants. Traditionally, HNO_3 has served as a widely used oxidizing agent, typically employed alongside other oxidative reagents like H_2SO_4, H_2O_2, and HF. This is followed

by a sonication-mediated approach aimed at eliminating metal impurities or amorphous carbons from highly stacked graphitic carbons, inclusive of CNT (carbon nanotubes).

In any attempt to convert coal into graphene, it is essential to safeguard the graphitic domains while addressing the transformation of aliphatic hydrocarbons present in coal. Mahajan and Lee [90] devised a cost-effective method for producing graphene from semi-anthracite coal while preserving these graphitic domains. A schematic illustration is given in figure 1.3. According to the authors, their innovative process, utilizing coal as the precursor, boasts an order of magnitude lower cost compared to the modified Hummers' method, which employs graphite as the precursor. The cost-effectiveness is attributed to the relatively lower consumption of chemicals, with only 16 M HNO_3 utilized.

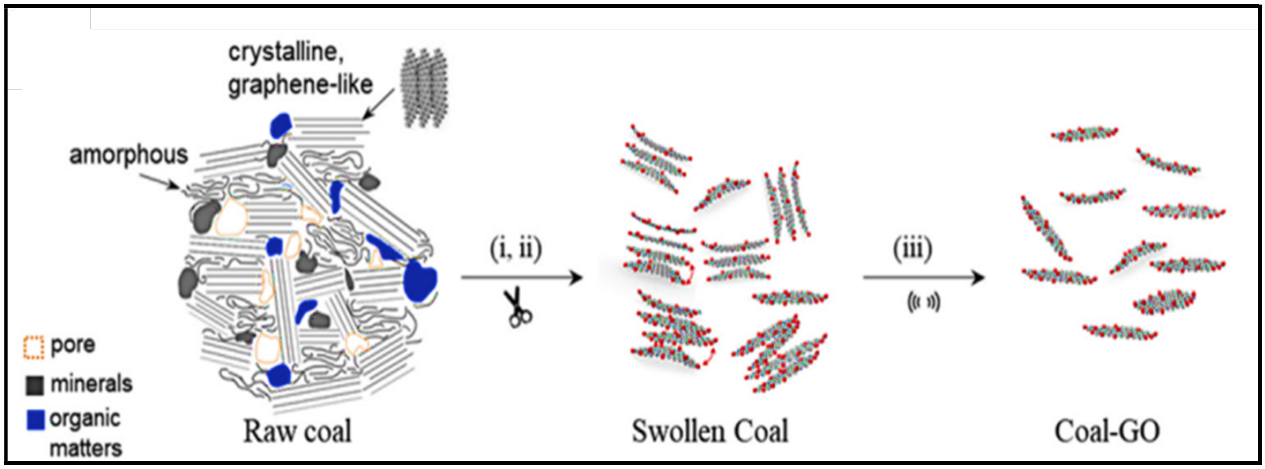

Figure 1.3. Schematic representation of one-pot process for Coal-GO synthesis (where, i, ii- coal purification followed by oxidative scissoring and iii- exfoliation) [91]

The unique coal structure facilitates a mild HNO_3 oxidation process to produce GO. Characterization through TEM and AFM reveals few-layered graphene nanosheets in Coal-rGO and Coal-GO with lateral sizes, 300-700 nm. While Coal-rGO shares morphological similarities with graphite-procured graphene, it differs in surface and structural features. In Coal-GO, carboxylic functionalities mainly emerge at the edges of graphene, minimizing the impact on *c*-

direction during HNO_3 oxidation. The basal plane damage to is negligible, preserving the graphene clusters in coal. Conventional thermal reduction converts Coal-GO to Coal-rGO, and the physicochemical properties are significantly influenced by the initial graphitic material. The general schematic representation of both modified Hummers' method and newly developed one-pot method is illustrated in figure 1.4.

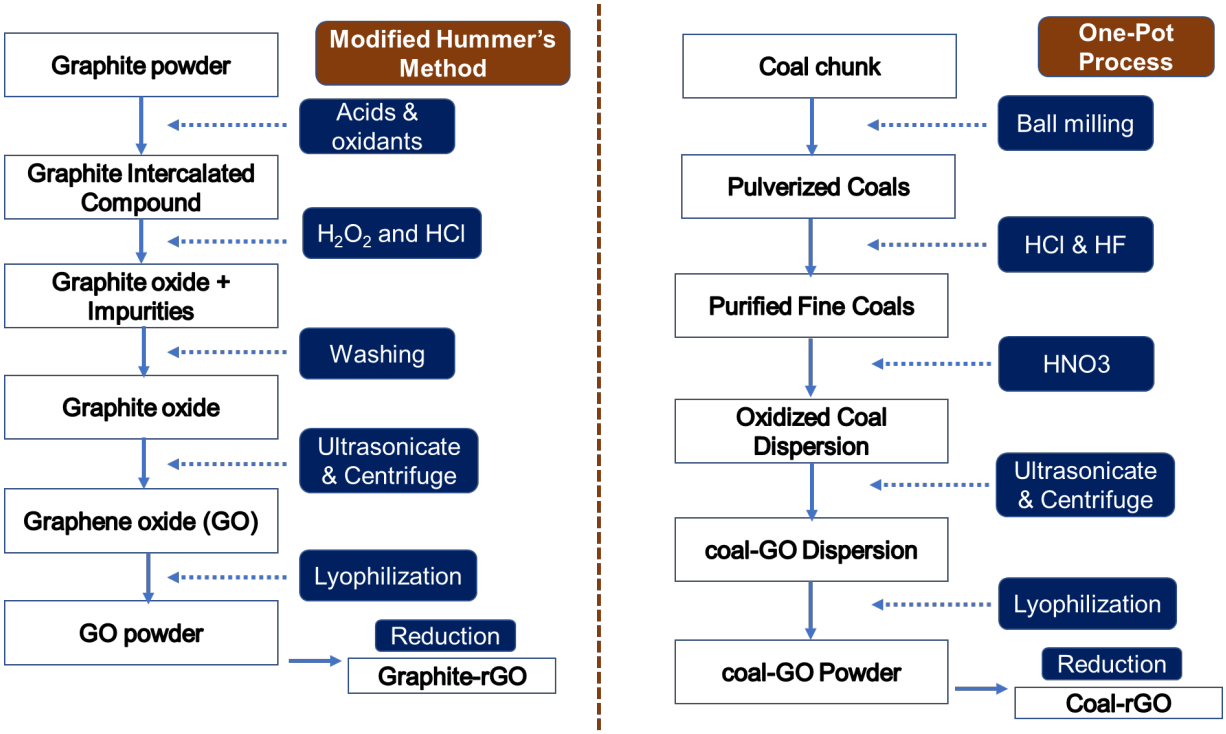

Figure 1.4. Schematic representation of conventionally used modified Hummers' method and the recent one-pot process for GO synthesis

The graphite received from the market is already purified via strong chemical washings, whereas the coal we purchase needs to be purified first, setting up a comparison between the two purified forms. The category of graphene derivatives has experienced rapid expansion, particularly in the past decade. The large-scale production via a facile and efficient approach is the ultimate need of the hour. With the suitable approach (cost-effectiveness at a large scale, lesser utilization of toxic chemicals leading to reduced gaseous emissions, reduced chemical waste disposal problems), one

can explore the full potential of graphene in polymer composites, sensing fields, optoelectronics, wastewater treatment plants, drug delivery operations, and various other fields [16].

1.4. Graphene oxide as reinforcing nanofiller in EGFPs for enhanced mechanical properties

Composite materials blend the properties of two or more materials, resulting in characteristics that cannot be achieved by either the fiber or matrix individually [94]. They exhibit anisotropic characteristics with distinct boundaries between the combined components, resulting in a unique set of properties and a superior strength-to-weight ratio. Glass fiber-reinforced polymeric (GFRP) composites, a widely utilized variant, have been effectively applied in engineering applications for several decades [95]. The matrix in GFRP composites consists of organic resins like polyester, thermostable resins such as vinyl ester and phenolic, and epoxy resins. Different types of glass fiber reinforcements, including long longitudinal, woven mat, chopped fiber (distinct), and chopped mat, have been incorporated into the composites to improve their mechanical and tribological properties. The mechanical behavior of fiber-reinforced composites relies on factors such as fiber strength and modulus, chemical stability, matrix strength, and the interface bonding between the fiber and matrix for effective stress transfer [96]. In general, the behavior of GFRPs is primarily influenced by the properties of glass fibers, the mechanical properties of the polymer matrix, and the interfacial adhesion between glass fibers and the polymer matrix.

Thermoset materials are typically in a liquid or malleable state before curing and cannot be reheated once they have hardened. Epoxy stands out as the most utilized thermosetting matrix in fiber-reinforced polymer nanocomposites due to its low density, high chemical stability, excellent bonding ability, and favorable mechanical properties [97]. Glass fiber-reinforced epoxy composites are known for their strong static mechanical properties, although they may lack in impact strength. The curing process involves the cross-linking of epoxy resins with a hardener through a polymerization reaction. The resulting cured resins exhibit superior characteristics,

including high strength, stiffness, and an elevated glass transition temperature [98]. Nevertheless, certain drawbacks highlight notably unsatisfactory properties, with a higher cross-link density leading to reduced fracture toughness, limiting their applicability. Several researchers have observed that the elevated cross-link density in pristine epoxies diminishes their fracture toughness due to internal stresses induced during the curing process. In high cross-link density epoxies, resistance to crack initiation is minimal, and void growth resulting from plastic deformation is constrained [99].

Addressing these drawbacks involves modifying epoxy resins by incorporating various nanofillers as a second microphase for advanced composite applications. The incorporation of nanofillers into epoxy resins represents a strategy to enhance the fracture toughness of thermosetting polymers. Figure 1.5 represents the structural aspects of potential nanofillers extensively used in GFRPs solely or in combination.

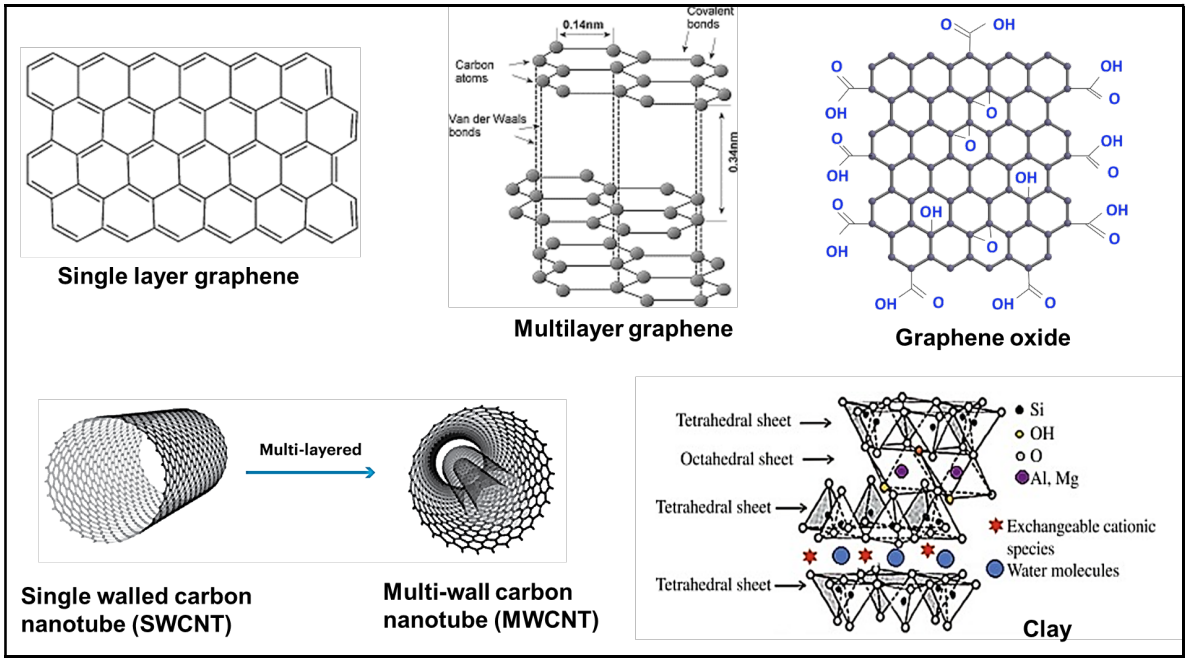

Figure 1.5. Different types of nanofillers used in GFRPs

While epoxy resins offer benefits such as good stiffness, specific strength, and low cure shrinkage, the addition of fillers allows for further enhancement and tailoring of epoxy performance for specific applications. The emergence of nanocomposites has garnered significant interest among researchers, with studies indicating that the mechanical properties and toughness of materials can be significantly improved through the use of promising fillers [100].

To attain optimal performance in nanocomposites, it is essential to ensure the proper dispersion of nanofillers within the resin [100]. Numerous researchers have investigated the dispersion of various nanomaterials into epoxy matrices [101]. Achieving homogeneous dispersions is crucial for adequate reinforcement, leading to a significant enhancement in nanocomposite performance through effective load transfer to the nanomaterials. Additionally, a higher aspect ratio, alignment, and stress transfer contribute to the improved performance of the polymer [102]. There are two primary methods for dispersing nanomaterials in the resin: mechanical and surface functionalization methods [103]. Techniques such as solution mixing, ultra-sonication, calendaring (three roll mills), and ball milling are commonly used for dispersion, depending on the type of nanomaterial. Solution mixing, which involves processing nanofiller/polymer by mixing with an appropriate solvent, is the most prevalent method. Additionally, ultra-sonication employs ultrasound energy to agitate nanomaterial particles, achieved using an ultrasonic probe [104][105].

Among the several nanomaterials, GO recognized for its single-layered atom-thick flatbed structure decorated with oxygen-based functional groups, has introduced a new dimension to the nanotechnology realm. GO comprises a layered carbon structure with oxygen-containing functional groups (=O, -OH, -O-, -COOH) attached to both sides of the layer and the edges of the plane [106]. GO is hydrophilic, making it relatively easy to prepare water- or organic solvent-based suspensions. Highly oxidized forms of GO act as electric insulators, with a bandgap of approximately 2.2 eV [107]. Prusty et al. [108] observed a notable improvement in both room temperature and sub-zero (-80 °C) flexural properties when GO was introduced into the epoxy

matrix. The enhanced properties were attributed to the effective bonding established between the epoxy matrix and GO. Wang et al. [109] explored the impact of incorporating chemically functionalized GO sheets of three different sizes (GO-1, GO-2, and GO-3) on the mechanical and thermal properties of GO/epoxy nanocomposites. The study demonstrated that the fracture toughness of GO/epoxy nanocomposites is influenced by the size and content of GO sheets. Notably, the addition of smaller-sized GO sheets (GO-3) outperformed the reinforcement with larger-sized GO sheets (GO-1 and GO-2) in the epoxy matrix. The incorporation of smaller GO sheets exhibited improved resistance to crack propagation, enhanced interfacial adhesion, and reduced stress concentration, as evidenced by fractographic examinations, resulting in increased toughness of GO/epoxy composites. Pathak and colleagues investigated the improved interfacial properties of a carbon fiber-reinforced epoxy nanocomposite incorporating graphene oxide [110]. The advantageous structure and characteristics of graphene derivatives are closely tied to factors such as size, shape, and functional moieties attached to the material's surface. Figure 1.6 represents the tensile behavior GO incorporated polymeric composites reported in literature spotting the potential of GO for GFRPs in enhancing the mechanical behaviour.

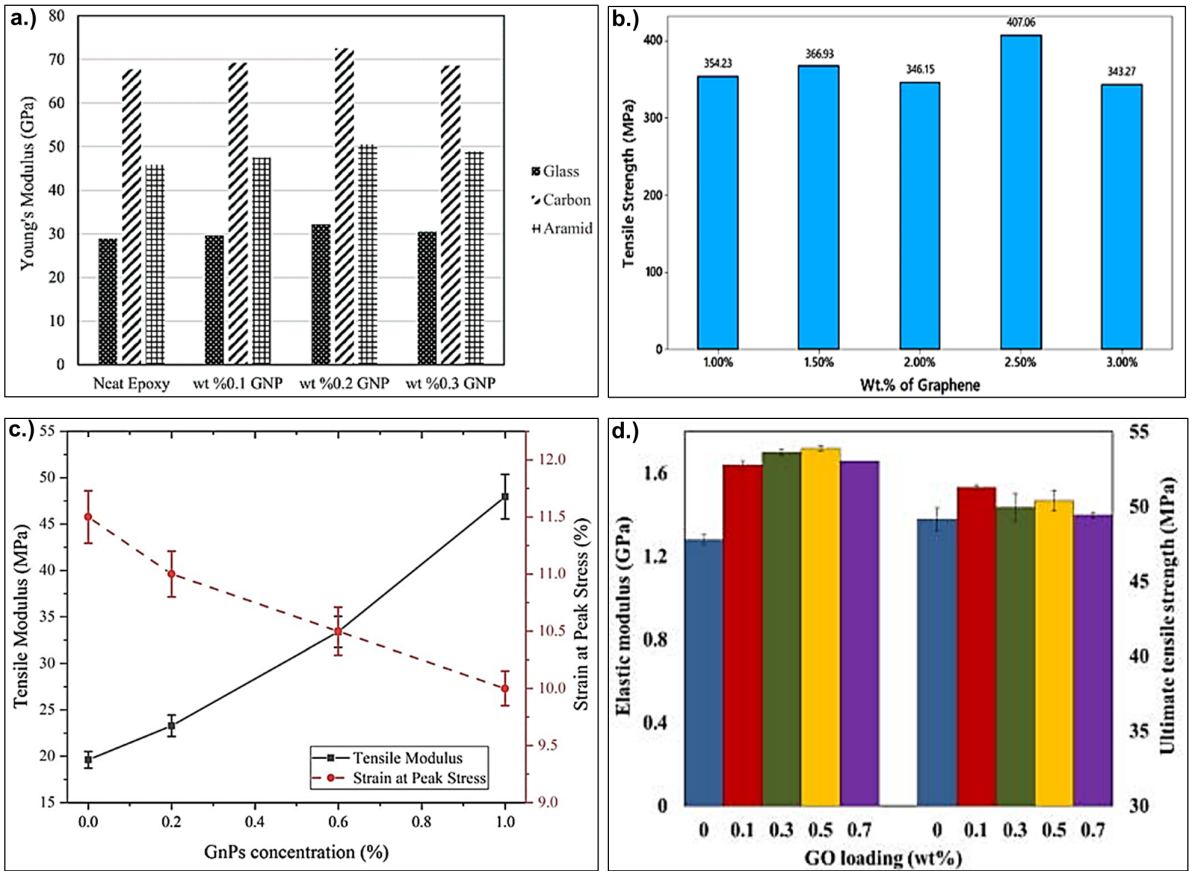

Figure 1.6. a.) Young's modulus changes with GNP content [111] **b.)** Tensile Strength vs wt. % of graphene in glass fiber and epoxy composites [112] **c.)** Tensile modulus and strain at peak stress plot as a function of GNPs concentration [113] **d.)** Elastic modulus and tensile strength of GO and epoxy nanocomposites [114]

Table 1.3. Literature review on Glass fiber reinforced polymer-based composites utilizing GO as the potential nanofiller

S.No.	Materials used	Key results	References
1.	Matrix: Epoxy Nano-reinforcement: Graphene oxide Fiber-reinforcement: Carbon fiber (T-300)	Examined the impact of GO inclusion on the thermal properties of CFRP hybrid composite. Various techniques including DMA, DSC, TGA, and TMA revealed that in GO-epoxy resin composites, both storage and loss moduli peaked at 0.3 wt% of GO. The glass transition temperature (Tg) determined from DMA and TMA analyses of	[110]

		GO-incorporated CFRP hybrid composites showed an increase in Tg by 4°C and 12°C, respectively, compared to CFRP composites without GO at the same loading level. This enhancement at the specified GO loading is attributed to the constraining effect of GO sheets on the mobility of polymer chains within the composite.	
2.	Matrix: Epoxy Nano-reinforcement: Graphene Fiber-reinforcement: Multi-walled Carbon Nanotube (MWNT) coated E-glass fiber	Explored the flexural properties of multiscale nanocomposites comprising glass fabric coated with multi-walled carbon nanotubes in an epoxy/graphene matrix. Noted that adding 0.1 wt.% of graphene to an epoxy matrix resulted in the highest increase in flexural properties compared to the pure epoxy. Furthermore, glass fabric was treated with polyvinylpyrrolidone (PVP) modified MWCNT, leading to enhanced flexural strength in its multiscale nanocomposites. Dynamic mechanical analysis (DMA) showed the mobility of epoxy chains in contact with PVP-coated MWCNT.	[115]
3.	Matrix: Epoxy Nano-reinforcement: Graphene oxide Fiber-reinforcement: T-300 Carbon fiber	Investigated the improved mechanical properties of carbon fiber/graphene oxide-epoxy hybrid composites. FTIR, XPS, NMR, XRD, and Raman spectroscopy confirmed the possession of different functional groups in synthesized GO responsible for interacting with epoxy resin and carbon fibers. The hybrid composite exhibits a 66% increase in flexural strength and a 72% increase in flexural modulus, along with a 25% increase in interlaminar shear strength when incorporating 0.3 weight% of graphene oxide into the carbon fiber reinforced polymer hybrid composites. This enhancement in composite properties at the percolation threshold of graphene oxide is attributed to hydrogen bonding and mechanical interlocking between GO, carbon fibers, and epoxy resin.	[116]
4.	Matrix: Epoxy Nano-reinforcement: Functionalized GO Fiber-reinforcement: Carbon fiber	Developed and analyzed nanocomposites comprising functionalized GO, carbon fiber, and epoxy. SEM analysis illustrated that the enhanced mechanical performance of the epoxy was attributed to the mechanism of carbon fibers being pulled out from the epoxy matrix.	[117]

		The findings demonstrate that diamine-functionalized GO can improve the interfacial bonding between the carbon fibers and the epoxy adhesive. Addition of functionalized graphene oxide (FGO) effectively enhances both tensile and flexural strengths, with the degree of enhancement depending on the type and percentage of GO functionalization. Furthermore, the inclusion of FGO in epoxy resin also increases both tensile and flexural moduli owing to the impressive elastic modulus of FGO.	
5.	Matrix: Epoxy Reinforcement: Graphene oxide	Examined the production of GO/epoxy nanocomposites with the goal of improving mechanical properties. Incorporating 0.1 wt.% of GO led to a roughly 50% boost in fracture toughness compared to neat epoxy. Furthermore, at a 0.5 wt% GO loading, the elastic modulus demonstrated an approximately 35% enhancement over neat epoxy. These improvements can be attributed to the outstanding properties of GO, such as its high specific surface area, enhanced interaction/adhesion due to oxygen functional groups, and its wrinkled, rough surface, along with its two-dimensional planar geometry.	[114]
6.	Matrix: Polyvinyl chloride (PVC) Reinforcement: Graphene oxide	Investigated the homogeneous dispersion of PVC with GO, and it was achieved by ultrasonic treatment. SEM analysis reveals that the majority of GO has been uniformly dispersed throughout the polymer matrix. FTIR spectra of PVC/GO composite films display C-H stretching vibrations of PVC. Also, the peak of the OH-stretching vibration in GO broadens at higher loading of GO (1.5 wt%) in composite material. Optical microscopic images revealed that even at very low concentrations (0.5 wt%), GO had been dispersed homogeneously throughout the PVC matrix (higher concentration, agglomeration). AFM images reveal that GO as the filler has a significant influence on the surface morphology of composite films. FTIR spectroscopy revealed structural changes with respect to different wt% of GO	[118]

		loading.	
7.	Matrix: Epoxy Reinforcement: Graphene oxide	Investigated graphene-epoxy system by amino-functionalization of graphene oxide (fGO). SEM images of the epoxy fGO composite's fractured surface drastically increase upon adding the fGO sheet to the matrix compared to the neat resin (due to fine dispersion of graphene sheets throughout matrix). AFM studies revealed the fracture surface of neat resin appears to be very smooth. Flexural modulus of epoxy increased monotonically by adding fGO and increased from 2800±25MPa (neat resin) to 3670±60MPa for composites containing 0.4 vol% fGO.	[119]
8.	Matrix: Epoxy Reinforcement: Graphene oxide	Significant enhancements in thermal conductivity (approximately 36%), tensile strength, and storage modulus (exceeding 13%) were observed upon incorporating 2 wt% of rGO.	[120]
9.	Matrix: Epoxy Reinforcement: Graphene nanosheets	Mechanical testing results indicated a peak in tensile and flexural strength for samples containing 0.1 wt.% graphene. Tensile strength experienced a 13% improvement, while flexural strength increased by 3.3%. Microscopic observations revealed that the primary toughening mechanism in graphene-epoxy nanocomposites was the deflection of crack paths.	[121]
10.	Matrix: PMMA Reinforcement: Graphene and CNTs separately	Results show an 18% increment in Young's modulus, 8.7% higher in tensile strength, and 5% higher in surface crack energy obtained for the composites by incorporation of graphene sheet than those by incorporation of CNT.	[122]
11.	Matrix: Epoxy Nano-reinforcement: Graphene nanoplatelets Fiber-reinforcement: E-glass fiber	The composite's flexural strength saw a 20% increase until 5% wt. GNPs and ultimate tensile strength (UTS) by 7%.	[123]
12.	Matrix: Epoxy Nano-reinforcement: Graphene	The maximum UTS increase can be observed for the maximum sonication time and GNPs content tested, i.e. 60 min. sonication and 5% wt. GNPs.	[124]

	nanoplatelets Fiber-reinforcement: E-glass fiber		
13.	Matrix: Epoxy Nano-reinforcement: Graphene oxide	Incorporating 1.5 vol.% GO into the epoxy matrix led to enhancements in the tensile strength, hardness, and Young's modulus of the composite compared to the pure epoxy matrix. SEM shows that adding more GO roughens the fracture surface. The cracks become more randomly dispersed, indicating that the GO network acts as an obstacle to crack propagation.	[125]
14.	Matrix: Epoxy Nano-reinforcement: Graphene aerogels	A remarkable 64% enhancement in composite's fracture toughness in comparison to neat epoxy was achieved at 1.4 wt.% graphene content.	[126]
15.	Matrix: Epoxy Nano-reinforcement: Expanded graphene nanoplatelets (EGNP)	The fracture toughness elevated by 66% over epoxy with 0.1 wt.% EGNP whereas the flexural modulus exhibited a steady rise with the addition of EGNPs from 0.1 to 2.0 wt.% Nanoindentation studies the hardness and modulus of the nanocomposites exhibiting a steady increase with the addition of EGNPs up to 1.5 wt.%.	[127]
16.	Matrix: Epoxy Nano-reinforcement: Graphene oxide	Mechanically gripped interface at -80°C promotes effective stress transfer resulting in a superior flexural strength of nanocomposite, which is 82% higher than neat epoxy.	[108]
17.	Matrix: Epoxy Nano-reinforcement: Graphene Fiber-reinforcement: E-glass fiber	The Laminate of 2.5 wt.% of graphene was found to exhibit superior properties in contrast to the other laminates of different weight percentages.	[112]
18.	Matrix: Epoxy Nano-reinforcement: GNPs Fiber-reinforcement: E-glass fiber	The impact resistance increased by 45%, and tensile strength improved by 114% compared to the pristine composite.	[113]

Table 1.3 denotes the remarkable potential of graphene derivatives in E-glass fiber-based epoxy composites for improved mechanical properties. These graphene-reinforced GFRP composites can effectively be utilized in the manufacture of aircraft bodies, ballistic missiles, sporting equipment, marine applications, and extraterrestrial ventures.

1.5. Other nanofillers- Multiwall Carbon nanotubes (MWCNT) and Halloysite nanotubes (HNTs) as reinforcing nanofillers in EGFPs for enhanced mechanical behavior

Numerous researchers have focused on carbon nanotubes (CNTs) because of their larger aspect ratio and distinctive properties, including high strength, stiffness, thermal conductivity, and electrical conductivity. CNTs, one-dimensional cylindrical structures with more than one graphitic layer and an inner diameter of approximately 4 nm, are available as SWCNTs (single-walled carbon nanotubes) and MWCNTs (multi-walled carbon nanotubes). These sp^2 hybridized materials, characterized by their curved rather than straight structure, possess high aspect ratios, contributing to superior mechanical and electrical properties [128]. MWCNTs consist of concentrically nested SWCNTs and demonstrate increased stiffness in compression compared to SWCNTs. Li et al. [129] studied the mechanical properties of epoxy composites reinforced with SWCNTs at varying content (0 wt% to 5 wt%). The results showed a 75% increase in elastic modulus and a 30% increase in hardness with 5 wt% SWCNTs. However, higher nanofiller contents (3 and 5 wt%) caused SWCNT agglomeration, leading to break-offs, pull-outs, and surface protrusions in the SWCNTs/epoxy composites. Martone et al. [130] examined the mechanical reinforcement efficiency, represented by the composite modulus, of MWCNTs in an epoxy matrix. The MWCNTs demonstrated the highest reinforcement efficiency of 1.780 TPa at an extremely low loading of 0.05 wt% (referred to as the percolation threshold limit). Beyond this limit, the reinforcement efficiency decreased significantly due to a reduction in the effective aspect ratio and the formation of micron-sized clusters of CNTs. Similarly, Singh et al. [131] explored the tensile and compressive properties of MWCNTs/epoxy composites.

Similarly, HNTs are unique one-dimensional natural nanomaterials characterized by predominantly hollow tubular nanostructures and high aspect ratios. With notable attributes such as high mechanical strength, thermal stability, biocompatibility, and abundance, HNTs hold great promise for various applications in polymer nanocomposites and even as a replacement for costly nanofillers like MWCNT. HNTs exhibit a high aspect ratio, typically around 10–50. This characteristic aids in reinforcing polymers within composites by facilitating optimal load transfer from the matrix to the nanotubes. Additionally, the elastic modulus of HNTs is 140 GPa, compared to the theoretical range of 230–340 GPa. In a 5 wt.% aqueous solution, the mean particle size of HNTs is 143 nm, with sizes ranging from 50 to 400 nm [132]. Structurally, Halloysite ($Al_2Si_2O_5(OH)_4.2H_20$) is chemically related to kaolin. HNTs contain two types of hydroxyl groups, inner and outer hydroxyl groups, which are situated between layers and on the surface of the nanotubes, respectively. The surface of HNTs is mainly composed of O Si O groups and the siloxane surface. These functionalities account for better bonding with the polymer matrix and ultimately owing to better dispersion than other nanoclays like MMT, kaolinite and even MWCNT. As per the findings of Tang et al. [133], HNTs were identified as effective additives for enhancing the fracture toughness of cured epoxies without compromising other crucial physical properties. Ye et al. [134] conducted a study on HNT as a reinforcing nanofiller to enhance the impact strength of the epoxy matrix. In all specimens, the load increased linearly with displacement until reaching the maximum load, initiating crack formation. Subsequently, there was a gradual decrease in crack propagation. In a study by M. Rajaei et al. [135], the impact of two nanoclays, HNT and layered double hydroxide (LDH), on the fire and mechanical properties of an epoxy composite with ammonium polyphosphate was compared. The findings indicated that HNT remarkably decreased the heat release of the epoxy resin by 87%. Additionally, HNT demonstrated superior tensile properties and proved to be a more cost-effective choice compared to LDH. Ramamoorthi et al. [136] incorporated HNT into epoxy glass fiber composites and

investigated the impact of varying HNT concentrations (1-10 wt%) on mechanical performance. The tensile strength and modulus exhibited a rapid increase up to 4 wt% HNT, reaching 33.71% and 31.01% higher than the neat epoxy/glass fiber composite, but decreased thereafter up to 10 wt%. Lapcik et al. [137] investigated the ductility and plasticity of HNTs/epoxy composites and graphene/epoxy composites separately. The graphene-based nanocomposite samples exhibited enhanced ductility, with an increase in elongation at break from 0.33 mm (neat matrix) to 0.46 mm (1 wt% graphene), representing a 39% increase. Existing literature suggests the potential improvement in mechanical properties with the addition of HNTs as nanofillers in GFRP composites. Also, Prasanthi et al. [138] identified carbon fiber-reinforced epoxy composites by incorporating carbon-based nano-reinforcements, including CNTs and GNPs, into the epoxy matrix. They compared the tensile modulus, tensile strength, flexural modulus, and flexural strength of the prepared composites. Carbon/carbon GNPs exhibited a 95.93% enhancement in tensile strength, and a 23.83% improvement was observed in carbon fiber/CNTs mixed epoxy compared to pure carbon/epoxy composites. Figure 1.7 shows the obtained mechanical properties along with the % improvement by utilizing CNTs and GNPs in carbon/epoxy composites.

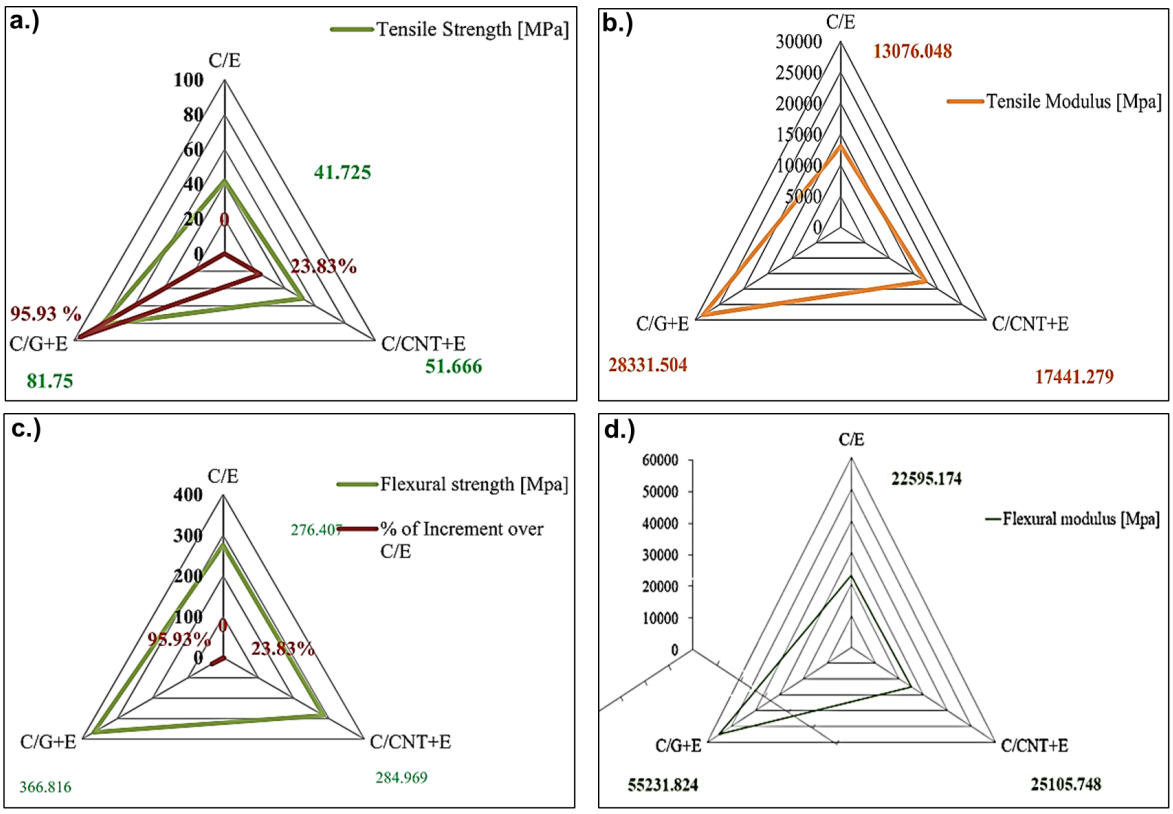

Figure 1.7. a, b.) Tensile strength and tensile modulus c, d.) Flexural strength and flexural modulus of carbon fiber reinforced CNT or Graphene-based polymer composites [134]

E-Glass fiber-reinforced nanocomposites (EGFPs) are widely employed for their cost-effectiveness and lightweight properties. They exhibit unique characteristics, including an excellent strength-to-weight ratio, high tensile and flexural properties (strength and modulus), robust interfacial shear strength, and resistance to chemical and environmental degradation. These materials find extensive applications in industries such as aviation, automotive, marine, and the military [139]. Their use contributes to reduced overall weight, enhanced fuel efficiency, and decreased emissions [140][141][142]. The major applications of EGFPs are shown in figure 1.8.

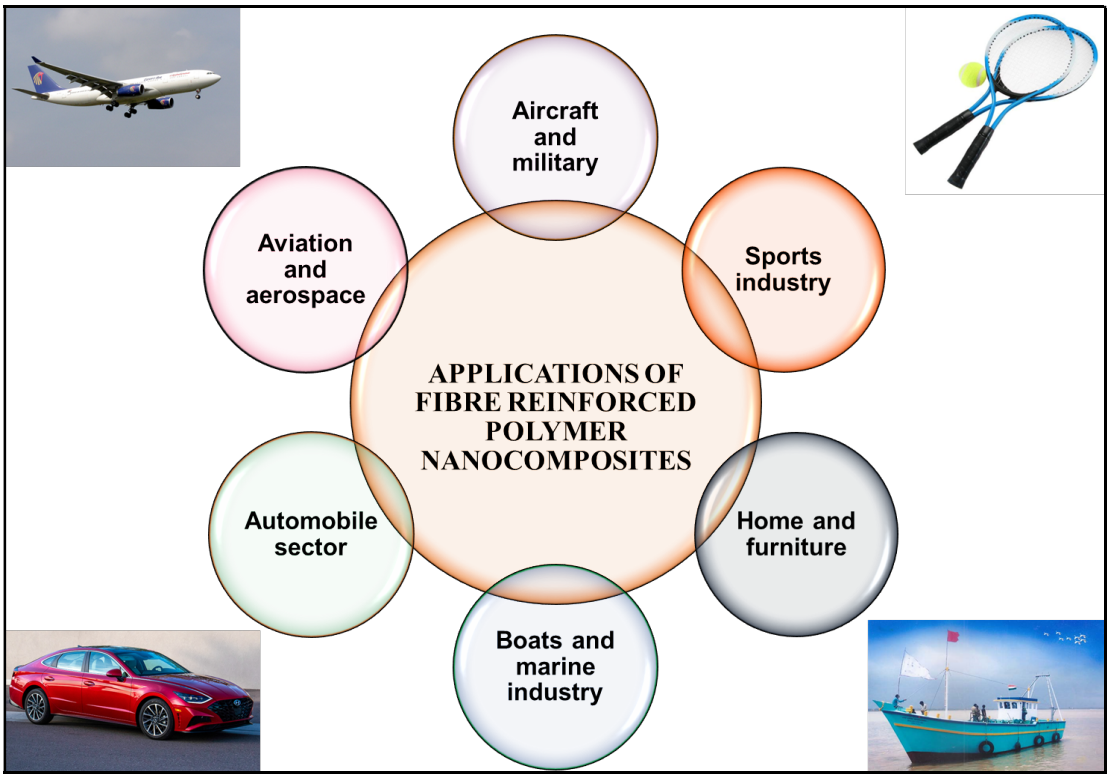

Figure 1.8. Applications of fiber-reinforced polymer composites in different sectors

Conclusion

In light of the above literature review, the proposal was made to enhance the mechanical properties of epoxy-based EGFP nanocomposites by introducing different carbon-based nanofillers such as graphene oxide, multilayer graphene, MWCNT, and other nanofillers like HNTs and even their hybrid reinforcements. However, the key to improving the properties of multi-constituent reinforced epoxy nanocomposites is ensuring proper dispersion and good compatibility among the various constituents of the composite system. Also, synthesis of GO through abundantly available cost-effective precursors, like Coal through a recently developed one-pot method has been explored and comparative of each study with conventionally prepared GO through a modified Hummers' method from graphite has been done. The reproducible fabrication of epoxy-based GFRPs featuring a multi-hybrid nanofiller system proved challenging due to the resulting high viscosity of the system. However, despite these challenges, the present

research successfully processed EGFPs with markedly elevated mechanical properties. The established processing procedure in this study is anticipated to pave the way for innovative avenues in further research aimed at enhancing the mechanical properties of epoxy-based EGFP nanocomposites.

- In the next chapter, the feasibility of using a facile one-pot process with HNO_3 has been carried out to synthesize graphene oxide (GO) from bituminous coal (BC) as well as anthracite coal procured from coalfields in India. The synthesized graphene oxide from different precursors has been characterized using various techniques including SEM-EDX, FTIR, XRD, XPS, BET-BJH, LRS, TEM, SAED, AFM, and DLS. Also, the potential application of coal-derived GO has been shown by studying the mechanical properties of glass fiber-reinforced polymer nanocomposites with AC-GO as a nanofiller.

References

[1] K.E. Whitener Jr, P.E. Sheehan, Graphene synthesis, Diam. Relat. Mater. 46 (2014) 25–34.

[2] M. Xu, T. Liang, M. Shi, H. Chen, Graphene-like two-dimensional materials, Chem. Rev. 113 (2013) 3766–3798.

[3] V. Georgakilas, J.A. Perman, J. Tucek, R. Zboril, Broad family of carbon nanoallotropes: classification, chemistry, and applications of fullerenes, carbon dots, nanotubes, graphene, nanodiamonds, and combined superstructures, Chem. Rev. 115 (2015) 4744–4822.

[4] M.J. Allen, V.C. Tung, R.B. Kaner, Honeycomb Carbon : A Review of Graphene, (2010) 132–145.

[5] R. Ye, J.M. Tour, Graphene at fifteen, ACS Nano. 13 (2019) 10872–10878.

[6] Z. Wei, Multiscale Modelling of Wettability of Graphene/Graphite, (2023).

[7] S. Chehreh Chelgani, M. Rudolph, R. Kratzsch, D. Sandmann, J. Gutzmer, A review of graphite beneficiation techniques, Miner. Process. Extr. Metall. Rev. 37 (2016) 58–68.

[8] R.K. Singh, R. Kumar, D.P. Singh, Graphene oxide: strategies for synthesis, reduction and frontier applications, Rsc Adv. 6 (2016) 64993–65011.

[9] S. Navalon, A. Dhakshinamoorthy, M. Alvaro, M. Antonietti, H. García, Active sites on graphene-based materials as metal-free catalysts, Chem. Soc. Rev. 46 (2017) 4501–4529.

[10] C. Kumunda, A.S. Adekunle, B.B. Mamba, N.W. Hlongwa, T.T.I. Nkambule, Electrochemical detection of environmental pollutants based on graphene derivatives: A review, Front. Mater. 7 (2021) 616787.

[11] C. Soldano, A. Mahmood, E. Dujardin, Production, properties and potential of graphene, Carbon N. Y. 48 (2010) 2127–2150.

[12] H. Huang, H. Shi, P. Das, J. Qin, Y. Li, X. Wang, F. Su, P. Wen, S. Li, P. Lu, The chemistry and promising applications of graphene and porous graphene materials, Adv. Funct. Mater. 30 (2020) 1909035.

[13] A. Garg, S. Basu, N.P. Shetti, K.R. Reddy, 2D materials and its heterostructured photocatalysts: Synthesis, properties, functionalization and applications in environmental remediation, J. Environ. Chem. Eng. 9 (2021) 106408. https://doi.org/10.1016/j.jece.2021.106408.

[14] C. Lee, X. Wei, J.W. Kysar, J. Hone, Measurement of the elastic properties and intrinsic strength of monolayer graphene, Science (80-.). 321 (2008) 385–388.

[15] G. Yang, L. Li, W.B. Lee, M.C. Ng, Structure of graphene and its disorders: a review, Sci. Technol. Adv. Mater. 19 (2018) 613–648.

[16] J. Sturala, J. Luxa, M. Pumera, Z. Sofer, Chemistry of graphene derivatives: Synthesis, applications, and perspectives, Chem. Eur. J. 24 (2018) 5992–6006.

[17] A.K. Geim, Graphene prehistory, Phys. Scr. 2012 (2012) 14003.

[18] A.K. Geim, K.S. Novoselov, The rise of graphene, Nat. Mater. 6 (2007) 183–191.

[19] M. Batzill, The surface science of graphene: Metal interfaces, CVD synthesis, nanoribbons, chemical modifications, and defects, Surf. Sci. Rep. 67 (2012) 83–115.

[20] L. Liu, M. Qing, Y. Wang, S. Chen, Defects in graphene: generation, healing, and their effects on the properties of graphene: a review, J. Mater. Sci. Technol. 31 (2015) 599–

606.

[21] M. Acik, Y.J. Chabal, Nature of graphene edges: a review, Jpn. J. Appl. Phys. 50 (2011) 70101.

[22] A.T. Dideikin, A.Y. Vul', Graphene oxide and derivatives: the place in graphene family, Front. Phys. 6 (2019) 149.

[23] A. V Talyzin, G. Mercier, A. Klechikov, M. Hedenström, D. Johnels, D. Wei, D. Cotton, A. Opitz, E. Moons, Brodie vs Hummers graphite oxides for preparation of multi-layered materials, Carbon N. Y. 115 (2017) 430–440.

[24] H.L. Poh, F. Šaněk, A. Ambrosi, G. Zhao, Z. Sofer, M. Pumera, Graphenes prepared by Staudenmaier, Hofmann and Hummers methods with consequent thermal exfoliation exhibit very different electrochemical properties, Nanoscale. 4 (2012) 3515–3522.

[25] J. Chen, Y. Li, L. Huang, C. Li, G. Shi, High-yield preparation of graphene oxide from small graphite flakes via an improved Hummers method with a simple purification process, Carbon N. Y. 81 (2015) 826–834.

[26] F. Pendolino, N. Armata, Graphene oxide in environmental remediation process, Springer, 2017.

[27] M. Yi, Z. Shen, A review on mechanical exfoliation for the scalable production of graphene, J. Mater. Chem. A. 3 (2015) 11700–11715.

[28] Y. Zhu, D.K. James, J.M. Tour, New routes to graphene, graphene oxide and their related applications, Adv. Mater. 24 (2012) 4924–4955.

[29] M. Park, N. Kim, J. Lee, M. Gu, B.-S. Kim, Versatile graphene oxide nanosheets via covalent functionalization and their applications, Mater. Chem. Front. 5 (2021) 4424–4444.

[30] F.J. Sonia, M. Aslam, A. Mukhopadhyay, Understanding the processing-structure-performance relationship of graphene and its variants as anode material for Li-ion batteries: A critical review, Carbon N. Y. 156 (2020) 130–165.

[31] A. Ahmed, A. Singh, S.-J. Young, V. Gupta, M. Singh, S. Arya, Synthesis techniques and advances in sensing applications of reduced graphene oxide (rGO) composites: A

review, Compos. Part A Appl. Sci. Manuf. (2022) 107373.

[32] U. Gupta, D. Gautam, V. Jain, B. Mukherjee, Design and synthesis of two-dimensional materials and their heterostructures, in: 2D Nanoscale Heterostruct. Mater., Elsevier, 2020: pp. 13–54.

[33] R. Al-gaashani, A. Najjar, Y. Zakaria, S. Mansour, M.A. Atieh, XPS and structural studies of high quality graphene oxide and reduced graphene oxide prepared by di ff erent chemical oxidation methods, Ceram. Int. 45 (2019) 14439–14448. https://doi.org/10.1016/j.ceramint.2019.04.165.

[34] A.T. Habte, Synthesis and Characterization of Reduced Graphene Oxide (rGO) Started from Graphene Oxide (GO) Using the Tour Method with, 2019 (2019).

[35] J. Jia, C. Kan, X. Lin, X. Shen, J. Kim, Effects of processing and material parameters on synthesis of monolayer ultralarge graphene oxide sheets, Carbon N. Y. (2014) 1–11. https://doi.org/10.1016/j.carbon.2014.05.027.

[36] J. Chen, B. Yao, C. Li, G. Shi, An improved Hummers method for eco-friendly synthesis of graphene oxide, Carbon N. Y. 64 (2013) 225–229. https://doi.org/10.1016/j.carbon.2013.07.055.

[37] A.L. Higginbotham, D. V Kosynkin, A. Sinitskii, Z. Sun, J.M. Tour, Lower-Defect Graphene Oxide Nanotubes, 4 (2010) 2059–2069.

[38] S. Stankovich, D.A. Dikin, R.D. Piner, K.A. Kohlhaas, A. Kleinhammes, Y. Jia, Y. Wu, Synthesis of graphene-based nanosheets via chemical reduction of exfoliated graphite oxide, 45 (2007) 1558–1565. https://doi.org/10.1016/j.carbon.2007.02.034.

[39] E. Andrijanto, S. Shoelarta, G. Subiyanto, S. Rifki, Facile synthesis of graphene from graphite using ascorbic acid as reducing agent, in: AIP Conf. Proc., AIP Publishing, 2016.

[40] Z.-J. Fan, W. Kai, J. Yan, T. Wei, L.-J. Zhi, J. Feng, Y. Ren, L.-P. Song, F. Wei, Facile synthesis of graphene nanosheets via Fe reduction of exfoliated graphite oxide, ACS Nano. 5 (2011) 191–198.

[41] H.-B. Zhang, J.-W. Wang, Q. Yan, W.-G. Zheng, C. Chen, Z.-Z. Yu, Vacuum-assisted synthesis of graphene from thermal exfoliation and reduction of graphite oxide, J. Mater. Chem. 21 (2011) 5392–5397.

[42] W. Jansomboon, P. Brikshasri, S. Sarawutanukul, P. Prapainainar, Characterization of graphene synthesized by modified hummers and liquid-phase exfoliation method, Appl. Sci. Eng. Prog. 12 (2019) 14–19.

[43] A. Saini, A. Kumar, V.K. Anand, S.C. Sood, Synthesis of graphene oxide using modified Hummer's method and its reduction using hydrazine hydrate, Int. J. Eng. Trends Technol. 40 (2016) 67.

[44] N. Méndez-Lozano, F. Pérez-Reynoso, C. González-Gutiérrez, Eco-friendly approach for graphene oxide synthesis by Modified Hummers method, Materials (Basel). 15 (2022) 7228.

[45] N. Selvakumar, U. Pradhan, S.B. Krupanidhi, H.C. Barshilia, Structural and Optical Properties of Graphene Oxide Prepared by Modified Hummers' Method., Comput. Mater. Contin. 52 (2016).

[46] M. Kaur, H. Kaur, D. Kukkar, Synthesis and characterization of graphene oxide using modified Hummer's method, in: AIP Conf. Proc., AIP Publishing, 2018.

[47] N.I. Zaaba, K.L. Foo, U. Hashim, S.J. Tan, W. Liu, C.H. Voon, Synthesis of Graphene Oxide using Modified Hummers Method : Solvent Influence, Procedia Eng. 184 (2017) 469–477. https://doi.org/10.1016/j.proeng.2017.04.118.

[48] A.L. Higginbotham, D. V Kosynkin, A. Sinitskii, Z. Sun, J.M. Tour, Lower-defect graphene oxide nanoribbons from multiwalled carbon nanotubes, ACS Nano. 4 (2010) 2059–2069.

[49] R. Ikram, B.M. Jan, W. Ahmad, An overview of industrial scalable production of graphene oxide and analytical approaches for synthesis and characterization, J. Mater. Res. Technol. 9 (2020) 11587–11610.

[50] A.M. Dimiev, Mechanism of formation and chemical structure of graphene oxide, Graphene Oxide Fundam. Appl. (2016) 36–84.

[51] N.S. Suhaimin, M.F.R. Hanifah, M. Azhar, J. Jaafar, M. Aziz, A.F. Ismail, M.H.D. Othman, M.A. Rahman, F. Aziz, N. Yusof, The evolution of oxygen-functional groups of graphene oxide as a function of oxidation degree, Mater. Chem. Phys. 278 (2022) 125629.

[52] S.M. Mousavi, S.A. Hashemi, M.Y. Kalashgrani, A. Gholami, M. Binazadeh, W.-H.

Chiang, M.M. Rahman, Recent Advances in Energy storage with Graphene Oxide-for Supercapacitor Technology, Sustain. Energy Fuels. (2023).

[53] J. Asenbauer, T. Eisenmann, M. Kuenzel, A. Kazzazi, Z. Chen, D. Bresser, The success story of graphite as a lithium-ion anode material–fundamentals, remaining challenges, and recent developments including silicon (oxide) composites, Sustain. Energy Fuels. 4 (2020) 5387–5416.

[54] Z. Ren, S. Mukherjee, G. Singh, Graphene-based hybrid materials for advanced batteries, in: 2D Nanomater. Energy Appl., Elsevier, 2020: pp. 73–95.

[55] Y.S. Zhang, K. Schneider, H. Qiu, H.L. Zhu, A perspective of low carbon lithium-ion battery recycling technology, Carbon Capture Sci. Technol. 5 (2022) 100074.

[56] A.D. Jara, A. Betemariam, G. Woldetinsae, J.Y. Kim, Purification, application and current market trend of natural graphite: A review, Int. J. Min. Sci. Technol. 29 (2019) 671–689.

[57] S.E. Lowe, Y.L. Zhong, Challenges of Industrial-Scale Graphene Oxide Production, Graphene Oxide Fundam. Appl. (2016) 410–431.

[58] M. Du, P.A. Advincula, X. Ding, J.M. Tour, C. Xiang, Coal-Based Carbon Nanomaterials: En Route to Clean Coal Conversion toward Net Zero CO2, Adv. Mater. (2023) 2300129.

[59] B.J. Arnold, Coal formation, in: Coal Handb., Elsevier, 2023: pp. 3–21.

[60] X. Guo, X. Huan, X. Chen, Feasibility for High-Temperature Graphitization of Deformed Meager Coal, ACS Omega. (2023).

[61] Z. Liu, D. Cao, G. Chen, Z. Bi, Q. Chen, Experimental Verification for the Graphitization of Inertinite, Minerals. 13 (2023) 888.

[62] N. Rabiee, S. Ahmadi, S. Iravani, R.S. Varma, Natural resources for sustainable synthesis of nanomaterials with anticancer applications: A move toward green nanomedicine, Environ. Res. 216 (2023) 114803.

[63] X. Zhang, S. Wang, H. Chen, X. Wang, J. Deng, X. Li, Y. Zhang, Observation of carbon nanostructure and evolution of chemical structure from coal to graphite by high temperature treatment, using componential determination, X-ray diffraction and high-

resolution transmission electron microscope, Fuel. 332 (2023) 126145.

[64] Y. Shibuta, J.A. Elliott, Interaction between two graphene sheets with a turbostratic orientational relationship, Chem. Phys. Lett. 512 (2011) 146–150.

[65] R.E. Franklin, The interpretation of diffuse X-ray diagrams of carbon, Acta Crystallogr. 3 (1950) 107–121.

[66] B. Manoj, Synthesis of Coal-based Nanocarbon Advances and Applications, Pure Funct. Carbon Based Nanomater. (2020) 52–79.

[67] B. Pakhira, S. Ghosh, S. Maity, D.N. Sangeetha, A. Laha, A. Allam, S. Sarkar, Extraction of preformed graphene oxide from coal: its clenched fist form entrapping large molecules, RSC Adv. 5 (2015) 89076–89082.

[68] J. Yan, M. Zhong, C. Yu, J. Zhang, M. Ma, L. Li, Q. Hao, F. Gao, Y. Tian, Y. Huang, Multilayer graphene sheets converted directly from anthracite in the presence of molten iron and their applications as anode for lithium ion batteries, Synth. Met. 263 (2020) 116364.

[69] V. Purwandari, S. Gea, B. Wirjosentono, Synthesis of Graphene Oxide from The Sawahlunto- Sijunjung Coal Via Modified Hummers Method, 020065 (2018). https://doi.org/10.1063/1.5082470.

[70] D.P. Savitskii, Preparation and characterization of colloidal dispersions of graphene-like structures from different ranks of coals, J. Fuel Chem. Technol. 45 (2017) 897–907.

[71] B. Das, R. Kundu, S. Chakravarty, Preparation and characterization of graphene oxide from coal, Mater. Chem. Phys. 290 (2022) 126597. https://doi.org/10.1016/j.matchemphys.2022.126597.

[72] Y. Wu, Y. Ma, Y. Wang, L. Huang, N. Li, T. Zhang, Y. Zhang, X. Wan, Y. Huang, Y. Chen, Efficient and large scale synthesis of graphene from coal and its film electrical properties studies, J. Nanosci. Nanotechnol. 13 (2013) 929–932.

[73] E. Senthil Kumar, V. Sivasankar, R. Sureshbabu, S. Raghu, R. A Kalaivani, Facile synthesis of few layer graphene from bituminous coal and its application towards electrochemical sensing of caffeine, Adv. Mater. Lett. 8 (2017) 239–245.

[74] S. Hashmi, A. Mushtaq, R. Ahmed, Z.U. Ali, Synthesis and characterization of reduced graphene oxide from indigenous coal: A non-burning solution, Int. J. Membr. Sci. Technol. 9 (2022) 1–12.

[75] Y.-M. Wang, C.-H. Zhang, Reduced Graphene Oxide Derived from Low-Grade Coal for High-Performance Flexible Supercapacitors with Ultrahigh Cyclability, Nanomaterials. 12 (2022) 2989.

[76] P. Sahoo, L. Shubhadarshinee, B.R. Jali, P. Mohapatra, A.K. Barick, Synthesis and characterization of graphene oxide and graphene from coal, Mater. Today Proc. 56 (2022) 2421–2427.

[77] M. Bora, S.M. Benoy, J. Tamuly, B.K. Saikia, Ultrasonic-assisted chemical synthesis of activated carbon from low-quality subbituminous coal and its preliminary evaluation towards supercapacitor applications, J. Environ. Chem. Eng. 9 (2021) 104986.

[78] V. Purwandari, M. Rianna, I. Isnaeni, Y. Zou, M. Harahap, G. Halawa, R. Goei, A.I.Y. Tok, The role of biocatalysts in the synthesis of graphene nanosheets from sub-bituminous coal, Mater. Sci. Energy Technol. 6 (2023) 282–289.

[79] W.S. Arsyad, Y. Pranata, V.I. Variani, I. Usman, L. Aba, L. Agusu, Synthesize of rGO from coal (sub-bituminous) as a counter-electrode on dye-sensitized solar cells, in: J. Phys. Conf. Ser., IOP Publishing, 2021: p. 12005.

[80] K. Rane, J.J. Adams, J.M. Thode, B.M. Leonard, J. Huo, L. Goual, Multistep Fractionation of Coal and Application for Graphene Synthesis, ACS Omega. 6 (2021) 16573–16583.

[81] F. Islam, A. Tahmasebi, B. Moghtaderi, J. Yu, Structural investigation of the synthesized few-layer graphene from coal under microwave, Nanomaterials. 12 (2021) 57.

[82] S.H. Vijapur, D. Wang, D.C. Ingram, G.G. Botte, An investigation of growth mechanism of coal derived graphene films, Mater. Today Commun. 11 (2017) 147–155.

[83] A. Singh, A.K. Ojha, Coal derived graphene as an efficient supercapacitor electrode material, Chem. Phys. 530 (2020) 110607.

[84] S.H. Vijapur, D. Wang, G.G. Botte, Raw coal derived large area and transparent graphene films, ECS Solid State Lett. 2 (2013) M45.

[85] A.P.M. Leandro, M.A. Seas, K. Vap, A.S. Tyrrell, V. Jain, H. Wahab, P.A. Johnson, Evolution of structural and electrical properties in coal-derived graphene oxide nanomaterials during high-temperature annealing, Diam. Relat. Mater. 112 (2021) 108244.

[86] D. Wang, S.H. Vijapur, G.G. Botte, Coal char derived few-layer graphene anodes for lithium ion batteries, in: Photonics, MDPI, 2014: pp. 251–259.

[87] B. Manoj, A.G. Kunjomana, Systematic investigations of graphene layers in sub-bituminous coal, Russ. J. Appl. Chem. 87 (2014) 1726–1733.

[88] P. Ma, Y. Tang, R. Li, Q. Che, P. Luo, Preparation and characteristic analysis of graphene based on coal macerals of different rank, Fuel. 357 (2024) 130004.

[89] G. Liu, K. Li, J.I.A. Jia, Y. Zhang, Coal-based graphene as a promoter of TiO2 catalytic activity for the photocatalytic degradation of organic dyes, New Carbon Mater. 37 (2022) 1172–1180.

[90] Mahajan, R. L., & Seul-Yi, L. E. E. (2022). U.S. Patent Application No. 17/415,445..

[91] S.Y. Lee, R.L. Mahajan, A facile method for coal to graphene oxide and its application to a biosensor, Carbon. 181 (2021) 408–420. https://doi.org/10.1016/j.carbon.2021.05.007.

[92] Shafali, S. Singh, S.K. Kansal, Nanostructured Photocatalysts for Degradation of Environmental Pollutants, Catal. Clean Energy Environ. Sustain. Biomass Convers. Green Chem. 1. (2021) 823–863.

[93] N. Kumar, R. Salehiyan, V. Chauke, O.J. Botlhoko, K. Setshedi, M. Scriba, M. Masukume, S.S. Ray, Top-down synthesis of graphene: A comprehensive review, FlatChem. 27 (2021) 100224.

[94] B. Pukánszky, Interfaces and interphases in multicomponent materials: past, present, future, Eur. Polym. J. 41 (2005) 645–662.

[95] D.K. Rajak, P.H. Wagh, E. Linul, Manufacturing technologies of carbon/glass fiber-reinforced polymer composites and their properties: A review, Polymers (Basel). 13

(2021) 3721.

[96] T.P. Sathishkumar, Glass fiber composite materials, Light. Sustain. Mater. Automot. Appl. (2017) 239–276.

[97] N. Saba, M. Jawaid, O.Y. Alothman, M.T. Paridah, A. Hassan, Recent advances in epoxy resin, natural fiber-reinforced epoxy composites and their applications, J. Reinf. Plast. Compos. 35 (2016) 447–470.

[98] D. Gibhardt, A. Doblies, L. Meyer, B. Fiedler, Effects of hygrothermal ageing on the interphase, fatigue, and mechanical properties of glass fibre reinforced epoxy, Fibers. 7 (2019) 55.

[99] N. Domun, H. Hadavinia, T. Zhang, T. Sainsbury, G.H. Liaghat, S. Vahid, Improving the fracture toughness and the strength of epoxy using nanomaterials–a review of the current status, Nanoscale. 7 (2015) 10294–10329.

[100] M. Šupová, G.S. Martynková, K. Barabaszová, Effect of nanofillers dispersion in polymer matrices: a review, Sci. Adv. Mater. 3 (2011) 1–25.

[101] B. Bittmann, F. Haupert, A.K. Schlarb, Ultrasonic dispersion of inorganic nanoparticles in epoxy resin, Ultrason. Sonochem. 16 (2009) 622–628.

[102] Z. Baig, O. Mamat, M. Mustapha, Recent progress on the dispersion and the strengthening effect of carbon nanotubes and graphene-reinforced metal nanocomposites: a review, Crit. Rev. Solid State Mater. Sci. 43 (2018) 1–46.

[103] P.-C. Ma, S.-Y. Mo, B.-Z. Tang, J.-K. Kim, Dispersion, interfacial interaction and re-agglomeration of functionalized carbon nanotubes in epoxy composites, Carbon N. Y. 48 (2010) 1824–1834.

[104] Z. Anwar, A. Kausar, I. Rafique, B. Muhammad, Advances in epoxy/graphene nanoplatelet composite with enhanced physical properties: A review, Polym. Plast. Technol. Eng. 55 (2016) 643–662.

[105] J. Xi, A. Sallam, D.L. Safranski, R. Mirzaeifar, S. Shahab, Hydrophilic and hydrophobic shape memory polymer networks in high-intensity focused ultrasound fields, Smart Mater. Struct. 33 (2024) 25024.

[106] E.C. Girão, A. Macmillan, V. Meunier, Classification of sp2-bonded carbon allotropes

in two dimensions, Carbon N. Y. 203 (2023) 611–619. https://doi.org/10.1016/j.carbon.2022.12.001.

[107] E. Pop, V. Varshney, A.K. Roy, Thermal properties of graphene: Fundamentals and applications, MRS Bull. 37 (2012) 1273–1281.

[108] R.K. Prusty, D.K. Rathore, S. Sahoo, V. Parida, B.C. Ray, Mechanical behaviour of graphene oxide embedded epoxy nanocomposite at sub-and above-zero temperature environments, Compos. Commun. 3 (2017) 47–50.

[109] X. Wang, J. Jin, M. Song, An investigation of the mechanism of graphene toughening epoxy, Carbon N. Y. 65 (2013) 324–333.

[110] A.K. Pathak, H. Garg, M. Singh, T. Yokozeki, S.R. Dhakate, Enhanced interfacial properties of graphene oxide incorporated carbon fiber reinforced epoxy nanocomposite : a systematic thermal properties investigation, (2019).

[111] T. Topkaya, Y.H. Çelik, E. Kilickap, Mechanical properties of fiber/graphene epoxy hybrid composites, J. Mech. Sci. Technol. 34 (2020) 4589–4595.

[112] G.K. Arun, N. Sreenivas, K.B. Reddy, K.S. Krishna Reddy, M.E. Shashi Kumar, R. Pramod, Investigation on Mechanical Properties of Graphene Oxide reinforced GFRP, IOP Conf. Ser. Mater. Sci. Eng. 310 (2018). https://doi.org/10.1088/1757-899X/310/1/012158.

[113] G. V Vigneshwaran, B.P. Shanmugavel, R. Paskaramoorthy, S. Harish, Tensile, impact, and mode-I behaviour of glass fiber-reinforced polymer composite modified by graphene nanoplatelets, Arch. Civ. Mech. Eng. 20 (2020) 1–15.

[114] D. Galpaya, M. Wang, G. George, N. Motta, E. Waclawik, C. Yan, mechanical properties Preparation of graphene oxide / epoxy nanocomposites with significantly improved mechanical properties, 053518 (2014). https://doi.org/10.1063/1.4892089.

[115] A. Mani, P. Tambe, A. Rahaman, Flexural properties of multiscale nanocomposites containing multiwalled carbon nanotubes coated glass fabric in epoxy / graphene matrix multiwalled carbon nanotubes coated glass fabric in epoxy /, Compos. Interfaces. 00 (2019) 1–28. https://doi.org/10.1080/09276440.2019.1569396.

[116] A.K. Pathak, M. Borah, A. Gupta, T. Yokozeki, S.R. Dhakate, Improved mechanical properties of carbon fiber/graphene oxide-epoxy hybrid composites, Compos. Sci.

Technol. (2016). https://doi.org/10.1016/j.compscitech.2016.09.007.

[117] A. Ashori, H. Rahmani, R. Bahrami, Preparation and characterization of functionalized graphene oxide / carbon fi ber / epoxy nanocomposites, Polym. Test. 48 (2015) 82–88. https://doi.org/10.1016/j.polymertesting.2015.09.010.

[118] K. Deshmukh, S.M. Khatake, G.M. Joshi, Surface properties of graphene oxide reinforced polyvinyl chloride nanocomposites, (2013). https://doi.org/10.1007/s10965-013-0286-2.

[119] M.M. Gudarzi, F. Sharif, Enhancement of dispersion and bonding of graphene-polymer through wet transfer of functionalized graphene oxide, Express Polym. Lett. 6 (2012) 1017–1031. https://doi.org/10.3144/expresspolymlett.2012.107.

[120] G.B. Olowojoba, S. Eslava, E.S. Gutierrez, A.J. Kinloch, C. Mattevi, V.G. Rocha, A.C. Taylor, In situ thermally reduced graphene oxide/epoxy composites: thermal and mechanical properties, Appl. Nanosci. 6 (2016) 1015–1022.

[121] R. Eqra, K. Janghorban, H. Daneshmanesh, Mechanical properties and toughening mechanisms of epoxy/graphene nanocomposites, J. Polym. Eng. 35 (2015) 257–266.

[122] Y. Li, S. Wang, Q. Wang, M. Xing, A comparison study on mechanical properties of polymer composites reinforced by carbon nanotubes and graphene sheet, Compos. Part B Eng. 133 (2018) 35–41.

[123] G. V Seretis, G. Kouzilos, D.E. Manolakos, C.G. Provatidis, On the graphene nanoplatelets reinforcement of hand lay-up glass fabric/epoxy laminated composites, Compos. Part B Eng. 118 (2017) 26–32.

[124] G. V Seretis, I.D. Theodorakopoulos, D.E. Manolakos, C.G. Provatidis, Effect of sonication on the mechanical response of graphene nanoplatelets/glass fabric/epoxy laminated nanocomposites, Compos. Part B Eng. 147 (2018) 33–41.

[125] S.I. Abdullah, M.N.M. Ansari, Mechanical properties of graphene oxide (GO)/epoxy composites, HBRC J. 11 (2015) 151–156. https://doi.org/10.1016/j.hbrcj.2014.06.001.

[126] Z. Wang, X. Shen, M. Akbari Garakani, X. Lin, Y. Wu, X. Liu, X. Sun, J.-K. Kim, Graphene aerogel/epoxy composites with exceptional anisotropic structure and properties, ACS Appl. Mater. Interfaces. 7 (2015) 5538–5549.

[127] S. Chatterjee, J.W. Wang, W.S. Kuo, N.H. Tai, C. Salzmann, W.L. Li, R. Hollertz, F.A. Nüesch, B.T.T. Chu, Mechanical reinforcement and thermal conductivity in expanded graphene nanoplatelets reinforced epoxy composites, Chem. Phys. Lett. 531 (2012) 6–10.

[128] S. Mishra, K.T. Kumaran, R. Sivakumaran, S.P. Pandian, S. Kundu, Synthesis of PVDF/CNT and their functionalized composites for studying their electrical properties to analyze their applicability in actuation & sensing, Colloids Surfaces A Physicochem. Eng. Asp. 509 (2016) 684–696. https://doi.org/10.1016/j.colsurfa.2016.09.007.

[129] X. Li, H. Gao, W.A. Scrivens, D. Fei, X. Xu, M.A. Sutton, A.P. Reynolds, M.L. Myrick, Nanomechanical characterization of single-walled carbon nanotube reinforced epoxy composites, Nanotechnology. 15 (2004) 1416.

[130] A. Martone, C. Formicola, M. Giordano, M. Zarrelli, Reinforcement efficiency of multi-walled carbon nanotube/epoxy nano composites, Compos. Sci. Technol. 70 (2010) 1154–1160.

[131] S. Singh, V.K. Srivastava, R. Prakash, Characterisation of multi-walled carbon nanotube reinforced epoxy resin composites, Mater. Sci. Technol. 29 (2013) 1130–1134.

[132] M. Liu, B. Guo, M. Du, X. Cai, D. Jia, Properties of halloysite nanotube–epoxy resin hybrids and the interfacial reactions in the systems, Nanotechnology. 18 (2007) 455703.

[133] Y. Tang, S. Deng, L. Ye, C. Yang, Q. Yuan, J. Zhang, C. Zhao, Effects of unfolded and intercalated halloysites on mechanical properties of halloysite–epoxy nanocomposites, Compos. Part A Appl. Sci. Manuf. 42 (2011) 345–354.

[134] Y. Ye, H. Chen, J. Wu, C.M. Chan, Interlaminar properties of carbon fiber composites with halloysite nanotube-toughened epoxy matrix, Compos. Sci. Technol. 71 (2011) 717–723.

[135] M. Rajaei, N.K. Kim, S. Bickerton, D. Bhattacharyya, A comparative study on effects of natural and synthesised nano-clays on the fire and mechanical properties of epoxy composites, Compos. Part B Eng. 165 (2019) 65–74.

https://doi.org/10.1016/j.compositesb.2018.11.089.

[136] R. Ramamoorthi, P.S. Sampath, Experimental investigations of influence of halloysite nanotube on mechanical and chemical resistance properties of glass fiber reinforced epoxy nano composites, J. Sci. Ind. Res. (India). 74 (2015) 685–689.

[137] L. Lapčík, H. Sepetcioğlu, Y. Murtaja, B. Lapčíková, M. Vašina, M. Ovsík, M. Staněk, S. Gautam, Study of mechanical properties of epoxy/graphene and epoxy/halloysite nanocomposites, Nanotechnol. Rev. 12 (2023) 20220520.

[138] P.P. Prasanthi, M.S.R.N. Kumar, M.S. Chowdary, V.V.V. Madhav, K.K. Saxena, K.A. Mohammed, M.I. Khan, G. Upadhyay, S.M. Eldin, Mechanical properties of carbon fiber reinforced with carbon nanotubes and graphene filled epoxy composites: experimental and numerical investigations, Mater. Res. Express. 10 (2023) 25308.

[139] A. Bamido, N. Shettigar, A. Thyagrajan, D. Banerjee, Investigation of the Temperature-Dependent Mechanical Properties of Polydimethylsiloxane (PDMS) Membrane for Thermo-Mechanical Applications, in: 2021 20th IEEE Intersoc. Conf. Therm. Thermomechanical Phenom. Electron. Syst., IEEE, 2021: pp. 617–629.

[140] A. Rahaman, K.K. Kar, Carbon nanomaterials grown on E-glass fibers and their application in composite, Compos. Sci. Technol. 101 (2014) 1–10.

[141] A.K. Naskar, J.K. Keum, R.G. Boeman, Polymer matrix nanocomposites for automotive structural components, Nat. Nanotechnol. 11 (2016) 1026–1030.

[142] A. Rahman, I. Ali, S.M. Al Zahrani, R.H. Eleithy, A review of the applications of nanocarbon polymer composites, Nano. 6 (2011) 185–203.

2. Research Gaps

Fiber-reinforced polymer graphene oxide nanocomposites stand out as a superior choice compared to traditional materials due to their enhanced mechanical properties. Despite numerous reviews addressing the concept of glass/epoxy/graphene oxide materials, certain aspects and practical applications have been relatively neglected. The following enumerates the gaps identified in the existing literature:

1. In any attempt to convert coal into graphene, it is essential to maintain the integrity of graphitic domains while directing attention to the transformation of aliphatic hydrocarbons present in coal. Mahajan and Lee have devised a cost-effective approach for graphene production using semianthracite coal, specifically preserving these graphitic domains. According to the authors, their innovative process, employing coal as the precursor, boasts a cost that is an order of magnitude lower compared to the modified Hummers' method, which relies on graphite as the precursor. The reduced expenses are attributed to the relatively lower consumption of chemicals, utilizing only 16 M HNO_3. The method also eliminates the production of harmful gases produced during modified Hummers' method as it involves a very simplified route of utilizing a single oxidizing agent. This research has been focused on a single variety of semianthracite coal (Northeast Pennsylvania, USA) and has not been explored for other ranks of coal which gives the benefit of doubt whether the same recipe would be applicable to other ranks of coal or needs modification.

2. While some researchers have investigated the mechanical properties, including impact strength, flexural strength, and tensile strength, of epoxy/graphene oxide or glass/epoxy composites, there is a notable lack of research focusing on the impact of graphene oxide (GO) on the mechanical properties of glass fiber reinforced epoxy materials.

3. There is a lack of substantial research that fully explores the potential of coal-derived graphene oxide as a nanofiller in GFRP composites.

3. Objectives

Focusing on gaps in the literature, the following objectives have been framed for the synthesis and characterization of graphene oxide and the preparation of fiber-reinforced polymer nanocomposite with improved mechanical properties. The objectives to be fulfilled are:

1. Synthesis and characterization of graphene oxide (GO) from Indian anthracite and bituminous coals.

2. Effect of precursors & processing parameters on synthesis of GO.

3. Preparation of fiber-reinforced epoxy GO nanocomposite sheets and analysis of their mechanical properties.

Chapter 2. *One-Pot Synthesis of Graphene Oxide from Different Coals and its Application in Enhancing the Mechanical Performance of GFRP Nanocomposites*

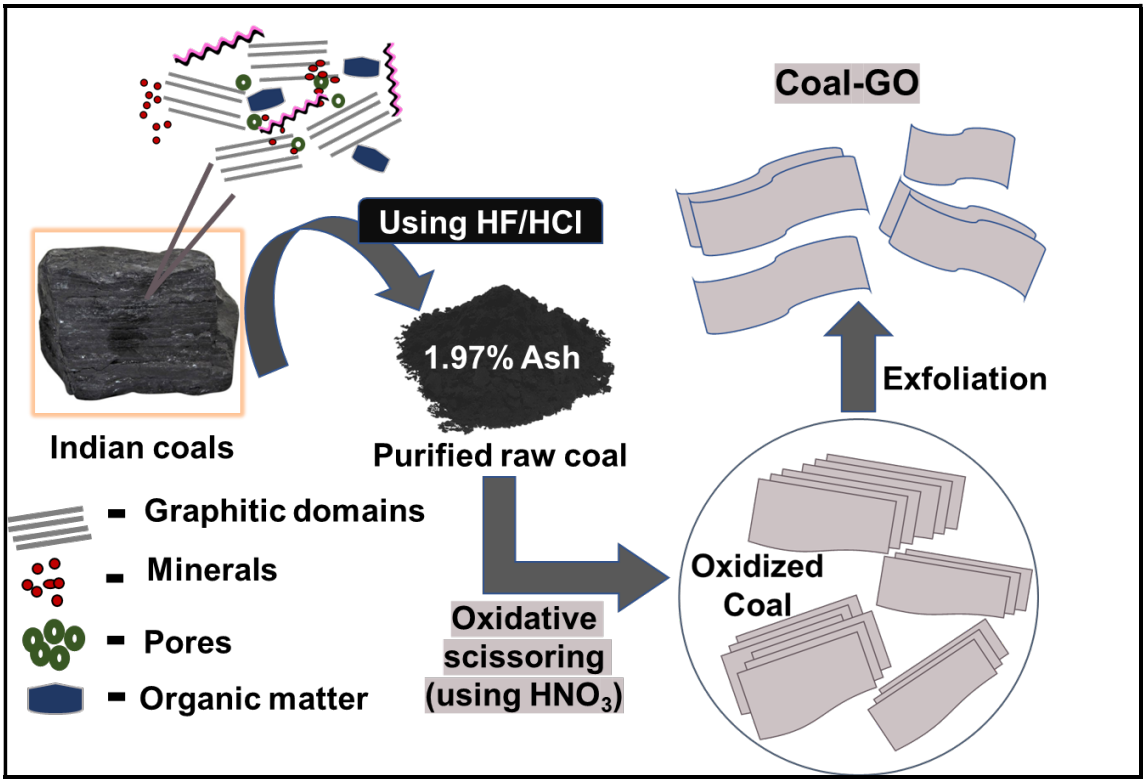

Highlights

- One-pot process using HNO_3 to extract GO from bituminous coal has been used.
- 5M HNO_3 concentration was sufficient for oxidation of the bituminous coal.
- Raw coal was purified using HF/HCl to avoid interference of mineral matter.
- TEM results showed the sheet-like morphology of BC-GO, typical of GO.

2.1. Introduction

Graphene, a crystalline carbon allotrope possesses high Young's modulus, exceptional thermal properties, and efficient electron mobility [1],[2]. Top-down techniques involving intensive chemical and mechanical exfoliation followed by reduction are commonly used for commercial-scale production of graphene oxide (GO) from graphite [3]. The widely used Hummers' method, originally utilizing $NaNO_3$ and $KMnO_4$ dissolved in H_2SO_4, has been extensively modified for the production of GO [4],[5]. Shahriary et al. [6] successfully synthesized ultrathin and homogeneous GO films obtaining the d-spacing of 0.77 nm using a modified Hummers' method. Choucair et al. [7] utilized a solvothermal process involving sonication of a solvent-interacting precursor for graphene sheet separation. The presence of defects adversely affected the quality of graphene. Tour et al. [8],[9] proposed an improved method by using a reaction mixture of H_2SO_4/H_3PO_4 in a ratio of 9:1 (by volume), along with increased amounts of $KMnO_4$, while eliminating $NaNO_3$ from Hummers' approach. This resulted in higher reaction yields and reduced release of toxic gases [10],[11]. However, this method requires larger quantities of $KMnO_4$ and H_2SO_4 compared to the modified Hummers' method, making it expensive and limiting its commercial potential.

Graphite has an oriented lattice structure with interconnected graphene sheets held by van der Waals forces [12], while coal has unorganized, or bent graphene layers, composed of heterogeneous aromatic units and short ether and aliphatic bonds [13],[14]. Natural graphite is limited and geographically localized. Additionally, synthesizing graphite is costly due to the use of petroleum by-products as precursors and the extremely high temperatures required, reaching up to 3000°C [15],[16],[17]. The size of sp^2-carbon crystals in coal varies with different fixed carbon contents depending on the coal rank [18],[19]. The diversity in structural composition of coal allows for flexibility in developing processes to synthesize graphene and its derivatives [20],[21],[22].

Pakhira et al. [23] reported their work on GO synthesis by leaching low-grade coal using HNO_3. After thermal elimination of excessive acid, large GO sheets were produced. However, these sheets exhibited instability in an acidic medium and underwent a spherical morphology, displaying both close and open behavior. Purwandari et al. [24] used bituminous coal and isolated graphite by a combination of exfoliation and Hummers' method. They observed higher d-spacing in GO than in coal-graphite, along with the presence of several functional groups. Savitskii et al. [25] investigated a similar approach involving chemical oxidation of different types of coal such as brown coal, anthracite, low-volatile bituminous and, bituminous coal. Their results showed anthracite coal to be an efficient precursor for colloidal dispersion of GO. The size distribution was in the range of 122–190 nm. The existence of oxygen functionalities at 3420 cm^{-1} (OH), 1053 and 1226 cm^{-1} (C-O), and 1293 and 1720 cm^{-1} (C=O) was also reported. Using Hummers' method, Hatakeyama et al. [26] prepared "Coal Oxide" from anthracite coal. The derived coal oxide contained carboxylic functionalities with minimal amount of oxygen-containing groups and amorphous framework. It showed similar properties to graphite-derived GO, such as raised proton conductivity and electrical insulation. Park et al. [27] optimized temperature, concentration, time allocated for reactions, and processing solvents in a mixed-acid oxidation processes with HNO_3 coupling to prevent graphitic carbon damage. Das et al. [28] used semi-bituminous coal from eastern Indian coal mines to synthesize graphene oxide (GO). XRD analysis showed a diffraction peak at $2\theta = 12.5°$, corresponding to the (001) crystalline plane with a d-spacing of approximately 0.789 nm, confirming the formation of GO. Hashmi et al. [29] used sub-bituminous coal to synthesize graphene oxide (GO). XRD analysis showed a broad peak from 15° to 22°, indicating amorphous nature of GO. Table 2.1 summarizes the recent literature on synthesis of GO using both graphite and bituminous coal.

Table 2.1. An overview of the literature search

Technique used (Year)	Precursor	Processing	Product characteristics	Advantages/Disadvantages of the process	Ref.
Solvothermal synthesis (2006)	Graphitic materials	Use of a solvent interacting with precursor; detachment of graphene sheets by sonication	Highly crystalline and larger surface area of graphene sheets, XRD peak of graphene was observed at 2Θ=26.5°, confirming well-ordered graphitic structures.	**Advantage:** Simple method of sonication **Disadvantage:** Poor quality of graphene	[7]
Tour method (2010)	Graphite	Use of large $KMnO_4$ quantity, 9:1 mixture of H_2SO_4/H_3PO_4,	Production of good oxidized graphene with hydrophilic nature and higher oxidation effectiveness.	**Advantage:** Elimination of $NaNO_3$ **Disadvantage:** Costly because of excess use of $KMnO_4$, limiting its commercialization	[8]
Wu et. al (2013)	Coal (China)	Synthesized in concentrated H_2SO_4 and was oxidized by $NaNO_2$, further diluted by 1M HNO_3	XRD diffraction peak at 2Θ= 21.5°, came from the inter-GO diffraction, showed a d-spacing of 0.41 nm, a little larger than that of the normal graphite, the presence of functional groups but smaller than those of GO from graphite.	**Advantage:** Utilization of coal as an alternative to graphite, cost-effective **Disadvantage:** Use of mixed acids (H_2SO_4 followed by HNO_3).	[30]
Kumar et. al (2017)	Bituminous coal (Sigma-Aldrich)	Synthesized in concentrated H_2SO_4 and was oxidized by $NaNO_2$, further diluted by 1M HNO_3	XRD peak of graphene oxide, appeared at 2Θ= 11.3° and had interlayer distance of 0.8 nm, the laminar structure with higher the d-spacing was observed in graphene oxide. Peak at 2θ=25.01◦, the d spacing indicates that the distance of graphite layers	**Advantage:** Utilization of coal as an alternative to graphite, cost-effective **Disadvantage:** Use of mixed acids (H_2SO_4 followed by HNO_3) & additional oxidant	[31]

			had efficiently increased during the thermal treatment.		
Exfoliation associated with altered Hummers' method (2018)	Bituminous coal	Graphite isolated from coal using oxidative process	Higher d-spacing in graphene oxide than coal graphite was observed which relates to the occurrence of carboxyl, epoxy, and other functional moieties in XRD spectra.	**Advantage:** Utilization of coal, cost-effective **Disadvantage:** Unsuitable for large scale production	[24]
Modified Hummers' method (2019)	Graphite	Graphite slurry mixed with $NaNO_3$, H_2SO_4, $KMnO_4$; involves the usage of harsh oxidants and the release of toxic gases	SEM images reveals ultrathin morphology of graphene films, 0.77 nm d-spacing in the XRD spectra, and maximum absorption peak at ~237 nm attributable to π-π* transition of the atomic C-C bonds.	**Advantage:** High yield, use of different oxidants to fully exfoliated graphene **Disadvantage:** Unsuitable for large scale production	[6]
Lee and Mahajan One-pot synthesis (2021)	Coal	Successfully excludes aliphatic compounds while preserving graphene domains during oxidization and subsequent exfoliation; utilization of single acid, HNO_3	Coal-GO shows a considerable amount of COOH graphs compared to the other oxygen groups; influential in oxidative scissoring of coal edges with significantly less effect on coal swelling towards c-direction.	**Advantage:** Utilization of a single oxidant (HNO_3) during the whole process, coal as a precursor, high reaction yield, suitable for large scale production **Disadvantage:** Use of high concentration of HNO_3.	[32]
Hashmi et. al (2022)	Sub-bituminous coal (Pakistan)	Hummers' method	A broad shoulder was observed in GO analysis from 15° to 22°, indicating that the graphene oxide produced	**Advantage:** Utilization of coal, cost-effective **Disadvantage:** Release of toxic gases, unsuitable for large scale production	[29]

			is amorphous. This shoulder after reduction shifted towards a higher degree, confirming that the material has exfoliated after reduction, and the rGO produced has smaller interplanar spacing than GO.		
Wang et al. (2022)	Lignite (Puhe Coal Mine, Shenbei Mining Area, Liaoning Province, China)	Hummers' method	The calculated interlayer distance from the (002) peak of GO is 8.27 Å (2θ = 10.7◦), which is larger than the value for synthetic graphite (3.38 Å); raw coal shows the 2θ around 24◦.	**Advantage:** Utilization of coal, cost-effective **Disadvantage:** Release of toxic gases, unsuitable for large scale production	[33]
Purwandari et. al (2023)	Sub-bituminous coal (Selensen Village - Riau, Indonesia)	Hydrothermal process and exfoliation	XRD patterns in coal indicate the spectral peak at 21.40°broad and low intensity, the peak of 12.22° indicates the presence of carbonyl groups with the distance between layers (d) 7.336 Å. XRD data confirmed the presence of graphene nanosheets (2theta peaks 24.86° and 43.96°), the distance between layers (d) 2.583 Å (right shift indicating reduction)	**Advantage:** Utilization of coal, cost-effective **Disadvantage:** Release of toxic gases, unsuitable for large scale production	[34]

In any endeavour to convert coal into graphene, it is crucial to preserve the graphitic domains while focusing on the transformation of aliphatic hydrocarbons in coal. Mahajan and Lee developed a cost-effective method of producing graphene from semi-anthracite coal by preserving these graphitic domains [35]. The authors assert that their new process, which utilizes coal as the precursor, has an order of magnitude lower cost compared to the modified Hummers' method that employs graphite as the precursor. The cost savings are attributed to relatively lower usage of chemicals (only 16M HNO_3) [32].

Given the inherent structural variations among coals of different ranks, we hypothesized that the application of the one-pot process developed for semi-anthracite coal to bituminous coal may require a weaker oxidizing agent. We also anticipated potential differences in process parameters and in the properties of the synthesized graphene oxide (GO). Before testing this hypothesis, our initial objective was to evaluate the applicability of the original one-pot process for the semi-anthracite coal from a different mine and identify any necessary modifications.

The current study was designed to test our hypothesis by synthesizing semi-anthracite and bituminous coal-derived graphene oxides (GOs) using Mahajan & Lee's one-pot process, as detailed in Section 2 (experimental). Comprehensive characterizations of the synthesized GOs were conducted using SEM-EDX, LRS, TEM-SAED, DLS, BET-BJH, XRD, XPS, and FTIR techniques. Section 3 presents the results and discussion, and Section 4 elucidates the proposed mechanism followed by conclusion. In Section 5, we demonstrate the potential application of coal-GO as a nanofiller in enhancing the mechanical performance of glass fiber reinforced polymer (GFRP) composites. This exemplar application holds particular relevance in industries such as automotive, aerospace, marine, and sports, where the use of mechanically robust and lightweight structural materials is highly desired. The paper concludes with a few remarks highlighting the major findings of the paper.

2.2. Experimental Section

2.2.1. Materials

Raw chunks of anthracite coal were sourced from the coalfields in Kashmir (supplied by SVISPAT Pvt Ltd, Pune, Maharashtra, India), while bituminous coal was procured from the north-eastern region of India (supplier, RK & Sons, Patiala, Punjab). Hydrochloric acid, hydrofluoric acid, nitric acid, ethanol, potassium permanganate, and hydrogen peroxide were acquired from Merk. All the reagents were of analytical grade and were used without purification except raw coal chunks, which were purified before oxidation. The epoxy resin (Araldite CY 230-1) and the hardener (Aradur HY 951) were procured from Huntsman Advanced Materials, India (used in a 10:1 ratio as recommended by the supplier). E-glass fiber mats were obtained from Revex Plasticizers Pvt. Ltd., India. Double-distilled water was used for preparing reagents and washing procedures throughout the experiments.

2.2.2 Synthesis of bituminous-derived Coal-GO (BC-GO) and semi-anthracite Coal-GO (AC-GO)

2.2.2.1 Processing and purification of raw coal powders

Nut-sized raw coal chunks of both bituminous and semi-anthracite coals, as-received, were powdered using a mortar pestle and then sieved using a 150μ mesh. Further, the sieved coal powder was processed utilizing a wet ball milling process to obtain a particle size below 10μ. The slurry of the ball-milled coal solution was filtered using cellulose filter paper. For purification, this coal powder was dissolved in a mixture of 5% HCl and 10% HF with 500 ml of distilled water followed by 36 hours of magnetic stirring. The mixture was allowed to rest for 12 hours after which black precipitates were visible near the bottom of beaker. The top layer of the solution was discarded without losing the precipitates. The solution was then neutralized by adding distilled water, following which the purified coal slurry was filtered via cellulose filter paper. All the steps

involving purification and the use of HF acid were carried out in a polypropylene bottle as HF is highly reactive to glass.

2.2.2.2 Oxidation, Exfoliation, and Centrifugation of Purified Bituminous Coal (PBC) and Purified Semi-Anthracite Coal (PAC)

Following the protocol in [32], three grams of purified bituminous coal were oxidized/swelled using different concentrations of HNO_3 (16 M, 10 M and 5 M) at 120^0C to determine the optimum concentration to test our hypothesis that a lower concentration of HNO_3 may suffice. For each concentration, five different values of the oxidation time— 72 hours, 48 hours, 24 hours, 5 hours, and 3 hours—were tried. The highly acidic GO solution was transferred to a one litre container filled with distilled water. After allowing the solution to settle for 12 hours, the top layer solution containing pale brown particles was discarded, while retaining the brown precipitates at the bottom. The solution was again diluted with distilled water, resulting in a gradient of brown coloration. The resulting brown solution (no longer extremely acidic) was filtered using a nylon membrane filter with a pore size less than 0.2 μ. The filtered solution was dried, resulting in 0.5 g oxidized powder material, which was transferred to 150 ml of distilled water. To exfoliate the oxidized coal to GO, the solution was subjected to ultrasonication. To further enhance the GO quality, an additional round of centrifugation was done at 5,000 rpm for 1 hour. The pellet obtained at the bottom of centrifuge tube was discarded as it probably contained highly stacked graphitic carbons or unreacted coal whereas the supernatant (the brown solution) was retrieved and stored in a bottle. For characterization purposes, for which the dry powder is required, this solution was freeze-dried after pre-treatment at -80^0C.

For synthesis of AC-GO, the original one-pot process advocated in [32] was used for synthesizing GO. It essentially follows the same procedure outlined above except that only one concentration of HNO_3 16M, at 120^0C for 5 hours was used for oxidation, as in the original process in [32]. Figure

2.1 shows the schematic diagram/camera visuals for the one-pot process used in the synthesis of GO.

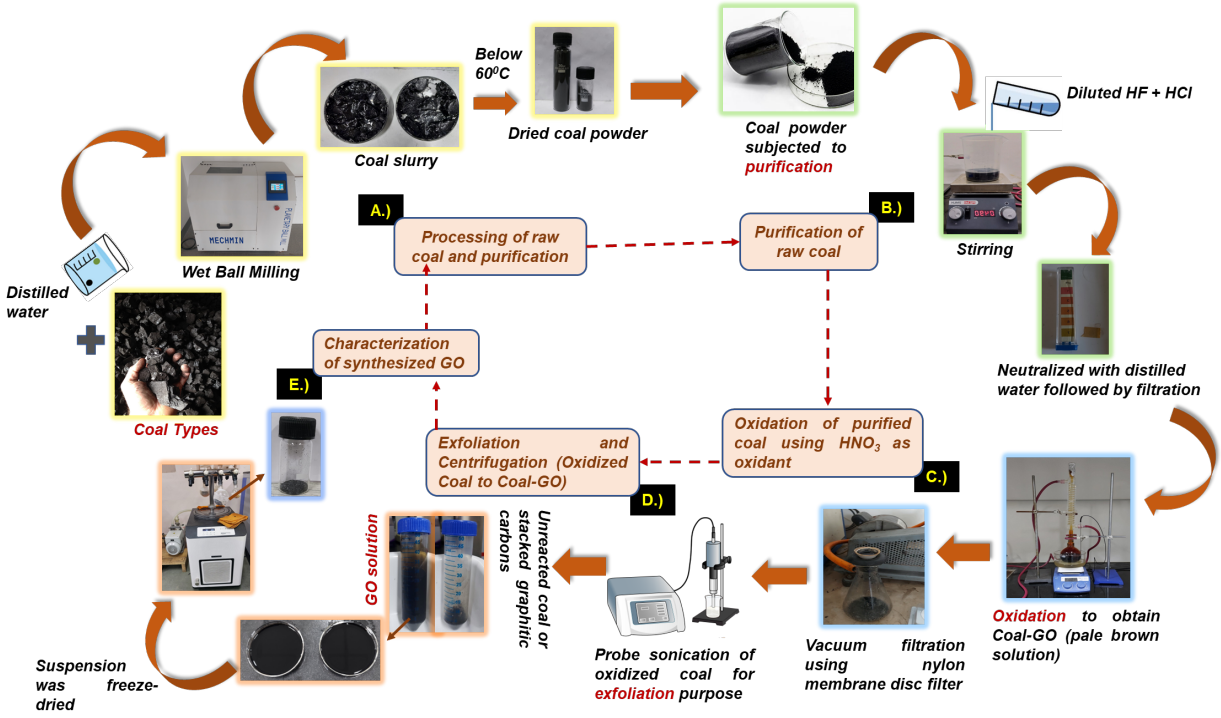

Figure 2.1. Schematic diagram/camera visuals of the one-pot method applied for GO synthesis from coal

2.2.3. Synthesis of GO using modified Hummers' method

For benchmarking the AC-GO and BC-GO synthesized using the one-pot or modified one pot process, graphene oxide (GO) was also synthesized using modified Hummers' method using BC, AC, and graphite as precursors. To this end, the mixture of graphite powder/semi-anthracite coal and sodium nitrate ($NaNO_3$) was added to 46 ml of conc. sulphuric acid (H_2SO_4). The resulting solution was kept in an ice-bath to maintain the temperature below 20°C and stirred for 4 h. Later, approximately 6 g of potassium permanganate ($KMnO_4$) was introduced to the solution and vigorously stirred for another hour. Thereafter, 220 ml distilled water was added dropwise, accompanied by continuous stirring, and dropwise addition of 30% of 10 ml hydrogen peroxide

(H_2O_2). Lastly, the solution was washed using 5% hydrochloric acid (HCl) and distilled water. The product was dried in an oven overnight to procure dry powdered GO.

2.2.4. Fabrication of GFRP composites using AC-GO

Initially, AC-GO was dispersed in the epoxy resin at different concentrations ranging from 0.06 to 0.75 phr. The mixture was homogenized at 20,000 rpm for 10 minutes and then subjected to probe sonication at 80% amplitude for 10 minutes in an ice bath to dissipate excess heat. Subsequently, the solution was mechanically stirred at 500 rpm for 10 minutes, and the hardener was added. The resulting mixture was infused into the VARIM (Vacuum Assisted Resin Infusion Mold). The VARIM table was cleansed with a cleansing agent and coated with a mold release agent to prevent sticking.

For the tensile and flexural property tests, two-ply mats, conforming to ASTM standards, were utilized. To prepare specimens for impact testing, twelve layers of the mat were employed. A separator cloth was placed on top of the uppermost layer of glass-fiber mat, and a perforated sheet was positioned on the separator cloth to ensure even resin dispersion. A wire-mesh was used to establish a resin flow path, and an infusion pipe was secured over the wire-mesh using sealant tape. To facilitate resin flow, a breather cloth was placed over the wire-mesh, creating a bridge. Finally, the entire setup was covered with a lamination sheet and supported with sealant tape. A vacuum pump maintained a vacuum pressure of approximately 1 mbar. The vacuum pump assisted in the resin infusion process, ensuring proper impregnation of the fiber mat with resin. After infusion, the nanocomposite sheets were cured and subsequently post-cured for 6 hours at 23 ℃ and an additional 6 hours at 60 ℃.

2.2.5. Characterization

The BET surface area analyzer from Microtrac Belsorp Mini-II (Bel, Japan, Inc) was used for the surface area estimation of graphene oxide at the liquid nitrogen temperature of -196ºC. To remove

impurities, pre-treatment of the samples was done for 5-6 h at 100ºC. The Barrett–Joyner–Halenda (BJH) method was employed to determine the pore size distribution from N_2 adsorption-desorption isotherms. Energy-dispersive X-ray (EDX) and Scanning electron microscope (SEM) were used for studying the surface morphology and carbon-oxygen weight% of the as-prepared graphene oxide material and its precursors through a Carl Zeiss Sigma 500 FEG-SEM at an accelerating voltage of 5 kV. X-Ray Diffraction analysis (XRD) was carried out through a PANalytical X-ray diffractometer with Ni-filtered Cu Kα radiations (λ = 0.1504 nm) with a scan rate of 2^o min^{-1} and range of 10–90º at 45 kV. X-ray photoelectron spectroscopy (XPS) analysis was done through PHI-5000 VersaProbe-III system with a monochromatic Al Kα X-ray source (1486.7 eV) to determine the elemental nature of the as-prepared Coal-GO and the precursor coal used. Particle size distribution and zeta potential measurements were done utilizing a dynamic light-scattering method (DLS, Zetasizer, Malvern) of graphene oxides and respective coals dispersed in deionized water. Fourier transform infrared (FTIR) spectra were recorded for oxygen-associated functionalities by RZX (Perkin Elmer), and high-resolution transmission electron microscopy (TEM-SAED) was scrutinized via Hitachi (H-7500) for a clear understanding of the morphological features of GO. Laser Raman Spectroscopy (LRS) was carried out using HR800-UV confocal micro-Raman spectrometer to identify the structural fingerprint and to analyze the synthesized materials for defects and impurities.

2.3. Results and Discussion

2.3.1 Proximate analysis of coals

The structural and surface properties of the raw coal vary based on the geological atmosphere and coalification degree. Coal consists of graphitic domains and amorphous carbons leading to a very complex network possessing different structural properties and functionalities. The non-purified

coal contains several minerals which might interfere in graphitic regions or release several noxious side-products. Therefore, we purified the respective coals as detailed in the experimental section.

Proximate analysis of the as received semi-anthracite and bituminous coals, before and after their cleaning, was done to evaluate moisture, ash content, volatile matter, and fixed C in coals. The results are shown in Table 2.2.

Table 2.2. Proximate analysis of non-purified and purified bituminous and semi-anthracite coals

	Parameters	**Unit**	**Non-purified bituminous coal (NPBC)**	**Purified bituminous coal (PBC)**	**Non-purified semi-anthracite coal (NPAC)**	**Purified anthracite coal (PAC)**
1	Moisture	%	4.31	0.90	4.58	0.88
2	Ash	%	**3.34**	**1.97**	**6.75**	**1.02**
3	Volatile matter	%	27.46	27.09	8.74	8.41
4	Fixed Carbon	%	64.89	70.04	79.93	89.69

The data shows that cleaning reduced the ash content from 3.34% to 1.97% for the bituminous coal, and from 6.75% to 1.02% for the semi-anthracite coal. It is noted that reducing the level of ash in the purified coal is desirable to minimize interference of the impurities on the subsequent GO synthesis process [36]. It is interesting that the same cleaning procedure used for both bituminous and semi-anthracite coal was more effective in reducing the ash content of the semi-anthracite coal compared to the bituminous coal.

2.3.2 Optimum Process Parameters for the Synthesis of BC-GO and AC-GO

As mentioned in Section 2.2.2, we tried combinations of the concentration of HNO_3 and oxidation time to determine the optimum parameters. Initially, for bituminous coal, we followed the recommended combination of 16 M HNO_3 and 72 hours, as originally suggested in [35],[32] for semianthracite coal. Under these conditions, the bituminous coal we used got completely dissolved without any observed precipitates. We gradually decreased the oxidation time to 48

hours, 24 hours, 5 hours and finally 3 hours, but still did not observe any precipitates. Even when we switched to 10 M HNO_3 concentration with oxidation times of 5 hours and then 3 hours, the bituminous coal dissolved entirely. However, further reducing down the concentration to 5 M with oxidation times of 5 hours and 3 hours, we finally observed oxidized coal precipitated at the bottom of the beaker. To confirm the composition of these precipitates, we subjected them to EDX analysis, yielding the following spectra. With 5 M concentration and 5 hours of oxidation time, the spectra indicated a composition of 70.34 wt% C and 29.66 wt% O, while with 3 hours of oxidation, the spectra indicated 84.12 wt% C and 15.88 wt% O. Another parameter we considered for optimizing the oxidation time with 5M HNO_3 was the yield of the oxidized PBC. The yield for 5 hour oxidation time was found to be 75%, much higher than the yield observed for 10 hours, which was only 11%. Based on these results, we concluded that for the bituminous coal sample used in this study, the optimum process parameters are concentration of 5 M HNO_3 and oxidation time of 5 hours.

To assess the suitability of the recipe developed for the synthesis of GO from purified semi-anthracite, as outlined in [35],[32], we conducted tests to determine if any fine tuning of the process parameters was required when applied for our locally obtained semi-anthracite coal. Following the procedure outlined in 2.2.2, we tested 10 M and 5M concentration of HNO_3 in addition to 16M in the original 16M concentration. We also tried two oxidation times: 5 hours and 72 hours. After analyzing the EDX results, which showed reduced levels of oxygen content, we reverted to the original recipe of 16 M HNO_3 and 72 hours as the optimal parameters for obtaining GO from semi-anthracite coal.

2.3.3 Structural characteristics of bituminous coal-derived GO (BC-GO) and semi-anthracite coal derived GO (AC-GO) using one-pot method

X-ray diffraction (XRD) analysis was done to provide detailed information on structural factors such as crystallite size, interlayer spacing (d), and stacking height in the BC-GO (graphene oxide synthesized from bituminous coal), and AC-GO (graphene oxide synthesized from semi-anthracite coal), using one-pot method [32], see Figure 2.2A.

Referring to Figure 2.2A, the main peak observed in PBC corresponds to the crystalline carbon (002) reflection and occurs at $2\theta = 24.6^0$ for PBC, and at $2\theta = 25.2^0$ in PAC. Similarly, the peak at $2\theta = 42.8^0$ in PBC and $2\theta = 43.2^0$ in PAC represents the plane reflection of graphite (100). The presence of these peaks suggests a larger interlayer spacing and the existence of loosely stacked graphene sheets in purified coals, indicating a turbostratic carbon structure. The d-spacing, calculated using $n\lambda=2d\sin\theta$, was calculated to be 0.361 nm for PBC and 0.353 nm for PAC. We note that the above-mentioned values of 2θ and d-spacing for PAC closely match those reported in [31], which are $2\theta = 25.0^0$, $2\theta=42.5^0$, and d-spacing=0.353 nm.

Focusing back on the GO synthesized from PBC, the XRD data in Figure 2.2A reveals a shift in the value of 2θ, decreasing from 24.6^0 in PBC to 20.9^0 for the BC-GO. In addition, the d-spacing increased from 0.361 nm in the PBC to 0.424 nm in the BC-GO. This increase in d-spacing can be attributed to the swollen layers of graphene oxide, resulting from oxidation process using HNO_3. These values are listed in Table 2.3 which also shows the crystallite height, L_c and the number of layers, N_c. The former was calculated using Scherrer's equation, a method commonly used to quantify the stacked layers in graphene derivative ($N_c= (L_c/\text{d-spacing})+1$). It can be observed that both L_c and N_c decrease in BC-GO in comparison to those for PBC. Specifically, the L_c for GO is only 0.49 nm, and it contains very few stacked sheets. For AC-GO, our values of 2θ (002) = 23.9

and d-spacing = 0.372, listed in Table 2.3 compare favorably with those reported in [31], which are 2θ (002) = 23.6^0, and d-spacing = 0.374 nm.

Table 2.3. Structural parameters of coals and their synthesized materials: PAC, PBC (purified coals) and AC-GO, BC-GO (synthesized GOs)

Sample codes	**2 Theta (degree) (002)**	**d (002) (nm)**	**Crystallite height, L_c (nm)**	**No. of graphene stacked layers, (N_c)**
PAC	25.2	0.353	1.02	2.89 (2-3)
AC-GO	23.9	0.372	0.75	2.02 (2)
PBC	24.6	0.361	0.64	1.77 (1-2)
BC-GO	20.9	0.424	0.49	1.16 (2)

Furthermore, the d-spacing increases from 0.353 nm for PAC to 0.372 nm for AC-GO, while both L_c and N_c decrease for AC-GO. These trends are similar to those observed in the oxidation of PBC and BC-GO, as well as those reported for AC-GO in [31]. It is worth noting that the C(002) peak in AC-GO (16M) is more symmetrical and narrower as compared to BC-GO produced at low HNO_3 concentration, indicating a highly ordered structure of AC-GO (16M). At this high concentration of HNO_3, the aliphatic side-groups get removed at a faster rate, leaving behind mostly the aromatic groups [31].

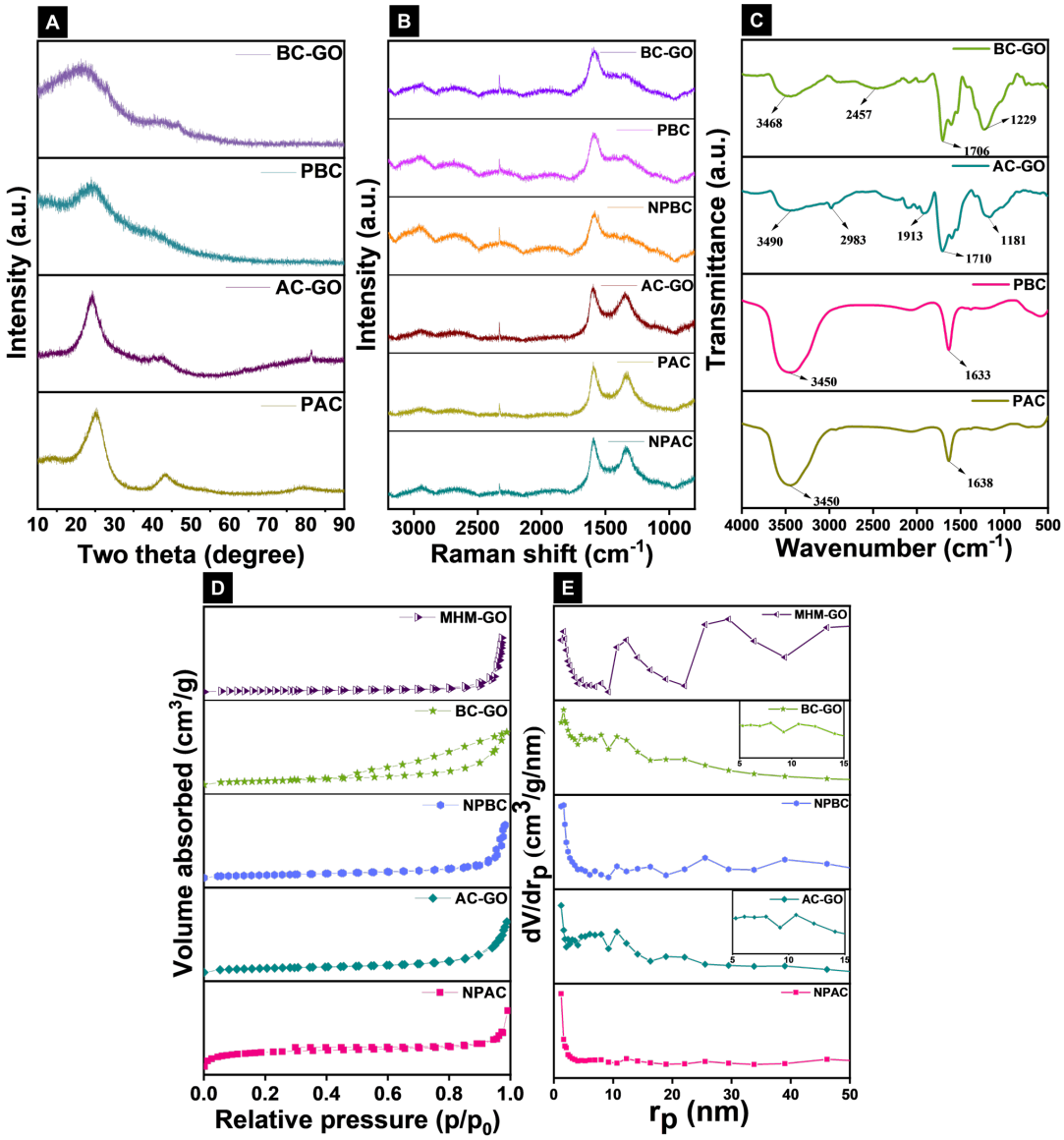

Figure 2.2. A) XRD spectra, B) Raman spectra, C) FTIR spectra, D) BET nitrogen adsorption/desorption isotherms, E) BJH plots of precursors and synthesized GO from respective coals and graphite

In addition to the XRD analysis, Raman analysis was also conducted for the GO samples. In most carbon-constituting materials, a typical Raman spectrum refers to prominent bands as the D and G bands at 1350 cm^{-1} and 1590 cm^{-1}, respectively [37]. The D-band represents structural defects caused by k-point phonons in the breathing mode of A_{1g} symmetry, while the G-band corresponds

to in-plane vibrations of E_{2g} phonons associated with sp^2 C-atoms [38]. The existence of band at 2700 cm^{-1} refers to 2D-band corresponding to active lattice vibration. The 2D band has a pronounced higher intensity in single-layered graphene, whereas in multilayer graphene, the band broadens and reduces in intensity [39]. Furthermore, the band-intensity ratio (I_D/I_G) is commonly used to assess product quality [40]. In carbonaceous materials, higher I_D/I_G points to higher disorder.

In our investigation, as shown in Figure 2.2B, the NPBC, PBC, and BC-GO samples display a weak and disordered D-band caused by the oxidation over the edges of the graphitic domains under milder HNO_3 treatment. These characteristics of D-band might be due to the relatively low concentration of HNO_3 used in the oxidation of NPBC to BC-GO. In contrast, synthesis of GO from PAC, which required higher concentration of HNO_3 (16M), a more distinct D-band was observed, as also reported in [32]. Furthermore, we observed that the 2-D band which appears at approximately 2700 cm^{-1} is bumpier and more ill-defined as compared to AC-GO. This difference could again be attributed to the low concentration of HNO_3 used in the synthesis of BC-GO. This finding is in alignment with the Raman spectra presented in [32] for AC-GO synthesized for different concentrations of HNO_3, which exhibited progressively shallower and more irregular peak at approximately 2700 cm^{-1}. A bumpy 2-D band suggests highly disordered and defective samples, leading to inaccuracy in quantifying the exact number of layers. We will further discuss this behavior in Section 3.3 when examining the TEM images of our samples, which will provide additional insight into the structural characteristics of these materials.

Table 2.4. Raman spectroscopy: Microstructural parameters

Sample codes	I_D/I_G	L_a (nm)
NPAC	1.44	30.2
PAC	1.23	35.3
AC-GO	1.16	37.5

From Table 2.4, the I_D/I_G ratio for AC-GO synthesized from the PAC decreased from 1.23 to 1.16, indicating a decrease in defects relative to graphitic regions, alongside an increase in L_a resulting from HNO_3 oxidative treatment. This result is different than that reported in [31], in which I_D/I_G increased from 1.78 to 1.83. Recalling that the structural and surface properties of the raw coal vary based on the geological atmosphere and coalification degree, this difference in the I_D/I_G ratio of AC-GO can be traced back to the coalfield from where the coal was sourced. In [32], the raw chunks of coal were obtained from the anthracite coal region in Northeast Pennsylvania, USA (US PAC), while the one we used in this study was from Kashmir, India where anthracite coal mines are predominant. Further, the I_D/I_G of Indian PAC was measured at 1.23. lower than of US PAC reported in [31] at 1.78. This indicates that Indian PAC has fewer defects compared to the former. However, in Indian AC-GO, the evolution of clustered graphitic regions far outweighs the defects originating from the oxygen-based functionalities in the one-pot process, even at 16 M HNO_3 concentration, which is still insufficient to disrupt the graphitic clusters in PAC. Another potential reason for this discrepancy could be the introduction of oxygen functionalities on the edges of Coal-GO. In other words, the presence of carboxyl groups may have had a limited effect on the partial intercalation step (oxidation) in the basal plane of Coal-GO implying to the lower I_D/I_G ratio. The one-pot process is more favorable than others in scissoring of the coal to extract sp^2 graphene domain made through the mild oxidation which introduces oxygen-based functionalities over the graphene-like edges, while simultaneously ostracizing the unwanted aliphatic complexes. This could justify the favourable graphene derivatives production from coal.

The pore volume and surface area of a material are important for assessing its applicability in different areas of catalysis, adsorption studies, etc. To calculate these quantities, Brunauer-Emmett-Teller (BET) analysis is an excellent tool. It provides a quantitative information about the specific surface area of coals and synthesized carbonaceous materials, enabling the study of surface porosity and particle size effects. The Barnett-Joyner-Halinda (BJH) analysis is often used in conjunction with BET analysis to evaluate specific pore volume and its area using adsorption/desorption methods [41]. We utilized both techniques to generate Figures 2.2D and 2.2E, which illustrate the BET nitrogen adsorption-desorption isotherms and BJH plots for the synthesized GO from different coals, respectively. In addition to valuable information about specific surface area, pore diameter, the BJH plots confirm the mesoporous nature of the synthesized samples as well as of the precursors. As depicted in Figure 2.2E, BC-GO shows a H1 hysteresis loop which validates the mesoporous nature of BC-GO. Examining the data in Table 2.5, we observe a decrease in the specific surface area of BC-GO in comparison to NPBC. One possible reason for this could be the more compact structure of GO, resulting from the formation of nicely stacked multilayers.

Table 2.5. Surface area, pore size, and pore-volume of ball-milled coals and synthesized GO

	NPAC	**NPBC**	**AC-GO**	**BC-GO**	**MHM-GO**	**AC-GO (MHM)**
Specific surface area (m^2/g)	97.75	87.50	16.50	12.60	12.40	9.00
Mean pore diameter (nm)	4.67	20.40	15.82	16.90	20.50	14.70
Total pore volume (cm^3/g)	0.11	0.44	0.06	0.05	0.06	0.04

The surface area of AC-GO decreased significantly relative to NPAC but was found to be almost comparable to BC-GO, as indicated in Table 2.5. The mean pore diameter of AC-GO was considerably larger than of NPAC (15.82 nm compared to 4.67 nm). This can be attributed to the presence of inorganic substances in coal such as kaolinite, siderite ($FeCO_3$), feldspar (composed of SiO_2, Al_2O_3, Fe_2O_3, K_2O, Na_2O) and some impurities such as CaO and MgO. These inorganic components have varying chemical reactivity, with some exhibiting low reaction abilities and others being chemically active. When reacted with HNO_3, for example, solid Fe_2O_3 reacts with HNO_3 to form soluble $Fe(NO_3)_2$. With the solubilization of these substances, other associated inorganic components, such as kaolinite and quartz lose support and adhesive force, and then separate from coal. This further explains the observed increase in pore volumes and pore sizes [42].

2.3.4 Topological and morphological properties of BC-GO and AC-GO using one-pot method

The Dynamic Light Scattering (DLS) technique helps measure the size of particles by quantifying the random variations in the scattering of light intensity from a suspension. This approach is particularly suitable for submicron particles and can be utilized for measuring sizes of particles smaller than a nanometre. In our investigation, we applied this technique to determine the apparent size of graphitic materials prepared in distilled water. Tiny particles in the suspension undergo random movements, which are modelled by Stokes-Einstein equation as given below:

$$D_h = k_B T / 3\pi \eta_0 D_t$$

where D_h represents the hydrodynamic diameter, k_B the Boltzmann constant, T the temperature (kelvin), η_0 the solvent's dynamic viscosity, and D_t is the translational diffusion coefficient. The calculations were handled by the instrument software, all the data was plotted with Gaussian fit. The average hydrodynamic diameter decreases sharply for AC-GO compared to PAC, reducing

from 681 nm to 171 nm as shown in Figure 2.3(A, B). For bituminous coal, on the other hand, the decrease in the average hydrodynamic diameter as PBC got converted to BC-GO was relatively small, declining from 627 nm in PBC to 296 nm in BC-GO, as depicted in Figure 2.3(C, D). The reduction in diameter may not only be attributed to the high sonication rate during the one-pot process but also to the improved interactions between the oxygen moieties on the GO surfaces and water molecules. Relatively sharper decrease in the hydrodynamic diameter of AC-GO is due to higher HNO_3 concentration (16M) used in oxidation process compared to only 5M for PBC.

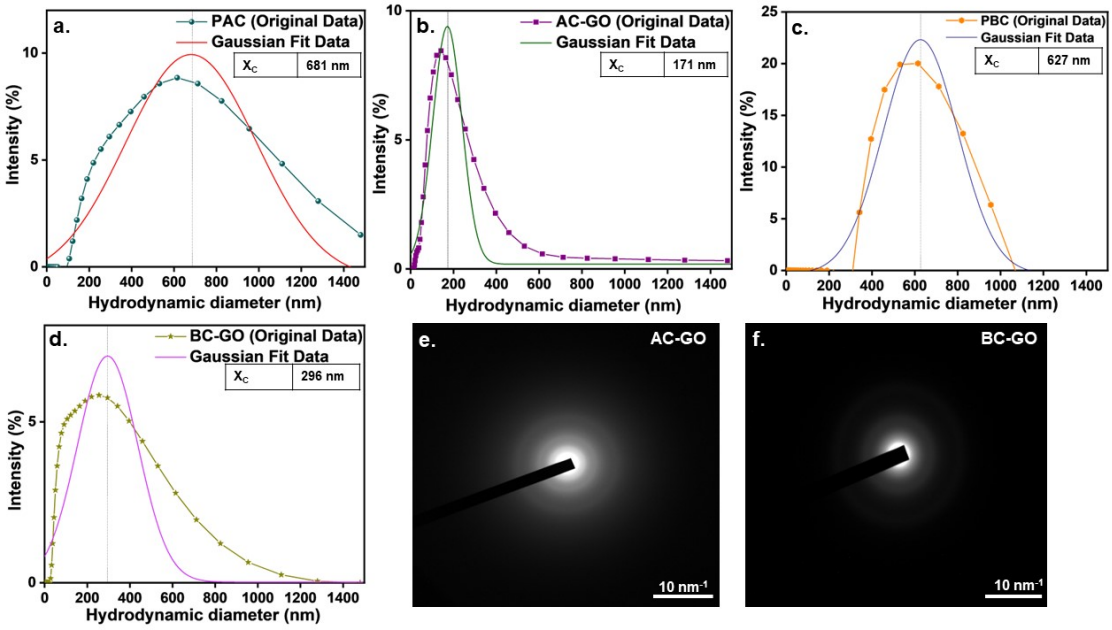

Figure 2.3. Representation of (A-D) DLS studies; (E,F) SAED patterns of AC-GO and BC-GO

To analyze the elemental composition of precursors (raw coals) and the synthesized product (BC-GO), EDX analysis was performed. The results are presented in Table 2.6 and displayed in Figure 2.4. In the raw bituminous and semi-anthracite coal, the EDX spectra reveal the presence of C, O, Si, S, Al, Cl, K, Ti, Fe.

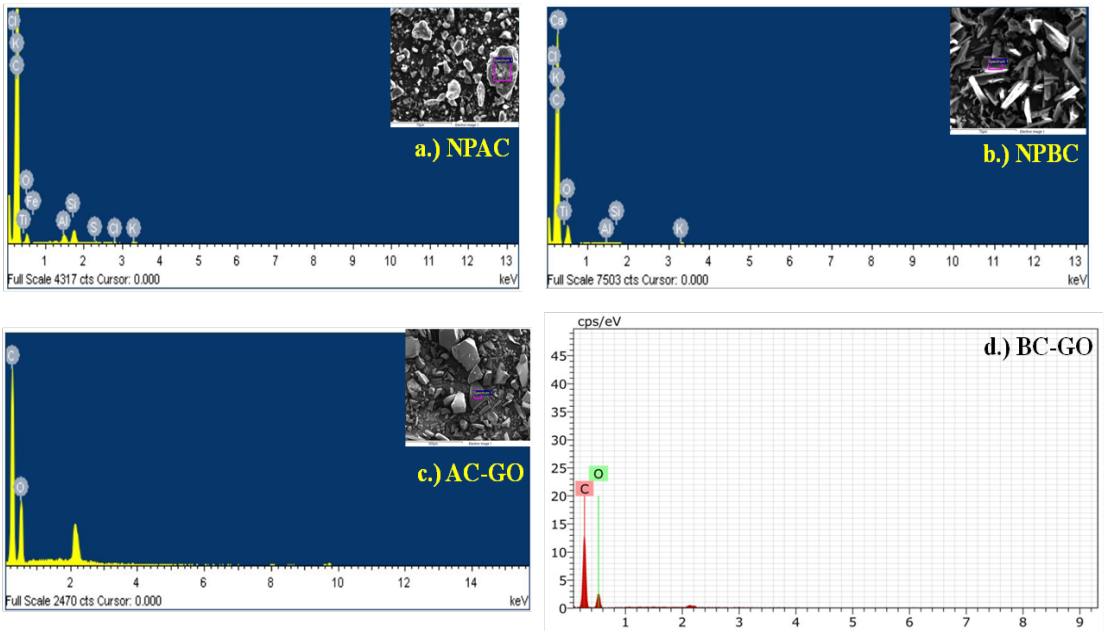

Figure 2.4. EDX spectra for a.) NPAC, b.) NPBC, c.) AC-GO, d.) BC-GO

However, in BC-GO and AC-GO, only C and O were observed as the major constituent element, as indicated by the atomic % and weight % in Table 2.6. The lower wt% of oxygen in BC-GO can be attributed to the lower concentration of HNO_3 used in the synthesis process. In a study by Zhao et al. [43], they synthesized GO by Hummers' method to immobilize rhodium on it for catalytic applications. The oxygen composition in their synthesized GO was determined to be 24.29%, which is lower than of the prepared BC-GO. This again suggests the favourable efficiency of HNO_3 as an oxidant at a much lower concentration of HNO_3 (5M with BC).

Zhang et al. [44] synthesized GO via modified Hummers' method utilizing $KMnO_4$ as an oxidant. Their EDX spectra indicated oxygen composition in their GO to be 31.72 wt% oxygen composition, which is lower than that 40.97 wt% obtained in the AC-GO synthesized with HNO_3 as an oxidizing agent), and slightly higher than in the BC-GO (26.44 wt%). Table 2.7 and the spectra in the Figure 2.5 shows the wt% of C and O in AC-GO and BC-GO obtained at different time intervals. The caveat arising from our experimental studies on different coals for synthesizing graphene oxide (GO) is that while the one-pot process utilizing HNO_3 (as a single acid) remains

consistent across all coal varieties, there may be variations in the oxidation time and the concentration of HNO_3 required for each specific type of coal.

Table 2.6. Elemental composition of precursors and synthesized GO

Elements	**NPAC Weight %**	**NPAC Atomic %**	**AC-GO Weight %**	**AC-GO Atomic %**	**NPBC Weight %**	**NPBC Atomic %**	**BC-GO Weight %**	**BC-GO Atomic %**
C	82.75	88.10	59.03	65.74	67.73	73.85	67.62	73.56
O	12.34	9.86	40.97	34.26	31.14	25.64	32.38	26.44
Al	1.26	0.60	-	-	0.00	0.00	-	-
Si	2.28	1.04	-	-	0.13	0.06	-	-
S	0.15	0.06	-	-	0.10	0.04	-	-
Cl	0.15	0.05	-	-	0.06	0.02	-	-
K	0.37	0.12	-	-	0.48	0.16	-	-
Ca	-	-	-	-	0.37	0.12	-	-
Ti	0.07	0.02	-	-	0.13	0.04	-	-
Fe	0.63	0.14	-	-	0.26	0.06	-	-
Total	100.00		100.00		100.00		100.00	

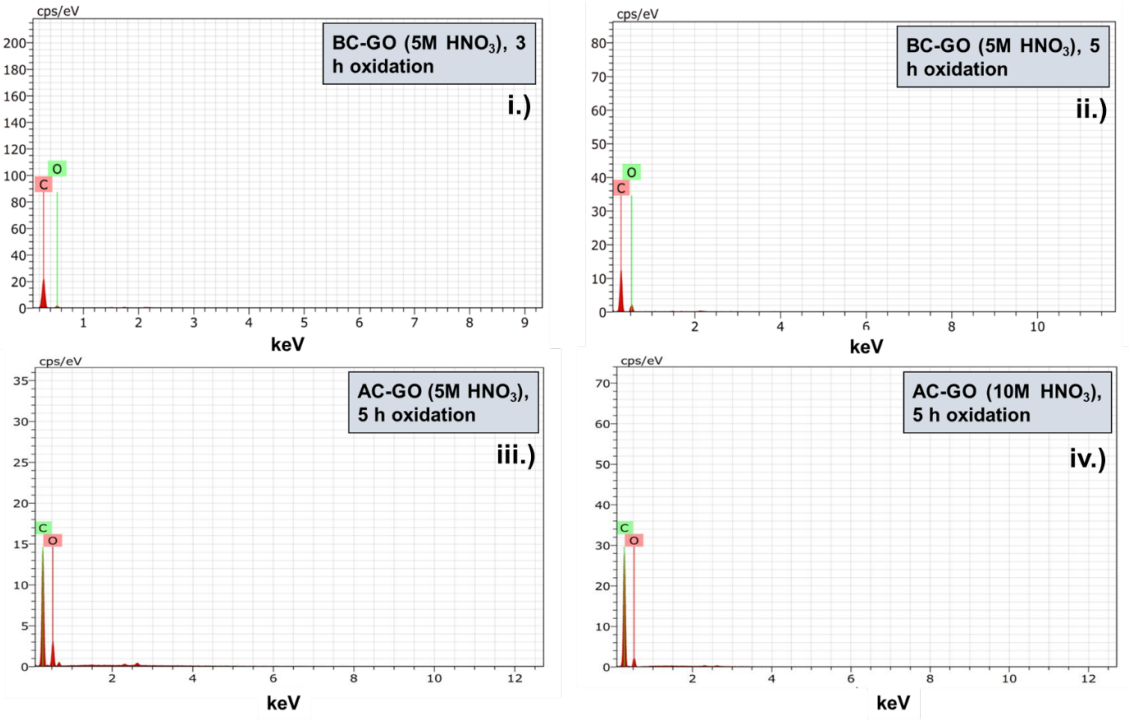

Figure 2.5. EDX spectra for i.) 5 M HNO_3 subjected BC-GO with oxidation reaction time, 3 hours, ii.) 5 M HNO_3 subjected BC-GO with oxidation reaction time, 5 hours, iii.) 5 M HNO_3 subjected AC-GO with oxidation reaction time, 5 hours, iv.) 10 M HNO_3 subjected BC-GO with oxidation reaction time, 5 hours

Table 2.7. Elemental composition of AC-GO and BC-GO at different acid concentration and oxidation time

Elements	**BC-GO (5M HNO_3), 3h oxidation Weight %**	**BC-GO (5M HNO_3), 3h oxidation Atomic %**	**BC-GO (5M HNO_3), 5h oxidation Weight %**	**BC-GO (5M HNO_3), 5h oxidation Atomic %**	**AC-GO (5M HNO_3), 5h oxidation Weight %**	**AC-GO (5M HNO_3), 5h oxidation Atomic %**	**AC-GO (10M HNO_3), 5h oxidation Weight %**	**AC-GO (10M HNO_3), 5h oxidation Atomic %**
C	84.12	87.59	70.34	75.95	80.48	84.60	67.07	73.07
O	15.88	12.41	29.66	24.05	19.52	15.40	32.93	26.93
Total	100.00		100.00		100.00		100.00	

SEM analysis was conducted for raw coals before and after ball milling to examine their morphological changes. Figures 2.6 (a, b) and Figures (d, e) display the SEM images of bituminous coal before and after ball milling. The images clearly depict a significant reduction in particle size. Prior to ball milling, raw AC and BC appear as big chunks, but after ball milling, smaller chunks became dominant. Most of the particles were less than 10 microns, which were later subjected to purification. The SEM images for AC-GO and BC-GO, as shown in Figure 2.6c and 2.6f, revealed a flaky texture. The irregular shape and inconsistent particle size may be attributed to cracking of structure during oxidation step accompanied by high temperatures during the one-pot process.

The TEM images in Figures 2.6g-6j reveal a multilayer structure for the prepared samples. The observed layered structure of AC-GO and BC-GO is consistent with previous studies. For instance, Aziz et al. [45] showed the morphology of synthesized GO via TEM micrographs. The images showed flat flaky texture with irregular and random particle size, which is consistent with the findings of our study. Similarly, Yang et al. [46] worked on reduced graphene oxide sheets synthesis adorned with gold nanoparticles. The TEM image of bare GO in their work also revealed few-layered GO with few microns dimension.

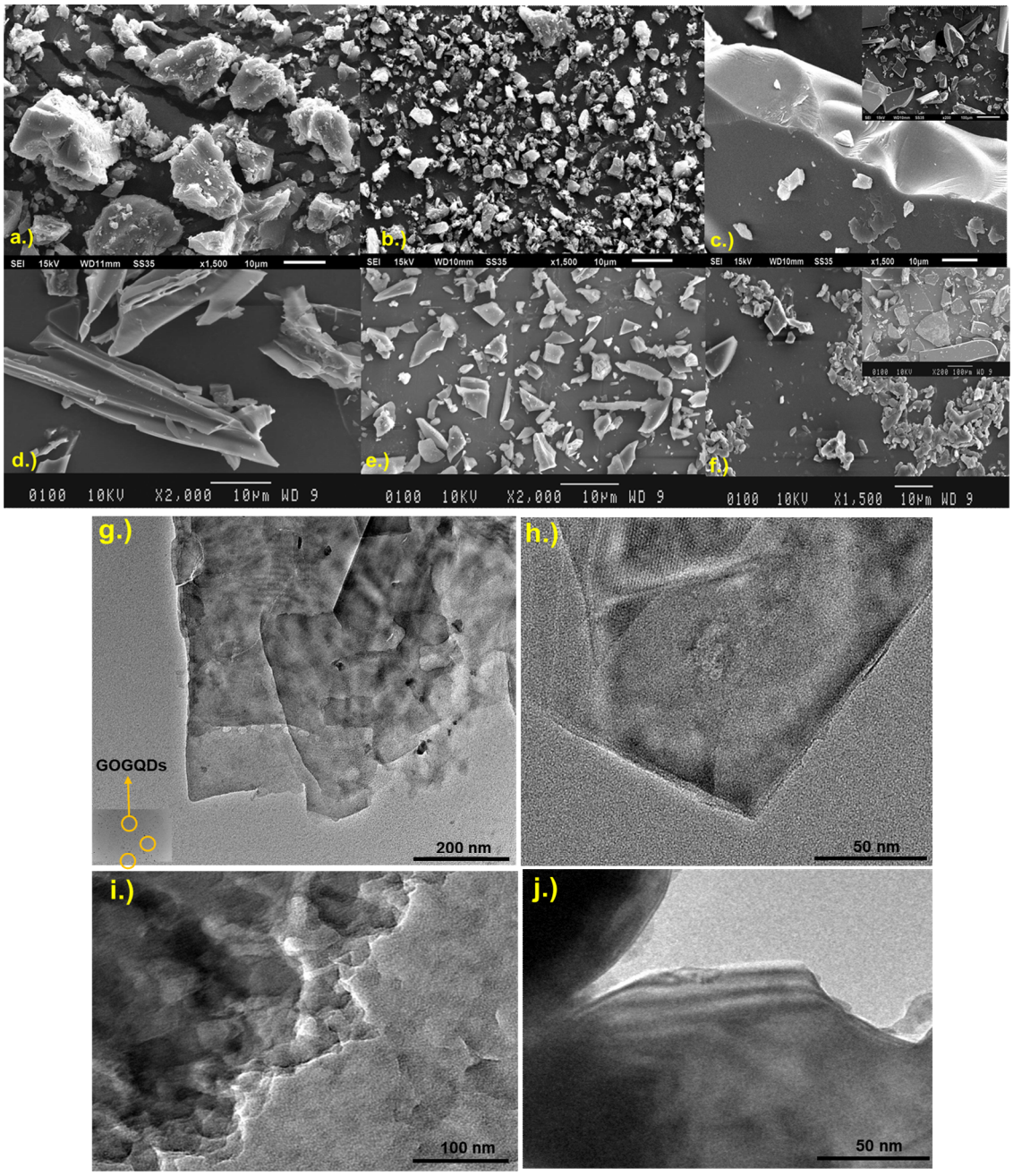

Figure 2.6. i) SEM images: a) Raw anthracite coal chunks, b) Ball milled anthracite coal, c) AC-GO, d) Raw bituminous coal chunks, e) Ball milled bituminous coal, f) BC-GO; ii) TEM images: g, h) AC-GO (the yellow circles in 4g refer to graphene oxide quantum dots formed during the synthesis of AC-GO, i, j) BC-GO

Ciplak et al. [47] prepared Graphene/Ag nanocomposite for their study. Their GO FTIR spectra reveal a strong O-H stretching vibration at 3410 cm^{-1} because of extensive oxidation. This strong O-H vibration is observed in the AC-GO and BC-GO in our study as well. The other peaks in their study corresponds to C=O, O-H, C-O vibrations consistent with our results. Mostly, the results procured and analyzed in the current study are consistent with the previous studies.

The Atomic Force Microscopy (AFM) analysis revealed that the height of BC-GO primarily ranged between 2.5 and 3.0 nm, with lateral dimensions smaller than 170 nm, as depicted in Figure 2.7. These findings, coupled with the previously mentioned TEM images, provide additional substantiation for the successful extraction of thin layered nanostructures of BC-GO through HNO_3 treatment of bituminous coal.

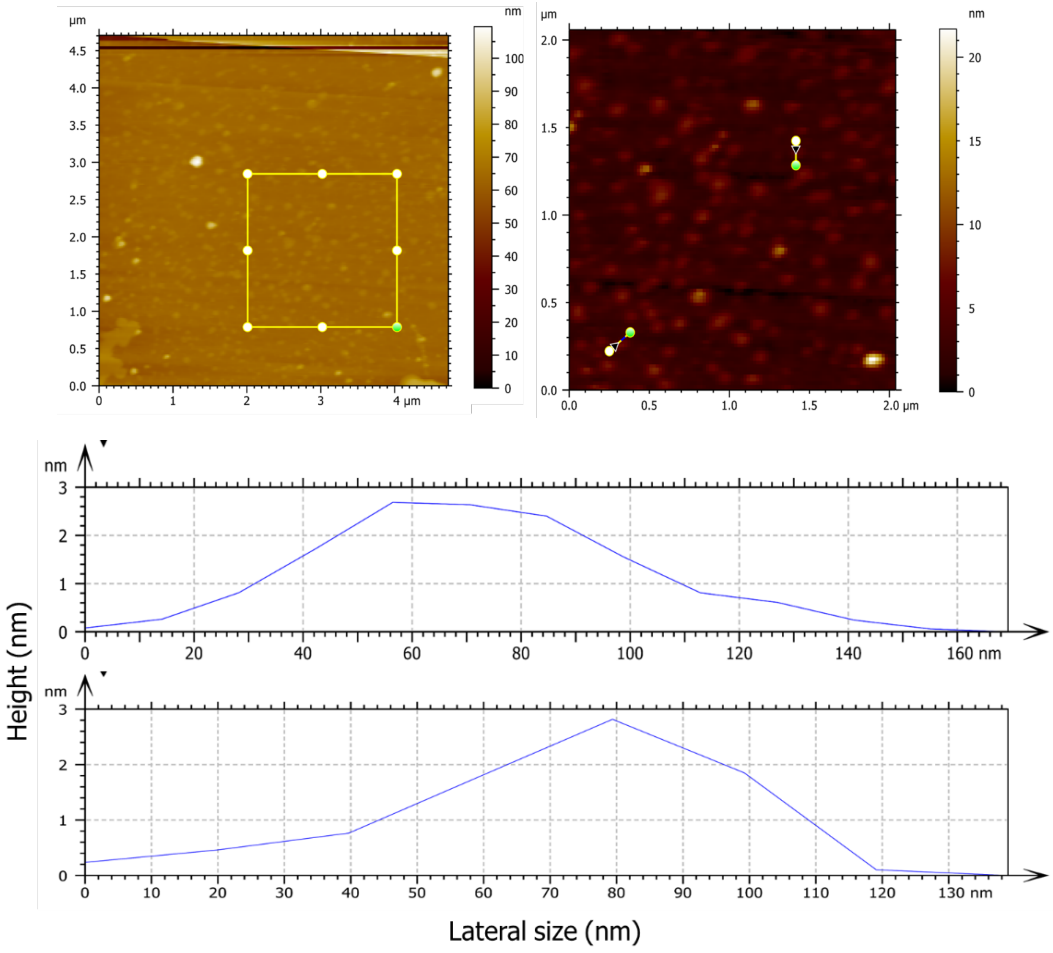

Figure 2.7. AFM image of BC-GO and corresponding height profile

2.3.5 Surface properties of BC-GO and AC-GO

XPS was used for analyzing the internal bonding in the samples and elemental analysis of the samples [48]. For purified coals, BC-GO and AC-GO, the C1s spectra ranged from 280 eV to 294 eV (Figure 2.8(a-d)), with a dominant peak at 284.8 eV corresponding to C=C, sp^2 C groups or C-H group and a region of extended tailing into the higher binding energy characterized by 285.8 eV ± 0.2 eV (C-C, sp^3 carbon bonded directly to oxygen in OH configurations), 286.5 eV ± 0.2 eV (C-O-C, epoxide), and 287.6 eV ± 0.2 eV (>C=O, carbonyl).

The presence of phenolic functional groups in the graphitic samples was identified by the bifurcation of the singlet O1s peaks. The samples exhibit bands at 532.38 eV for PAC, 533.17 eV for PBC, 532.43 eV for BC-GO and around 532.63 eV for AC-GO. These peaks correspond to C = O (oxygen double bonded to aromatic carbon), C–O (oxygen single bonded to carbon), and C-OH (carbon single bond to the hydroxyl group), respectively as depicted in Figure 2.8(e-h). In Figure 2.8(i-l), the N XPS spectrum displays a peak signifying amine R-NH_2 in carbon samples and pyrrole-type N at 400 eV.

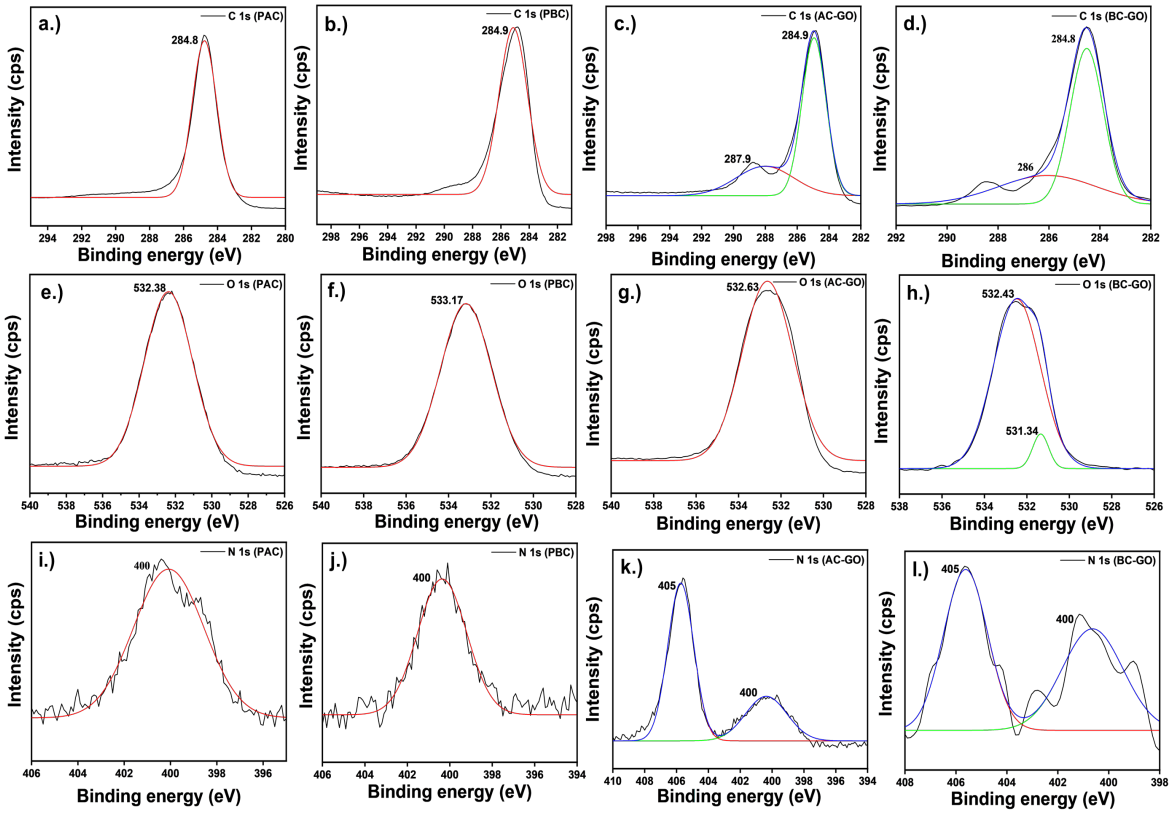

Figure 2.8. XPS analysis: a-d) C 1s spectra of PAC, PBC, AC-GO, BC-GO; e-h) O 1s spectra of PAC, PBC, AC-GO, BC-GO i-l) N 1s spectra of PAC, PBC, AC-GO, BC-GO

For the PAC and PBC, the results are consistent with the EDX analysis, suggesting that the N content may have been inherited from the coalification process. However, the peak at 405 eV in both synthesized AC-GO and BC-GO can be attributed to graphitic N, which is a result of the one-pot process employed in our synthesis. Figure 2.9 contains the survey spectrum for respective synthesized GO and their precursor moieties.

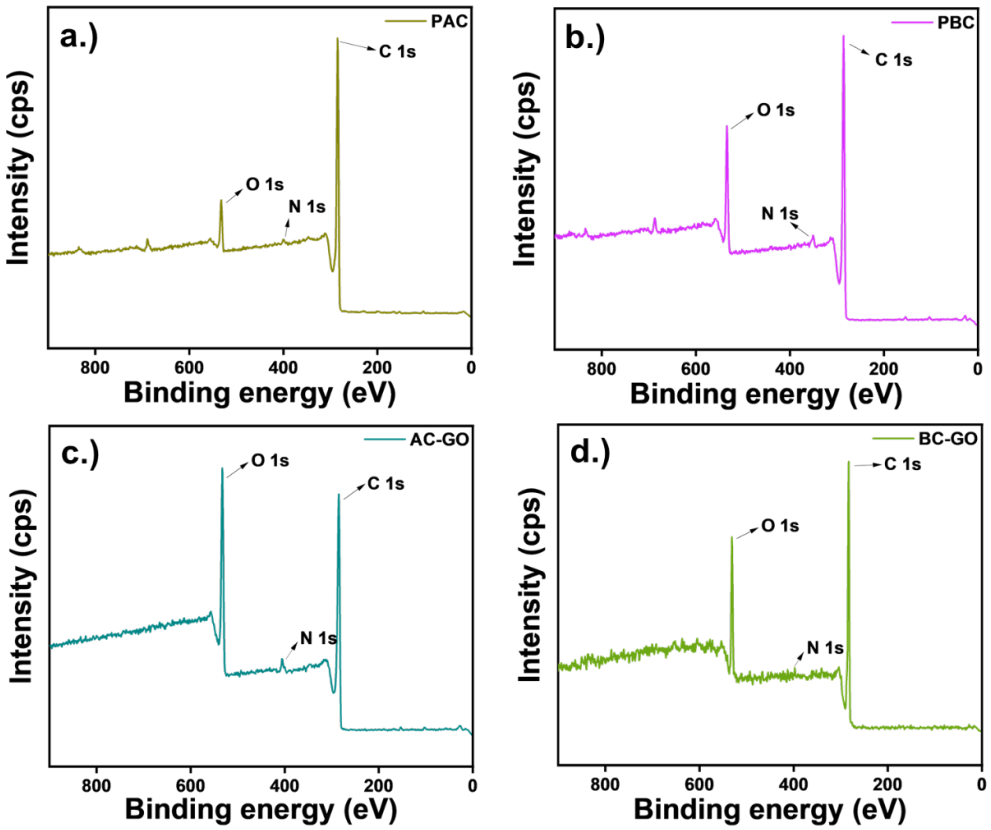

Figure 2.9. XPS survey spectrum for precursors, PAC and PBC and synthesized GO, AC-GO and BC-GO

To investigate the diverse functionalities and molecular structure of our samples, we conducted FTIR analysis [49]. The FTIR spectrum was recorded in the range of 4000-500 cm^{-1}, as depicted in Figure 2.2C. In purified Indian semi-anthracite coal and bituminous coal, a broad and noticeable absorption peak was observed at 3450 cm^{-1}, indicating the presence of O-H functionalities in their stretching vibration mode. Additionally, peaks observed at 1638 cm^{-1} and 1633 cm^{-1} in PAC and PBC, respectively, correspond to strong C=C stretching vibrations. The purified coals exhibited significantly fewer functional groups. In the synthesized AC-GO and BC-GO, additional functional groups were observed. The peaks at 3490 cm^{-1} and 3468 cm^{-1} in AC-GO and BC-GO correspond to the O-H stretching mode [50]. This finding is in alignment with the GO FTIR spectra presented by Ciplak et al. [47] in their study on graphene/Ag nanocomposite, where they

observed a strong O-H stretching vibration at 3410 cm^{-1} due to extensive oxidation. The presence of other peaks in their study corresponding to C=O, O-H, C-O vibrations are also consistent with our results. The peaks at 2983 cm^{-1}, 1913 cm^{-1}, 1710 cm^{-1}, and 1181 cm^{-1} correspond to C-H stretching vibration, C=C=C stretch, C=O stretching and C-N stretching vibrational mode, where C-N stretch refers to the presence of N in coal's inherent structure, arising from degraded plant matter. In the case of synthesized BC-GO, the peaks at 2457 cm^{-1}, 1706 cm^{-1}, and 1229 cm^{-1} are associated with vibrational bands of $-CH_2$, C=O stretching, and C-N stretching mode, respectively. Moreover, distribution and content of oxygen-related functional groups, may vary and cannot be directly compared with conventionally prepared GO, as synthesis scheme, oxidative agents, and level of application are different.

2.3.6 Structural, topological, and morphological properties of GO synthesized using modified Hummers' method

In this section, we compare the structural, topological and morphological properties of graphene oxide synthesized from semi-anthracite coal and graphite using modified Hummers' method. Our main objective was to assess the effect of different oxidizing agents used in the modified Hummers' method on the properties of the two GOs: one obtained from graphite (MHM-GO) and other from semi-anthracite coal (AC-GO (MHM)). Initially, we aimed to include GO synthesized from bituminous coal using MHM, but unlike the semi-anthracite coal, the bituminous coal completely dissolved under the influence of such strong oxidizing conditions.

First, we focus on the XRD spectra for MHM-GO and AC-GO (MHM). For MHM-GO, the XRD spectrum displays characteristic peaks at $2\theta = 9.1^0$ and 44^0 corresponding to (001) and (100) plane, respectively (Figure 2.10a). Further, consistent with previous studies, the calculated values of L_c and N_c for MHM-GO are 5.01 and 6-7 layers which are lower than those for graphite ($2\theta = 26^0$, L_c = 32 and N_c = 95-96 layers), suggesting thorough exfoliation of graphite by intercalating oxygen functionalities during oxidation in Hummers' method. This is consistent with the finding reported

by Lee et al. [51] in their study on the fabrication of GO/rGO Janus film in which they prepared GO via Hummers' method using graphite as precursor. Their XRD analysis showed the typical diffraction peak at $2\theta = 10.5^0$ of C (001), which indicates thorough exfoliation of graphite by the intercalation of oxygen functionalities.

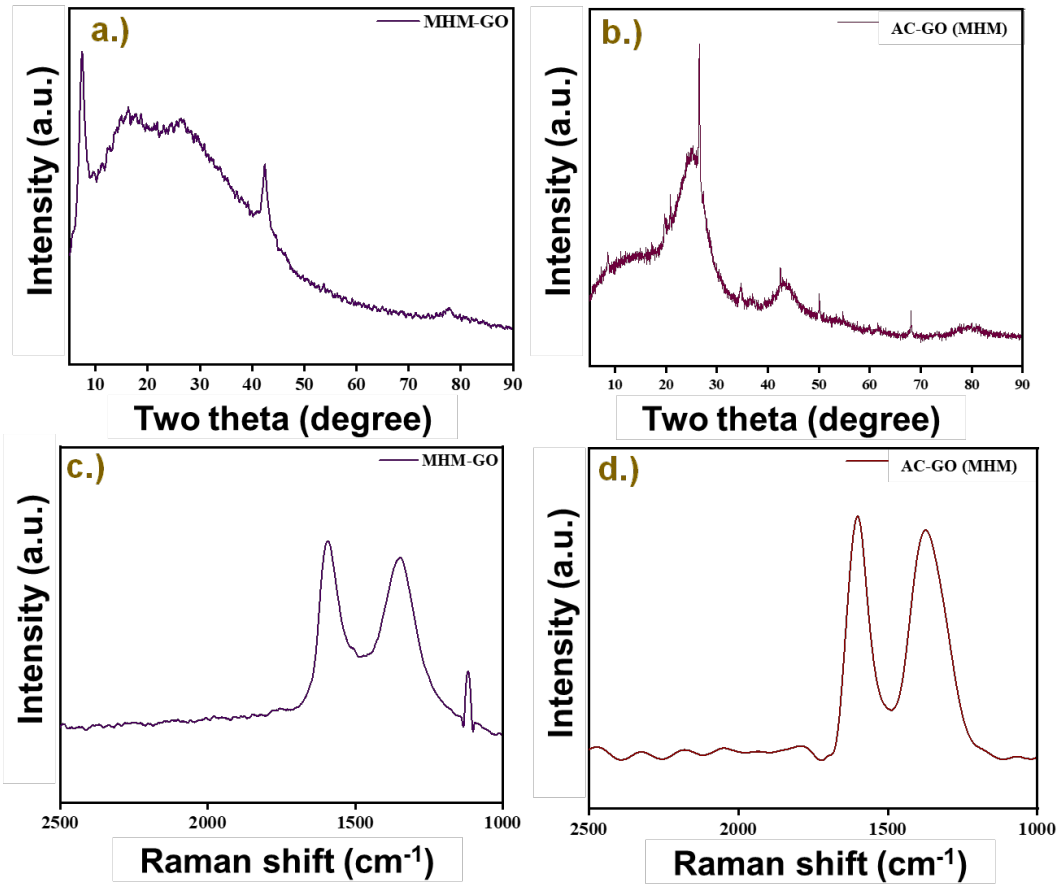

Figure 2.10. a.) XRD spectra of graphite derived GO (MHM-GO), b.) XRD spectra of coal derived GO (Coal-GO (MHM)), c.) Raman spectra of graphite derived GO (MHM-GO), d.) Raman spectra of coal derived GO (Coal-GO (MHM))

The AC-GO (MHM), on the other hand, shows additional peaks, corresponding to the impurities, apart from the (002) graphitic phase, indicating the unsuitability of the MHM for synthesizing GO from semi-anthracite coal (Figure 2.10b). In addition, we compared the yield of GO produced from semi-anthracite using MHM with that obtained through the one-pot process. The former is found to be eight times lower than the latter, clearly indicating that the one-pot process is the

preferred route for converting coal to GO. This is due to two entirely different mechanisms at play in the two methods of synthesis (one-pot and modified Hummers'). As pointed out in [31], the modified Hummers' method allows the exfoliation of nicely stacked AB-carbon of bulk graphite in the *c*-direction in which the graphene sheets are orderly stacked in a large number, whereas the newly developed one-pot method is based on scissoring of the links between amorphous and graphitic domains and extraction of those graphitic regions of coal, which unlike graphite contains turbostatic graphitic carbon arrangement.

Next, we analyze the Raman spectra for MHM-GO and AC-GO (MHM) for differences, if any. The Raman spectrum of MHM-GO (Figure 2.10c) is typical of graphite-derived GO, exhibiting a D band at 1353 cm^{-1} and a G band at 1605 cm^{-1}. The I_D/I_G ratio of 0.86 indicates a highly ordered structure of graphite-GO. The Raman spectrum of AC-GO (MHM) is almost similar to that of the MHM-GO suggesting the presence of similar structural moieties in both of them (Figure 2.10d).

Figure 2.11 depicts the BET/BJH plots for AC-GO (MHM). Interestingly, the specific surface area for the MHM-GO was also comparable to the BC-GO but the surface area for AC-GO (MHM) was also quite low.

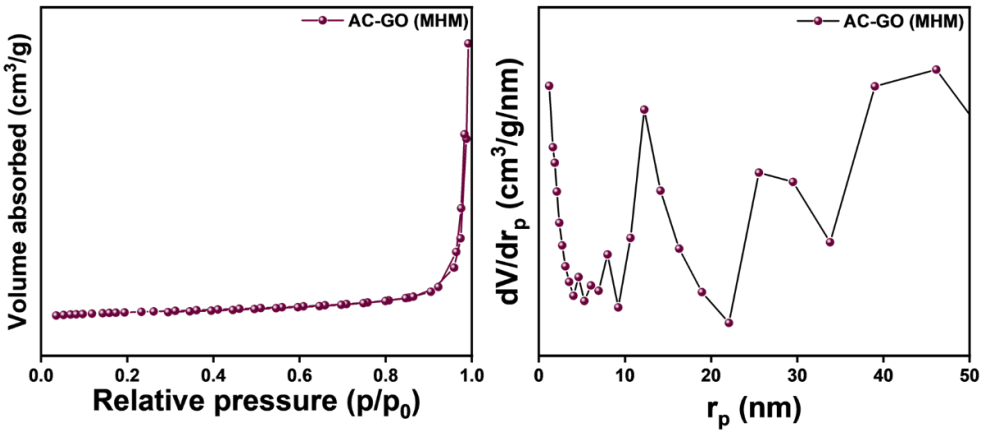

Figure 2.11. BET/BJH of AC-GO (MHM)

Moving on to the FTIR spectra, Figure 2.12a shows the spectrum for MHM-GO, where the peak at 1620 cm^{-1} is attributed to C=C stretching of the unoxidized graphite. The peaks at 1727 cm^{-1}

and 1170 cm^{-1} represent the C=O stretches of carboxyl group and the C-OH stretches of alcoholic group, respectively. In contrast, in the FTIR spectrum (Figure 2.12b) for AC-GO (MHM), the O-H peak almost disappears, indicating a lower level of oxygen functionalities in it.

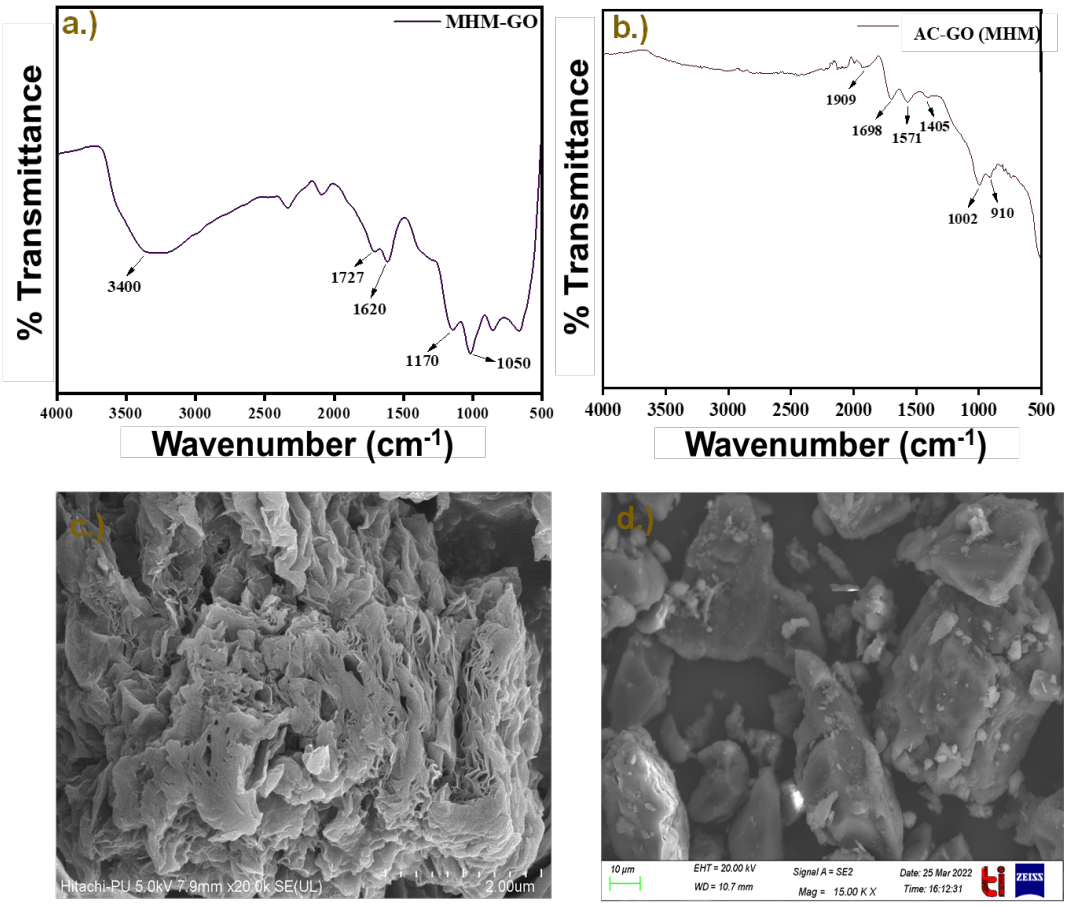

Figure 2.12. a-b.) FTIR spectra for MHM-GO and AC-GO (MHM), c-d.) SEM images of MHM-GO and AC-GO (MHM)

The peak at 1050 cm^{-1} is attributed to C-O stretching vibrations of C-O-C group. It is worth noting that the functional groups in AC-GO and BC-GO prepared by the one-pot method are comparable to those in GO synthesized using modified Hummers' method. The SEM morphology of AC-GO (MHM) is also quite similar to that of AC-GO and BC-GO, see Figure 2.12d. In the case of MHM-GO, the SEM image reveals the aggregated morphology of GO sheets, as represented in

Figure 2.12c. Thus, collectively, the FTIR and XPS analyses confirm that AC-GO and BC-GO have abundant functionalities comprising of oxygen and nitrogen, along with graphitic structures.

2.4. Mechanism for one-pot synthesis of GO from Indian coals

Graphite has been the precursor of choice for synthesizing graphene oxide via Hummers' method or its modified versions [52]. The mechanism which is accepted involves the formation of three intermediates during the synthesis, which are as follows:

1. First intermediate (H_2SO_4–GIC): Transformation of graphite to the sulfuric acid–graphite intercalation compound (GIC) in an acidic oxidizing medium.
2. Second intermediate (PGO): GIC is an oxidized form of graphite (pristine graphite oxide, PGO) in which oxidant diffusion takes place into preoccupied graphite galleries.
3. Third intermediate (GO): Alteration of PGO to graphene oxide involving the reaction of PGO with water.

Essentially, oxidation initiates at the active sites of the graphitic surfaces. In presence of strong oxidizing agents deployed in the Hummers' method, oxidation advances and penetrates into adjacent stacked layers of graphene on the basal plane by splitting O_2 gas in adjoining graphene layers [31,46]. Exfoliation of graphite takes place corresponding to AB-stacked carbon in c-direction, and graphene layers are largely piled up in regular fashion.

For GO synthesized from coals using HNO_3 as an oxidizing agent, the mechanism is quite different. As first postulated by Lee and Mahajan [32], scissoring of linkages in-between graphitic and amorphous domains and extraction of those domains occurs where graphite layering are irregularly arranged. Based on a study by Lyubchik et al. [53] on the reaction between anthracite coal and NO_3 acid leading to coal swelling and subsequent release of NO_2 as a by-product, Lee and Mahajan [32] proposed the following model:

$$2HNO_3\ (g) \longrightarrow 2HNO_3\ (ad) \longleftrightarrow NO_2^+\ (ad) + NO_3^-\ (ad) + H_2O$$

$$C_n + NO_2^+ (ad) \longrightarrow C_n^+ + NO_2 (g)\uparrow$$

$$C_n^+ + NO_3^- (ad) + mHNO_3 (ad) \longrightarrow C_n^+NO_3^n nmHNO_3^n (IC\ compound)$$

where, g represents the gas phase; ad shows adsorption on surface of carbon; IC is the abbreviation for intercalation. It was further noticed that increase in HNO_3 concentration pertaining to intercalation behaviour resulted in decrease of crystalline structure. Figure 2.13(a,b) shows a comparative flow chart/mechanism for oxidation and exfoliation of GO from graphite using Hummers' method, and from coals using one-pot process. Although there are variations in the concentration of HNO_3 and the oxidation time for anthracite and bituminous coals, we believe that the mechanism proposed above applies to both the coals.

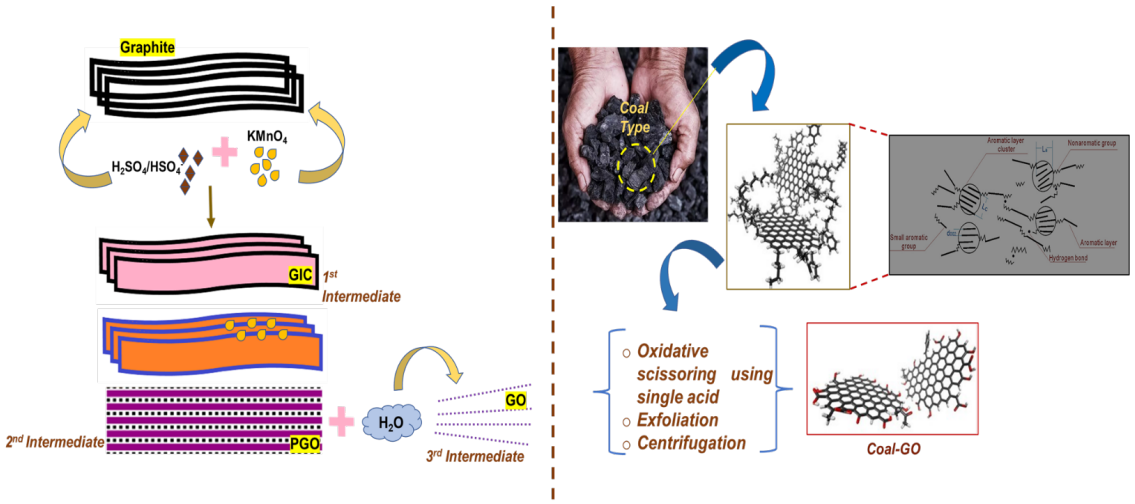

Figure 2.13. Mechanistic scheme for comparison between two different approaches of GO synthesis (a) Hummers' method, (b) One-pot process

2.5. Application of Coal-GO in Glass fiber-based epoxy nanocomposites for improved mechanical behaviour of GFRP nanocomposites

The use of graphene oxide (GO) as an additive, either alone or in conjunction with glass fibers, has garnered significant attention in recent years, from both academia and industry [54]. This is due to its remarkable ability to considerably improve mechanical, electrical, and thermal

properties, even at very low concentrations. A growing amount of interest in GO-based technology has been seen in both academia and industry [54]. The improvement in strength and toughness of nano composites obtained by incorporating nanoparticles in polymer matrices is attributed to the multiple effects such as increase in the interfacial bonding between the epoxy matrix and the nanofillers, leading to improved load transfer and stress distribution within the composite material, and acting as reinforcing agents by limiting the movement of polymer chains, preventing crack propagation [55]. Several studies have demonstrated the potential of graphite-derived GO as a nanofiller in glass fiber-reinforced polymer (GFRP) nanocomposites in improving mechanical performance [56],[57],[58]. However, to the best of our knowledge no study has been conducted to investigate the potential of coal-derived GO synthesized using the one-pot method in GFRP nanocomposites.

We have conducted a systematic study in which we utilized anthracite-coal-derived GO and studied its reinforcement effect in GFRP nanocomposites, utilizing epoxy as the matrix. The methodology followed for fabrication of GFRPs using AC-GO is described in Section S3. All calculations and data analysis were compared to the control composite (epoxy and glass-fiber), abbreviated as $GFRP_0$.

As illustrated in Figure 2.14, at 0.125 phr loading of AC-GO in GFRP (referred to as A-$EGF_{0.125}$), all the mechanical properties reached their maximum levels compared to GFRP composite with no loading ($GFRP_0$). The tensile strength, tensile modulus, flexure strength and flexure modulus were enhanced by 18.3%, 30.9%, 22.7% and 25.1%, respectively, as shown in Figures 2.14a, b, c, and d. The impact strength, however, experienced a relatively smaller increase of only 6% compared to $GFRP_0$, see Figure 2.14e. These rather significant improvements in mechanical properties can be attributed to the presence of abundant functional groups in AC-GO, which promote better dispersion and enhanced adhesion between oxygen-related functional groups on GO and epoxy resin and hardener. Furthermore, dynamic light scattering (DLS) studies revealed an average

particle size distribution of 0.17 μm for AC-GO. This small particle size distribution provides a larger surface area available for polymer/filler bonding, promoting effective dispersion, and the associate benefits discussed earlier. It is clear from the bar charts in Figure 2.14 that increasing the concentration of GO beyond the optimized value leads to a significant drop in the mechanical strength of the composites. This decrease can be attributed to the high viscosity of the resin system and the aggregation of AC-GO at higher nanofiller loadings, which act as stress concentration sites [59].

Figure 2.14f presents the XRD spectra of $GFRP_0$ and the synthesized A-EGF nanocomposites at different concentrations of nanofillers. The absence of d(002) peak, which varies in shape among different compositions, and the presence of an identical peak across different AC-GO compositions indicate that the morphology of the reinforced EGFPs is largely exfoliated, irrespective of the composition. These XRD results are consistent with the studies reported in [60],[61]. Additionally, the oxygen-based functional groups present on the glass fiber react with the hydroxyl functional groups on the surface of the GOs during the curing process, resulting in a substitution reaction. GO also bonds with epoxy polymer via hydrogen bonding [62].

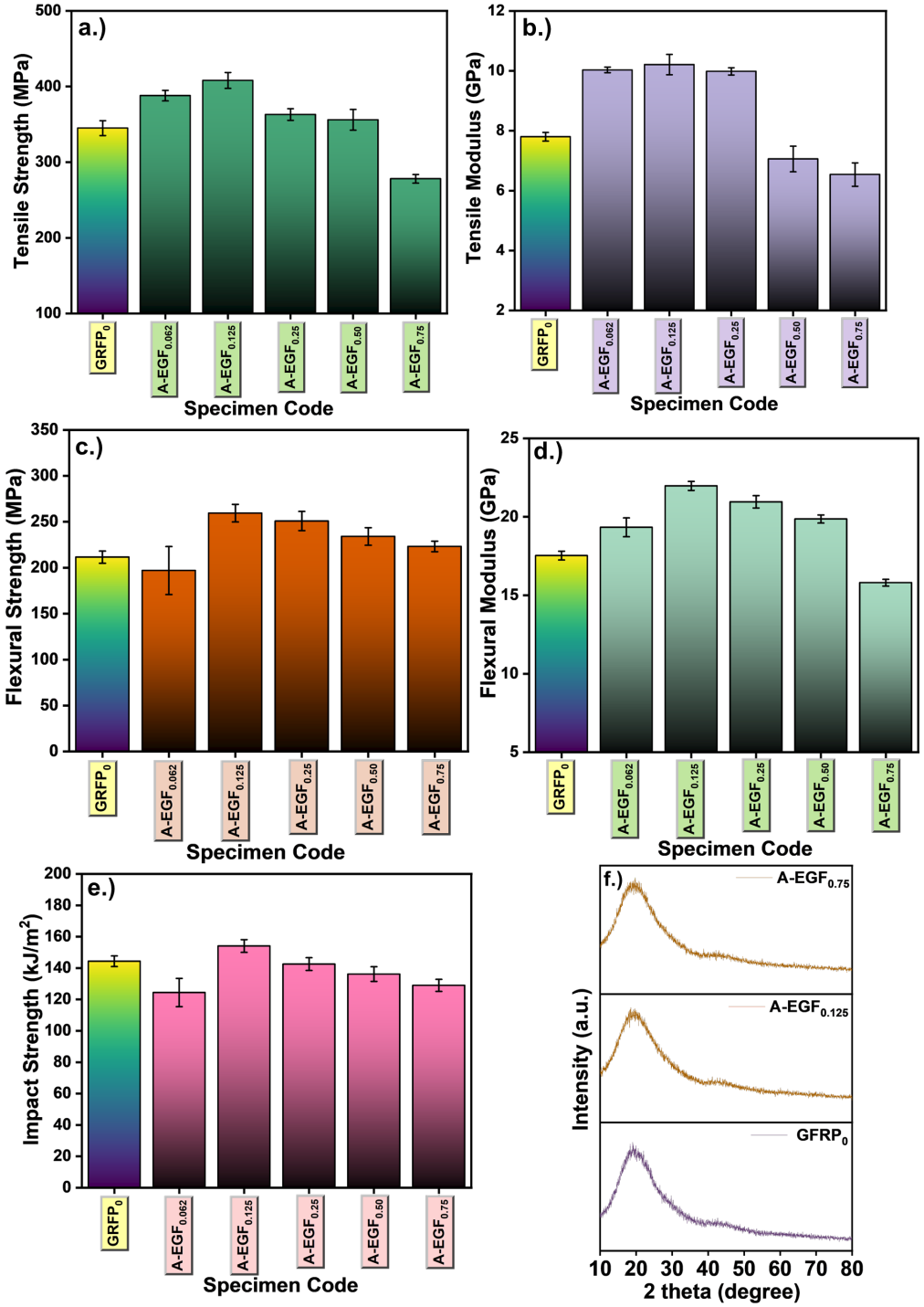

Figure 2.14. Mechanical properties of AC-GO based GFRP composites a,b) Tensile strength and Tensile modulus c, d) Flexural strength and Flexural modulus e) Impact strength f) XRD spectra of control sample, GFRP and AC-GO incorporated GFRP

GFRPs offer an ideal solution for applications where enhanced mechanical properties (tensile, flexural and impact strength) are the prime requirement, while maintaining low weight of the structures. The data presented in this paper suggests that the versatility of these materials can be further expanded by the availability of various precursors and associated processing techniques. This flexibility in the choice of the precursor and associated processing methods extends beyond GFRPs to other applications using GO such as electronic devices, energy storage devices, supercapacitors, membranes, catalysts, and water purification systems [63],[64][65].

Conclusion

In this comprehensive investigation, we have conducted an extensive experimental study aimed at extending the recently developed one-pot process for synthesizing GO for semi-anthracite coal to bituminous coal, which is abundantly available in India. Additionally, we also assessed the applicability of the original process to anthracite coal available in India. Another focus of our study was to explore the potential applications of coal-derived GO and evaluate its impact as a nanofiller on the mechanical properties of a commonly used Glass Fiber Resin Polymer (GFRP). The major takeaways from our study are as follows:

- We identified the optimal processing parameters for bituminous coal, including a concentration of 5M HNO_3 and an oxidation time of 5 hours.
- Interestingly, we observed that at higher HNO_3 concentrations, bituminous coal dissolved completely, and even at 5 M with extended oxidation times (> 5 hours), it either dissolved completely or very less yield was obtained. The inference is that the concentration and oxidation time are important parameters in the synthesis of GO.
- For the semi-anthracite coal in India, with minor changes in composition from the sample used in the development of the original process, the original recipe using 16 M HNO_3 and 72 hours of oxidation worked well.

- TEM and SEM analyses revealed the flaky texture and stacked sheets of GO synthesized from both bituminous and semi-anthracite coal. FTIR studies indicated the appearance of carboxylic functionalities predominantly at the edges of the graphitic surface predominantly, suggesting minimal impact of HNO_3 in the c-direction.
- Raman spectra of BC-GO shows quite low I_D in comparison to AC-GO which correlates well with the use of less concentrated HNO_3 used, resulting in fewer defects and preservation of the graphitic domains. Furthermore, BC-GO exhibited a broad H1 loop, suggesting the presence of mesopores.
- Incorporating AC-GO as a nanofiller in GFRP composites resulted in significant improvements in their mechanical properties. The tensile strength and tensile modulus increased by 18.3% and 30.9% while the flexural strength and flexural modulus increased by 22.7% and 25.1%, respectively. Additionally, a small increase (6.7%) was observed in the impact strength at a loading of 0.125 phr of AC-GO in GFRP composites.

Looking ahead, future research and development efforts can continue to explore and harness the potential of GO in various industries. The versatility and unique properties of GO offer opportunities for advancements and these areas, leading to advancements and breakthroughs in various applications such as electronics, energy storage devices, membranes, catalysts, and water purification systems, to name a few. Mostly, the results procured and analyzed in the current study are consistent with the previous studies. In addition to low hazardous chemicals footprint, the one-pot process extended to bituminous coal lends itself to scale-up. This should open up opportunities for applications in different market segments such as sensing, fiber-reinforced polymer nanocomposites, drug delivery, Li-ion batteries and others.

- In the next chapter, a comparative study for the effect of various precursor-based graphene oxide (GO) nanofillers on enhancing the mechanical performance of E-glass fiber reinforced

epoxy resin composites (EGFPs) has been carried out. GO derived from bituminous coal (BC-GO) and graphite (Gr-GO) were dispersed into epoxy resin matrix. The resulting mixture was combined with E-glass fiber mats using vacuum-assisted resin infusion molding. The synthesized BC-GO and Gr-GO based EGFPs have been evaluated for different mechanical properties (Tensile, Flexural and Impact properties).

References

[1] P.P. Brisebois, M. Siaj, Harvesting graphene oxide-years 1859 to 2019: A review of its structure, synthesis, properties and exfoliation, J. Mater. Chem. C. 8 (2020) 1517–1547. https://doi.org/10.1039/c9tc03251g.

[2] A. Garg, S. Basu, N.P. Shetti, K.R. Reddy, 2D materials and its heterostructured photocatalysts: Synthesis, properties, functionalization and applications in environmental remediation, J. Environ. Chem. Eng. 9 (2021) 106408. https://doi.org/10.1016/j.jece.2021.106408.

[3] Y. Zhu, D.K. James, J.M. Tour, New routes to graphene, graphene oxide and their related applications, Adv. Mater. 24 (2012) 4924–4955.

[4] W.S. Hummers, R.E. Offeman, Preparation of Graphitic Oxide, J. Am. Chem. Soc. 80 (1958) 1339. https://doi.org/10.1021/ja01539a017.

[5] J. Sturala, J. Luxa, M. Pumera, Z. Sofer, Chemistry of graphene derivatives: Synthesis, applications, and perspectives, Chem. Eur. J. 24 (2018) 5992–6006.

[6] L. Shahriary, A. a. Athawale, Graphene Oxide Synthesized by using Modified Hummers Approach, Int. J. Renew. Energy Environ. Eng. 02 (2014) 58–63.

[7] M. Choucair, P. Thordarson, J.A. Stride, Gram-scale production of graphene based on solvothermal synthesis and sonication, Nat. Nanotechnol. 4 (2009) 30–33.

https://doi.org/10.1038/nnano.2008.365.

[8] D.C. Marcano, D. V Kosynkin, J.M. Berlin, A. Sinitskii, Z. Sun, A. Slesarev, L.B. Alemany, W. Lu, J.M. Tour, Improved Synthesis of Graphene Oxide, 4 (n.d.).

[9] A.T. Habte, D.W. Ayele, M. Hu, Synthesis and Characterization of Reduced Graphene Oxide (rGO) Started from Graphene Oxide (GO) Using the Tour Method with Different Parameters, Adv. Mater. Sci. Eng. 2019 (2019). https://doi.org/10.1155/2019/5058163.

[10] F. Farjadian, S. Abbaspour, M.A.A. Sadatlu, S. Mirkiani, A. Ghasemi, M. Hoseini-Ghahfarokhi, N. Mozaffari, M. Karimi, M.R. Hamblin, Recent Developments in Graphene and Graphene Oxide: Properties, Synthesis, and Modifications: A Review, ChemistrySelect. 5 (2020) 10200–10219. https://doi.org/10.1002/slct.202002501.

[11] J. Chen, B. Yao, C. Li, G. Shi, An improved Hummers method for eco-friendly synthesis of graphene oxide, Carbon N. Y. 64 (2013) 225–229. https://doi.org/10.1016/j.carbon.2013.07.055.

[12] A. Bianco, H.M. Cheng, T. Enoki, Y. Gogotsi, R.H. Hurt, N. Koratkar, T. Kyotani, M. Monthioux, C.R. Park, J.M.D. Tascon, J. Zhang, All in the graphene family - A recommended nomenclature for two-dimensional carbon materials, Carbon N. Y. 65 (2013) 1–6. https://doi.org/10.1016/j.carbon.2013.08.038.

[13] M. Cai, D. Thorpe, D.H. Adamson, H.C. Schniepp, Methods of graphite exfoliation, J. Mater. Chem. 22 (2012) 24992–25002. https://doi.org/10.1039/c2jm34517j.

[14] Y. Yan, F.Z. Nashath, S. Chen, S. Manickam, S.S. Lim, H. Zhao, E. Lester, T. Wu, C.H. Pang, Synthesis of graphene: Potential carbon precursors and approaches, Nanotechnol. Rev. 9 (2020) 1284–1314. https://doi.org/10.1515/ntrev-2020-0100.

[15] S. Abdolhosseinzadeh, H. Asgharzadeh, H.S. Kim, Fast and fully-scalable synthesis of reduced graphene oxide, Sci. Rep. 5 (2015) 1–7. https://doi.org/10.1038/srep10160.

[16] C. Botas, P. Álvarez, C. Blanco, R. Santamaría, M. Granda, M.D. Gutiérrez, F. Rodríguez-Reinoso, R. Menéndez, Critical temperatures in the synthesis of graphene-like materials by thermal exfoliation-reduction of graphite oxide, Carbon N. Y. 52 (2013) 476–485. https://doi.org/10.1016/j.carbon.2012.09.059.

[17] V.C. Hoang, M. Hassan, V.G. Gomes, Coal derived carbon nanomaterials – Recent advances in synthesis and applications, Appl. Mater. Today. 12 (2018) 342–358. https://doi.org/10.1016/j.apmt.2018.06.007.

[18] S.H. Vijapur, D. Wang, G.G. Botte, The growth of transparent amorphous carbon thin films from coal, Carbon N. Y. 54 (2013) 22–28. https://doi.org/10.1016/j.carbon.2012.10.065.

[19] H. Zeng, B. Xing, C. Zhang, Y. Nie, X. Qu, Applied Surface Science Edge-boron-functionalized coal-derived graphite nanoplatelets prepared via mechanochemical modification for enhanced Li-ion storage at low-voltage plateau, Appl. Surf. Sci. 621 (2023) 156870. https://doi.org/10.1016/j.apsusc.2023.156870.

[20] A.P.M. Leandro, M.A. Seas, K. Vap, A.S. Tyrrell, V. Jain, H. Wahab, P.A. Johnson, Evolution of structural and electrical properties in coal-derived graphene oxide nanomaterials during high-temperature annealing, Diam. Relat. Mater. 112 (2021) 108244.

[21] A. Kundu, B. Maity, S. Basu, Coal-derived graphene quantum dots with a Mn2+/Mn7+ nanosensor for selective detection of glutathione by a fluorescence switch-off-on assay, New J. Chem. 46 (2022) 7545–7556. https://doi.org/10.1039/d2nj00220e.

[22] H. Zeng, B. Xing, Y. Cao, B. Xu, L. Hou, H. Guo, S. Cheng, G. Huang, C. Zhang, Q. Sun, Insight into the microstructural evolution of anthracite during carbonization-graphitization process from the perspective of materialization, Int. J. Min. Sci. Technol. 32 (2022) 1397–1406. https://doi.org/10.1016/j.ijmst.2022.06.009.

[23] B. Pakhira, S. Ghosh, S. Maity, D.N. Sangeetha, A. Laha, A. Allam, S. Sarkar, Extraction of preformed graphene oxide from coal: its clenched fist form entrapping large molecules, RSC Adv. 5 (2015) 89076–89082.

[24] V. Purwandari, S. Gea, B. Wirjosentono, A. Haryono, Synthesis of graphene oxide from the Sawahlunto-Sijunjung coal via modified hummers method, AIP Conf. Proc. 2049 (2018). https://doi.org/10.1063/1.5082470.

[25] D.P. Savitskii, Preparation and characterization of colloidal dispersions of graphene-like structures from different ranks of coals, J. Fuel Chem. Technol. 45 (2017) 897–907.

[26] K. Hatakeyama, C. Ogata, M. Koinuma, T. Taniguchi, S. Hayami, K. Kuroiwa, Y. Matsumoto, Coal Oxide as a Thermally Robust Carbon-Based Proton Conductor, ACS Appl. Mater. Interfaces. 7 (2015) 23041–23046. https://doi.org/10.1021/acsami.5b06470.

[27] T.J. Park, S. Banerjee, T. Hemraj-Benny, S.S. Wong, Purification strategies and purity visualization techniques for single-walled carbon nanotubes, J. Mater. Chem. 16 (2006) 141–154. https://doi.org/10.1039/b510858f.

[28] B. Das, R. Kundu, S. Chakravarty, Preparation and characterization of graphene oxide from coal, Mater. Chem. Phys. 290 (2022) 126597. https://doi.org/10.1016/j.matchemphys.2022.126597.

[29] S. Hashmi, A. Mushtaq, R. Ahmed, Z.U. Ali, Synthesis and characterization of reduced graphene oxide from indigenous coal: A non-burning solution, Int. J. Membr. Sci. Technol. 9 (2022) 1–12.

[30] Y. Wu, Y. Ma, Y. Wang, L. Huang, N. Li, T. Zhang, Y. Zhang, X. Wan, Y. Huang, Y. Chen, Efficient and large scale synthesis of graphene from coal and its film electrical properties studies, J. Nanosci. Nanotechnol. 13 (2013) 929–932.

[31] E. Senthil Kumar, V. Sivasankar, R. Sureshbabu, S. Raghu, R. A Kalaivani, Facile synthesis of few layer graphene from bituminous coal and its application towards electrochemical sensing of caffeine, Adv. Mater. Lett. 8 (2017) 239–245.

[32] S.Y. Lee, R.L. Mahajan, A facile method for coal to graphene oxide and its application to a biosensor, Carbon. 181 (2021) 408–420. https://doi.org/10.1016/j.carbon.2021.05.007.

[33] Y.M. Wang, C.H. Zhang, Reduced Graphene Oxide Derived from Low-Grade Coal for High-Performance Flexible Supercapacitors with Ultrahigh Cyclability, Nanomaterials. 12 (2022). https://doi.org/10.3390/nano12172989.

[34] V. Purwandari, M. Rianna, I. Isnaeni, Y. Zou, M. Harahap, G. Halawa, R. Goei, A.I.Y. Tok, The role of biocatalysts in the synthesis of graphene nanosheets from sub-bituminous coal, Mater. Sci. Energy Technol. 6 (2023) 282–289.

[35] Mahajan, R. L.; Seul-Yi, L. E. E. U.S. Patent Application No. 17/415 4452022.

[36] R. Pietrzak, H. Wachowska, Low temperature oxidation of coals of different rank and different sulphur content, Fuel. 82 (2003) 705–713. https://doi.org/10.1016/S0016-2361(02)00364-2.

[37] O. Beyssac, B. Goffé, J.P. Petitet, E. Froigneux, M. Moreau, J.N. Rouzaud, On the

characterization of disordered and heterogeneous carbonaceous materials by Raman spectroscopy, Spectrochim. Acta - Part A Mol. Biomol. Spectrosc. 59 (2003) 2267–2276. https://doi.org/10.1016/S1386-1425(03)00070-2.

[38] Z.B. Siddique, S. Basu, P. Basak, Development of Graphene Oxide Dispersed Natural Ester Based Insulating Oil for Transformers, IEEE Trans. Dielectr. Electr. Insul. 28 (2021) 1326–1333. https://doi.org/10.1109/TDEI.2021.009445.

[39] A. Armano, S. Agnello, Two-Dimensional Carbon: A Review of Synthesis Methods, and Electronic, Optical, and Vibrational Properties of Single-Layer Graphene, C — J. Carbon Res. 5 (2019) 67. https://doi.org/10.3390/c5040067.

[40] A. Kaniyoor, S. Ramaprabhu, A Raman spectroscopic investigation of graphite oxide derived graphene, AIP Adv. 2 (2012) 0–13. https://doi.org/10.1063/1.4756995.

[41] J. Jo, S. Lee, J. Gim, J. Song, S. Kim, V. Mathew, M.H. Alfaruqi, S. Kim, J. Lim, J. Kim, Facile synthesis of reduced graphene oxide by modified Hummer's method as anode material for Li-, Na- And K-ion secondary batteries, R. Soc. Open Sci. 6 (2019). https://doi.org/10.1098/rsos.181978.

[42] S. Kai-Yi, T. Xiu-Xiang, H. Fen-Fen, H. Huan, J. Yong-Hua, L. Ji-Lan, Mechanism of oxidation of low rank coal by nitric acid, J. Coal Sci. Eng. 18 (2012) 396–399. https://doi.org/10.1007/s12404-012-0411-6.

[43] Q. Zhao, D. Chen, Y. Li, G. Zhang, F. Zhang, X. Fan, Rhodium complex immobilized on graphene oxide as an efficient and recyclable catalyst for hydrogenation of cyclohexene, Nanoscale. 5 (2013) 882–885. https://doi.org/10.1039/c2nr33290f.

[44] W.L. Zhang, H.J. Choi, Silica-graphene oxide hybrid composite particles and their electroresponsive characteristics, Langmuir. 28 (2012) 7055–7062.

https://doi.org/10.1021/la3009283.

[45] M. Aziz, F.S.A. Halim, J. Jaafar, Preparation and characterization of graphene membrane electrode assembly, J. Teknol. (Sciences Eng. 69 (2014) 11–14. https://doi.org/10.11113/jt.v69.3388.

[46] H. Yang, W. Zhou, B. Yu, Y. Wang, C. Cong, T. Yu, Uniform decoration of reduced graphene oxide sheets with gold nanoparticles, J. Nanotechnol. (2012). https://doi.org/10.1155/2012/328565.

[47] Z. Çiplak, N. Yildiz, A. Cąlimli, Investigation of graphene/Ag nanocomposites synthesis parameters for two different synthesis methods, Fullerenes Nanotub. Carbon Nanostructures. 23 (2015) 361–370. https://doi.org/10.1080/1536383X.2014.894025.

[48] F.T. Johra, J.W. Lee, W.G. Jung, Facile and safe graphene preparation on solution based platform, J. Ind. Eng. Chem. 20 (2014) 2883–2887. https://doi.org/10.1016/j.jiec.2013.11.022.

[49] S.R.B. Nazri, W.W. Liu, C.S. Khe, N.M.S. Hidayah, Y.P. Teoh, C.H. Voon, H.C. Lee, P.Y.P. Adelyn, Synthesis, characterization and study of graphene oxide, AIP Conf. Proc. 2045 (2018). https://doi.org/10.1063/1.5080846.

[50] Sudesh, N. Kumar, S. Das, C. Bernhard, G.D. Varma, Effect of graphene oxide doping on superconducting properties of bulk MgB2, Supercond. Sci. Technol. 26 (2013). https://doi.org/10.1088/0953-2048/26/9/095008.

[51] S.Y. Lee, R.B. Moore, R.L. Mahajan, An Al-assisted GO/rGO Janus film: Fabrication and hygroscopic properties, Carbon N. Y. 171 (2021) 585–596. https://doi.org/10.1016/j.carbon.2020.09.002.

[52] A.M. Dimiev, J.M. Tour, Mechanism of graphene oxide formation, ACS Nano. 8

(2014) 3060–3068. https://doi.org/10.1021/nn500606a.

[53] S.B. Lyubchik, L.Y. Galushko, A.M. Rego, Y. V. Tamarkina, O.L. Galushko, I.M. Fonseca, Intercalation as an approach to the activated carbon preparation from Ukrainian anthracites, J. Phys. Chem. Solids. 65 (2004) 127–132. https://doi.org/10.1016/j.jpcs.2003.10.006.

[54] A. Landesmann, C.A. Seruti, E.D.M. Batista, Mechanical properties of glass fiber reinforced polymers members for structural applications, Mater. Res. 18 (2015) 1372–1383. https://doi.org/10.1590/1516-1439.044615.

[55] D. kumar Gara, G. Raghavendra, P. Syam Prasad, O. S, Enhanced mechanical properties of glass fibre epoxy composites by 2D exfoliated graphene oxide filler, Ceram. Int. 47 (2021) 34860–34868. https://doi.org/10.1016/j.ceramint.2021.09.027.

[56] A.K. Pathak, H. Garg, M. Singh, T. Yokozeki, S.R. Dhakate, Enhanced interfacial properties of graphene oxide incorporated carbon fiber reinforced epoxy nanocomposite : a systematic thermal properties investigation, (2019).

[57] T. Topkaya, Y.H. Çelik, E. Kilickap, Mechanical properties of fiber/graphene epoxy hybrid composites, J. Mech. Sci. Technol. 34 (2020) 4589–4595.

[58] M.F. Maqsood, M.A.A. Zubair, M.A. Raza, S.M.Z. Mehdi, N. Lee, Z.U. Rehman, K. Park, M.U. Bhatti, U. Latif, A. Tawakkal, Fabrication and characterization of graphene oxide and glass fiber-based hybrid epoxy composites, Polym. Compos. 43 (2022) 8072–8083. https://doi.org/10.1002/pc.26952.

[59] T. Nanda, G. Sharma, R. Mehta, D. Shelly, K. Singh, Mechanisms for enhanced impact strength of epoxy based nanocomposites reinforced with silicate platelets, Mater. Res. Express. 6 (2019). https://doi.org/10.1088/2053-1591/ab1023.

[60] R. Umer, Y. Li, Y. Dong, H.J. Haroosh, K. Liao, The effect of graphene oxide (GO) nanoparticles on the processing of epoxy/glass fiber composites using resin infusion, Int. J. Adv. Manuf. Technol. 81 (2015) 2183–2192. https://doi.org/10.1007/s00170-015-7427-1.

[61] R.K. Prusty, S.K. Ghosh, D.K. Rathore, B.C. Ray, Reinforcement effect of graphene oxide in glass fibre/epoxy composites at in-situ elevated temperature environments: An emphasis on graphene oxide content, Compos. Part A Appl. Sci. Manuf. 95 (2017) 40–53. https://doi.org/10.1016/j.compositesa.2017.01.001.

[62] Z. Li, R.J. Young, R. Wang, F. Yang, L. Hao, W. Jiao, W. Liu, The role of functional groups on graphene oxide in epoxy nanocomposites, Polymer (Guildf). 54 (2013) 5821–5829. https://doi.org/10.1016/j.polymer.2013.08.026.

[63] D. Sharma, S. Kanchi, M.I. Sabela, K. Bisetty, Insight into the biosensing of graphene oxide: Present and future prospects, Arab. J. Chem. 9 (2016) 238–261. https://doi.org/10.1016/j.arabjc.2015.07.015.

[64] J. Sun, J.Y. Hwang, P. Jankowski, L. Xiao, J.S. Sanchez, Z. Xia, S. Lee, A. V. Talyzin, A. Matic, V. Palermo, Y.K. Sun, M. Agostini, Critical Role of Functional Groups Containing N, S, and O on Graphene Surface for Stable and Fast Charging Li-S Batteries, Small. 17 (2021). https://doi.org/10.1002/smll.202007242.

[65] X. Wang, H. Zhang, S. Ham, R. Qiao, Graphene Oxide and Its Derivatives as Adsorbents for PFOA Molecules, J. Phys. Chem. B. 127 (2023) 9620–9629.

Chapter 3. *Enhancing the Mechanical Performance of E-Glass Fiber Epoxy Composites using Coal-Derived Graphene Oxide*

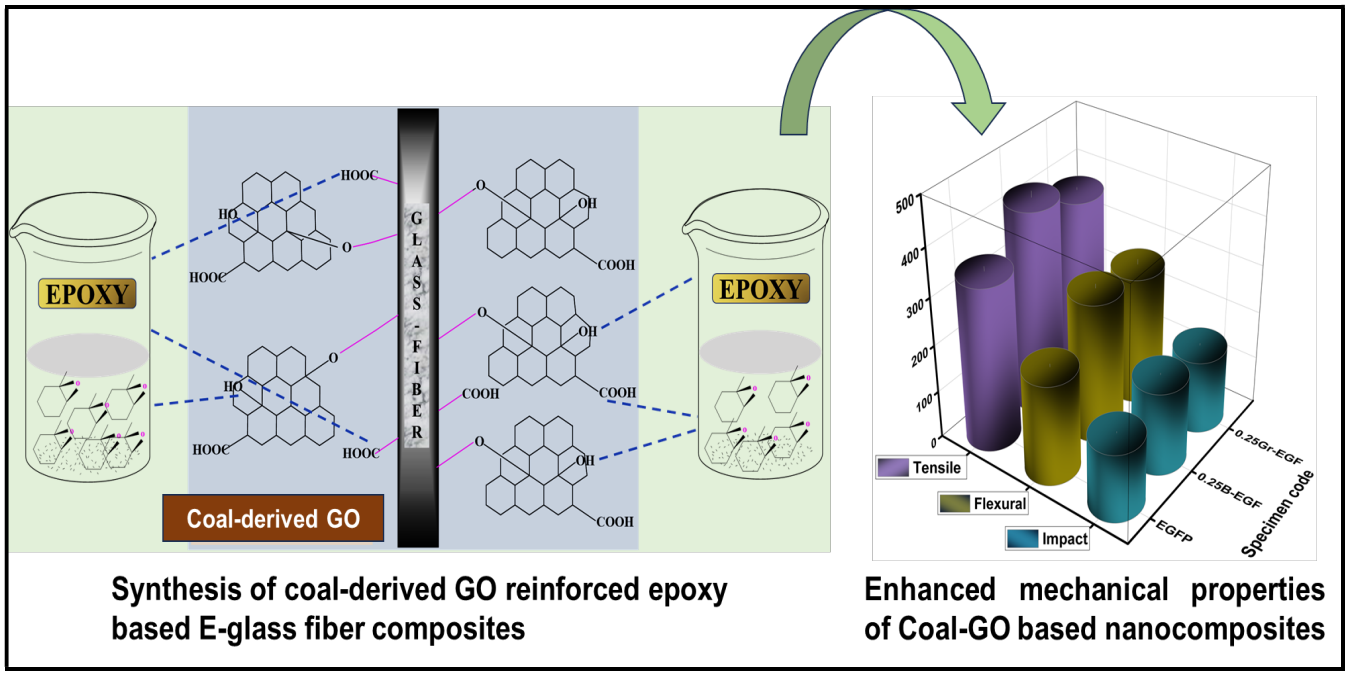

Synthesis of coal-derived GO reinforced epoxy based E-glass fiber composites

Enhanced mechanical properties of Coal-GO based nanocomposites

Highlights

- BC-GO demonstrates superior mechanical performance compared to Gr-GO in EGFPs.
- 0.25 phr BC-GO improves 38.9 % flexural, 22.9 % tensile & 21.6 % impact strengths.
- Beyond 0.25 phr, BC-GO and Gr-GO showed a decline in mechanical enhancement.
- Role of particle size, loading & adhesion to matrix analyzed using XRD, FTIR, DLS.
- Coal-GO is an attractive alternative nanofiller for EGFPs.

3.1. Introduction

Because of superior mechanical and chemical properties, E-glass fibers and graphene oxide (GO) have been used as reinforcement materials in a wide range of applications [1]. E-glass fiber reinforced polymers (EGFPs) have been extensively utilized in important market sectors such as aircraft, automotives, wind energy, and construction. The mechanical characteristics of these EGFPs depend on the attributes of the polymer matrix and the interfacial adhesion between the glass fibers and the matrix [2,3]. EGFPs have a few attractive features such as low density, high stiffness, strength, excellent thermal stability, and chemical and corrosion resistance. However, these materials are susceptible to different types of damage, such as matrix cracking, interfacial debonding, and fiber breakage during fracture. These failures mainly result from the weak fiber-matrix interface, which affects the mechanical behavior of EGFPs. Improving the interfacial adhesion between the fiber and the polymer matrix is, therefore, critically important to enhance the mechanical and functional properties of EGFPs. To this end, researchers have proposed various methods, including incorporating nanoparticles to reinforce the polymer matrix, and modifying the fiber surface through surface treatment [4,5]. Additionally, researchers have also tried adding particulates, not necessarily nano, to improve interfacial adhesion. For example, in [6], Mekonen and co-workers evaluated the mechanical properties of hybrid polymer composites, using epoxy resin as the matrix material, and E-glass fiber and bone particulate as reinforcement materials in different weight percentages (wt.%) and various combinations. Their results showed that the highest values for tensile and compressive strength were achieved at a composition ratio of 40 % E-glass fiber and 60 % epoxy matrix, measuring 254.96 MPa and 37.52 MPa, respectively. The maximum flexural strength achieved at this composition was measured at 250.52 MPa. However, the bone particulate-reinforced composites showed the lowest tensile strength. The hybrid composites demonstrated performance between the bone particulate and E-glass fiber reinforced composites. The authors opined that this deficit in performance could be due

to poor adhesion between the bone particulates and glass fibers with the matrix or due to the presence of air bubbles in the composition. In addition to poor adhesion with the epoxy composites, E-glass fiber as reinforcement in epoxy composites can also exhibit lower mechanical enhancement than expected due to factors such as improper resin impregnation, fiber misalignment, voids or defects in the composite structure, and limitations of the epoxy matrix itself.

Another potential approach that has been explored to improve interfacial adhesion between fibers and the polymer matrix in EGFPs is replacing E-glass fiber with natural fibers [7]. However, natural fibers have their own drawbacks, including higher water absorption, inadequate matrix-fiber adhesion, and poor fiber dispersion compared to synthetic fibers. These drawbacks negatively affect the performance and overall properties of composites. Chopra et. al [8] focused on the mechanical properties of E-glass fiber reinforced epoxy composites by incorporating plain weave copper strips mesh amidst layers of fiberglass. The findings indicated that the tensile strength, flexural strength, impact strength, density, and hardness of the hybrid composite increased by 16.3 %, 29.0 %, 55.5 %, 57.2 %, and 113.8 %, respectively, compared to those of the EGFP composite. Other researchers have explored the addition of various other types of filler materials to achieve specific desired outcomes [9]. For instance, borosilicate glass microspheres were incorporated into epoxy composites [10], copper metal powder was added to create a hybrid composite [11], waste products like fly ash, Linz-Donawintz slag, a solid waste produced during steel manufacturing were used for making hybrid composites [12–14], and iron fillings were included in FRP composites [15]. According to these studies, the choice between hybrid composites made with epoxy, E-glass, and particulates or another type of fiber depends on the effect of the filler (fiber or particulates) on the overall adhesion between the matrix and the additives.

An important inference that can be drawn from the above-mentioned studies and other related research is that nanofillers have the potential to significantly enhance the strength and stiffness of EGFP composites. These nanofillers acting as reinforcing agents can also effectively distribute stress and improve load-bearing capabilities. Their incorporation improves the strength and toughness of nanocomposites by suppression of crack propagation [16].

In recent years, graphene oxide (GO) has gained growing attention in both academia and industry due to its ability to significantly enhance mechanical, electrical, and thermal properties, either on its own or in combination with glass fibers, even at exceedingly low concentrations [17]. Umer et al. [18] studied the influence of GO on EGFP composites, synthesized using resin infusion technique in which GO was added at different wt.% (0.05, 0.1, and 0.2 wt.%). The test data for flexural properties showed a 21 % increase in flexural modulus and a 30 % increase in flexural strength, with the addition of GO by 0.2 wt.%. Prusty et al. [19] conducted an assessment of the flexural strength of epoxy/glass fiber composite with 0.5 wt.% graphene oxide (GO) and reported an increase of 21.1 %. Du et al. [20] analyzed the flexural and tensile properties of short glass fibers coated with GO as a reinforcement material in polyethersulfone (PES) composites. Different weight percentages of GO ranging from 0.05 to 1.0 were used. The composite with 0.5 wt.% GO coating on short fibers showed an enhanced improvement of 10.2 % in tensile strength, 25.4 % in Young's modulus, 9.4 % in flexural strength, and 15.9 % in flexural modulus.

However, the properties of composites comprising graphene and glass fiber are subject to two crucial constraints [21]. Firstly, suboptimal interfacial adhesion impedes effective load transfer from the graphene nanofiller to the matrix across the interphase. Secondly, graphene sheets tend to aggregate in polymer matrices due to their larger particle size, higher surface energy, and intrinsic van der Waals bonding [22]. As a consequence, the mechanical properties do not increase monotonically with increasing GO concentration. Instead, they rather peak at a specific value of

GO concentration. This is due to the aggregation of GO particles even after employing techniques like homogenization and ultrasonication. The aggregation of GO particles leads to substantially reduced exposed surface area of GO, leading to fewer functional groups available for bonding with the epoxy matrix, and thereby reducing the efficiency of stress transfer from the matrix to the reinforcing GO. These two limitations can be addressed by uniformly dispersing GO fillers in epoxy and employing appropriate surface treatment of the constituents [23,24]. This is facilitated to some extent by the fact that GO sheets accommodate a large number of functional groups on their surfaces and edges such as hydroxyl, epoxy, and carboxylic groups [25], which facilitate the dispersion and interaction of GO within the matrix.

In addition to the use of GO nanosheets incorporated in EFGPs, they have also been used in conjunction with carbon fibers. For example, Pathak et al. [26] studied the interfacial properties of GO incorporated carbon fiber reinforced epoxy nanocomposites. Their data showed that the amount of GO needed to achieve optimal thermal properties in hybrid carbon fiber reinforced plastic (CFRP) composites was 0.3 wt.%. By adding this amount of GO to the CFRP composites, the thermal stability of the material was enhanced by 16°C. This improvement can be attributed to the layered structure of GO, which creates a convoluted path that acts as a barrier, impeding the penetration of oxygen. In our research, we have opted to utilize GO instead of pristine graphene because of the abundant functionalities present on the GO surface, which facilitate easier dispersion of GO in epoxy resins and enhance its compatibility with the polymer matrix. In contrast, pristine graphene tends to agglomerate, which leads to poor dispersion and diminished mechanical properties of the composite [27,28]. Secondly, the functional groups on GO enable it to form stronger chemical bonds with the epoxy resin and the glass fibers. This significantly improves the interfacial bonding, thereby leading to better load transfer between the polymer matrix and the fibers, resulting in increased mechanical properties [25,29–33].

The integration of macroscopic fibers and micro- and nano-fillers by means of grafting techniques can result in hierarchical reinforcements that improve the interface shear strength of fiber-based composites. This approach allows for the uniform dispersion of nano-scale reinforcement, which can enhance the mechanical properties of the resulting composites. Li et al. [34] proposed a hierarchical reinforcement strategy that involved grafting GO onto carbon fibers (CF) through a chemical process, using polyamidoamine (PAMAM) dendrimers as bridging agents. Morphological characterization confirmed the uniform distribution of GO sheets onto CF. This uniform distribution of nanoscale filler over macroscale reinforcement contributed to the high mechanical strength of the resulting composites. Liu et al. [35] investigated the interfacial properties of hierarchical reinforcement of carbon fibers modified with GO through different modes of bonding (van der Waals forces, zwitterionic interactions, and covalent bonds). The resulting CF/GO composites exhibited higher flexural strength, interlaminar shear strength, and interfacial shear strength compared to pristine CF, with increases of 28.7 %, 22.7 %, and 50.6 %, respectively. The interfacial interaction between CF-GO and polymer matrix has been shown to enhance significantly, demonstrating excellent potential for improving the interfacial properties of fiber-GO composites for various applications.

The most common method commercially deployed for the synthesis of graphene, to date, has been the modified Hummers' method with graphite as the precursor [36–40]. But due to the rising cost of graphite and regional localization, researchers have been exploring other readily accessible precursors such as coal, biomass, etc. [41]. Additionally, the modified Hummers method is quite tedious and requires harsh chemicals and results in the release of detrimental gases such as NO_x and ClO_x. To address these concerns, Lee and Mahajan [41] have developed a simplified one-pot process to synthesize GO that uses semi anthracite coal as a precursor and a single acid (HNO_3) for oxidative scissoring of the sp^2 graphitic domains from the coal edges. More recently, Garg et al. [42] extended this process to bituminous coal obtained from one of the mines in India and

showed that the original recipe for bituminous coal needs fine-tuning for optimal production of GO.

In a recent study by Bhardwaj et al. [43], the authors investigated the thermal performance of non-silicone-based thermal interface materials by incorporating different carbonaceous additives, including multilayer graphene derived from graphite (Gr-MLG), using the Hummers' method [36–40], and multilayer graphene synthesized from semi-anthracite coal (AC-MLG), using one-pot method [44]. The experimental data revealed as much as ~350 % higher thermal conductance with the AC-MLG compared to Gr-MLG. This gain was attributed to the higher thermal percolation threshold of AC-MLG, which, in turn, was linked to a larger distribution of phenolic oxygen functional groups. Their study highlighted the critical role played by the precursor material and the accompanying process parameters used for the synthesis of graphene in determining the properties of graphene or graphene oxide. Based on these findings, it is reasonable to deduce that the choice of precursor material and the process used to synthesize GO nanofillers may significantly impact the mechanical properties of GO-reinforced EGFP composite. While EGFPs with Gr-GO have been studied extensively, including the interaction of Gr-GO with the epoxy-fiber matrix, there is limited knowledge about the interfacial adhesion of coal-derived GO in EGFPs [45–47].

To address this research gap, we have conducted an investigation, with a focus on comparing the enhancement or degradation in the mechanical properties such as tensile strength, flexural strength, and impact strength of glass fiber epoxy composites, using GO synthesized from bituminous coal (BC-GO) via the one-pot method in comparison to GO derived from graphite (Gr-GO). Importantly, we wanted to ascertain whether the mechanical threshold (optimum) i.e., the level of the loading fraction of the additive that can be dispersed in the matrix before the onset of agglomeration, is higher for the bituminous coal-derived GO composites as compared to other prepared composites. The novelty of our work stems from the utilization of BC-GO, synthesized

through a simplified a one-pot method, into EGFP composites, rendering it more practical and accessible for real-world applications. This unique approach capitalizes on the utilization of an abundantly available and cost-effective source, i.e., bituminous coal as a precursor for synthesizing GO used as a nanofiller in the reinforcement in EGFPs. As elaborated in the text, when BC-GO was tested for its mechanical potential in EGFP, its properties were superior to conventionally used Gr-GO in EGFPs. We believe this to be possible due to the ability of BC-GO to possess abundant functional groups, which improve the adhesion between oxygen-related functional groups on GOs and epoxy resin and hardener. For the higher value of mechanical threshold, a larger improvement in mechanical properties would be possible. Additionally, we also wanted to investigate the role of particle size on load transfer and mechanical properties. These issues are discussed in detail in the following sections. Section 3.2 provides an overview of the materials and synthesis techniques used, while Section 3.3 briefly describes the characterization and testing tools deployed. Sections 3.4-3.6 present a comprehensive analysis of the experimental data, including the mechanical properties (tensile, flexural, and impact strength) of the composites under different nanofiller loading conditions. Section 3.7 delves into the crucial insights into the mechanism for interfacial bonding between GO and EGFP, and Section 3.8 summarizes the main findings of the study.

3.2. Materials and methods

3.2.1. Materials

The epoxy resin (Araldite CY 230-1) and the curing agent (Aradur HY 951) were procured from Huntsman Advanced Materials, India. These epoxy resin and the curing agents have the functionality of diglycidyl ether and aliphatic amine, as reported. The epoxy and curing agent were mixed in the weight ratio of 10:1. E-glass fiber mats were obtained from Revex Plasticizers Pvt. Ltd., India. BC-GO was synthesized in the laboratory using the recently developed one-pot

process while Gr-GO was synthesized using a modified Hummers' method. Raw chunks of bituminous coal were sourced from the north-eastern region of India (supplier, RK & Sons, Patiala, Punjab). Graphite fine powder was obtained from Loba Chemie Pvt. Ltd. Merk supplied hydrochloric acid, ethanol, hydrofluoric acid, and nitric acid. Double distilled water was used to prepare reagents and for washing during the experiments.

3.2.2. Synthesis of coal-derived GO via one-pot method

The nut-size raw coal was ball milled to obtain a particle size below 10 µm. Acids including 37 % HCl and 50 % HF were used to purify raw coal powder with 500 ml of distilled water. This mixture was subjected to magnetic stirring for 36 h. For the next 12 h, the mixture was kept at rest and black precipitates were obtained from the bottom of the beaker. Three grams of the purified coal were subjected to oxidation, using 5 M HNO_3 for 5 h at 80°C. The oxidized Coal-GO solution was neutralized and subjected to probe sonication for 4 h and finally centrifuged. The obtained BC-GO solution was dried in an oven below 60°C to obtain the powdered form of GOs.

3.2.3. Synthesis of graphite-derived GO via modified Hummers' method

Following the recipe in [38], 46 ml of conc. sulphuric acid (H_2SO_4), 1 g of graphite powder, and 1 g of sodium nitrate ($NaNO_3$) were subjected to 4 hour stirring in an ice bath. Subsequently, 6 g of $KMnO_4$ was added to the solution, followed by vigorous stirring for 1 h. While continuously stirring, distilled water (220 ml) and hydrogen peroxide (H_2O_2), with a concentration of 30 %, were added dropwise into the solution. To eliminate any metal impurities, the solution was washed using 5 % HCl and distilled water. Finally, drying of the solution was carried out overnight to obtain the powdered form of Gr-GO.

3.2.4. Fabrication of EGFP nanocomposites

Based on previous studies [19,48–51], the starting concentration range of nanofillers in the EGFP system was chosen in the range 0.1 – 0.75 phr (parts per hundred resin). Initially, coal-derived GO

(BC-GO) and graphite-derived GO (Gr-GO) were dispersed separately in the epoxy resin and homogenized at 20,000 rpm for 10 minutes, followed by probe sonication at 80 % amplitude for 10 minutes in an ice bath to allow dissipation of excessive heat. Afterward, the solution was mechanically stirred at 500 rpm for 10 minutes, and the hardener was added to this mixture. This mixture was then infused in the VARIM (Vacuum Assisted Resin Infusion Mold), which was cleaned with the cleansing agent and then coated with a mold release agent to prevent sticking.

As per the ASTM standards, two-ply mats were used for testing tensile and flexural properties (ASTM D-3039 for tensile samples and ASTM D 790-02 for flexural samples), while the impact testing specimens were constructed using twelve layers of the mat in accordance with ASTM D 256–02. The upper-most layer of glass-fiber mat was covered with a separator cloth on the top of which a perforated sheet was placed to ensure uniform dispersion of resin. Lastly, a wire mesh was used to provide a path for the resin flow. An infusion pipe was placed over the wire mesh and secured with sealant tape. A breather cloth was again used to create a bridge over the wire mesh to facilitate resin flow. In the last step of fabrication process, the whole setup was covered with a lamination sheet and supported with sealant tape. A vacuum pump maintained about 1 mbar of vacuum pressure. The infusion of resin was carried out with the assistance of a vacuum pump, ensuring proper impregnation of the fiber mat with resin. After infusion, the nanocomposite sheets were cured and post-cured for 6 h at 23 ℃ and 6 h at 60 ℃, respectively. The general scheme/camera visuals are shown in Figure 3.1, which represents the protocol followed during the preparation of sheets.

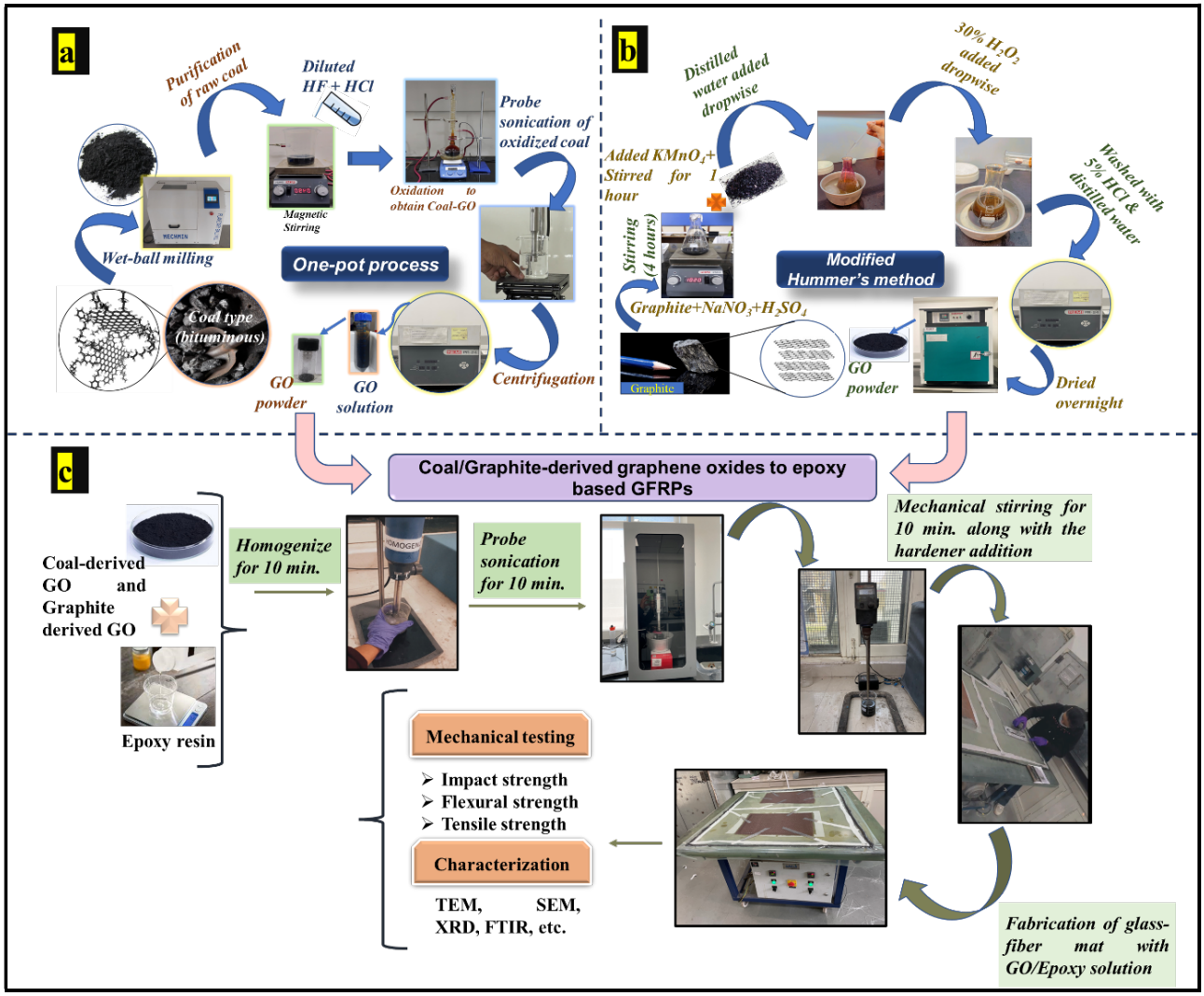

Figure 3.1. (a) & (b): Schematic representation/camera visuals of the one-pot process, and modified Hummers' method for the preparation of GO, respectively, and (c): synthesis of EGFP nanocomposites using VARIM

3.3. Characterization and Mechanical testing

Characterizations of GO in FRP nanocomposites were conducted using various analytical techniques: SEM, TEM, XRD, and FTIR. X-Ray Diffraction analysis (XRD) was carried out through a PANalytical X-ray diffractometer equipped with Ni-filtered Cu Kα radiations (λ = 0.1504 nm). The scan rate was set at 2° min^{-1} in the range of 10–90° at an applied voltage of 45

kV. TEM characterization was carried out using Hitachi (H-7500) operating at an acceleration voltage of 110 kV. Fractographic analysis of various samples of fractured composites was conducted using a ZEISS scanning electron microscope (SEM) at an accelerating voltage of 5 kV. A Shimadzu FTIR spectrophotometer (IRTacer-100) in the scan range of 400-4000 cm^{-1} was used to analyze the functional groups present in different concentrations in the prepared composites and identify any chemical modifications that might have occurred after the addition of GOs. The particle size distribution of graphene oxide dispersed in deionized water was determined by using a dynamic light-scattering method (DLS) with a Zetasizer from Malvern. For mechanical testing (impact, tensile and flexural strength), the composite specimens were prepared according to the ASTM D 256–02, ASTM D 3039, and ASTM D 790–02, respectively. The tensile strength and flexural strength were tested via a Universal Testing Machine, UTM from Zwick/Roell, Germany. For impact testing, Tinius Olsen (model-IT504) impact tester was used. To ensure reproducibility, five specimens were prepared and tested for each strength property of all the composites.

3.4. Results and Discussion

3.4.1. Characterizations of EGFP nanocomposites

Figure 3.2a illustrates the XRD patterns for different GO samples, including bituminous coal-derived GO (BC-GO) via a modified one-pot process [42], and graphite-derived GO (Gr-GO) by modified Hummers' method [38]. Additionally, the XRD pattern of the EGFP composite without any nanofillers is shown in Figure 3.2a. Figure 3.2b displays the XRD spectra of different composites prepared by incorporating BC-GO and Gr-GO as nanofillers in EGFP composites.

In Figure 3.2a, Gr-GO exhibits an XRD diffraction peak at around $2\theta = 10.19°$ corresponding to the (002) plane with a d-spacing of 0.86 nm. Alam et al. [52] reported the (002) crystalline plane peak around $2\theta = 10.11°$. The existence of a diffraction peak of (100) crystalline plane at $2\theta = 43°$ is suggestive of the turbostratic disorder in the graphene oxide, likely caused by defects in the GO

system [16,53]. In contrast, the XRD patterns of BC-GO show the diffraction peak at $2\theta = 20.9^0$, respectively which are consistent with those reported by Garg et al. [42]. Lastly, the XRD spectrum of EGFP without any nano reinforcement shows a diffraction peak at $2\theta = 19.02^0$, attributed to the residual crystalline silica in the composite. Since no other identifiable diffraction peaks were observed in the EGFP composite, it can be assumed that the composite is amorphous in nature. The absence of identifiable peaks in the EGFP composite without any nanofillers implies a uniform distribution of glass fibers within the matrix [54]. For simplicity, in the text to follow, we use the following nomenclature: the initial of the precursor from which GO has been derived comes first, followed by E for epoxy polymer and GF for glass fiber, with a subscript showing the concentration of GO in that composite. For instance, B-EGF_x stands for bituminous coal-derived GO in epoxy glass fiber composite with x as the concentration of GO being used as a filler. The XRD diffractograms of B-EGF_x and Gr-EGF_x (Figure 3.2b) for different values of x, when compared with those of EGFP alone (Figure 3.2a), clearly show no other distinct peaks corresponding to the crystalline planes of the respective graphene oxides. This implies that the incorporation of graphene oxide sheets does not influence the degree of crystallinity of the corresponding EGFP composites [55]. The analysis also reveals negligible transformation to the trans-crystalline phase at the system interface, indicating that there is no change to the fundamental 3-dimensional cured epoxy network crystal structure with the addition of GOs as a nanofiller [54]. Another possible reason could be the exfoliation of GO layers in the presence of epoxy [56]. The absence of d(002) peak around $2\theta = 19°$ (very close to the silica residual peak) would also suggest that GOs are largely exfoliated in the epoxy matrix. The missing d(002) peak, which varies in shape among different compositions, and the presence of an identical peak across all GO compositions indicate that the morphology of the reinforced EGFPs is largely exfoliated, irrespective of the composition and source of GO. The presence of another peak of GOs around $2\theta = 43°$ was observed in all GO modified EGFP samples, suggesting the presence of GO.

Similar observations were reported by Kanny et al. [57] on the incorporation of nanoclay in the epoxy matrix at lower values of the concentration of nanoclay. No separate peak was observed for 3 wt.% dispersed nanoclay, indicating a randomly dispersed structure throughout the matrix, referred to as an exfoliated structure. However, at 4 wt.% and 5 wt.% nano clays, composites exhibited distinct diffraction patterns at 2θ of 4.7° and 5.1°, respectively, suggesting that the epoxy had successfully intercalated into the gallery spacing of the clay particles (referring it as an intercalated structure). Their TEM analysis confirmed their inference/conclusions about the structure suggested by the XRD data. In the range of concentration of GO nanofiller in our study, we did not observe the intercalated structure.

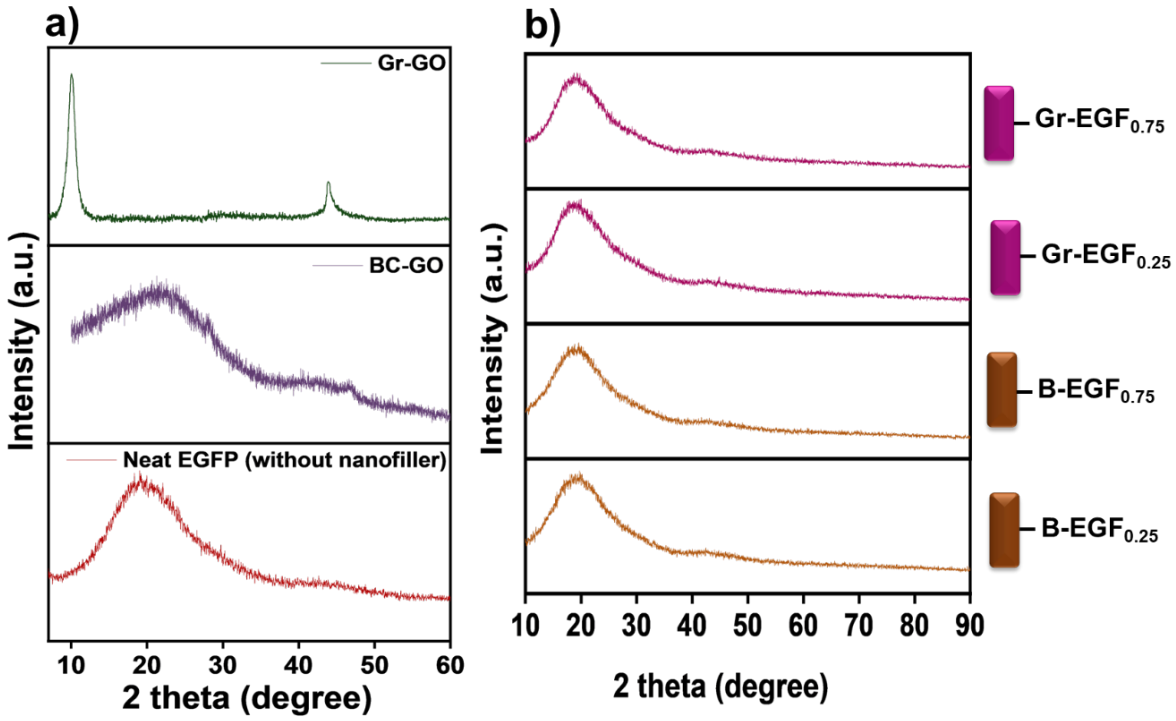

Figure 3.2. XRD spectra of various synthesized coal/graphite-derived GO and EGFP composites

One of the highly preferable tools to determine the mechanistic interpolymer hydrogen bonding is FTIR. It offers a non-destructive, highly effective method to obtain the molecular fingerprint of various compositions. The FTIR spectra of cured epoxy/glass fiber composites with/without any

nanofiller at different loadings are shown in Figure 3.3. For brevity, only the spectra of the concentration of interest are shown as all the peaks were almost similar. Notably, the spectra were similar for composites, both with and without the nanofiller. This is due to the presence of abundant functional groups, such as epoxides, carbonyls, hydroxyl in epoxy and glass fiber [58], and also a significant amount of oxygen-based functional groups in graphene oxide [59], resulting in overlapping peaks. As discussed later, the incorporation of these functional groups into the network with epoxy and glass fiber networks, (also shown in Figure 3.11) contributes to enhanced mechanical strength observed in the composites.

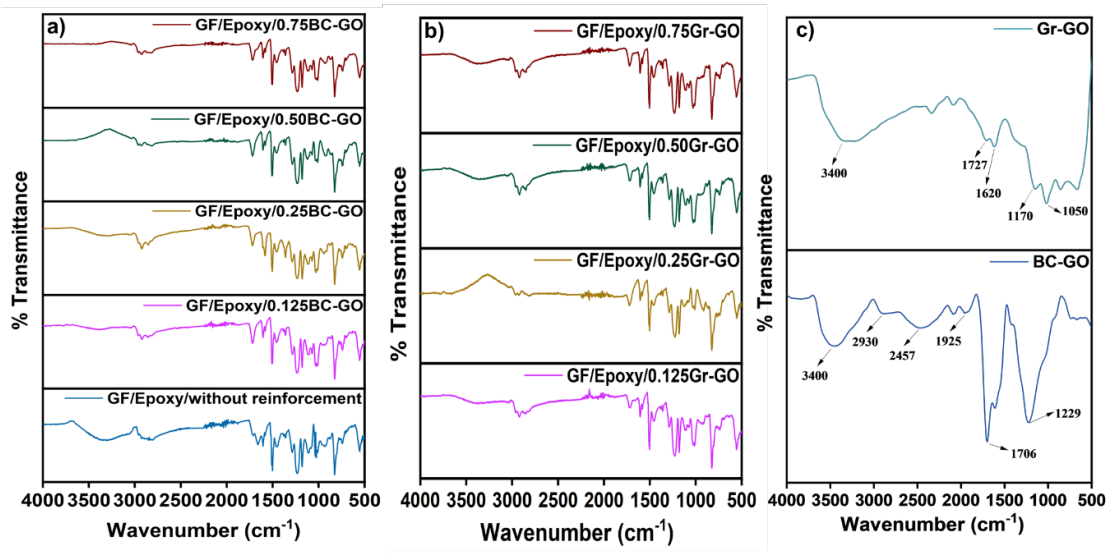

Figure 3.3. (a), (b): FTIR spectra of EGFPs synthesized, with the incorporation of different levels of nanofillers derived from two precursors, bituminous coal (BC) and graphite (Gr), and (c): FTIR spectra of nanofillers

The strong and broad peaks observed between 3319 cm^{-1} to 2910 cm^{-1} can be attributed to the presence of hydroxy (-OH stretch) groups. The peaks arising between 1598 cm^{-1} to 1715 cm^{-1}, and 1438 cm^{-1} to 1450 cm^{-1} are attributable to the bending vibrations of C-H bonds in the composite material [57]. In the case of B-$EGF_{0.25}$ composite, the peak at 1598 cm^{-1} could also be indicative of N-H bending vibrations, arising from the presence of N in the microstructure of coal-derived

GO, as reported in [42,44]. The peak at 1360 cm^{-1} in these composites shows the presence of phenolic functionality based -OH group. Lastly, the peaks from 1234 cm^{-1} to 1015 cm^{-1} depict the C-O stretching vibration, while those at 820 cm^{-1}, 738 $cm^{-1,}$ and 729 cm^{-1} are associated with C-H bending vibration.

The observed peaks in the FTIR spectra of BC-GO and Gr-GO provide valuable information about the functional groups and molecular bonds present within these nanofillers. In the case of BC-GO, the peak at 3400 cm^{-1} (Figure 3.3c) is attributed to the stretching mode of N−H bond, while peaks at 2930 cm^{-1}, 1925 cm^{-1}, and 1706 cm^{-1} denote stretching vibrations of C−H bonds, C=C=C bonds, and C=O bonds, respectively. The presence of N within the inherent structure of coal, originating from the degradation of plant matter, is signified by the N-H stretching vibrational mode. Moving on to Gr-GO, the peak observed at 3400 cm^{-1} corresponds to O-H stretch whereas the peak at 1620 cm^{-1} can be attributed to the stretching of C=C bonds within the unoxidized graphite component (Figure 3.3c). Furthermore, the peaks at 1727, 1170 and 1050 cm^{-1} correspond to the stretching vibrations of C=O bonds in the carboxyl group, the stretching vibrations of C−OH bonds in the alcoholic group, and the stretching mode of C-O-C epoxide bonds [42]. The FTIR spectra of both the nanofillers provide a better understanding of the comparative functional groups present and the possible bonds they tend to make with polymer which is further explained in section 3.7.

3.4.2. Tensile and Flexural properties of EGFP composites reinforced with BC-GO and Gr-GO nanofillers

In this section, we investigate the impact of incorporating BC-GO and Gr-GO nanofillers on the mechanical behavior of glass fiber-reinforced polymer composites (EGFPs). First, consider the tensile strength and tensile modulus data displayed in Figure 3.4a and 3.4b, respectively, for B-EGF and Gr-EGF with four different loadings ranging from 0.125 phr to 0.75 phr. For both

nanofillers, the tensile strength initially increases with an increase in the loading rate, reaching a maximum at 0.25 phr. Beyond this optimal, an increase in the loading rate leads to a decrease in tensile strength due to agglomeration of the nanofillers. Agglomeration reduces the exposed surface area of GO, leading to fewer functional groups available for bonding with the epoxy matrix and poorer dispersion of particles in the matrix, thereby reducing the efficiency of stress transfer from the matrix to the reinforcing GO. The observed presence of a threshold limit of concentration of the nanofillers for optimal strength is similar to that demonstrated in [60] where the authors investigated the effect of different levels of concentration of single wall carbon nanotubes (SWCNTs) on the thermal, electrical, and mechanical properties of epoxy-SWCNT composites. Notably, the incorporation of BC-GO leads to a relatively higher increase in tensile strength (22.9 %) compared to Gr-GO (9.3 %) at the optimal loading of 0.25 phr. Additionally, the tensile modulus for both BC-GO and Gr-GO is also higher than that of EGFP, see Figure 3.4b, it being 31.5 % for B-EGF$_{0.25,}$ and 28.6 % for Gr-EGF$_{0.25.}$ However, as the numbers indicate, the relative advantage in the tensile modulus of BC-GO over Gr-GO is much smaller than the improvement observed for the tensile strength.

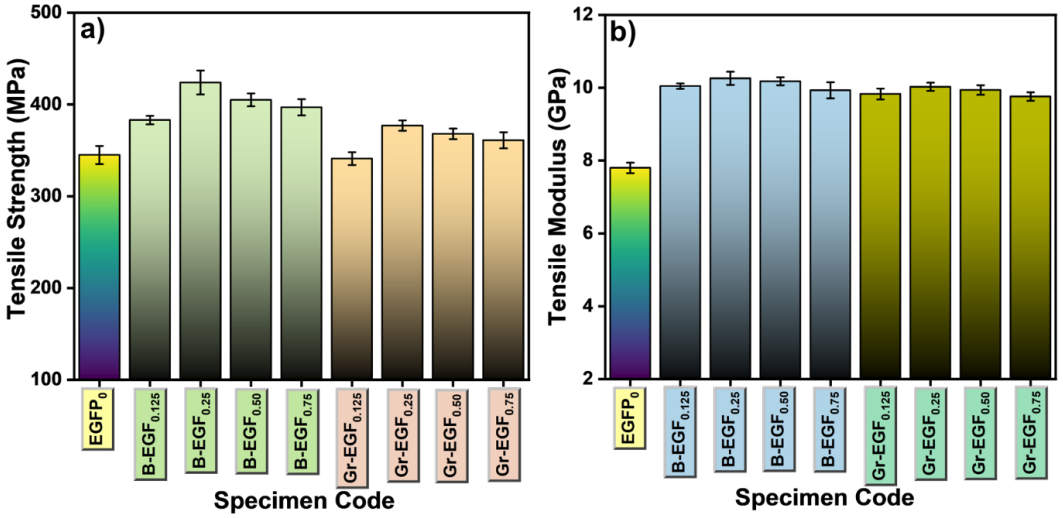

Figure 3.4. Histograms representing a) Tensile strength, and b) Tensile modulus of GO reinforced EGFP composites

Figure 3.5 displays the data for flexure strength and flexure modulus of the EGFP composites with BC-GO and Gr-GO at different loadings. Similar to tensile properties, the maximum gains in flexural strength and flexure modulus were observed at a loading of 0.25 phr for both BC-GO and Gr-GO. Among the two GO-based composites, B-EGF exhibited the highest increase in flexural strength (38.9 %) compared to a 28 % increase for Gr-$EGF_{0.25}$ over the flexural strength of EGFP. Similarly, the flexural modulus showed an increase of 30.8 % for B-$EGF_{0.25}$ and a 26.7 % increase for Gr-$EGF_{0.25,}$ both as compared to EGFP. Increasing the filler concentration in the composites results in an increase in both tensile and flexural strength, attributed to the reinforcing effect where the filler particles effectively share the applied load. However, this effect is more pronounced when there is good adhesion and interaction between the filler and the matrix material at an optimal concentration. Notably, the changes in the composites' tensile and flexural strength with a change in the filler percentage depend on a complex interplay of various factors including the filler type, filler-matrix interaction, and the level of dispersion.

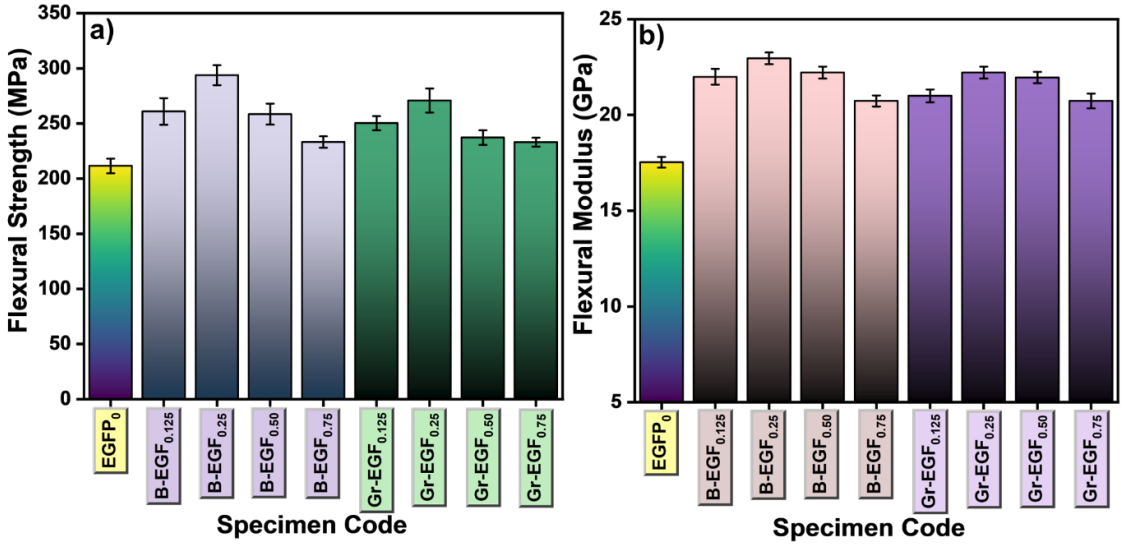

Figure 3.5. Histograms representing a) Flexural strength, and b) Flexural modulus of GO reinforced EGFP composites

3.4.2.1. The effect of particle size: To gain a deeper understanding of the observed behavior, we measured the particle size distribution of BC-GO and Gr-GO using Dynamic Light Scattering (DLS). Particle size is one of the critical factors influencing the mechanical properties of such composites, see, for example, a comprehensive review, by Fu et al. [61]. The authors emphasized the significant role played by particulate size, in addition to the impact of particle/matrix interface, and particle loading, in determining the mechanical behavior of composites. The particle size distributions for BC-GO and Gr-GO are shown in Figure 3.6a and 3.6b, respectively. As indicated there, the mean particle size of BC-GO is 0.29 µm, while Gr-GO possesses a larger mean size of 5.18 µm. The larger particle size in Gr-GO can be attributed to the presence of sheets with greater lateral dimensions.

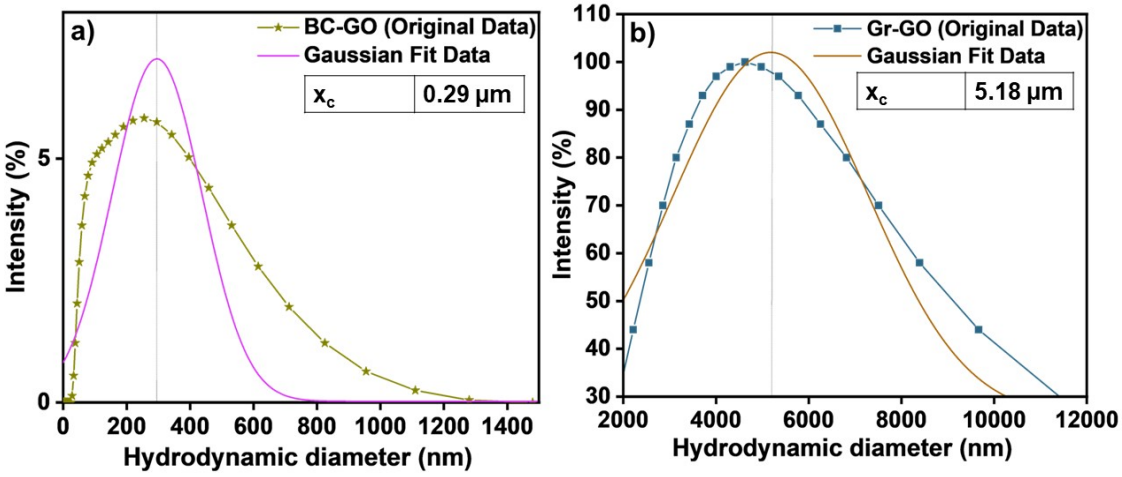

Figure 3.6. DLS graphs of BC-GO and Gr-GO

The relatively narrower size distribution of BC-GO facilitates its more uniform dispersion within the epoxy network. In alignment with [61], our data indicates that all the mechanical properties of composites are influenced by the interplay among three factors: particle/matrix interface, particle loading, and particle size, with the specific interaction being different for each property. For instance, they noted that particle size has a more pronounced effect on tensile strength than on

tensile modulus, as is also observed in our data in Figs. 4a and 4b, which show that the relative gain in tensile modulus is not as significant as that for tensile strength. Further, there is a critical particle size above which there is no further effect of the particle size on the composite modulus [61]. The particle distribution data shown in Figure 3.6a and Figure 3.6b for the BC-GO and Gr-GO, respectively, suggests that for both GO fillers, the particle size may be above the critical value, confirming the minimal observed effect of particle size on the composite modulus. It is worth noting that the magnitude of this critical particle size is difficult to predict *apriori* since it depends on the particulars of the particle, matrix, and particle-matrix adhesion [61].

For the tensile strength, on the other hand, the smaller particle size in BC-GO promotes strong interfacial adhesion, which contributes to effective stress transfer from the matrix to the nanofiller, thereby increasing the strength as compared to Gr-GO, which possesses bigger particle size than BC-GO. Interestingly, in a recent study by Siraj et al. [62] in which the authors investigated the impact of two particle sizes (5 μm and 25 μm) of silica particles in high-density polyethylene (HDPE)-based composites, they drew different conclusions from their data. For the composite material developed with a 25μm filler size, an improvement in mechanical properties was observed as the concentration of silica particles increased from 0 to 20 %, beyond which there was a degradation in improvement, attributable again to the agglomeration of particles, which is consistent with our data as well as of other investigators [61]. However, for the 5 μm filler size, the authors did not observe any improvement as the concentration of silica particles was increased from 0 to 20 %. This suggests that for the smaller particle size filler, the critical value for maximum improvement in mechanical properties might be at a lower concentration, which was not explored in their experiments.

In summary, the particle size of the GO fillers plays a crucial role in determining the mechanical properties of fiber-reinforced polymer composites. Smaller nanofiller particle sizes, as observed in

BC-GO, have the potential to enhance the mechanical properties by a combination of reinforcement effect, filler-matrix interaction, and particle packing density.

3.4.2.2 Role of functional groups: Apart from particle size, the presence of functional groups on the GO fillers also impacts the mechanical properties of the GO-based composites. This effect is particularly significant for coal-GO, which possesses abundant functional groups that improve the adhesion between the oxygen-related functional groups on GOs and the epoxy resin and hardener. The dispersion of BC-GO in the epoxy matrix is better, which results in a larger surface area being available for bonding between the polymer and filler. The combined effect is to enhance better stress transfer between the filler, GO, and the epoxy matrix. This mechanism is explained in more detail in Section 7.

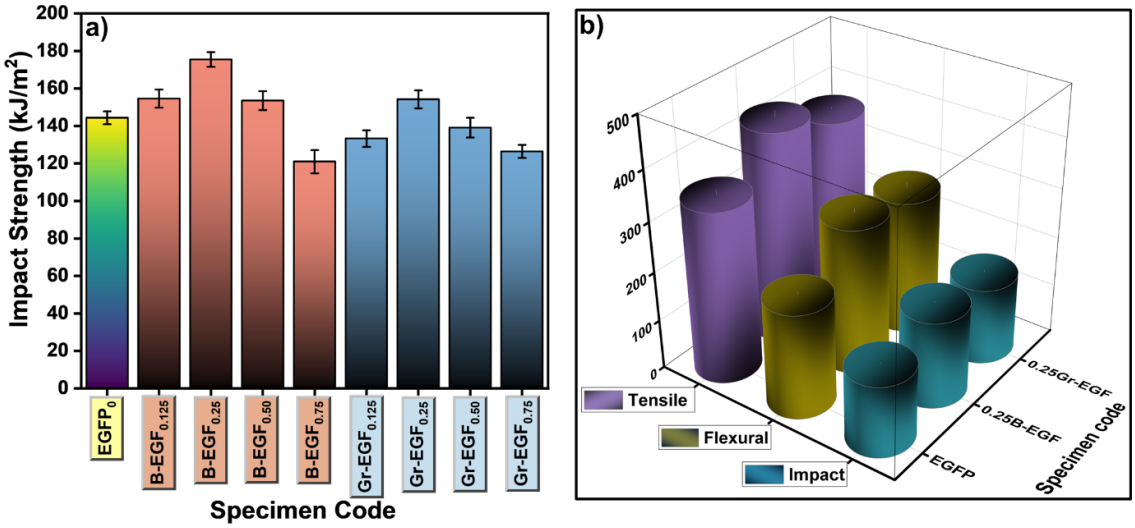

Figure 3.7. a) Impact strength of different synthesized EGFP composites b) Compilation of the mechanical properties of best-suited compositions of different nanofillers in FRPs

3.4.3 Impact Strength of B-EGF and Gr-EGF Composites

To complete our study of the effect of BC-GO and Gr-GO fillers on the mechanical properties of their composites with EGFP, we present in Figure 3.7a, the impact strength of all the composites,

with or without nano reinforcements, to determine their load-bearing capacity under sudden loading conditions. The relative increase in impact strength of B-EGF$_{0.25}$ and Gr-EGF$_{0.25}$ over that of EGFP was assessed to be 21.6 % and 6.8 %, respectively. The exfoliated layers of both the graphene oxide in EGFP composites serve as crack inhibitors and create a complex pathway for crack propagation, resulting in enhanced impact strength at 0.25 phr concentration. However, as with the other mechanical properties discussed above, when the concentration of BC-GO and Gr-GO in EGFP composites increases beyond the optimized value, the fillers act as sites of stress concentration, leading to a decrease in the impact strength [63]. As before, the smaller particle size of BC-GO (Figure 3.6) also contributes to the improved impact strength of B-EGFP composite as compared to Gr-EGFP, because at the same concentration loading, there will be a greater number of small particles to suppress the crack progression as compared to large particles. For convenience, the mechanical properties of the optimized compositions of BC-GO and Gr-GO in the EGFP composites are graphically presented in Figure 3.7b.

3.5. SEM images of fractured surfaces of FRP composites

SEM analysis was conducted to examine the fractured surfaces of impact samples and study dispersion and compatibility—the two major factors that govern the interaction between glass fiber and the epoxy polymer matrix [64,65]. The SEM micrograph of the control sample (glass fiber and epoxy composite without GOs) displayed in Figure 3.8a, b shows pulled-out fibers from the matrix. A few large gaps between the fibers and the epoxy matrix are observed, indicating weak interfacial adhesion. The poor bonding between the fiber and the matrix contributes to large fiber pull-out, ultimately leading to reduced resistance to fracture. Thus, when stress is applied, the fibers easily detach from the matrix, resulting in the formation of some voids and leading to an uncomplicated fracture of the material. Because of the weak interfacial adhesion, a relatively low load is required for deformation. In other words, EGFPs without GO fillers have low strength [19].

On the other hand, the composites showing higher impact strength (B-EGF$_{0.25}$, and Gr-EGF$_{0.25}$), as shown in Figure 3.8c and 3.8d, the failure specimens exhibit reduced fiber pull-out, indicating higher stress transfer between the fiber and the matrix, thereby contributing to higher strength.

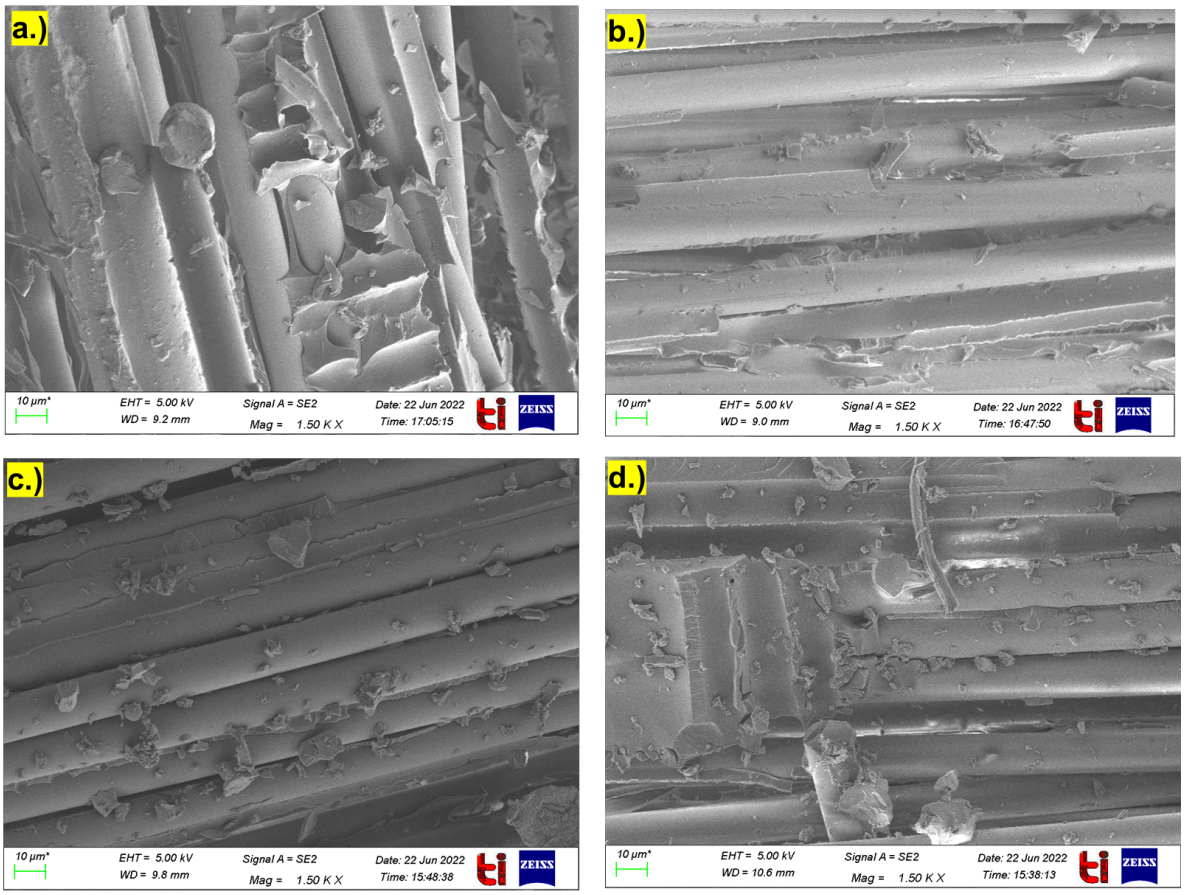

Figure 3.8. SEM micrographs of the fractured surfaces of impact strength specimens of EGFP composites: a,b) EGFP, c) B-EGF$_{0.25}$, and d) Gr-EGF$_{0.25}$

The basic mechanism of increase in the impact strength of polymer matrix reinforced with nano-filler is well understood and can be described as follows. During the initial stage of deformation, when a crack propagates in the composite material, it encounters multiple nanofillers and fiber-matrix interfaces that hamper the propagation of the crack. This resistance from fillers compels the crack to alter its direction, thereby, elongating the crack. Alternatively, the crack may also cause the fillers themselves to get splintered or fractured when it propagates through the material. This

process requires a large amount of energy [66,67]. In addition, the integration of nanofillers in glass fiber-reinforced epoxy-based composites results in a synergistic effect between the fillers and the glass fibers, leading to a substantial increase in the tensile and flexural properties of the composite material.

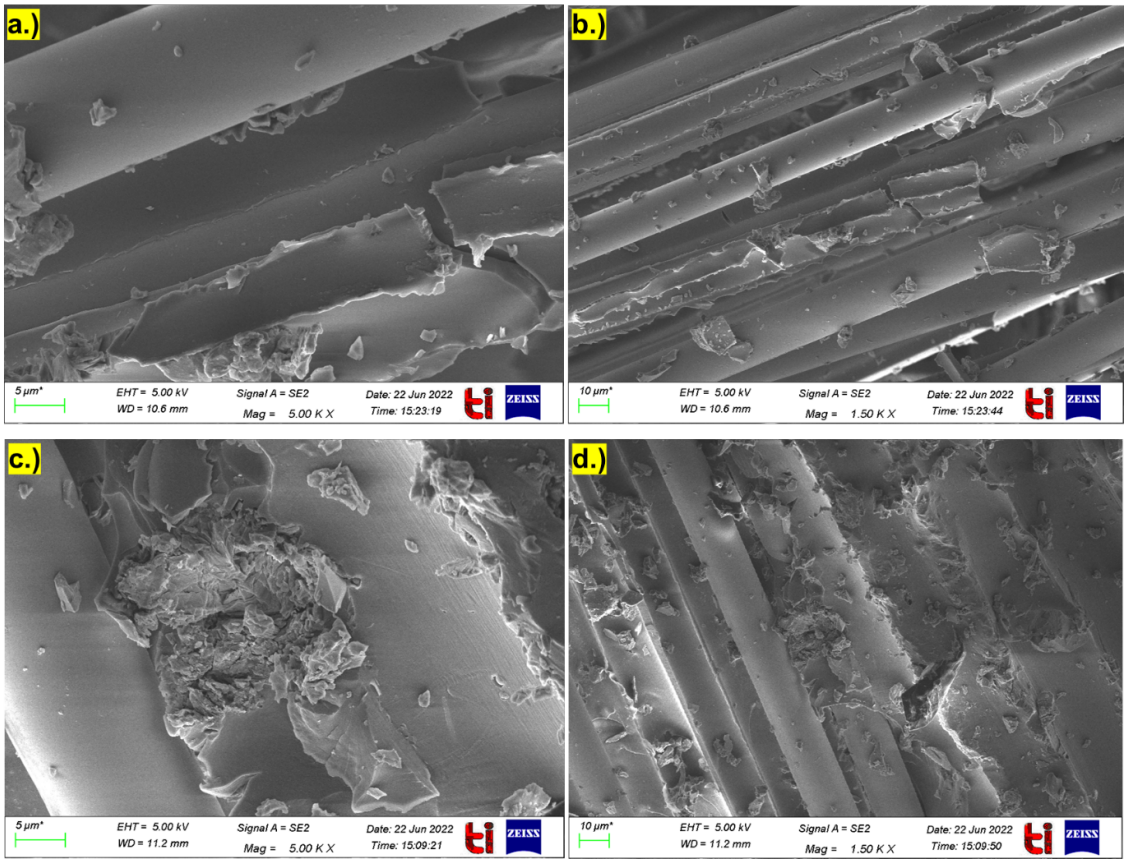

Figure 3.9. SEM micrographs of the fractured surface of impact strength specimens of EGFP composites a-b) B-EGF$_{0.75}$ c-d) Gr-EGF$_{0.75}$

We also wanted to use SEM micrographs in support of our argument that beyond the optimal concentration of BC-GO and Gr-GO in the composites (for instance, 0.75 phr), a decrease in mechanical properties is attributable to particle aggregation and poor bonding. However, clear identification of GO in the polymer matrix from the SEM micrograph is more difficult as compared to other fillers such as CNTs and CNFs, which possess cylindrical morphology. We,

therefore decided to analyze GO dispersion in terms of the size of agglomerates. From the SEM micrographs in Figure 3.9, it can be predicted that the size of aggregates is much bigger at higher filler loadings (0.75 phr) than the ones observed at lower filler loadings. Therefore, it can be concluded that up to the optimized loading of GO, GO can be well-distributed in the matrix with the current processing parameters, and higher addition of GO will lead to agglomeration. The SEM studies are consistent with the results obtained for the mechanical properties of different polymer composites.

3.6. TEM analysis of FRP composites

TEM analysis was also conducted for the optimized composition, and the results are presented in Figure 3.10 which shows the TEM micrographs for B-EGF$_{0.25}$. It can be observed that the graphene oxide sheets are apart from each other (encircled in the image) and the spacing between the platelets is also non-uniform. This suggests an exfoliated morphology, consistent with the results obtained for XRD.

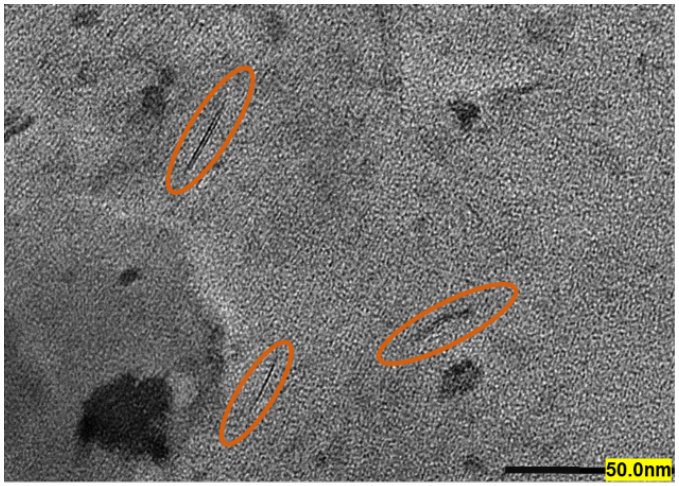

Figure 3.10. TEM micrograph of epoxy-based EGFP composites with 0.25 phr BC-GO (B-EGF$_{0.25}$)

3.7. Proposed mechanism for the role of functional groups in enhancing the mechanical properties of GF-epoxy composites using GO derived from different precursors

Well-functionalized GO, such as BC-GO, promotes better bonding with glass-fiber and epoxy matrix, ultimately leading to improved mechanical performance [68]. For example, the hydroxyl functional group of GF undergoes a substitution reaction with the epoxy groups on the GO surface at the curing temperature [26], with GO also bonding with epoxy polymer via hydrogen bonding [69]. All the possible chemical reactions for bonding between epoxide molecule of epoxy resin and various functionalities on GO or GF surface are depicted in Figure 3.11.

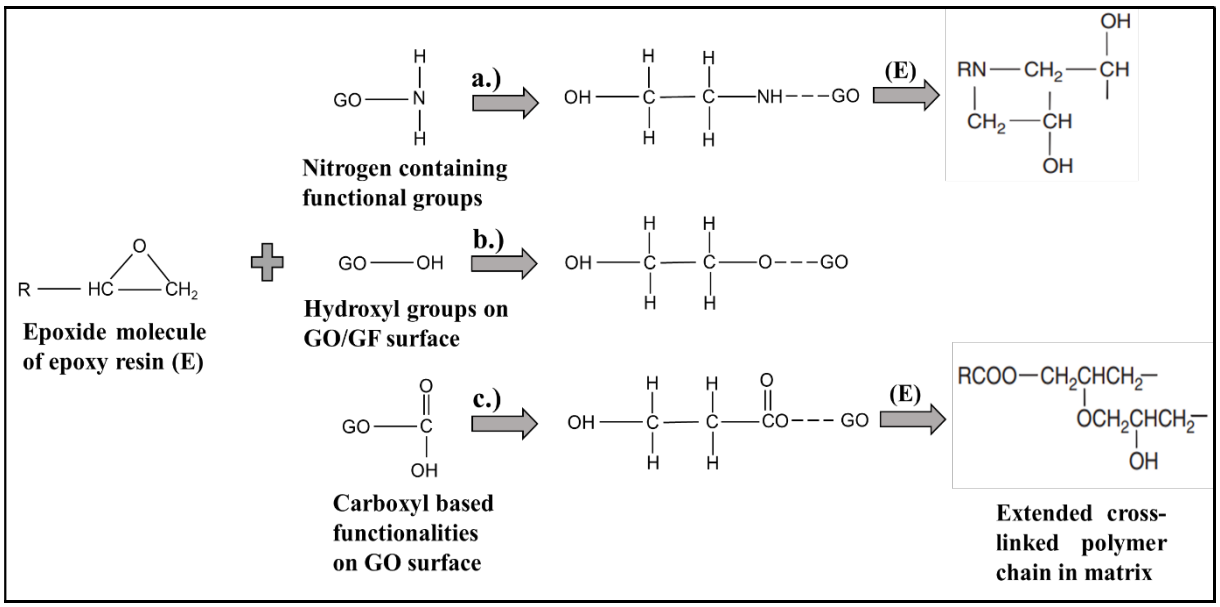

Figure 3.11. Polymerization between epoxide group and different types of functional groups on GO surface or GF surface

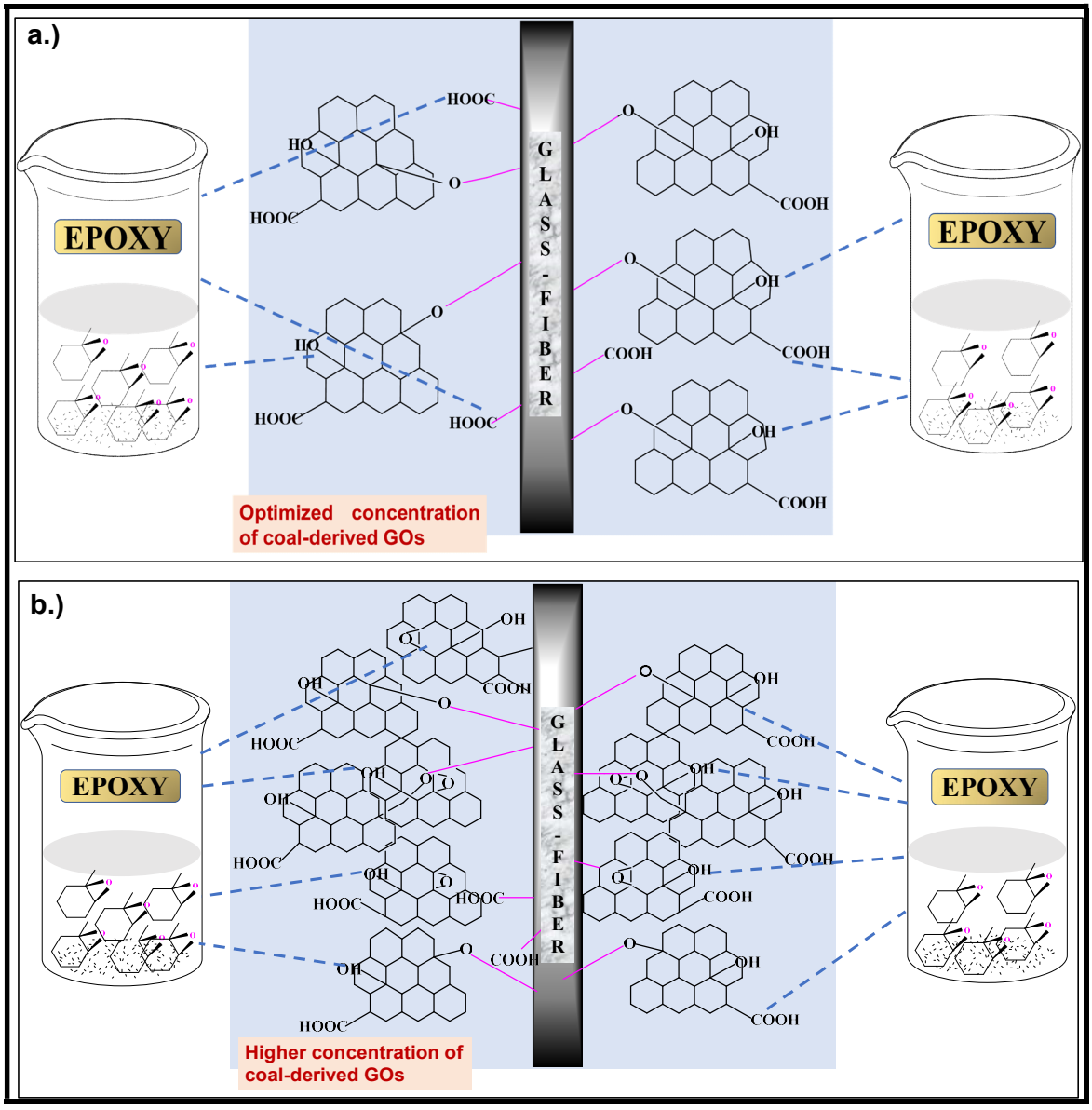

Figure 3.12. Mechanism showing the effective bonding among coal-derived GO/epoxy/glass-fiber at optimum and higher concentration of nanofiller

While Figure 3.11 illustrates the role of functional groups on GO or GO surfaces in facilitating reactions between various constituents of the composite, in Figure 3.12 we propose a mechanism to explain the greater enhancement of mechanical properties with BC-GO at its optimal concentration (0.25 phr), Figure 3.12 (a), and degradation in these properties beyond the optimal

concentration, Figure 3.12 (b), primarily due to agglomeration. We also posit why BC-GO performs better than Gr-GO in enhancing the mechanical properties.

Consider, for example, B-EGF$_{0.75}$, beyond the optimal value of GO filler. The agglomeration of GO within the system introduces steric hindrance, which leads to fewer GO platelets beyond the optimal concentration that can effectively bond with the epoxy. This, in turn, contributes to a deterioration in the mechanical properties of the composite. Additionally, the agglomeration of graphene oxide platelets reduces the aspect ratio of the filler, which further contributes to the degradation in mechanical properties [70].

In our previous work [42], we presented the mechanical properties of semi-anthracite coal-derived GO (AC-GO) in EGFP composites. It was reported that the optimal concentration of the AC-GO filler was 0.125 phr rather than 0.25 phr, which has been observed in the case of BC-GO in the present study. The difference in the optimum filler content loading between AC-GO and BC-GO can be explained based on the difference in particle size distribution calculated from DLS studies [42]. The smaller particle size distribution in AC-GO leads to a larger surface area-to-volume ratio compared to larger particles of BC-GO, which contributes to achieving better mechanical properties of AC-GO based composites at lower concentrations of nanofiller loading in EGFP systems as compared to BC-GO. Secondly, AC-GO possesses more functional groups as deduced from higher oxygen wt.% in AC-GO, 40.97 % compared to BC-GO, 26.44 % oxygen wt.% (as seen in EDX analysis [42]). Therefore, the enhancement in mechanical properties observed in AC-GO would be maximum at a lower AC-GO loading, since the greater number of functional groups can bond in a better way with epoxy resin and hardener. The enhancement in the mechanical properties at the respective optimum BC-GO loading in B-EGF composites is more than of AC-GO based composites. The possible reason for this can be the synthesis method and the influence of HNO_3 used in the process on the degree of oxidation. During the synthesis of AC-GO, we

utilized 16 M HNO_3 (for the reaction period of 3 days), while for BC-GO, we used only 5 M HNO_3 for a reaction time of 5 hours only (much milder conditions). A higher concentration of HNO_3 leads to a higher degree of oxidation in AC-GO. A similar argument has been substantiated by Fan et al. [71], who modulated the oxidation degree in their study to achieve adjustable interfaces between GO and the epoxy matrix. They observed that though the dispersion was fine at a higher degree of oxidation, yet the tensile properties tend to deteriorate at higher degree of oxidation due to impaired modulus and strength of GO sheets.

As far as the comparison of the performance of BC-GO and Gr-GO as a nanofiller in improving the mechanical properties of the composite is concerned, we note that in the case of Gr-GO, the formation of epoxide between two neighbouring carbon atoms eliminates the possibility to have delocalized π orbitals resulting in the formation of single bonds. Thus, some of the bonds lose their stiffness leading to a decrease in Young's modulus. Similar argument has been reported for Gr-GO by [72]. Unlike Gr-GO, BC-GO has fewer of these epoxide groups. They possess mostly hydroxyl, carboxyl, and nitrogen-based groups on the surface, which as explained earlier, lead to enhanced bonding between the glass fiber and the epoxy resin, but fewer epoxide groups [42]. The outcome is larger enhancement in mechanical properties in B-EGF composites as compared to Gr-EGF composites.

Conclusion

In this study, we conducted a comprehensive experimental study to assess the impact of bituminous coal-derived graphene oxide (BC-GO) and graphite-derived graphene oxide (Gr-GO) nanofillers on the mechanical properties of an E-glass fiber and epoxy resin composite (EGFP). The key takeaways from this study are:

The results clearly demonstrate that the incorporation of BC-GO and Gr-GO as nanofillers in EGFP significantly improves the effective bonding and strength of the glass fiber/matrix interface, as is evident from SEM micrographs, leading to overall improvements in mechanical properties.

Significant enhancements were observed in EGFPs reinforced with BC-GO at a loading of 0.25 phr (B-EGF$_{0.25}$). These are a 38.9 % increase in flexural strength, a 22.9 % increase in tensile strength, and a 21.6 % increase in impact strength. In comparison, the improvements for EGFPs reinforced with Gr-GO (Gr-EGF$_{0.25}$) are 28 %, 9.3 %, and 6.8 %, respectively. Both the tensile modulus and flexural modulus for B-EGF$_{0.25}$ and Gr-EGF$_{0.25}$ GO surpassed those of EGFP, with an increase of 31.5 % and 30.8 % for B-EGF0.25 and 28.6 % and 26.7 % for Gr-EGF$_{0.25}$, respectively.

DLS and FTIR studies showed that BC-GO possesses much smaller particles and abundant functionalities compared to Gr-GO, which contribute to a greater improvement in the mechanical properties of BC-GO based composites. These findings are significant as they offer insights into the design and optimization of an important class of composites, specifically GFRPs. Proper selection of a precursor and careful control of nanofiller concentration can yield nanocomposites with superior mechanical properties—critical for various industrial applications in the aerospace, marine, sports equipment, and defense sectors.

We anticipate that the promising results of our research will stimulate further exploration of different precursors, including other ranks of coal, biomass, along with various other polymers, thereby facilitating the development of cost-effective and environment-friendly advanced composite materials with tailored properties for a wide spectrum of industrial applications. Moreover, an additional facet that merits exploration within the scope of our current research is rheological studies. Conducting rheological analysis can shed light on the curing and curing kinetics of these composites, thereby facilitating better control over the manufacturing process.

Ultimately, this can lead to the development of composites with superior properties for practical applications.

- In the next chapter, we follow up the similar protocol and study the synergistic performance of two different nanofillers, namely halloysite nanotubes (HNT) clay and multiwalled carbon nanotubes (MWCNT), in conjunction with a fixed concentration (0.125 phr) of semi-anthracite coal-derived graphene oxide (AC-GO) on enhancing the mechanical properties of E-glass fiber reinforced epoxy resin composites (EGFPs).

References

[1] A. Landesmann, C.A. Seruti, E.D.M. Batista, Mechanical properties of glass fiber reinforced polymers members for structural applications, Mater. Res. 18 (2015) 1372–1383. https://doi.org/10.1590/1516-1439.044615.

[2] D. kumar Gara, G. Raghavendra, P. Syam Prasad, O. S, Enhanced mechanical properties of glass fibre epoxy composites by 2D exfoliated graphene oxide filler, Ceram. Int. 47 (2021) 34860–34868. https://doi.org/10.1016/j.ceramint.2021.09.027.

[3] F. Achema, B.S. Yahaya, E.S. Apeh, J.O. Akinyeye, Application of Glass Fibre Reinforced Composite in the Production of Light Weight Car Bumper (A Case Study of the Mechanical Properties), Int. J. Eng. Res. Technol. 6 (2017) 575–579.

[4] M. Garg, S. Sharma, R. Mehta, Role of curing conditions and silanization of glass fibers on carbon nanotubes (CNTs) reinforced glass fiber epoxy composites, Compos. Interfaces. 24 (2017) 233–253. https://doi.org/10.1080/09276440.2016.1201373.

[5] A. Purohit, V. Tripathy, S.K. Mishra, P.T.R. Swain, P.K. Patnaik, Mechanical and Tribo-performance Analysis of Linz Donawitz Sludge-Filled Glass–Epoxy Composites using Taguchi Experimental Design, J. Inst. Eng. Ser. E. 103 (2022) 245–251. https://doi.org/10.1007/s40034-021-00236-y.

[6] S.W. Mekonen, S. Palani, B. Ravi, S.M. Atnaw, M. Desta, Y. Regassa, Mechanical Properties of Bone Particulate and E-Glass Fiber Reinforced Hybrid Polymer Composite, Adv. Mater. Sci. Eng. 2022 (2022). https://doi.org/10.1155/2022/5902616.

[7] M.S. Salit, M. Jawaid, N. Bin Yusoff, M.E. Hoque, Manufacturing of natural fibre reinforced polymer composites, Springer, 2015. https://doi.org/10.1007/978-3-319-07944-8.

[8] R. Chopra, R.K. Gupta, M. Kumar, N. Akhtar, Experimental study on mechanical properties of E-Glass fiber reinforced with epoxy resin composite and compare its properties with hybrid composite, Mater. Today Proc. 63 (2022) 417–421. https://doi.org/10.1016/j.matpr.2022.03.435.

[9] P. Pradhan, A. Purohit, S.S. Mohapatra, C. Subudhi, M. Das, N.K. Singh, B.B. Sahoo, A computational investigation for the impact of particle size on the mechanical and thermal properties of teak wood dust (TWD) filled polyester composites, Mater. Today Proc. 63 (2022) 756–763.

[10] S. Ren, X. Tao, X. Ma, J. Liu, H. Du, A. Guo, J. Xu, Fabrication of fl y ash cenospheres-hollow glass microspheres / borosilicate glass composites for high temperature application, Ceram. Int. (2017) 0–1. https://doi.org/10.1016/j.ceramint.2017.10.089.

[11] A. Godwin Antony, P. Lakshmanan, S. V. Kajendira Kumar, S. Dinesh, K. Rajaguru, P. Parameswaran, Experimental evaluation of hybrid composites by the Cu addition, Mater. Today Proc. 21 (2020) 411–414. https://doi.org/10.1016/j.matpr.2019.06.378.

[12] V.K. Srivastava, P.S. Shembekar, R. Prakash, Fracture behaviour of fly-ash filled FRP composites, Compos. Struct. 10 (1988) 271–279. https://doi.org/10.1016/0263-

8223(88)90006-2.

[13] S.K. Shejkar, B. Agrawal, A. Agrawal, G. Gupta, Physical, mechanical, and sliding wear behavior of epoxy composites filled with surface modified walnut shell particulate, Polym. Compos. 43 (2022) 7526–7537. https://doi.org/10.1002/pc.26847.

[14] A. Purohit, P.T.R. Swain, P.K. Patnaik, Mechanical and sliding wear characterization of LD sludge filled hybrid composites, Mater. Today Proc. 26 (2019) 1654–1659. https://doi.org/10.1016/j.matpr.2020.02.345.

[15] H. Abushammala, J. Mao, Waste Iron Filings to Improve the Mechanical and Electrical Properties of Glass Fiber-Reinforced Epoxy (GFRE) Composites, J. Compos. Sci. 7 (2023) 90. https://doi.org/10.3390/jcs7030090.

[16] M.A. Rafiee, J. Rafiee, I. Srivastava, Z. Wang, H. Song, Z.Z. Yu, N. Koratkar, Fracture and fatigue in graphene nanocomposites, Small. 6 (2010) 179–183. https://doi.org/10.1002/smll.200901480.

[17] V. Cech, E. Palesch, J. Lukes, The glass fiber-polymer matrix interface/interphase characterized by nanoscale imaging techniques, Compos. Sci. Technol. 83 (2013) 22–26. https://doi.org/10.1016/j.compscitech.2013.04.014.

[18] R. Umer, Y. Li, Y. Dong, H.J. Haroosh, K. Liao, The effect of graphene oxide (GO) nanoparticles on the processing of epoxy/glass fiber composites using resin infusion, Int. J. Adv. Manuf. Technol. 81 (2015) 2183–2192. https://doi.org/10.1007/s00170-015-7427-1.

[19] R.K. Prusty, S.K. Ghosh, D.K. Rathore, B.C. Ray, Reinforcement effect of graphene oxide in glass fibre/epoxy composites at in-situ elevated temperature environments: An emphasis on graphene oxide content, Compos. Part A Appl. Sci. Manuf. 95 (2017) 40–

53. https://doi.org/10.1016/j.compositesa.2017.01.001.

[20] S. Sen Du, F. Li, H.M. Xiao, Y.Q. Li, N. Hu, S.Y. Fu, Tensile and flexural properties of graphene oxide coated-short glass fiber reinforced polyethersulfone composites, Compos. Part B Eng. 99 (2016) 407–415. https://doi.org/10.1016/j.compositesb.2016.06.023.

[21] S.P. Yeole, P.S. Jadhav, G.M. Joshi, Recent Scenario of Surfactants Modified Graphene and Its Derivatives-Based Polymer Nanocomposites, Macromol. Chem. Phys. 224 (2023) 2300122.

[22] A. Erklig, N.F. Dogan, M. Bulut, Charpy impact response of glass fiber reinforced composite with nano graphene enhanced epoxy, Period. Eng. Nat. Sci. 5 (2017) 341–346. https://doi.org/10.21533/pen.v5i3.121.

[23] Z. Li, R.J. Young, R. Wang, F. Yang, L. Hao, W. Jiao, W. Liu, The role of functional groups on graphene oxide in epoxy nanocomposites, Polymer (Guildf). 54 (2013) 5821–5829. https://doi.org/10.1016/j.polymer.2013.08.026.

[24] H. Ahmad, M. Fan, D. Hui, Graphene oxide incorporated functional materials: A review, Compos. Part B Eng. 145 (2018) 270–280. https://doi.org/10.1016/j.compositesb.2018.02.006.

[25] B. Zhang, R. Asmatulu, S.A. Soltani, L.N. Le, S.S.A. Kumar, Mechanical and thermal properties of hierarchical composites enhanced by pristine graphene and graphene oxide nanoinclusions, J. Appl. Polym. Sci. 131 (2014) 1–8. https://doi.org/10.1002/app.40826.

[26] A.K. Pathak, H. Garg, M. Singh, T. Yokozeki, S.R. Dhakate, Enhanced interfacial properties of graphene oxide incorporated carbon fiber reinforced epoxy

nanocomposite : a systematic thermal properties investigation, (2019).

[27] P. yan Hung, K. tak Lau, B. Fox, N. Hameed, J.H. Lee, D. Hui, Surface modification of carbon fibre using graphene–related materials for multifunctional composites, Compos. Part B Eng. 133 (2018) 240–257. https://doi.org/10.1016/j.compositesb.2017.09.010.

[28] Y. Lin, E. Bilotti, C.W.M. Bastiaansen, T. Peijs, Transparent semi-crystalline polymeric materials and their nanocomposites: A review, Polym. Eng. Sci. 60 (2020) 2351–2376. https://doi.org/10.1002/pen.25489.

[29] B.K. Kandola, F. Magnoni, J.R. Ebdon, Flame retardants for epoxy resins: Application-related challenges and solutions, J. Vinyl Addit. Technol. 28 (2022) 17–49.

[30] J. Tamuly, D. Bhattacharjya, B.K. Saikia, Graphene/graphene derivatives from coal, biomass, and wastes: Synthesis, energy applications, and perspectives, Energy & Fuels. 36 (2022) 12847–12874.

[31] B. Das, R. Kundu, S. Chakravarty, Preparation and characterization of graphene oxide from coal, Mater. Chem. Phys. 290 (2022) 126597. https://doi.org/10.1016/j.matchemphys.2022.126597.

[32] S. Pareek, D. Jain, R. Shrivastava, S. Dam, S. Hussain, D. Behera, Tunable degree of oxidation in graphene oxide: Cost effective synthesis, characterization and process optimization, Mater. Res. Express. 6 (2019) 85625. https://doi.org/10.1088/2053-1591/ab243a.

[33] J.C. Pandey, M. Singh, Dielectric polymer nanocomposites: Past advances and future prospects in electrical insulation perspective, SPE Polym. 2 (2021) 236–256.

https://doi.org/10.1002/pls2.10059.

[34] Y. Li, Q. Peng, X. He, P. Hu, C. Wang, Y. Shang, R. Wang, W. Jiao, H. Lv, Synthesis and characterization of a new hierarchical reinforcement by chemically grafting graphene oxide onto carbon fibers, J. Mater. Chem. 22 (2012) 18748–18752. https://doi.org/10.1039/c2jm32596a.

[35] L. Liu, F. Yan, M. Li, M. Zhang, L. Xiao, L. Shang, Y. Ao, Improving interfacial properties of hierarchical reinforcement carbon fibers modified by graphene oxide with different bonding types, Compos. Part A Appl. Sci. Manuf. 107 (2018) 616–625. https://doi.org/10.1016/j.compositesa.2018.02.009.

[36] M. Quaresimin, K. Schulte, M. Zappalorto, S. Chandrasekaran, Toughening mechanisms in polymer nanocomposites: From experiments to modelling, Compos. Sci. Technol. 123 (2016) 187–204. https://doi.org/10.1016/j.compscitech.2015.11.027.

[37] R. Atif, I. Shyha, F. Inam, Mechanical, thermal, and electrical properties of graphene-epoxy nanocomposites-A review, Polymers (Basel). 8 (2016). https://doi.org/10.3390/polym8080281.

[38] N.I. Zaaba, K.L. Foo, U. Hashim, S.J. Tan, W. Liu, C.H. Voon, Synthesis of Graphene Oxide using Modified Hummers Method : Solvent Influence, Procedia Eng. 184 (2017) 469–477. https://doi.org/10.1016/j.proeng.2017.04.118.

[39] S.S. Shams, L.S. Zhang, R. Hu, R. Zhang, J. Zhu, Synthesis of graphene from biomass: A green chemistry approach, Mater. Lett. 161 (2015) 476–479. https://doi.org/10.1016/j.matlet.2015.09.022.

[40] D.C. Marcano, D. V Kosynkin, J.M. Berlin, A. Sinitskii, Z. Sun, A. Slesarev, L.B. Alemany, W. Lu, J.M. Tour, Improved Synthesis of Graphene Oxide, 4 (n.d.).

[41] Mahajan, R. L.; Seul-Yi, L. E. E. U.S. Patent Application No. 17/415 4452022.

[42] A. Garg, S. Basu, S.-Y. Lee, R.L. Mahajan, R. Mehta, Simplified One-Pot Synthesis of Graphene Oxide from Different Coals and its Potential Application in Enhancing the Mechanical Performance of GFRP Nanocomposites, ACS Appl. Nano Mater. (2023).

[43] Bharadwaj B, Singh P, Mahajan RL. Thermal performance of different carbonaceous nanoparticles as additives to thermal paste as an Interface material. International Electronic Packaging Technical Conference and Exhibition. Vol 85505. American Society of Mechanical Engineers; 2021, October: V001T08A002.

[44] S.Y. Lee, R.L. Mahajan, A facile method for coal to graphene oxide and its application to a biosensor, Carbon N. Y. 181 (2021) 408–420. https://doi.org/10.1016/j.carbon.2021.05.007.

[45] D. Ren, K. Li, L. Chen, S. Chen, M. Han, M. Xu, X. Liu, Modification on glass fiber surface and their improved properties of fiber-reinforced composites via enhanced interfacial properties, Compos. Part B Eng. 177 (2019) 107419. https://doi.org/10.1016/j.compositesb.2019.107419.

[46] K. Prabhakar, S. Debnath, M. Anwar, K. Palanikumar, Experimental Analysis on the Effect of Surface Treatment of Glass Fibers & Nanoclay on Mechanical Properties of Glass Fiber Reinforced Polymer Nanocomposites, IOP Conf. Ser. Mater. Sci. Eng. 495 (2019). https://doi.org/10.1088/1757-899X/495/1/012091.

[47] M.B. Aberem, W. Feng, A. Ait-Kadi, B. Riedl, J. Brisson, Modification of glass fiber surface by nylon-6,6 grafting, Compos. Interfaces. 12 (2005) 425–443. https://doi.org/10.1163/1568554054275715.

[48] G.K. Arun, N. Sreenivas, K.B. Reddy, K.S. Krishna Reddy, M.E. Shashi Kumar, R.

Pramod, Investigation on Mechanical Properties of Graphene Oxide reinforced GFRP, IOP Conf. Ser. Mater. Sci. Eng. 310 (2018). https://doi.org/10.1088/1757-899X/310/1/012158.

[49] N. V. Pujar, N. V. Nanjundaradhya, R.S. Sharma, Effect of graphene oxide nano filler on dynamic behaviour of GFRP composites, AIP Conf. Proc. 1943 (2018). https://doi.org/10.1063/1.5029683.

[50] S.A. Bansal, A.P. Singh, A. Kumar, S. Kumar, N. Kumar, J.K. Goswamy, Improved mechanical performance of bisphenol-A graphene-oxide nano-composites, J. Compos. Mater. 52 (2018) 2179–2188. https://doi.org/10.1177/0021998317741952.

[51] M.F. Maqsood, M.A.A. Zubair, M.A. Raza, S.M.Z. Mehdi, N. Lee, Z.U. Rehman, K. Park, M.U. Bhatti, U. Latif, A. Tawakkal, Fabrication and characterization of graphene oxide and glass fiber-based hybrid epoxy composites, Polym. Compos. 43 (2022) 8072–8083. https://doi.org/10.1002/pc.26952.

[52] S.N. Alam, N. Sharma, L. Kumar, Synthesis of Graphene Oxide (GO) by Modified Hummers Method and Its Thermal Reduction to Obtain Reduced Graphene Oxide (rGO)*, Graphene. 06 (2017) 1–18. https://doi.org/10.4236/graphene.2017.61001.

[53] Z.B. Siddique, S. Basu, P. Basak, Development of Graphene Oxide Dispersed Natural Ester Based Insulating Oil for Transformers, IEEE Trans. Dielectr. Electr. Insul. 28 (2021) 1326–1333. https://doi.org/10.1109/TDEI.2021.009445.

[54] O. Adekomaya, A.A. Adediran, K. Adama, Characterization and morphological properties of glass fiber reinforced epoxy composites fabricated under varying degrees of hand lay-up techniques, J. Appl. Sci. Environ. Manag. 22 (2018) 110. https://doi.org/10.4314/jasem.v22i1.20.

[55] H. Alhumade, H. Rezk, A.M. Nassef, M. Al-Dhaifallah, Fuzzy Logic Based-Modeling and Parameter Optimization for Improving the Corrosion Protection of Stainless Steel 304 by Epoxy-Graphene Composite, IEEE Access. 7 (2019) 100899–100909. https://doi.org/10.1109/ACCESS.2019.2930902.

[56] S.I. Abdullah, M.N.M. Ansari, Mechanical properties of graphene oxide (GO)/epoxy composites, HBRC J. 11 (2015) 151–156. https://doi.org/10.1016/j.hbrcj.2014.06.001.

[57] K. Kanny, T.P. Mohan, Resin infusion analysis of nanoclay filled glass fiber laminates, Compos. Part B Eng. 58 (2014) 328–334. https://doi.org/10.1016/j.compositesb.2013.10.025.

[58] J. Deng, Y. Song, Z. Lan, Z. Xu, Y. Chen, B. Yang, H. Hao, The surface modification effect on the interfacial properties of glass fiber-reinforced epoxy: A molecular dynamics study, Nanotechnol. Rev. 11 (2022) 1143–1157. https://doi.org/10.1515/ntrev-2022-0068.

[59] Y. S, Effect of Epoxy Functional Groups on the Properties of Carbon Fiber-Epoxy Composites, J. Appl. Mech. Eng. 06 (2017) 4–10. https://doi.org/10.4172/2168-9873.1000276.

[60] Sundaram V, Finch DS, Hooker SA, Mahajan RL. Thermal, electrical, and mechanical characterization of carbon nanotubes epoxy composites, Proceedings, HT-FED 2004 ASME Heat Transfer/Fluids Engineering Summer Heat Transfer Conference, Chrolette, NC, USA, July 11–16, pp. 1–6.

[61] S.Y. Fu, X.Q. Feng, B. Lauke, Y.W. Mai, Effects of particle size, particle/matrix interface adhesion and particle loading on mechanical properties of particulate-polymer composites, Compos. Part B Eng. 39 (2008) 933–961.

https://doi.org/10.1016/j.compositesb.2008.01.002.

[62] S. Siraj, A.H. Al-Marzouqi, M.Z. Iqbal, W. Ahmed, Impact of Micro Silica Filler Particle Size on Mechanical Properties of Polymeric Based Composite Material, Polymers (Basel). 14 (2022). https://doi.org/10.3390/polym14224830.

[63] T. Nanda, G. Sharma, R. Mehta, D. Shelly, K. Singh, Mechanisms for enhanced impact strength of epoxy based nanocomposites reinforced with silicate platelets, Mater. Res. Express. 6 (2019). https://doi.org/10.1088/2053-1591/ab1023.

[64] A. Purohit, G. Gupta, P. Pradhan, A. Agrawal, Development and erosion wear analysis of polypropylene/Linz-Donawitz sludge composites, Polym. Compos. 44 (2023) 6556–6565. https://doi.org/10.1002/pc.27579.

[65] A. Purohit, J. Dehury, L.N. Rout, S. Pal, A Novel Study of Synthesis, Characterization and Erosion Wear Analysis of Glass–Jute Polyester Hybrid Composite, J. Inst. Eng. Ser. E. 104 (2023) 1–9.

[66] A.N. Gent, C. Wang, Matrix cracking initiated by fibre breaks in model composites, J. Mater. Sci. 27 (1992) 2539–2548. https://doi.org/10.1007/BF01105067.

[67] A.L. Yesgat, R. Kitey, Effect of filler geometry on fracture mechanisms in glass particle filled epoxy composites, Eng. Fract. Mech. 160 (2016) 22–41. https://doi.org/10.1016/j.engfracmech.2016.03.034.

[68] H. Mahmood, M. Tripathi, N. Pugno, A. Pegoretti, Enhancement of interfacial adhesion in glass fiber/epoxy composites by electrophoretic deposition of graphene oxide on glass fibers, Compos. Sci. Technol. 126 (2016) 149–157. https://doi.org/10.1016/j.compscitech.2016.02.016.

[69] J. Keyte, K. Pancholi, J. Njuguna, Recent Developments in Graphene Oxide/Epoxy

Carbon Fiber-Reinforced Composites, Front. Mater. 6 (2019) 1–30. https://doi.org/10.3389/fmats.2019.00224.

[70] O. Shakuntala, G. Raghavendra, A. Samir Kumar, Effect of filler loading on mechanical and tribological properties of wood apple shell reinforced epoxy composite, Adv. Mater. Sci. Eng. 2014 (2014). https://doi.org/10.1155/2014/538651.

[71] J. Fan, J. Yang, H. Li, J. Tian, M. Wang, Y. Zhao, Cryogenic mechanical properties of graphene oxide/epoxy nanocomposites: Influence of graphene oxide with different oxidation degrees, Polym. Test. 96 (2021) 107074. https://doi.org/10.1016/j.polymertesting.2021.107074.

[72] M. Tavakol, A. Montazeri, S.H. Aboutalebi, R. Asgari, Mechanical properties of graphene oxide: The impact of functional groups, Appl. Surf. Sci. 525 (2020) 146554. https://doi.org/10.1016/j.apsusc.2020.146554.

Chapter 4. *Enhancement in Mechanical Properties of GFRP-Coal-derived Graphene Oxide Composites by Addition of Multiwalled Carbon Nanotubes and Halloysite Nanotubes: A Comparative Study*

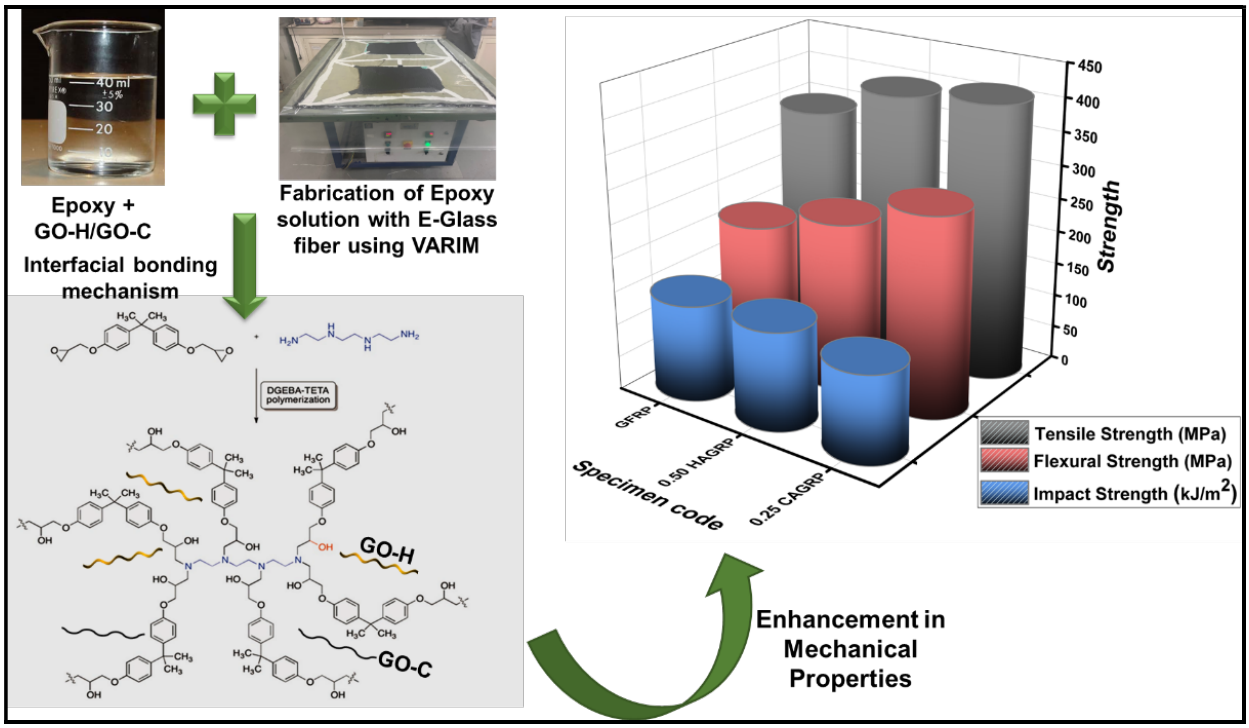

Highlights

- GO-H demonstrates superior mechanical performance comparable to GO-C in EGFPs.
- 0.50 phr HAGRP improves 18.3% flexural, 14.6% tensile, 1.8% impact strengths.
- Beyond 0.50 phr HAGRP and 0.25 phr CAGRP, mechanical properties were decreased.
- XRD, FESEM, FTIR revealed strong interfacial adhesion between nanofillers and epoxy.

4.1. Introduction

Over the past few decades, extensive research has been conducted on fiber-based polymeric nanocomposites in response to advancements in materials development and their potential applications in various domains [1], including but not limited to structural components of aircrafts, wind blades, marine, and sports equipment [2]. Composite materials, utilizing advanced material preparation techniques, optimize properties by the synergy of two or more material components with distinct properties, resulting in the creation of multiphase solid materials [3][4]. The remarkable characteristics of fiber-based composite materials, such as their lightweight composition, high strength, corrosion resistance, and exceptional durability, have garnered significant interest within the scientific and engineering community.

The exceptional performance of polymer matrix composites reinforced with E-glass fiber has been extensively acknowledged and supported by documented evidence. Among thermosetting polymers, epoxy resins have emerged as the predominant choice for high-performance applications, including fiber-reinforced composites, coatings, structural adhesives, and various other engineering applications. Epoxy resins are distinguished by their outstanding mechanical and thermal properties, remarkable chemical and corrosion resistance, minimal curing shrinkage, and adaptability to diverse processing conditions [5]. Nevertheless, the inherent rigidity and brittleness of highly cross-linked epoxy resins hinder their applicability in various end-use applications, particularly as structural materials, due to their poor crack resistance [6]. To address these challenges, the industry uses several nanofillers in fiber-based composites to transfer the stress from the matrix to the nanofiller by adding a small concentration of nanofillers, thereby enhancing their mechanical properties [7,8].

Among different nanofillers, carbon nanotubes (CNTs) have been extensively explored as a versatile reinforcement material in polymer matrices due to their exceptional mechanical, electrical, and thermal properties [9][10][11]. For example, they have been used to synthesize

Multi-Walled Carbon Nanotubes Glass Fiber Reinforced Polymer (MWCNT-GFRP) composites, which find specific applications in aircraft fairing skins, crucial for achieving streamlined surfaces and reducing drag, and closing gaps in aircraft components. These nanocomposites are also employed in wind farms to effectively absorb radar and radio frequency microwave energy [12]. Mahato et al. [13] conducted a study to assess the impact of adding MWCNTs at different concentrations (0.1, 0.3, and 0.5 wt.%) into GFRP composites, with a focus on elucidating the tensile behavior under varying crosshead speeds (1, 10, 100 mm/min). The results showed that the tensile strength steadily increased with an increase in the concentration of MWCNTs from 0.1 to 0.3 wt.% for all crosshead speeds, reaching an optimum at 0.3 wt.%. However, upon further addition of MWCNTs, extending to 0.5wt.%, there was a slight decrease in tensile modulus, attributable to the clustering of MWCNTs in the polymer matrix. In a study by Yip et al. [14], MWCNTs-GFRP composite laminates were created using ultrasonication and the hand lay-up method. The aim was to investigate the interlaminar shear strength (ILSS) and flexural strength of composites with varying amounts of MWCNTs. The findings revealed that the mechanical properties were optimized when the MWCNT content reached 0.75 percent hundred resin (phr). The ILSS exhibited a substantial improvement of 15.7%, and the flexural strength increased by 9.2%. Zhang et al. [15] investigated the effects of different wt.% of MWCNTs (0.4, 0.75, and 1.1) in the epoxy system of pre-stretched GFRP composites, finding that GFRP samples with 0.75 wt.% of MWCNTs exhibited higher tensile strength with minimal damage. Moreover, GFRP samples containing 0.4 wt.% of MWCNTs showed superior flexural strength and failure strain compared to the neat GFRP samples. Panchagnula et al. [16] studied the impact of varying MWCNT concentrations on the mechanical properties of glass fiber-reinforced plastics, for which epoxy resins were modified with different wt.% of MWCNTs: 0.1%, 0.2%, 0.3%, and 0.4%. Among the tested samples, the GFRP reinforced with 0.3% MWCNTs exhibited superior tensile strength at 242.22 MPa and flexural strength at 332.53 MPa compared to the neat GFRPs (178.05

MPa and 238.42 MPa, respectively) without MWCNTs. Additional studies on MWCNT-GFRP nanocomposites [17–20], fabricated with varying concentrations of MWCNTs, also demonstrated improved mechanical properties when compared to neat GFRP composites.

Although CNTs show promise as nanofillers in GFRP composites, their high production costs have hindered their commercial feasibility [17]. The production of CNTs involves complex and specialized manufacturing processes like chemical vapor deposition (CVD) or laser ablation, which require sophisticated equipment and precise control over reaction conditions. These factors contribute to the high production costs of CNTs [21,22]. Additionally, producing CNTs with consistent properties and high purity is still a challenge, which results in a restricted supply [23,24]. As a result, the demand for CNTs often exceeds the available quantity, driving up their prices.

Halloysite nanoclay (HNT), characterized by the general chemical formula of $Al_2Si_2O_5(OH)_4.nH_2O$, is a promising substitute for CNTs [25]. Originating from the prolonged weathering of alumina silicates, halloysite is a naturally occurring mineral. It commonly exists as fine, tubular structures with specific dimensions, featuring a length range of 300-1500 nm, an inner diameter ranging from 15 to 100 nm, and an outer diameter falling within 40-120 nm. Due to their high aspect ratio and satisfactory mechanical strength, these tubular halloysite structures (HNTs) hold the potential as a cost-effective alternative to carbon nanotubes (CNTs) in reinforcing polymers [26]. However, despite these promising attributes, limited studies have explored HNT-reinforced E-glass fiber-based epoxy nanocomposites. M. Rajaei et al. [27] conducted a study comparing the effects of two nanoclays (halloysite nanotubes (HNT) and layered double hydroxide (LDH)) on the fire resistance and mechanical properties of an epoxy composite containing ammonium polyphosphate. The results showed that reinforcing with HNT nanoclay significantly reduced the heat release of the epoxy resin by 87%. Moreover, HNT

exhibited superior tensile properties and was a more cost-effective option compared to LDH nanoclay.

Kim et al. [28] studied the impact of heat-treated HNTs (at various temperatures) on the mechanical properties of epoxy resin in a humid environment. The findings indicated that glass fiber-reinforced plastic (GFRP) with 0.5 wt.% heat-treated HNTs at 700°C exhibited superior resistance to moisture absorption, as well as increased tensile strength and interlaminar shear strength. The reinforcement of HNTs in the carbon fiber for improved mechanical behaviour has also been reported. In [26], the infusion of HNT into epoxy resin was successfully achieved, and these composites were utilized for the impregnation of carbon fiber textiles. At 2 wt.% HNT content, the impact strength of the hybrid composite increased by 25%, compared to that of neat composite without HNT. Ramamoorthi et al. [29] employed HNTs to augment epoxy glass fiber composites and investigated the effect of varying HNT concentrations (1-10 wt.%) on mechanical properties. The tensile strength and modulus rapidly increased with an increase in the concentration of HNTs, peaking at 4 wt.% HNT, accompanied by 33.71% and 31.01% increase, respectively, over those for the neat epoxy/glass fiber composite, A subsequent increase to 10 wt.% resulted in a decline in these mechanical properties. In [30], the authors presented the preparation method for synthesizing composites of HNTs and graphene oxide (GO). The process required modifications to the nanofillers (3-chloropropyl trimethoxysilane for chlorinated HNTs and ethylenediamine for GO modification) to achieve compatibility for preparing the composite. The results showed that the modified HNT/GO composite produced through this innovative approach exhibited excellent adsorption capabilities for levofloxacin across the pH range of 1-10. Notably, both nanofillers underwent functionalization, HNT using an expensive silane agent, and GO through ethylenediamine.

Hashmi et al. [31] exclusively utilized HNTs to fabricate epoxy-HNT nanocomposites using the solution-casting approach. Their investigation of the mechanical behavior of these composites

demonstrated that the nanocomposite containing 3 wt.% of HNTs, homogenized through ultrasonication, displayed superior mechanical strength as compared to other counterparts within this study. Lapcik et al. [32] studied the ductility and plasticity of the HNTs/epoxy composites and graphene/epoxy composites, separately. Enhanced ductility was observed in the graphene-based nanocomposite samples, with an increase in elongation at break from 0.33 mm (neat matrix) to 0.46 mm (1 wt.% graphene), representing a 39% increase. Taken together, these studies indicate the potential of HNTs as effective nanofillers in GFRP composites to improve their mechanical properties.

In our recent research reported in [33], we utilized semi-anthracite coal-derived GO (AC-GO) synthesized through the one-pot method as a nanofiller in the epoxy-based E-glass fiber-reinforced GFRP composites. The impact of this addition was substantial, with an 18.35% increase in tensile strength and a 30.9% boost in tensile modulus. Similarly, flexural strength and flexural modulus recorded improvements of 22.7% and 25.1%, respectively. Even the impact strength experienced a modest increase of 6.7% when AC-GO was loaded at 0.125 phr in the GFRP composites. These results demonstrate the potential of AC-GO in enhancing the mechanical strength of epoxy-based, fiber-reinforced composites. Building upon the existing literature on the reinforcement of GFRP composites with MWCNTs or HNTs and leveraging insights from our recent investigation on semi-anthracite coal-derived graphene oxide (AC-GO) based GFRP composites for improved mechanical strength, we formulated a hypothesis to guide our present study. It centers around the question whether the addition of a small amount of AC-GO to HNT-based GFRP composites can enhance mechanical properties comparable to those achieved with AC-GO and MWCNT-based GFRP composites. Both HNTs and MWCNTs are one-dimensional (1D) nanofillers and possess a cylindrical morphology. It is reasonable to postulate that if both nanofillers can deliver similar enhancements in the mechanical performance of GFRPs, this could significantly contribute to

overcoming the challenges associated with the high cost and limited availability of MWCNTs. Notably, HNTs are abundantly available and more cost-effective compared to MWCNTs.

To test our hypothesis, we systematically characterized and tested the mechanical properties of both HNT- and MWCNT-based GFRP composites at various concentration levels of these nanofillers. For simplicity, we adopt the following nomenclature scheme throughout this text: 'x' denotes the varying concentration of HNTs or MWCNTs, followed by 'H' for HNTs or 'C' for MWCNTs, and 'A' for AC-GO (maintained at a fixed concentration of 0.125phr in all the composites). Accordingly, a GFRP composite is named as 'xHAGRP' or 'xCAGRP'. When referring to nanofillers only, they are abbreviated as 'GO-H' and 'GO-C', with varying concentrations of HNT or CNT (ranging from 0.125 phr to 0.75 phr) but a fixed concentration of AC-GO (0.125 phr).

The materials and methods employed to synthesize these composites, their characterization using different techniques, and the resulting mechanical properties are detailed in Sections 4.2-4.5. Section 4.6 delves into essential insights regarding the interfacial bonding mechanism between AC-GO, HNTs, or MWCNTs, and GFRP, while the last section summarizes the key findings of our study.

4.2. Materials and methods

4.2.1 Materials

The epoxy resin, Araldite CY 230-1, along with the curing agent Aradur HY 951, was obtained from Huntsman Advanced Materials in India. Known for their diglycidyl ether functionality and aliphatic amine functionality [34], these materials were blended in a weight ratio of 10:1 to form the epoxy resin. Glass fiber mats were acquired from Revex Plasticizers Pvt. Ltd. in India. Halloysite nanotubes (HNTs) were purchased from Sigma Aldrich, while Multiwalled carbon nanotubes (MWCNTs) were obtained from Reinste Nano Ventures Pvt Ltd in New Delhi, India. AC-GO was synthesized in-house using a facile one-pot method [31]. Raw chunks of semi-

anthracite coal were sourced from coalfields in Kashmir, supplied by SVISPAT Pvt Ltd in Pune, Maharashtra, India. Merk provided hydrochloric acid, ethanol, hydrofluoric acid, and nitric acid. Double distilled water was utilized to prepare reagents and for washing purposes during the experimental procedures.

4.2.2. Synthesis of coal-derived GO via one-pot method

The raw coal, initially of nut size, was subjected to ball milling in order to reduce its particle size to below 100 μm. To purify the raw coal powder, a solution of acids, 37% HCl, and 50% HF in 500 ml of distilled water was employed. The resulting mixture was stirred using a magnetic stirrer for 36 hours. Following this agitation, the mixture was left undisturbed for 12 hours, resulting in the formation of black precipitates settling at the bottom of the beaker. Subsequent to this step, three grams of purified coal were oxidized using 16 M HNO_3 at a temperature of 120°C for 5 hours. The resultant solution, containing oxidized Coal-GO, was then neutralized and subjected to probe sonication for 4 hours, followed by centrifugation. The resulting AC-GO solution was subsequently dried in an oven at a temperature lower than 60°C [33,35].

4.2.3. Fabrication of GFRP nanocomposites

Drawing from our previous work [33], which identified the optimal mechanical properties for AC-GO at a concentration of 0.125 phr, we fixed this value of the concentration of AC-GO for the current investigation and varied the concentration range for HNTs and MWCNTs (0.125 phr - 0.75 phr) in the E-glass fiber reinforced epoxy (EGFP) composites. Initially, AC-GO along with the varying concentrations of HNTs and MWCNTs, was dispersed in the epoxy resin and homogenized at 20,000 rpm for 10 minutes, followed by probe sonication at 80% amplitude for 10 minutes in an ice-bath to allow dissipation of excessive heat. This solution was mechanically stirred at 500 rpm for a duration of 10 minutes. The hardener was then introduced, and the resulting dispersion was infused into the VARIM (Vacuum Assisted Resin Infusion Molding)

mold. Following the procedure outlined in [33][34][36], the VARIM table was cleaned using a cleansing agent before coating it with a mold release agent to prevent sticking. Following the guidelines set by ASTM standards, two-ply mats were employed for testing tensile and flexural properties, while specimens for impact testing were prepared using twelve layers of this mat. To ensure uniform resin distribution, a separator cloth was placed on the top layer of the glass-fiber mat, followed by a placement of a perforated sheet. A wire-mesh was integrated to enhance resin flow, and an infusion pipe was secured over it using a sealant tape. Furthermore, a breather cloth was utilized to form a bridge across the wire-mesh to facilitate smooth resin flow. In the concluding phase of the manufacturing process, the entire setup was covered with a lamination sheet and sealed using sealant tape. To maintain a vacuum pressure of around 1 mbar, a vacuum pump was employed during the resin infusion process. This ensured that the fiber mat was thoroughly impregnated with the resin. After the infusion, the nanocomposite sheets underwent a curing stage, followed by two separate post-curing phases, each lasting 6 hours. The initial post-curing was conducted at a temperature of 23 ℃, followed by the second at 60 ℃. Figure 4.1 illustrates the overall protocol and visual representation of the process followed during preparation of sheets.

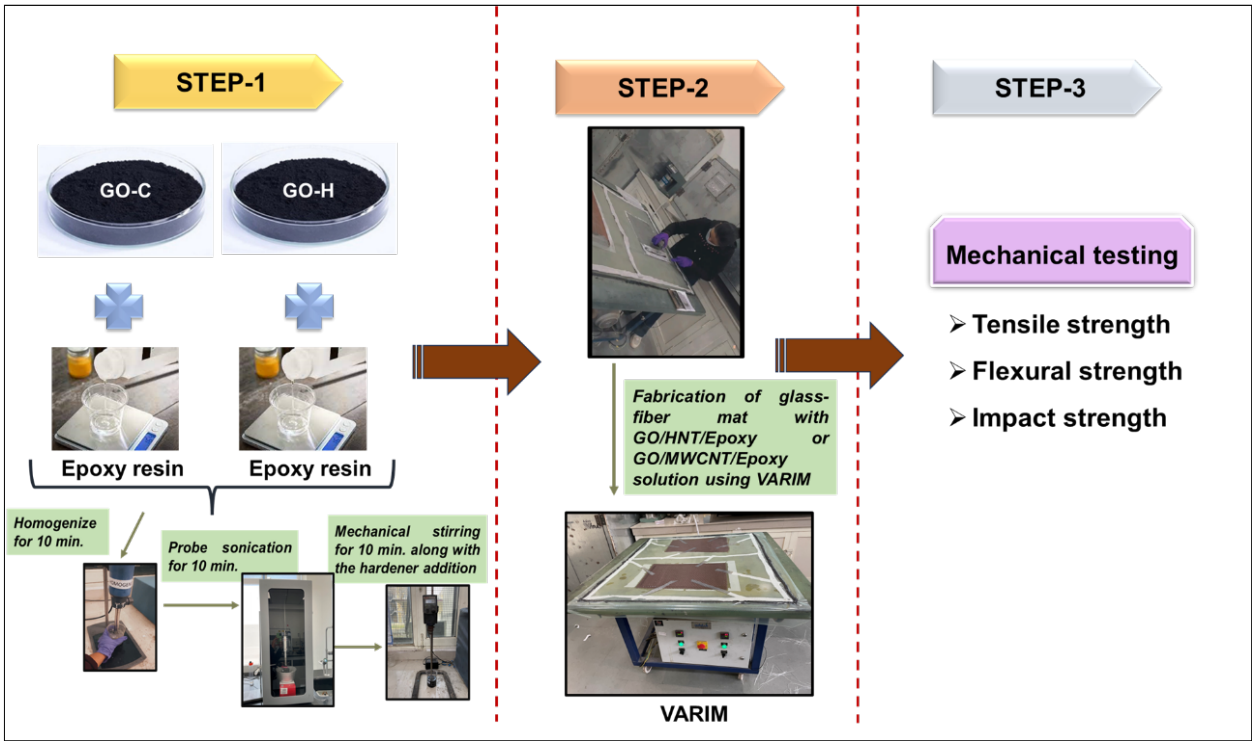

Figure 4.1. Schematic representation/camera visuals for the synthesis of GO-H and GO-C based EGFP nanocomposites using VARIM

4.3. Characterization and Mechanical testing

To assess the properties of nanocomposites comprising AC-GO, HNT clay, and MWCNT with EGFP, a range of analytical techniques was employed, including FESEM (Field Emission Scanning Electron Microscopy), TEM (Transmission Electron Microscopy), XRD (X-Ray Diffraction), and FTIR (Fourier Transform Infrared Spectroscopy). X-Ray Diffraction analysis (XRD) was conducted using a PANalytical X-ray diffractometer equipped with Ni-filtered Cu Kα radiations (λ = 0.1504 nm). The scanning rate was set at 2 degrees per minute in the 10–90º range, with an applied voltage of 45 kV. TEM characterization was performed using a Hitachi (H-7500) microscope operating at an acceleration voltage of 110 kV. Fractographic analysis of fractured composite samples was conducted using a ZEISS field emission scanning electron microscope (FESEM) with an accelerating voltage of 5 kV. To analyze the functional groups, present in different concentrations within the prepared composites and identify any chemical modifications

resulting from the addition of AC-GO/HNTs or MWCNTs, a Shimadzu FTIR spectrophotometer (IRTacer-100) was employed. FTIR analysis was conducted by scanning the range of 400-4000 cm^{-1}. Particle size distribution measurements of the dispersed graphene oxide in deionized water were performed using a dynamic light-scattering method (DLS) with the Zetasizer instrument from Malvern. The composite specimens for mechanical testing, including impact, tensile strength, and flexural strength were prepared following the guidelines outlined in ASTM D 256–02, ASTM D 3039, and ASTM D 790–02, respectively. The tensile strength and flexural strength of the composites were assessed using a Universal Testing Machine (UTM) manufactured by Zwick/Roell in Germany. For impact testing, a Tinius Olsen impact tester (model-IT504) was utilized. To ensure reproducibility, five specimens were prepared and tested for each strength property in all the composites.

4.4. Results and Discussion

4.4.1 XRD and FTIR of EGFP nanocomposites

The XRD patterns for different nanofillers, HNT clay, CNT, and AC-GO along with EGFP (without nanofiller) are shown in Figure 4.2a. The peak at 2θ (002) = 23.9^0 corresponds to the crystalline carbon and the other peak at 2θ = 42.3^0 in AC-GO represents the plane reflection of graphite (100) [33]. MWCNTs exhibit the typical peaks at 2θ = 25.8^0 and 42.7^0, corresponding to the graphite (002) and (100) reflections [37].

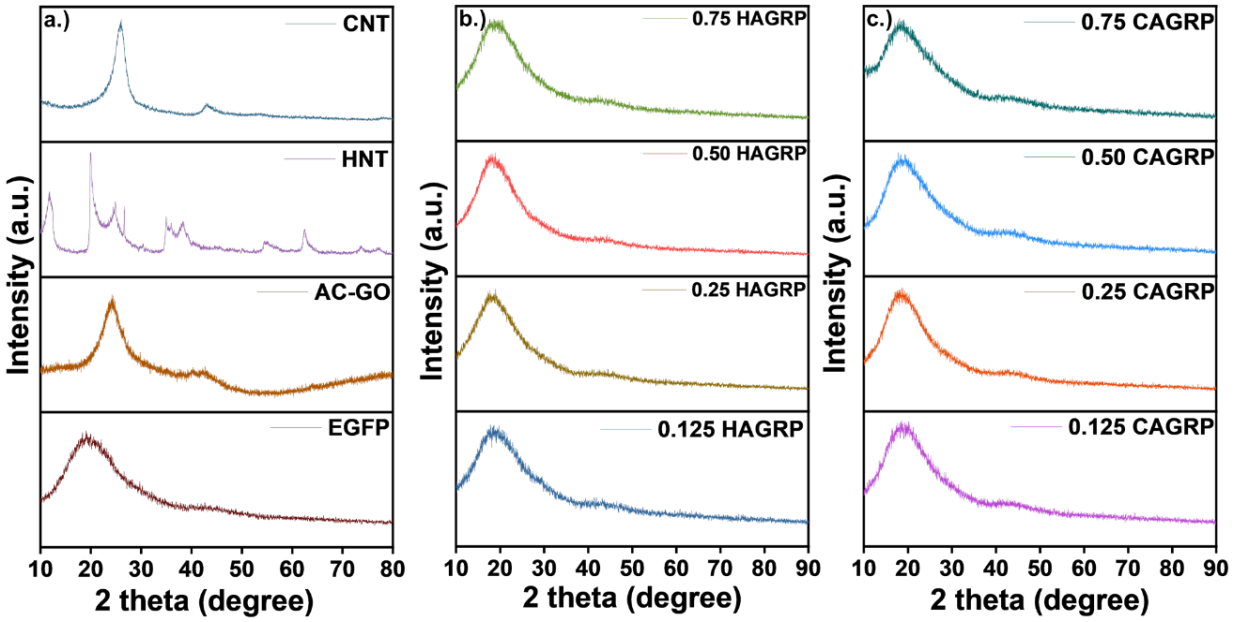

Figure 4.2. XRD spectra of various synthesized coal-derived GO, HNT, CNT, and EGFP composites.

The XRD pattern of the halloysite exhibits well-defined diffraction peaks, indicative of the crystalline nature of the HNT clay. This XRD pattern was matched and indexed to the ICDD (International Centre for Diffraction Data) 00-029-1487, which is associated with metahalloysite or aluminium silicate hydroxide. The diffraction peaks observed at 2θ values of 12.0^0, 20.3^0, 24.6^0, 35.1^0, 38.0^0, 54.7^0, and 62.5^0 correspond to the (001), (100), (002), (110), (003), (210), and (300) crystallographic planes, respectively. The presence of the (001) peak at $2\theta = 12.0^0$ indicates a layer spacing of 0.73 nm, characteristic of halloysite with a 7 Å layer structure. The dehydrated state of the material was further confirmed by the appearance of the (100) diffraction peak at $2\theta = 20.3^0$, corresponding to a layer spacing of 0.43 nm. In its hydrated form, halloysite exhibits a layer distance of 10 Å. However, upon dehydration, which is an irreversible process, the layer distance reduces to 7 Å. This is characteristic of tubular halloysite similar in morphology to MWCNT [38].

Conversely, in the absence of any nano reinforcement, the X-ray diffraction (XRD) spectrum of EGFP exhibits a distinct diffraction peak at $2\theta = 19.02^0$, which is attributed to the presence of residual crystalline silica within the composite material. As no other recognizable diffraction peaks were detected in the EGFP composite, it can be inferred that the composite, without the nanofiller, possesses an amorphous structure. Additionally, the absence of identifiable peaks without nanofillers indicates a homogeneous distribution of glass fibers throughout the matrix [39].

The XRD diffractograms of CAGRP and HAGRP composites (Figure 4.2b) for 0.125 phr of AC-GO (fixed) and different concentrations of HNTs or MWCNTs), when compared with that of EGFP alone (Figure 4.2a), clearly show no other distinct peaks corresponding to the crystalline planes of the respective HNTs or MWCNTs or AC-GO. This implies that the incorporation of nanofillers does not influence the degree of crystallinity of the corresponding EGFP composites [40]. The consistent presence of an identical peak in all EGFP composites, suggests that the morphology of the reinforced EGFPs is predominantly exfoliated. This observation holds true regardless of the specific composition or type of nanofiller employed.

The FTIR spectra of cured epoxy/glass fiber composites with AC-GO and HNT or CNT (different loadings) are shown in Figure 4.3. Figure 4.3a shows the FTIR spectra for different nanofillers used in the EGFP composites. In the synthesized AC-GO, additional functional groups are observed. The peaks at 3490 cm^{-1} and 3468 cm^{-1} in AC-GO correspond to O-H stretching mode, while those at 2983 cm^{-1}, 1913 cm^{-1}, 1710 cm^{-1}, and 1181 cm^{-1} are attributed to C-H stretching vibration, C=C=C stretch, C=O stretching and C-N stretching vibrational mode, respectively. The C-N stretch refers to the possession of N in coal's inherent structure, which is due to degraded plant matter. In HNT clay, specific absorption bands at 911 and 3695 cm^{-1} due to Al–O–OH bending and O–H stretching confirm the presence of HNT. A specific in-plane stretching vibration in HNT found at 1091 cm^{-1} and 1032 cm^{-1} is due to the presence of Si–O–Si [41]. FTIR spectra for

CNT didn't show any oxygen-related functionalities depicting its purity [42,43]. For brevity, only the spectra corresponding to the target concentration are presented, as all the peaks were almost similar.

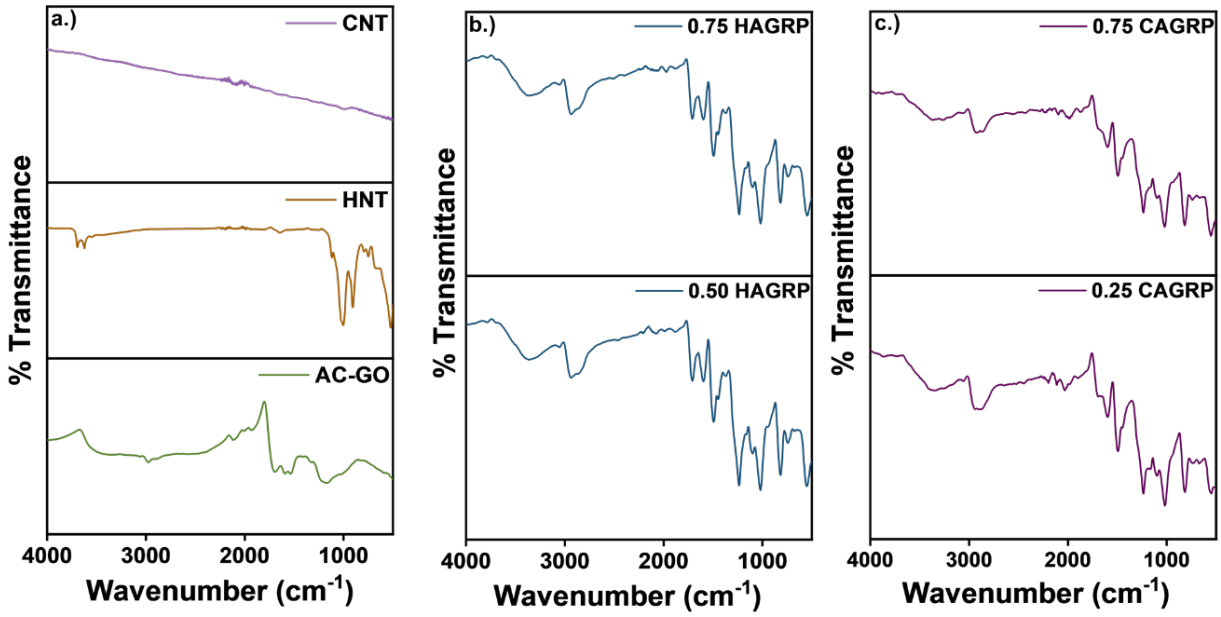

Figure 4.3. FTIR spectra a.) different nanofillers used; b, c.) synthesized EGFPs with the incorporation of reinforcement material, AC-GO with HNT clay, or AC-GO with MWCNT

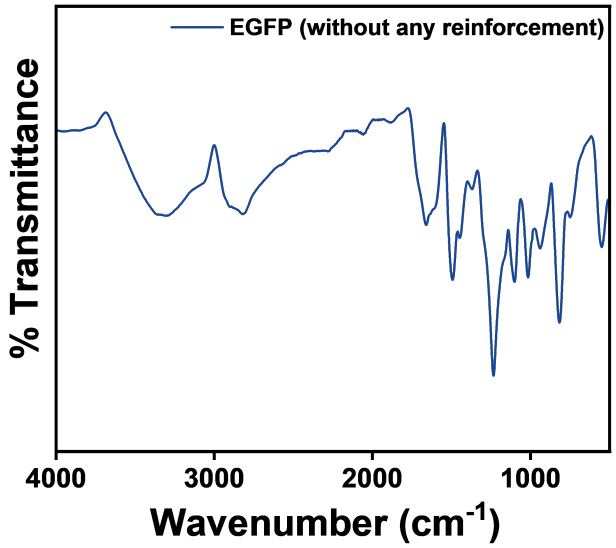

Figure 4.4. FTIR spectra of E-Glass fiber/epoxy composite (without any reinforcement)

Figure 4.4 shows the FTIR spectra of the EGFP composite without the addition of any nanofiller. Notably, the spectra are similar for composites, both with and without the nanofiller. This is due to the presence of abundant functional groups, such as epoxides, carbonyls, and hydroxyl in epoxy and glass fiber, as well as a significant amount of oxygen-based functional groups in graphene oxide, resulting in overlapping peaks. The strong and broad peaks observed between 3319 cm^{-1} to 2910 cm^{-1} can be attributed to the presence of hydroxy (-OH stretch) groups. The peaks arising between 1598 cm^{-1} to 1715 cm^{-1}, and 1438 cm^{-1} to 1450 cm^{-1} correspond to the bending vibrations of C-H bonds in the composite material. The peak at 1598 cm^{-1} could also be indicative of N-H bending vibrations, arising from the presence of N in the microstructure of coal-derived GO, as reported in [33,44].

The GO obtained from coal has an additional amino group functionality, which would enable a much more efficient stress transfer to the epoxy matrix, as compared to GO derived from commercially available graphite. The peak at 1360 cm^{-1} in these composites shows the presence of phenolic functionality based -OH group. Lastly, the peaks from 1234 cm^{-1} to 1015 cm^{-1} depict the C-O stretching vibration, while those at 820 cm^{-1}, 738 cm^{-1}, and 729 cm^{-1} are associated with C-H bending vibration.

4.4.2 Tensile and Flexural properties of EGFP composites reinforced with AC-GO and HNT clay or MWCNT nanofillers

In this section, we investigate the effect of incorporating AC-GO with HNT clay (GO-H) and AC-GO with MWCNT (GO-C) nanofillers on the mechanical behavior of glass fiber-reinforced polymer composites (EGFPs). First, consider the tensile strength and tensile modulus data displayed in Figures 4.5a and 4.5b for HAGRP and CAGRP with four different loadings of HNT or MWCNT ranging from 0.125 phr to 0.75 phr, with AC-GO fixed at 0.125 phr. For both GO-H and GO-C, the tensile strength initially increases with an increase in the loading rate, reaching a maximum at 0.50 phr for HNT and 0.25 phr for MWCNT. Beyond these optimal values, a further

increase in the loading rate led to a decrease in tensile strength due to agglomeration of the nanofillers. Agglomeration reduces the exposed surface area of GO-H and GO-C, leading to fewer functional groups available for bonding with the epoxy matrix and poorer dispersion of particles in the matrix, thereby reducing the efficiency of stress transfer from the matrix to the reinforcing GO-H and GO-C [45].

Notably, the incorporation of GO-H leads to a comparable increase in tensile strength (14.6%) at the optimal loading of 0.50 phr; for GO-C, this increase is 18.7% at the optimal loading of 0.25 phr. Additionally, the tensile modulus for both GO-H and GO-C is also higher than that of EGFP, see Figure 4.5b, it being 26.8% for 0.50 HAGRP, and 33.8% for 0.25 CAGRP. Interestingly, as the numbers indicate, the relative advantage in the tensile modulus of GO-H and GO-C is distinctly higher than the improvement observed for the tensile strength. This increase in tensile modulus can be attributed to the strong H-bonding interactions between the different nanotubes and AC-GO and their varying dispersion in the matrix which synergistically affect the overall moduli. Coleman et al. [46] reported that the modulus increase is maximized with the use of small-diameter multi-walled nanotubes (MWNTs). These materials tend to have a large surface area per unit volume which results in very good load transfer to the nanotube network. Single-walled nanotubes (SWNTs) are deemed unsuitable for composite reinforcement due to dispersion challenges leading to bundle formation [47]. HNTs have stronger bonding with AC-GO due to the additional advantage of possessing functional groups over their surface. Also, they possess weak tube-tube interactions owing to their better dispersion in the matrix, thereby mitigating bundle formation issues. Better dispersion and interactions synergistically lead to better load transfer from the matrix to the nanofiller, resulting in enhanced stiffness and consequently, a higher tensile modulus.

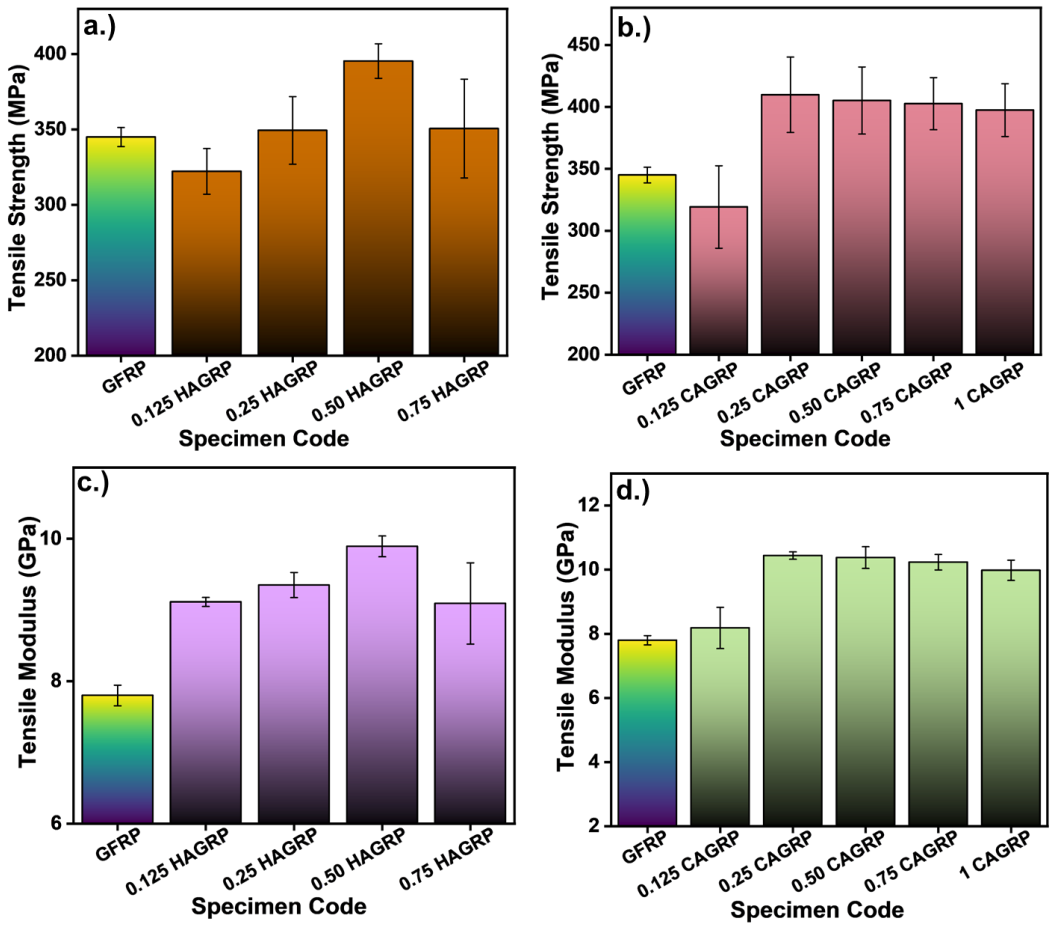

Figure 4.5. a,b) Tensile strength, and c,d) Tensile modulus of GO-H (AC-GO/HNT) and GO-C (AC-GO/MWCNT) reinforced EGFP composites

Figure 4.6 displays the data for flexural strength and flexure modulus of the EGFP composites with GO-H and GO-C at different HNT or MWCNT loadings, with a fixed AC-GO concentration. Similar to tensile properties, the maximum gains in flexural strength and flexure modulus were observed at a loading of 0.50 phr for HNT and 0.25 phr for MWCNT. Among the two GO-based composites, GO-C exhibited the highest increase in flexural strength (40.3%) compared to an 18.3% increase for GO-H over the flexural strength of EGFP. Yip et al. [14] synthesized the fabrication of CNTs/GFRP composite laminates using ultrasonication and the hand lay-up method to investigate interlaminar shear strength (ILSS) and flexural strength. At 0.75 phr of CNTs in the composite system, the ILSS was significantly improved by 15.7%, and flexural strength improved

by 9.2%. In our study, the addition of GO-C enhances the flexural strength by 40.3%, highlighting the combined effect of AC-GO and MWCNT. Also, Panchagnula et al. [16] observed that the flexural strength of MWCNT-GFRPs increased from 238.42 MPa (Neat GFRP) to 332.53 MPa (nearly 39.41%) with the addition of 0.3% of MWCNTs. Significantly, the flexural modulus was higher for GO-H, 38.9% than 28.6% for GO-C, both as compared to EGFP. Bozkurt et al. [48] conducted a study to assess the impact of clay incorporation, specifically Montmorillonite (MMT) and organically modified Montmorillonite (OMMT), on the mechanical and thermal properties of epoxy-clay GFRP nanocomposites. They varied the clay concentration at levels of 1%, 3%, 6%, and 10% by weight. The tensile modulus exhibited minimal variation with the addition of both MMT and OMMT, remaining relatively constant up to a clay concentration of 6%. In terms of tensile strength, there was a slight improvement observed in MMT/epoxy composites compared to OMMT/epoxy composites. For flexural properties, both flexural strength and modulus increased with the addition of clay, with more pronounced enhancements observed in the OMMT-based composites. Interestingly, the introduction of OMMT led to an increase in the fracture toughness of GFRP nanocomposites, while the presence of MMT had the opposite effect, decreasing fracture toughness.

Most of the literature emphasizes the need for functionalization for HNTs and CNTs to enhance their mechanical properties. In our study, the addition of a small concentration of AC-GO to HNT enhanced the mechanical performance comparative to CNTs. Increasing the filler concentration in the composites resulted in a rise in both tensile and flexural strength, attributed to the reinforcing effect where filler particles efficiently distribute the applied load. The impact is more significant with optimal adhesion and interaction between the filler and the matrix material. Variations in tensile and flexural strength due to alterations in filler percentage hinge on a complex interplay of factors such as filler type, filler-matrix interaction, and the degree of dispersion.

The modulus of the particulate composite depends on the relative magnitude of the particle size. There exists a critical particle size beyond which the composite modulus remains unaffected. Below this critical size, the impact on composite modulus is more substantial. The specific value of this critical particle size cannot be predetermined, as it depends on the particle, matrix, and particle/matrix adhesion. Aligning with [49], we decided to rule out the effect of particle size on modulus. Nevertheless, comparing the relative values for modulus and strength, we observed that flexural modulus was higher for GO-H than flexural strength. This can be attributed to the well-aligned HNT and AC-GO nanoparticles in the direction of stress where they can contribute more to the flexural modulus by resisting deformation in that direction. However, the impact on flexural strength might be less pronounced. Also, proper dispersion and distribution of HNT and AC-GO within the epoxy matrix are crucial. Uniform dispersion allows for better stress transfer and can enhance stiffness, contributing to a higher flexural modulus. In the case of GO-C, the flexural strength improves over modulus, highlighting the aspect ratio. Nanofillers with a high aspect ratio, such as nanotubes or nanowires, offer superior reinforcement by effectively bridging cracks and distributing stress within a matrix. The effect of aspect ratio on the optimal concentration and improvement in the properties is detailed in Section 4.6.

4.4.2.1. Role of interfacial strength in the overall improvement in mechanical properties

Han et al. [50] reported the introduction of graphene and CNTs into the epoxy resin, resulting in improved interfacial miscibility, attributed to the formation of a gradient interface layer between the fiber and the matrix. The gradient interface layer proves beneficial to reducing stress concentration, delaying crack propagation, and enhancing energy dissipation. It effectively redirects the crack path from the fiber surface to the interface area and promotes the transfer of stress from the matrix to the reinforcement. We believe this mechanism plays an important role in the 40.3% improvement in flexural strength and 18.7% increase in tensile strength observed in the case of GO-C based composites. In the case of GO-H based composites, the oxygen-containing

functional groups present on the surface of HNT, when decorated with AC-GO, can undergo chemical reactions with the polymer matrix, establishing a chemical connection between the fibers and the polymer. The carboxyl groups on GO-H, possessing nucleophilic characteristics, induce the ring opening of epoxy groups, initiating chemical reactions during the curing process. These reactions contribute to the formation of a robust multi-scale reinforced composite interface layer between glass fibers and GO-H. This interface layer serves to alleviate stress concentration, impede crack propagation, and enhance energy dissipation in the material, thereby contributing to the notable improvements observed in GO-H based EGFPs.

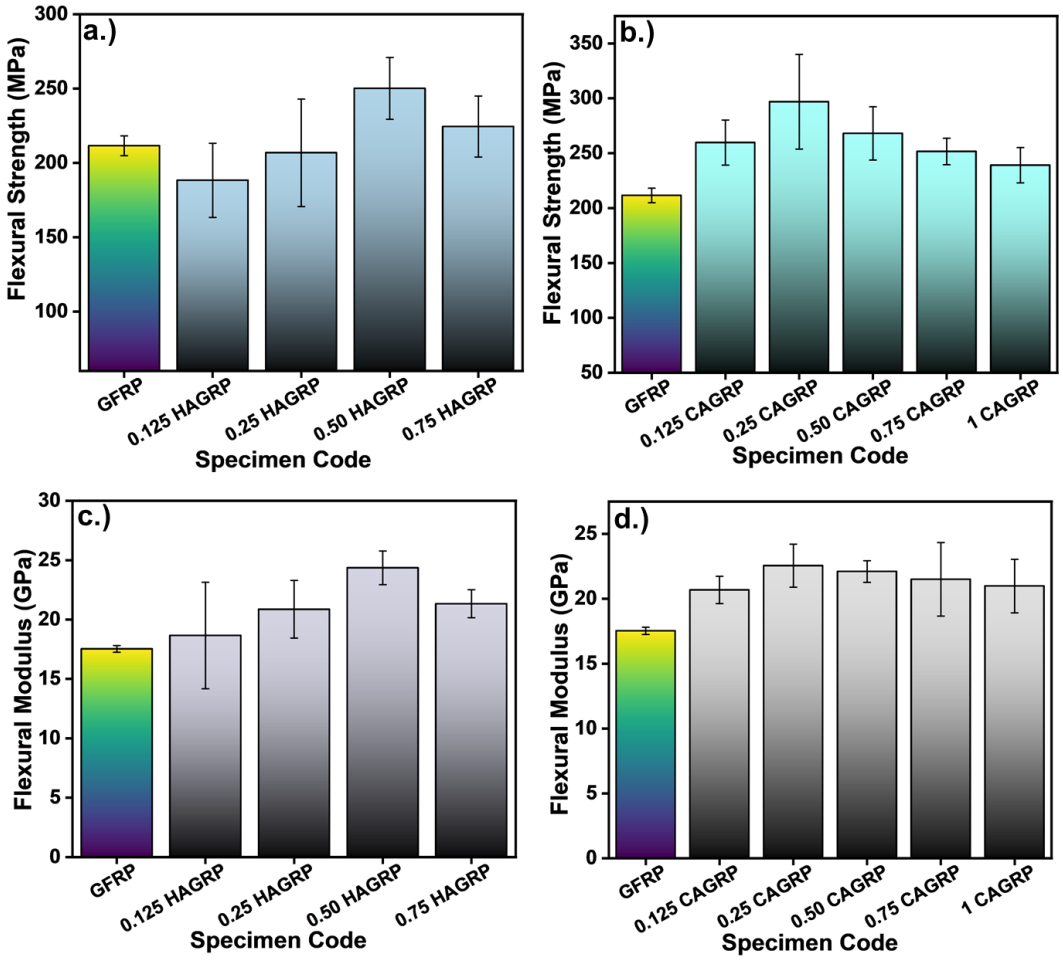

Figure 4.6. a,b) Flexural strength, and c, d) Flexural modulus of GO-H and GO-C reinforced EGFP composites

4.4.3 Impact Strength of EGFP composites reinforced with AC-GO and HNT clay or CNT nanofillers

To complete our study of the effect of GO-H and GO-C fillers on the mechanical properties of their composites with EGFP, we present in Figure 4.7, the impact strength of all the composites, both with or without nano reinforcements, to assess their load-bearing capacity under sudden loading conditions. The impact strength increased slightly by 1.8% for 0.50 HAGRP but for 0.25 CAGRP, it decreased by 10.5% compared to that of EGFP. It is noteworthy that both of these had the highest increase in tensile modulus within their respective categories.

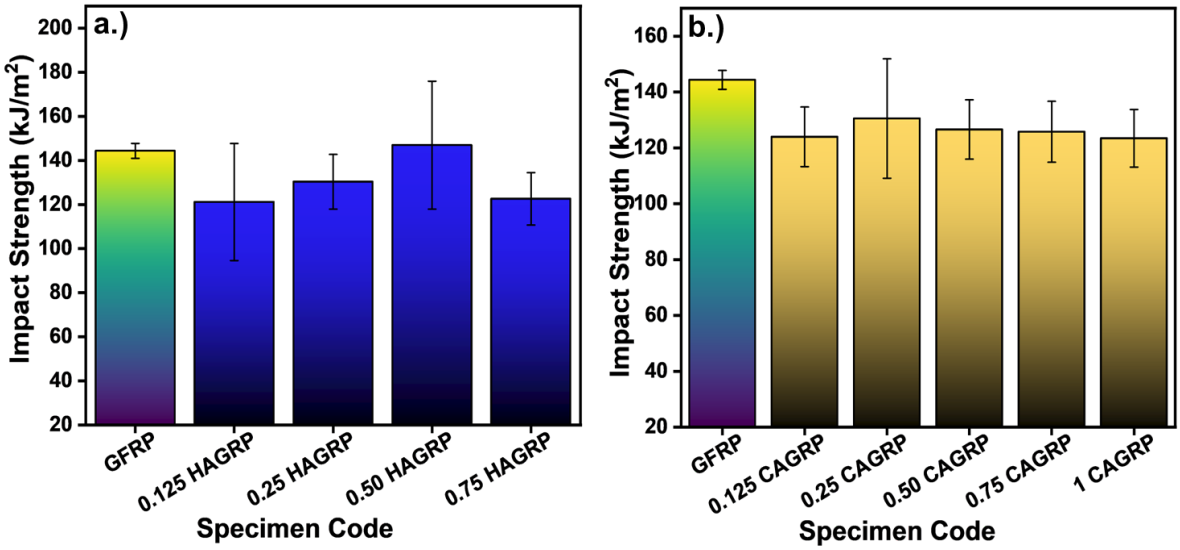

Figure 4.7. a, b) Impact strength of GO-H and GO-C reinforced EGFP composites

Lingaraju et al. [51] synthesized epoxy-clay GFRPs, incorporating two types of clays (HNTs and silica) to study the Izod impact strength of nanocomposites. They observed an 8% improvement in impact strength (with a 2.5 mm notch radius) with 2 wt.% HNT, but this enhancement diminished beyond this reinforcement level. In alignment with our earlier findings on tensile strength, their study reported an 11% improvement in tensile strength on the addition of HNT clay till 3 wt.%, which then declined with a further increase in clay content. The reduction in impact strength upon the incorporation of GO-C can be attributed to the introduction of defects or weak points in the

composite structure. These defects can act as initiation points for cracks, facilitating crack propagation under impact loading, and consequently reducing the overall impact strength [52].

4.5. FESEM images of fractured surfaces of FRP composites

FESEM analysis was conducted to examine the fractured surfaces of impact samples, focusing on dispersion and compatibility—two major factors that govern the interaction between glass fiber and the epoxy polymer matrix. Our examination revealed several noticeable wide gaps between fibers and the epoxy matrix, indicating a lack of strong interfacial adhesion. This lack of bonding between the fiber and the matrix contributes to a large fiber pull-out upon the application of stress, ultimately causing a decrease in the resistance to fracture, and the fibers detaching readily from the matrix. This detachment gives rise to the creation of voids, culminating in an uncomplicated material fracture. Due to the weak interfacial bonding, the material undergoes deformation under relatively low loads. In other words, EGFPs without GO-H and GO-C fillers have low strength [53].

On the other hand, the composites with enhanced tensile strength (0.50 HAGRP and 0.25 CAGRP) exhibited reduced fiber pull-out, see Figure 4.8a, b. The improved interfacial bonding contributed to higher stress transfer between the fiber and the matrix, thereby enhancing strength. The fundamental mechanism underlying the enhancement in impact strength of a polymer matrix reinforced with nano-fillers is well understood and essentially revolves around impeding crack propagation. As deformation initiates and a crack advances within the composite material, it encounters multiple nanofillers and interfaces between fibers and the matrix, which collectively impede the progression of the crack. The resistance exerted by the fillers forces the crack to alter its trajectory, effectively prolonging its path. Alternatively, the crack's advancement through the material may also result in the fracturing or splintering of the fillers themselves. This process requires a large amount of energy [54,55]. This requirement, coupled with the significant increase

in the tensile and flexural properties of the composite material, results in higher impact strength of the composites.

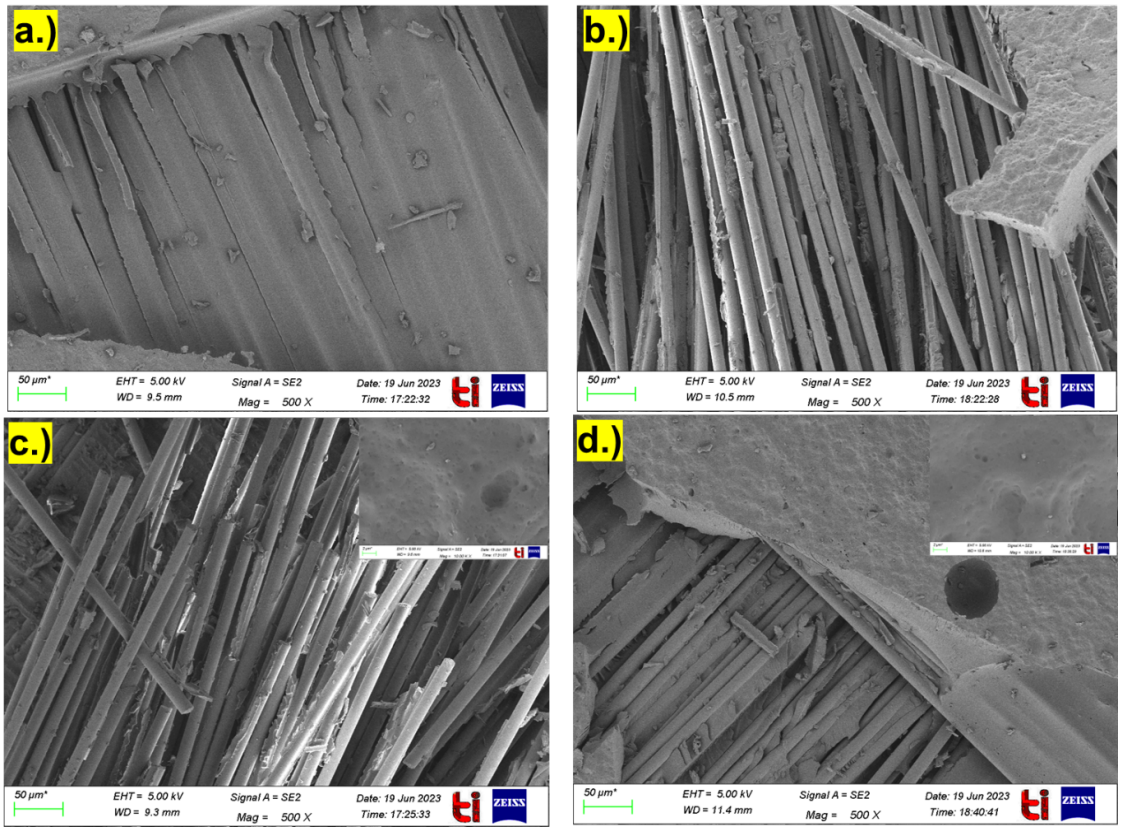

Figure 4.8. FESEM micrographs of a,b.) 0.50 HAGRP and 0.25 CAGRP c,d.) 0.75 HAGRP and 0.75 CAGRP

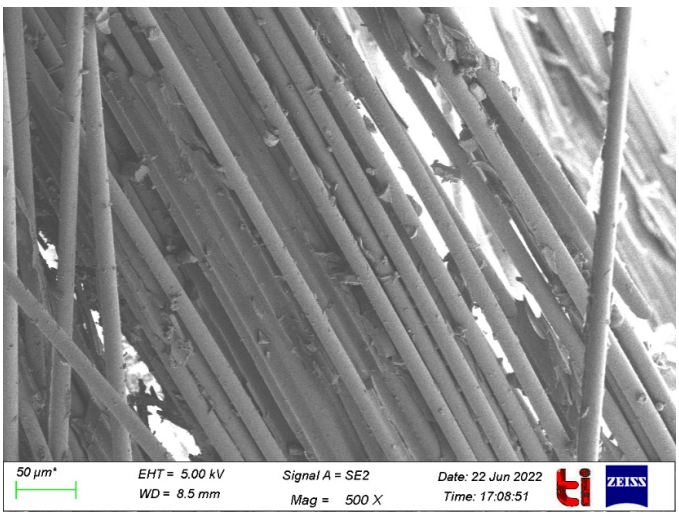

Figure 4.9. FESEM micrograph of E-Glass fiber/epoxy composite (without any reinforcement)

We also utilized FESEM micrographs in support of our argument that beyond the optimal concentration of HNT-based HAGRP and CNT-based CAGRP in the composites (for instance, 0.75 phr for HNT and CNT), a decrease in mechanical properties is attributable to particle aggregation and poor bonding. From the FESEM micrographs in Figure 4.8 c, d, it can be seen that the size of aggregates is much bigger at higher filler loadings (0.75 phr) than that observed at lower filler loadings, indicating agglomeration beyond optimized concentrations.

Noting that clear identification of GO-H and GO-C in the polymer matrix from the FESEM micrograph is quite difficult, we performed EDX analysis and elemental mapping to confirm the presence of our nanofillers. The EDX mapping (see Figure 4.10) confirms the presence of C, O (from AC-GO or CNT) as well as aluminosilicates (from HNT clay or Glass fiber).

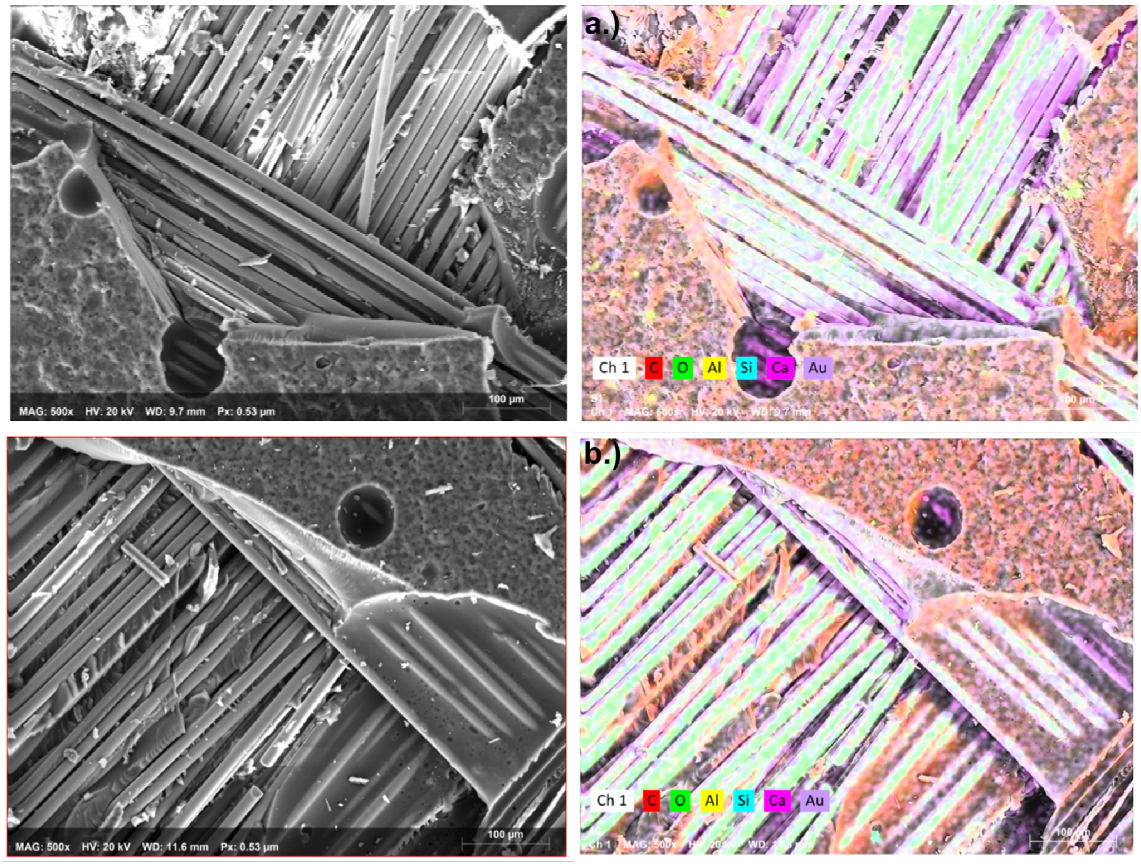

Figure 4.10. EDX mapping of a.) HAGRP composite and b.) CAGRP composite

4.6. Proposed mechanism for the role of functional groups and aspect ratio in enhancing the mechanical properties of GF-epoxy composites using GO-H and GO-C

4.6.1. Role of functional groups

Well-functionalized nanofillers, specifically GO-H and GO-C, play a pivotal role in improving the mechanical performance of glass-fiber-epoxy composites by fostering enhanced bonding with both the glass fiber and epoxy matrix [52]. Surface silanol groups on HNT are very advantageous for different types of functionalization purposes. In our previous work [33], we demonstrated that coal-derived GO oxidized using HNO_3, contains predominant carboxyl and hydroxyl functional groups on the surface. Silano groups on HNT engage in hydrogen bonding with these functional groups on the GO surfaces, forming additional interactions through π-π interactions and van der Waals forces. In contrast, MWCNTs lack abundant functional groups, as confirmed by FTIR. However, van der Waals interactions allow CNTs and GO to physically adsorb onto each other. This non-covalent interaction allows for the formation of hybrid structures where CNTs can be coated or decorated with GO sheets. In other words, AC-GO can be used as a platform for functionalization of CNTs. By attaching functional groups to GO, the dispersion and compatibility of CNTs within the epoxy are enhanced. Also, the π-π interactions between the aromatic rings of CNTs and AC-GO can facilitate the dispersion of CNTs on GO sheets or vice versa. These interactions contribute to the stability of hybrid structures and help prevent aggregation in the epoxy matrix.

Furthermore, GO-H and GO-C nanofillers with surface-exposed hydroxyl, carboxyl, and a few epoxides interact dominantly with the epoxy matrix as well as glass fiber through hydrogen bonding. Stronger and more stable interactions with epoxy and glass fiber, particularly when HNT is decorated with AC-GO, contribute to the composite's superior strength compared to GO-C.

4.6.2. Role of the aspect ratio of nanofillers

The aspect ratio of these nanofillers (ratio of length to diameter) is another key factor in determining how they influence the composite's mechanical behavior [56]. Nanofillers with high aspect ratio nanofillers, such as nanotubes or nanowires, provide enhanced reinforcement due to their ability to bridge cracks and distribute stress more effectively within a matrix. In our study, we have observed that GO-C exhibits its peak mechanical properties at 0.25 phr of CNT, whereas GO-H excels at 0.50 phr of HNT.

This enhanced performance of the two nanofillers may be attributed to the difference in their aspect ratios, with CNT and HNT possessing aspect ratios of 0.5 and 0.04, respectively. Relatively higher aspect-ratio CNTs contribute to improved mechanical properties by effectively transferring loads along their length [57]. Therefore, GO-C even at a lower nanofiller loading in EGFPs i.e., 0.25 phr of CNT, shows comparable mechanical enhancement to GO-H, whose optimal loading is 0.50 phr.

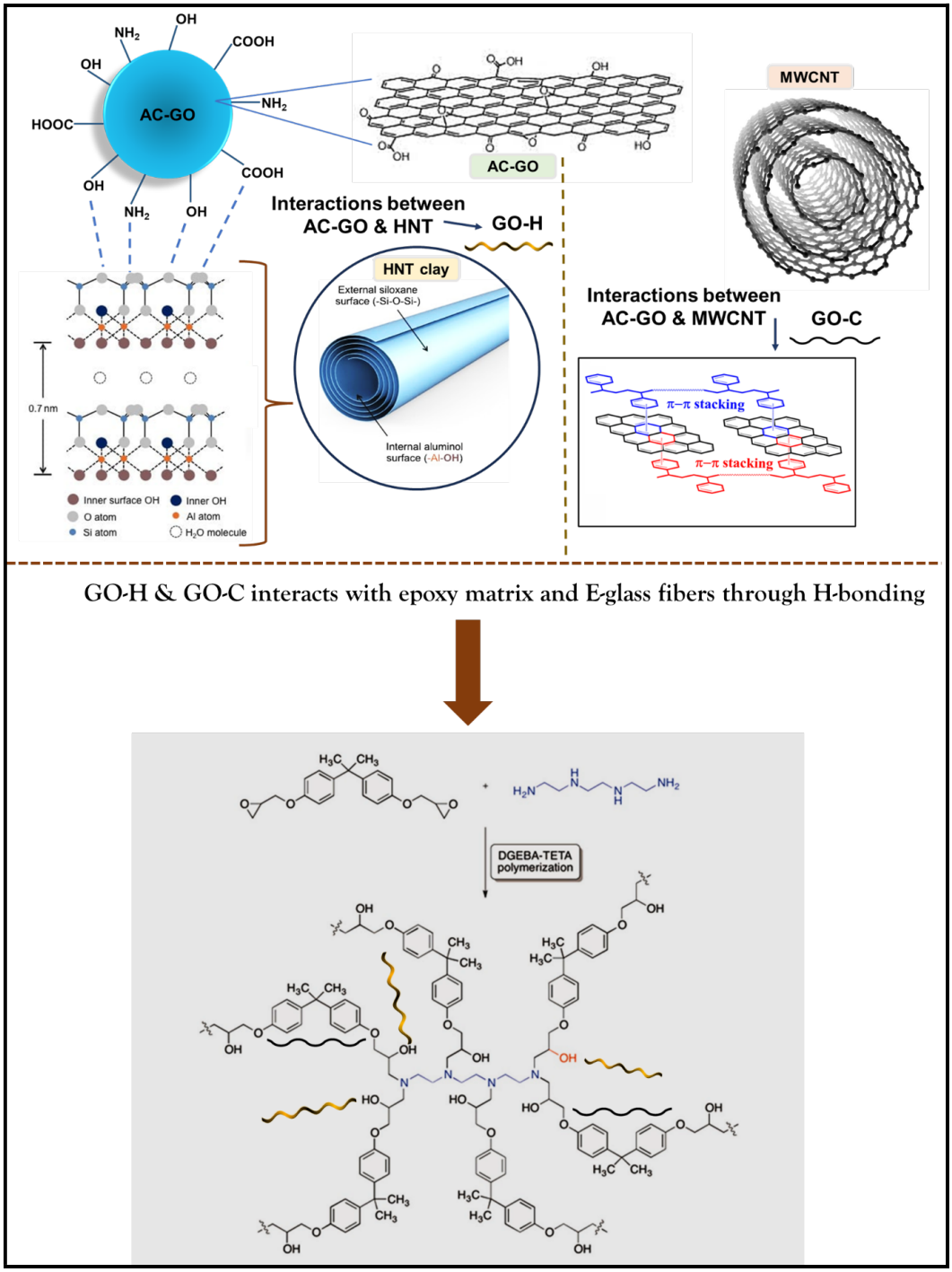

Figure 4.11. Mechanism showing the effective bonding among GO-H or GO-C/epoxy/glass-fiber at their optimum concentrations, respectively. *Note that we have shown the general mechanism for GO-H and GO-C together in the same epoxy cured structure, though we have conducted a separate investigation for both nanofillers based composites

In Figure 4.11, we propose a mechanism to explain the greater enhancement of mechanical properties observed with GO-H at its optimal concentration (0.50 HAGRP), Figure 4.11 (a). The subsequent decline in these enhancements beyond the optimal concentration, Figure 4.11 (b), primarily stems from agglomeration effects. The agglomeration of GO-H and GO-C in the composite induces steric hindrance, which leads to fewer GO platelets available to form a bond with epoxy at concentrations exceeding the optimum. This limitation, in turn, may contribute to the deterioration of the mechanical properties of the composite [54]. Additionally, the agglomeration of GO-H and GO-C reduces the aspect ratio of the filler, which further contributes to the degradation in mechanical properties [58].

Conclusion

In this extensive investigation, we conducted a comprehensive experimental study to evaluate the collective impact of GO-C and GO-H nanofillers on enhancing the mechanical properties of E-Glass fiber epoxy resin polymers, where GO-C and GO-H, denote the combinations of coal-derived graphene oxide with multiwalled carbon nanotubes (MWCNTs) combination, and halloysite nanotubes (HNT). These results were systematically compared with a control composite comprising E-glass fiber and epoxy resin (EGFP) without any nanofiller. The key conclusions of our study are as follows:

- Enhanced Mechanical Properties: The incorporation of GO-H and GO-C as nanofillers in EGFP significantly improves the effective bonding and strength of the glass fiber/matrix interface, as evident from SEM micrographs, leading to overall improvements in mechanical properties. The extent of these enhancements depends on the interplay of particle loading and particle-matrix adhesion.
- Optimal Filler Concentration: There is an optimal threshold concentration of the GO filler (0.50 phr for GO-H and 0.25 phr GO-C with a fixed concentration of 0.125 phr of AC-

GO), beyond which the mechanical properties decrease significantly due to particle aggregation, resulting in reduced available bonding sites for functional groups and reduced aspect ratio, ultimately leading to lower reinforcement efficiency.

These findings are significant as they offer insights into the design and optimization of an important class of composites—GFRPs. The proper selection of nanofiller and careful control of nanofiller concentration can yield nanocomposites with superior mechanical properties—critical for various industrial applications in aerospace, marine, sports equipment, and defense sectors.

We anticipate that the encouraging outcomes from our research will encourage additional investigation into diverse precursors, including HNT, MWCNT, and GO, coupled with a variety of polymers. This pursuit aims to pave the way for the synthesis of advanced composite materials with customized attributes for a broad spectrum of industrial applications, aligning with cost-effectiveness and environmental sustainability.

References

[1] Z. Arif, N.K. Sethy, L. Kumari, P.K. Mishra, S.N. Upadhyay, Recent advances in functionalized polymer-based composite photocatalysts for wastewater treatment, Nano-Materials as Photocatal. Degrad. Environ. Pollut. (2020) 39–64.

[2] P. Morampudi, K.K. Namala, Y.K. Gajjela, M. Barath, G. Prudhvi, Review on glass fiber reinforced polymer composites, Mater. Today Proc. 43 (2020) 314–319. https://doi.org/10.1016/j.matpr.2020.11.669.

[3] M. Fazeli, J.P. Florez, R.A. Simão, Improvement in adhesion of cellulose fibers to the thermoplastic starch matrix by plasma treatment modification, Compos. Part B Eng. 163 (2019) 207–216.

[4] P. Jadhav, G.M. Joshi, Recent trends in Nitrogen doped polymer composites: A review, J. Polym. Res. 28 (2021) 73.

[5] C. May, Epoxy resins: chemistry and technology, Routledge, 2018.

[6] J. Meister, Introduction to Polymer Modification, Polym. Modif. 60 (2020) 15–34. https://doi.org/10.1201/9781482269819-8.

[7] S. De, K.C. Nuli, A.O. Fulmali, P. Behera, R.K. Prusty, Elevated-temperature mechanical performance of GFRP composite with functionalized hybrid nanofiller, J. Appl. Polym. Sci. 139 (2022) e53223. https://doi.org/10.1002/app.53223.

[8] G. Rathinasabapathi, A. Krishnamoorthy, Comparative experimental investigations on mechanical properties of graphene and multi walled carbon nano tubes reinforced epoxy/glass fibre composites, in: AIP Conf. Proc., AIP Publishing LLC, 2019: p. 20094. https://doi.org/10.1063/1.5130304.

[9] B. Muralidhara, S.P. Kumaresh Babu, B. Suresha, Utilizing vacuum bagging process to prepare carbon fiber/epoxy composites with improved mechanical properties, Mater. Today Proc. 27 (2019) 2022–2028. https://doi.org/10.1016/j.matpr.2019.09.051.

[10] S. Mishra, K.T. Kumaran, R. Sivakumaran, S.P. Pandian, S. Kundu, Synthesis of PVDF/CNT and their functionalized composites for studying their electrical properties to analyze their applicability in actuation & sensing, Colloids Surfaces A Physicochem. Eng. Asp. 509 (2016) 684–696. https://doi.org/10.1016/j.colsurfa.2016.09.007.

[11] L. David, A. Feldman, E. Mansfield, J. Lehman, G. Singh, Evaluating the thermal damage resistance of graphene/carbon nanotube hybrid composite coatings, Sci. Rep. 4 (2014) 4311.

[12] B. Fiedler, F.H. Gojny, M.H.G. Wichmann, M.C.M. Nolte, K. Schulte, Fundamental aspects of nano-reinforced composites, Compos. Sci. Technol. 66 (2006) 3115–3125.

[13] K.K. Mahato, D.K. Rathore, R.K. Prusty, K. Dutta, B.C. Ray, Tensile behavior of MWCNT enhanced glass fiber reinforced polymeric composites at various crosshead speeds, in: IOP Conf. Ser. Mater. Sci. Eng., IOP Publishing, 2017: p. 12006. https://doi.org/10.1088/1757-899X/178/1/012006.

[14] M.C. Yip, Y.C. Lin, C.L. Wu, Effect of multi-walled carbon nanotubes addition on mechanical properties of polymer composites laminate, Polym. Polym. Compos. 19 (2011) 131–140. https://doi.org/10.1177/0967391111019002-313.

[15] X. Zhang, P. Wang, H. Neo, G. Lim, A.A. Malcolm, E.H. Yang, J. Yang, Design of glass fiber reinforced plastics modified with CNT and pre-stretching fabric for potential sports instruments, Mater. Des. 92 (2016) 621–631. https://doi.org/10.1016/j.matdes.2015.12.051.

[16] K.K. Panchagnula, P. Kuppan, Improvement in the mechanical properties of neat GFRPs with multi-walled CNTs, J. Mater. Res. Technol. 8 (2019) 366–376. https://doi.org/10.1016/j.jmrt.2018.02.009.

[17] M.-S. Kim, S.-E. Lee, W.-J. Lee, C.-G. Kim, Mechanical properties of MWNT-loaded plain-weave glass/epoxy composites, Adv. Compos. Mater. 18 (2009) 209–219.

[18] A. Tugrul Seyhan, M. Tanoglu, K. Schulte, Mode I and mode II fracture toughness of E-glass non-crimp fabric/carbon nanotube (CNT) modified polymer based composites, Eng. Fract. Mech. 75 (2008) 5151–5162. https://doi.org/10.1016/j.engfracmech.2008.08.003.

[19] P. Wang, X. Zhang, G. Lim, H. Neo, A.A. Malcolm, Y. Xiang, G. Lu, J. Yang, Improvement of impact-resistant property of glass fiber-reinforced composites by carbon nanotube-modified epoxy and pre-stretched fiber fabrics, J. Mater. Sci. 50

(2015) 5978–5992. https://doi.org/10.1007/s10853-015-9145-3.

[20] M.S. Chang, An investigation on the dynamic behavior and thermal properties of MWCNTs/FRP laminate composites, J. Reinf. Plast. Compos. 29 (2010) 3593–3599. https://doi.org/10.1177/0731684410379510.

[21] Z.A. Hamid, A.A. Azim, F.A. Mouez, S.S.A. Rehim, Challenges on synthesis of carbon nanotubes from environmentally friendly green oil using pyrolysis technique, J. Anal. Appl. Pyrolysis. 126 (2017) 218–229.

[22] Y.M. Manawi, Ihsanullah, A. Samara, T. Al-Ansari, M.A. Atieh, A review of carbon nanomaterials' synthesis via the chemical vapor deposition (CVD) method, Materials (Basel). 11 (2018). https://doi.org/10.3390/ma11050822.

[23] H. Dai, Carbon nanotubes: Opportunities and challenges, Surf. Sci. 500 (2002) 218–241. https://doi.org/10.1016/S0039-6028(01)01558-8.

[24] Q. Zhang, J.Q. Huang, M.Q. Zhao, W.Z. Qian, F. Wei, Carbon nanotube mass production: Principles and processes, ChemSusChem. 4 (2011) 864–889. https://doi.org/10.1002/cssc.201100177.

[25] M.S. Saharudin*, E. Elias, E.M. Sofian, B.T. Boschi, F. Inam, Flexural Properties of Halloysite Nanotubes (HNTS) and Carbon Nanotubes (CNTS) Toughened Epoxy Composites, Int. J. Innov. Technol. Explor. Eng. 9 (2020) 1670–1675. https://doi.org/10.35940/ijitee.d1520.029420.

[26] K. Prashantha, H. Schmitt, M.F. Lacrampe, P. Krawczak, Mechanical behaviour and essential work of fracture of halloysite nanotubes filled polyamide 6 nanocomposites, Compos. Sci. Technol. 71 (2011) 1859–1866. https://doi.org/10.1016/j.compscitech.2011.08.019.

[27] M. Rajaei, N.K. Kim, S. Bickerton, D. Bhattacharyya, A comparative study on effects of natural and synthesised nano-clays on the fire and mechanical properties of epoxy composites, Compos. Part B Eng. 165 (2019) 65–74. https://doi.org/10.1016/j.compositesb.2018.11.089.

[28] Y.H. Kim, S.J. Park, J.S. Choi, K.M. Moon, C.W. Bae, Effects of heat-treated HNTs on the mechanical properties of GFRP under moisture absorption, Int. J. Mod. Phys. B. 32 (2018) 1840070. https://doi.org/10.1142/S0217979218400702.

[29] R. Ramamoorthi, P.S. Sampath, Experimental investigations of influence of halloysite nanotube on mechanical and chemical resistance properties of glass fiber reinforced epoxy nano composites, J. Sci. Ind. Res. (India). 74 (2015) 685–689.

[30] H.X. Wang Qihui, Deng Guowei, Yang Min, Wang Jiexue, Qi Xiaodan, Preparation method and application of halloysite nanotube / graphene oxide composite material CN113244890B, (n.d.) 7–11.

[31] M.A. Hashmi, Enhancement of mechanical properties of epoxy/halloysite nanotube (HNT) nanocomposites, SN Appl. Sci. 1 (2019) 1–8.

[32] L. Lapčík, H. Sepetcioğlu, Y. Murtaja, B. Lapčíková, M. Vašina, M. Ovsík, M. Staněk, S. Gautam, Study of mechanical properties of epoxy/graphene and epoxy/halloysite nanocomposites, Nanotechnol. Rev. 12 (2023) 20220520.

[33] A. Garg, S. Basu, S.-Y. Lee, R.L. Mahajan, R. Mehta, Simplified One-Pot Synthesis of Graphene Oxide from Different Coals and its Potential Application in Enhancing the Mechanical Performance of GFRP Nanocomposites, ACS Appl. Nano Mater. (2023).

[34] A. Garg, S. Basu, R. Mehta, R.L. Mahajan, Enhancing the mechanical performance of E-glass fiber epoxy composites using coal-derived graphene oxide, Polym. Compos.

(2023).

[35] S.Y. Lee, R.L. Mahajan, A facile method for coal to graphene oxide and its application to a biosensor, Carbon N. Y. 181 (2021) 408–420. https://doi.org/10.1016/j.carbon.2021.05.007.

[36] D. Shelly, T. Nanda, R. Mehta, Synergistic effect of compatibilized nanoclay/polyethylene fibers on the impact strength of epoxy-glass fiber nanocomposites, Polym. Compos. 44 (2023) 6528–6541.

[37] M.L. Chen, W.C. Oh, Synthesis and highly visible-induced photocatalytic activity of CNT-CdSe composite for methylene blue solution, Nanoscale Res. Lett. 6 (2011) 1–8. https://doi.org/10.1186/1556-276X-6-398.

[38] T. Le Ba, A.Q. Alkurdi, I.E. Lukács, J. Molnár, S. Wongwises, G. Gróf, I.M. Szilágyi, A novel experimental study on the rheological properties and thermal conductivity of halloysite nanofluids, Nanomaterials. 10 (2020) 1–14. https://doi.org/10.3390/nano10091834.

[39] O. Adekomaya, A.A. Adediran, K. Adama, Characterization and morphological properties of glass fiber reinforced epoxy composites fabricated under varying degrees of hand lay-up techniques, J. Appl. Sci. Environ. Manag. 22 (2018) 110. https://doi.org/10.4314/jasem.v22i1.20.

[40] H. Alhumade, H. Rezk, A.M. Nassef, M. Al-Dhaifallah, Fuzzy Logic Based-Modeling and Parameter Optimization for Improving the Corrosion Protection of Stainless Steel 304 by Epoxy-Graphene Composite, IEEE Access. 7 (2019) 100899–100909. https://doi.org/10.1109/ACCESS.2019.2930902.

[41] T. Barot, D. Rawtani, P. Kulkarni, Physicochemical and biological assessment of

silver nanoparticles immobilized Halloysite nanotubes-based resin composite for dental applications, Heliyon. 6 (2020). https://doi.org/10.1016/j.heliyon.2020.e03601.

[42] K. Zhu, G. Wang, S. Zhang, Y. Du, Y. Lu, R. Na, Y. Mu, Y. Zhang, Preparation of organic-inorganic hybrid membranes with superior antifouling property by incorporating polymer-modified multiwall carbon nanotubes, RSC Adv. 7 (2017) 30564–30572. https://doi.org/10.1039/c7ra04248e.

[43] E.M. Benchafia, C. Yu, M. Sosnowski, N.M. Ravindra, Z. Iqbal, Plasma synthesis of nitrogen clusters on carbon nanotube sheets, Jom. 66 (2014) 608–615. https://doi.org/10.1007/s11837-014-0945-8.

[44] Mahajan, R. L.; Seul-Yi, L. E. E. U.S. Patent Application No. 17/415 4452022.

[45] A.N. Gent, C. Wang, Matrix cracking initiated by fibre breaks in model composites, J. Mater. Sci. 27 (1992) 2539–2548. https://doi.org/10.1007/BF01105067.

[46] J.N. Coleman, M. Cadek, R. Blake, V. Nicolosi, K.P. Ryan, C. Belton, A. Fonseca, J.B. Nagy, Y.K. Gun'ko, W.J. Blau, High performance nanotube-reinforced plastics: Understanding the mechanism of strength increase, Adv. Funct. Mater. 14 (2004) 791–798.

[47] N. Mohd Nurazzi, M.R.M. Asyraf, A. Khalina, N. Abdullah, F.A. Sabaruddin, S.H. Kamarudin, S. Ahmad, A.M. Mahat, C.L. Lee, H.A. Aisyah, Fabrication, functionalization, and application of carbon nanotube-reinforced polymer composite: An overview, Polymers (Basel). 13 (2021) 1047.

[48] E. Bozkurt, E. Kaya, M. Tanoğlu, Mechanical and thermal behavior of non-crimp glass fiber reinforced layered clay/epoxy nanocomposites, Compos. Sci. Technol. 67 (2007) 3394–3403. https://doi.org/10.1016/j.compscitech.2007.03.021.

[49] S.Y. Fu, X.Q. Feng, B. Lauke, Y.W. Mai, Effects of particle size, particle/matrix interface adhesion and particle loading on mechanical properties of particulate-polymer composites, Compos. Part B Eng. 39 (2008) 933–961. https://doi.org/10.1016/j.compositesb.2008.01.002.

[50] W. Han, J. Zhou, Q. Shi, Research progress on enhancement mechanism and mechanical properties of FRP composites reinforced with graphene and carbon nanotubes, Alexandria Eng. J. 64 (2023) 541–579.

[51] D. Lingaraju, K. Ramji, M.P. Devi, U.R. Lakshmi, Mechanical and tribological studies of polymer hybrid nanocomposites with nano reinforcements, Bull. Mater. Sci. 34 (2011) 705–712. https://doi.org/10.1007/s12034-011-0185-2.

[52] T. Nanda, G. Sharma, R. Mehta, D. Shelly, K. Singh, Mechanisms for enhanced impact strength of epoxy based nanocomposites reinforced with silicate platelets, Mater. Res. Express. 6 (2019). https://doi.org/10.1088/2053-1591/ab1023.

[53] R.K. Prusty, S.K. Ghosh, D.K. Rathore, B.C. Ray, Reinforcement effect of graphene oxide in glass fibre/epoxy composites at in-situ elevated temperature environments: An emphasis on graphene oxide content, Compos. Part A Appl. Sci. Manuf. 95 (2017) 40–53. https://doi.org/10.1016/j.compositesa.2017.01.001.

[54] O. Shakuntala, G. Raghavendra, A. Samir Kumar, Effect of filler loading on mechanical and tribological properties of wood apple shell reinforced epoxy composite, Adv. Mater. Sci. Eng. 2014 (2014). https://doi.org/10.1155/2014/538651.

[55] J. Fan, J. Yang, H. Li, J. Tian, M. Wang, Y. Zhao, Cryogenic mechanical properties of graphene oxide/epoxy nanocomposites: Influence of graphene oxide with different oxidation degrees, Polym. Test. 96 (2021) 107074.

https://doi.org/10.1016/j.polymertesting.2021.107074.

[56] C. Li, J. Wang, Y. Su, A dual-role theory of the aspect ratio of the nanofillers for the thermal conductivity of graphene-polymer nanocomposites, Int. J. Eng. Sci. 160 (2021) 103453. https://doi.org/10.1016/j.ijengsci.2020.103453.

[57] M. Mu, E. Teblum, Ł. Figiel, G.D. Nessim, T. McNally, Correlation between MWCNT aspect ratio and the mechanical properties of composites of PMMA and MWCNTs, Mater. Res. Express. 5 (2018) 45305. https://doi.org/10.1088/2053-1591/aab82d.

[58] M. Karevan, R. V. Pucha, M.A. Bhuiyan, K. Kalaitzidou, Effect of Interphase Modulus and Nanofiller Agglomeration on the Tensile Modulus of Graphite Nanoplatelets and Carbon Nanotube Reinforced Polypropylene Nanocomposites, Carbon Lett. 11 (2010) 325–331. https://doi.org/10.5714/cl.2010.11.4.325.

Take-aways and Future Perspectives

Take-aways from the entire work:

- This thesis primarily focused on synthesizing graphene-based materials through a one-pot method and their application as nanofillers in Glass Fiber Reinforced Polymer (GFRP) composites to enhance mechanical performance. We conducted a comprehensive experimental study with the objective of expanding the recently devised one-pot process for synthesizing graphene oxide (GO) from semi-anthracite and bituminous coals, abundant resources in India. Another focal point of our investigation was to explore potential applications of GO derived from coal and assess its influence as a nanofiller on the mechanical properties of a widely used GFRPs. In our subsequent in-depth exploration, we carried out an extensive experimental study to assess the cumulative influence of GO-C and GO-H nanofillers on improving the mechanical properties of E-Glass fiber epoxy resin polymers. Here, GO-C and GO-H represent combinations of AC-GO with MWCNTs (multiwalled CNTs) and HNT (halloysite nanotube), respectively. The key take-aways are as follows:
- The concentration and oxidation time of HNO_3 play a critical role in the synthesis of GO from coal. We noted that at elevated concentrations of HNO_3, bituminous coal exhibited complete dissolution. Even at 5 M HNO_3 with prolonged oxidation times (> 5 hours), either complete dissolution occurred or very low yields were obtained. In the case of semi-anthracite coal available in India, with slight adjustments in composition from the sample employed in the development of the original process, the initial recipe utilizing 16 M HNO_3 and 72 hours of oxidation proved to be effective.
- The introduction of AC-GO (semianthracite coal-derived GO) as a nanofiller in GFRP composites led to notable enhancements in their mechanical characteristics. Specifically, there was an 18.3% increase in tensile strength and a 30.9% increase in tensile modulus. Likewise, the flexural strength and flexural modulus exhibited improvements of 22.7% and 25.1%,

respectively. Furthermore, a modest increase of 6.7% was observed in impact strength at a loading of 0.125 phr of AC-GO in GFRP composites. EGFPs (E-Glass reinforced polymer composites) reinforced with BC-GO at a concentration of 0.25 phr exhibited noteworthy improvements. These include a 38.9% augmentation in flexural strength, a 22.9% increase in tensile strength, and a 21.6% enhancement in impact strength.

- Significant enhancements were evident in EGFPs reinforced with GO-H, featuring an 18.3% increase in flexural strength, a 14.6% rise in tensile strength, and a marginal uptick in impact strength (1.8%) at a loading of 0.50 phr of HNT, while maintaining an AC-GO concentration at 0.125 phr. Similarly, optimal values for GO-C-reinforced EGFPs at 0.25 phr included a 40.3% boost in flexural strength, an 18.7% increase in tensile strength, and a 10.5% reduction in impact strength. Importantly, considering that the cost of HNT clay is approximately 15 times cheaper than industrial-grade MWCNTs, these findings underscore the potential of GO-H as a very cost-effective reinforcement alternative to GO-C for polymer nanocomposites for various industrial applications.

Future Scope

The future of graphene oxide-based GFRP composites presents promising avenues for advancement and application across various domains. Here are some future directions:

- Investigating techniques to functionalize graphene oxide or modify its surface to enhance compatibility with different matrices can improve overall performance.
- Integrating coal-derived graphene oxide into GFRP composites for the development of smart materials that respond to external stimuli, such as temperature or strain, can open up applications in sensing and structural health monitoring.
- Exploring the incorporation of additional nanofillers or additives alongside graphene oxide in GFRP composites to achieve multi-functional properties, such as improved fire resistance, antibacterial properties, or self-healing capabilities.

- Scaling up production processes of graphene oxide-based GFRP composites and facilitating their integration into industrial applications is essential.
- Research efforts can be directed towards utilizing graphene oxide-based GFRP composites for lightweight, high-strength applications in sectors such as aerospace and automotive industries, where materials with superior strength-to-weight ratios are highly sought after.
- Continued research and innovation in these directions can unlock the full potential of graphene oxide-based GFRP composites and lead to their widespread adoption in various industrial applications.

Conferences and Workshops Attended

1. Poster presentation on the topic "**Graphene: Synthesis, Functionalization & Its Applications**" at International e-Conference on Nanomaterials & Nanoengineering APA NANOFORUM-2022 February 24-26, 2022.

2. Oral presentation on the topic "**Synthesis of Coal-derived Graphene oxide and Its Application in Glass-fiber based Polymer Composites for Improved Mechanical Performance**" at 1st International Conference on Futuristic Materials for Sustainable Development Goals-2024 (FMSDG-2024)- 8-9th, January, 2024.

3. Attended International Virtual Conference on **Modern Instrumental and Characterization Techniques in Applied Sciences**- 2020 (MICTAS-2020) organized by MIET Kumaon Haldwani & Department of Chemistry, H.N.B. Govt. P. G. College, Khatima, Uttarakhand in collaboration with USERC DST Dehradun & Department of Chemistry, R.H. Govt. P. G. College, Kashipur, Uttarakhand, India on July 5-6, 2020.

4. Attended DST STUTI workshop on "**ADVANCED CHARACTERIZATION TECHNIQUES IN CONDENSED MATTER**", held in BITS, Pilani from 17 Jan-23 Jan 2023.

5. Won the **Best Poster Award** in Poster Presentation Session on **CEEMS SCHOLAR'S DAY-2024** organized by TIET-VT Center of Excellence in Emerging Materials (CEEMS) on 15th February, 2024.

6. Oral presentation on the topic "**Synthesis of Coal-derived Graphene oxide and its Application in Glass-fiber based Polymer Composites for Improved Mechanical Performance**" at the International Conference on "Sustainable Development in Chemical and Environmental Engineering" (SDCEE) - 22-24, February, 2024.

Appendix-I Challenges Encountered During the Ph.D. Journey

This appendix provides a structured overview of the challenges encountered during the PhD journey, offering transparency and insight into my experiences and the resilience demonstrated in overcoming these obstacles.

During the initial phase, there were some **challenges regarding the Literature Review**. Firstly, difficulty in locating relevant and recent literature due to the vast amount of information available and secondly managing conflicting viewpoints and theories within the literature, leading to prolonged analysis and synthesis. Creating a comprehensive and detailed table that categorizes various precursors, highlights their differences, outlines synthesis methods, compares them, and organizes papers by year aids in distinguishing the literature effectively. This approach enhances clarity regarding why a specific methodology is being emphasized, facilitating a clearer understanding of the research focus. This approach has proven beneficial to me throughout my entire journey, yielding fruitful results from beginning to end.

In the preliminary stages of my research, I **aimed to explore the newly developed one-pot method tailored for Indian coal varieties**. We acquired semianthracite coal from the Kashmir coalfield and initially validated the use of a 16 M concentration of HNO_3, confirming its efficacy akin to its application in US-based anthracite coal. This initial success instilled confidence in the method's potential applicability across diverse coal types. Additionally, I obtained another variety of bituminous coal from Prof. Amjad Ali's Lab within our Department of Chemistry and Biochemistry. To my astonishment, when I applied the identical procedure, it failed to yield the expected results. No precipitates were obtained at the initial 16M concentration of HNO_3. However, upon reducing both the concentration and oxidation time, successful precipitation was achieved with a 5M HNO_3 concentration over 5 hours. Nevertheless, a significant limitation persisted: uncertainty regarding the precise origin of the coal. Through discussions with Prof.

Amjad Ali and my supervisors, it was tentatively identified as originating from the North-eastern region of India. Typically, sourcing specific coal mines proves challenging. However, Prof. Mahajan expressed uncertainty regarding the method's compatibility with different grades of bituminous coal, citing diverse experiences from his lab at Virginia Tech., USA. Consequently, I obtained another variety of bituminous coal with a slightly altered carbon content. Surprisingly, preliminary data indicated an optimal concentration of 14M for 5 hours with this new coal variety. Through rigorous experimentation, I concluded that while the use of a single oxidant, HNO_3, remained constant, the optimal oxidant concentration and oxidation time varied across different coal grades.

Subsequently, when incorporating semianthracite **coal-derived graphene oxide (AC-GO) into GFRP composites**, the optimal concentration for achieving its peak mechanical performance was determined to be 0.125 phr. Curious whether further reduction in concentration could enhance additional properties, I experimented with a concentration of 0.0625 phr for AC-GO, resulting in inferior mechanical properties. This brief example underscores the iterative nature of experimentation. Through numerous trials, I refined the concentration for each coal-derived GO and graphite-derived GO, facilitating a comprehensive comparison. Additionally, an extensive literature review enabled the identification of pivotal factors influencing nanofiller loading and the choice of nanofiller in GFRP composites, elucidating their diverse mechanical behaviors.

Moreover, crucially, instances of data loss stemming from hardware malfunctions require considerable efforts for recovery. Thus, it is imperative to prevent such occurrences by consistently updating our data.

However, despite of the several challenges faced, the research work flourished significantly owing to the invaluable guidance and support of my supervisors.